NASA CONTRACTOR REPORT

NASA CR-910

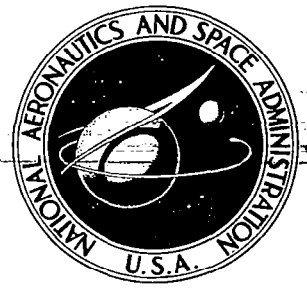

MEASURING HUMAN PERFORMANCE WITH A PARAMETER TRACKING VERSION OF THE CROSSOVER MODEL

by Glenn A. Jackson

Prepared by
UNIVERSITY OF MICHIGAN
Ann Arbor, Mich.
for

NATIONAL AERONAUTICS AND SPACE ADMINISTRATION • WASHINGTON, D. C. • OCTOBER 1967

NASA CR-910

MEASURING HUMAN PERFORMANCE WITH A PARAMETER TRACKING VERSION OF THE CROSSOVER MODEL

By Glenn A. Jackson

Prepared under Contract No. NASr 54(06) by
UNIVERSITY OF MICHIGAN
Ann Arbor, Mich.

for

NATIONAL AERONAUTICS AND SPACE ADMINISTRATION

For sale by the Clearinghouse for Federal Scientific and Technical Information
Springfield, Virginia 22151 – CFSTI price $3.00

Abstract

MEASURING HUMAN PERFORMANCE WITH A PARAMETER TRACKING VERSION OF THE CROSSOVER MODEL

Glenn A. Jackson

The purpose of this research is the evaluation of a particular parameter tracking system for use in measuring the performance of human operators in low order compensatory manual control systems. The system is based on a "crossover model" proposed by Duane McRuer, which assumes that the entire forward loop of the compensatory control system can be represented by a gain, an integration and a pure time-delay.

A continuous parameter tracking system is developed using an approximate version of the crossover model as the basic system model. The approximation involves the use of a first order Padé time-delay in place of the pure time-delay. The parameter tracking system is designed to adjust automatically the gain and time-delay parameters so that the instantaneous value of the square of the error between the model output and the compensatory system output is driven toward zero. The tracking method is similar to those developed by George Bekey and Hans Meissinger, except a nonlinear parameter adjustment technique has been added to give smoother performance.

The parameter tracking system is tested on subjects controlling single and double integrator plants, with input signals of bandwidth limited Gaussian noise. The gain and time-delay parameters are found to change significantly with training and with the bandwidth of the input signal. The parameters also vary between subjects and with the order of the plant being controlled.

Using spectral analysis, the parameter values determined by the parameter tracking system are confirmed. Also, the crossover model is shown to represent the compensatory system nearly as well as the best linear time-invariant model.

In addition to the experimental testing of the parameter tracking system, a theoretical analysis of the system is undertaken. It is shown that the convergence properties of the parameters can be calculated when the input signal is sinusoidal and the system is tracking a known constant coefficient system. The theoretical analysis is based on the method of Kryloff and Bogoliuboff. The extension of this analysis to the random input case is indicated.

It is concluded that, as long as the input bandwidth is properly chosen, the parameter tracking system developed is an excellent method for measuring human performance in certain low order compensatory control systems.

ACKNOWLEDGMENTS

The author wishes to express his gratitude to each committee member, especially to Dr. R.M. Howe, Dr. L.E. Fogarty, and Dr. R.W. Pew for their continued interest and suggestions.

The assistance of Mrs. Linda Fench in conducting the experiments, and the work of Mr. John Duffendack and Mr. John Overmars on the spectral analysis program are greatly appreciated.

The author is indebted to Mrs. Christine Long for her excellent work in typing the manuscript.

This research was sponsored in part by the National Aeronautics and Space Administration under contract NASr 54(06).

TABLE OF CONTENTS

LIST OF TABLES

LIST OF FIGURES

LIST OF APPENDICES

LIST OF SYMBOLS

A	Coefficient matrix
a	Acceleration input constant, $\theta_i(t) = at^2/2$
B	Coefficient matrix
C	Coefficient matrix
c(t)	Control stick output
$C_{iiq}(\alpha)$	Estimate of $R_{ii}(\alpha)$ computed from one sample of $\theta_i(t)$
$C_{ooq}(\alpha)$	Estimate of $R_{oo}(\alpha)$ computed from one sample $\theta_o(t)$
$C_{ioq}(\alpha)$	Estimate of $R_{io}(\alpha)$ computed from one sample of $\theta_i(t)$ and one sample of $\theta_o(t)$
$E(\cdot)$	Expected or mean value
$e(t, K, \tau)$	Output error of the parameter tracking system, $e(t, K, \tau) = Z(t, K, \tau) - \theta_o(t)$
$\overline{e^2(t)}$	$R_{ee}(0)$ = time average of $e^2(t)$
$e_1(t, K, \tau)$	Closed loop error of the assumed model, $e_1(t, K, \tau) = \theta_i(t) - Z(t, K, \tau)$
h(t)	Impulse response function
I	Unit matrix
I(t)	Performance index
IAE	Integral of the absolute value of the error
j	Square root of minus one
K	Crossover model gain of the assumed model
K*	Crossover model gain of the system being identified

k_K	Gradient gain in the parameter adjustment equation for K
k_τ	Gradient gain in the parameter adjustment equation for τ
L	Value of the limits on the parameter adjustment limiter
n(t)	Closed loop remnant referred to the output of the compensatory system
$n_1(t)$	Closed loop remnant referred to the output of the control stick
p	Differential operator
PM	Power match
PM_I	Ideal power match
$R_{ee}(\alpha)$	Time auto-correlation function of e(t)
$R_{ii}(\alpha)$	Time auto-correlation function of $\theta_i(t)$
$R_{oo}(\alpha)$	Time auto-correlation function of $\theta_o(t)$
$R_{io}(\alpha)$	Time cross-correlation function between $\theta_i(t)$ and $\theta_o(t)$
S(t)	Time signal associated with the correlated portion of the compensatory system output. If the remnant is referred to the output of the compensatory system, $\theta_o(t) = S(t) + n(t)$
sat(·)	Saturation function
T	Length of compensatory tracking task. Also used as the time constant of a first order filter
t_o	$t_o = t - \tau$
$u_o(t, K, \tau)$	Sensitivity coefficient for K
$u_1(t, K, \tau)$	Sensitivity coefficient for τ
V	Ramp input constant, $\theta_i(t) = Vt$
v	Normalized frequency, $v = \omega\tau$

$x_i(t)$	ith state variable of the parameter tracking system
$\vec{x}(t)$	Column vector of state variables
$Y_C(p)$	Transfer operator of the controlled element
$Y_P(p)$	Transfer operator representing the linear action of the subject
$\widehat{Y_P Y_C}(j\omega)$	Estimate of $Y_P Y_C(j\omega)$
$y_i(t)$	Perturbation variable related to $x_i(t)$
$\vec{y}(t)$	Column vector of perturbation variables
$Z(t, K, \tau)$	Output signal of the assumed parameter tracking model
α_i, β_i	Coefficients of a general parameter tracking model
$\vec{\alpha}, \vec{\beta}$	Column vectors with elements α_i and β_i
$\Delta K(t)$	$K(t) = K(0) + \Delta K(t)$
$\Delta\tau(t)$	$\tau(t) = \tau(0) + \Delta\tau(t)$
$\epsilon(t)$	Closed loop error of the compensatory control system, $\epsilon(t) = \theta_i(t) - \theta_o(t)$
$\theta_i(t)$	Input signal to the compensatory control system
$\theta_o(t)$	Output signal of the compensatory control system
$\widetilde{\theta_o^2(t)}$	Time average of $\theta_o^2(t) = R_{oo}(0)$
λ	Characteristic root of a matrix
ρ_o	Relative remnant
$\hat{\rho}_o^2$	Estimate of ρ_o^2
τ	Crossover model time-delay of the assumed model
τ^*	Crossover model time-delay of the system being identified

$\Phi_{ii}(j\omega)$	Spectral density of $\theta_i(t)$
$\Phi_{oo}(j\omega)$	Spectral density of $\theta_o(t)$
$\Phi_{io}(j\omega)$	Cross-spectral density between $\theta_i(t)$ and $\theta_o(t)$
$\Phi_{i\epsilon}(j\omega)$	Cross-spectral density between $\theta_i(t)$ and $\epsilon(t)$
$\hat{\Phi}_{ii}(j\omega)$	Estimate of $\Phi_{ii}(j\omega)$
$\hat{\Phi}_{oo}(j\omega)$	Estimate of $\Phi_{oo}(j\omega)$
$\hat{\Phi}_{io}(j\omega)$	Estimate of $\Phi_{io}(j\omega)$
$\phi_{iiq}(j\omega)$	Fourier transform of $C_{iiq}(\alpha)$
$\phi_{ooq}(j\omega)$	Fourier transform of $C_{ooq}(\alpha)$
$\phi_{ioq}(j\omega)$	Fourier transform of $C_{ioq}(\alpha)$
ω	Frequency in radians per second
ω_i	Cut-off frequency of the input filter in radians per second
$\triangleq$	Equal by definition
$\widetilde{(\cdot)}$	Time average
$\widehat{(\cdot)}$	Estimated value

Chapter 1

INTRODUCTION

1.1 Compensatory Tracking

One area of active research in the broad discipline called human performance, or human behavior, is compensatory tracking. In this type of tracking task the human operator (subject) serves as the controller in a conventional closed loop control system.

The subject is asked to manipulate the signal forcing a dynamic system in such a manner that the system output follows a given input signal. The magnitude of the signal forcing the dynamic system is determined by the position of a control stick which the subject moves with his hand, arm, or wrist, depending on the particular type of control stick being used. The error $\epsilon(t)$ between the system input $\theta_i(t)$ and the actual system output $\theta_o(t)$ is displayed on an oscilloscope located in front of the subject. The error signal is used by the subject to determine future control stick action. The system configuration is shown in Fig. 1.1.1.

The input signal is some unpredictable signal, such as low frequency filtered Gaussian white noise, or a sum of sinusoids that is

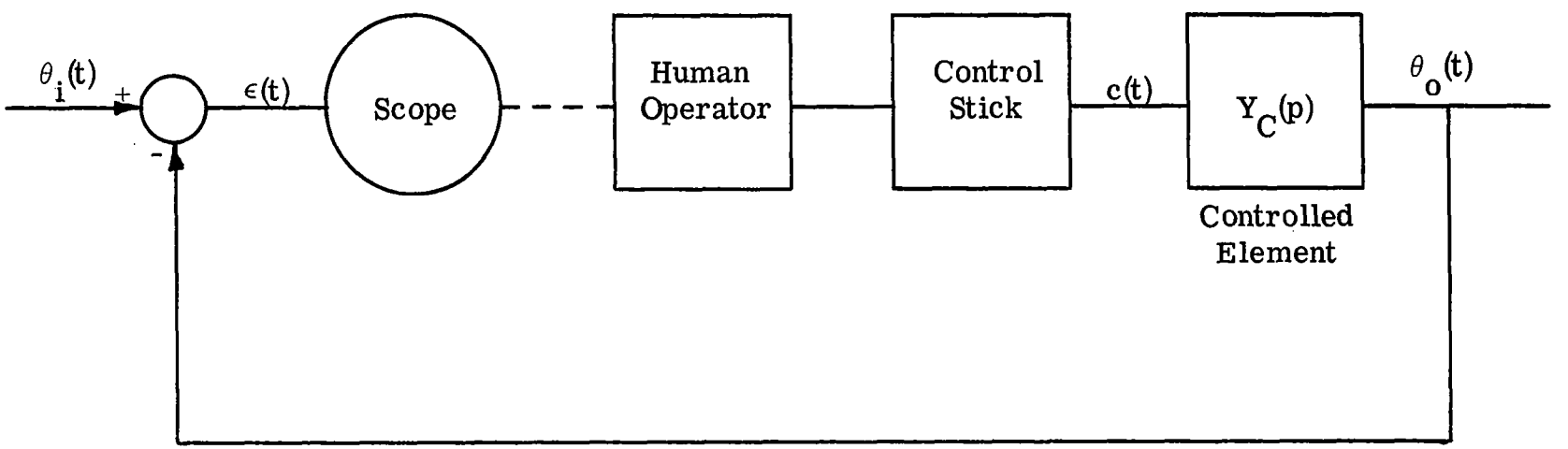

Figure 1.1.1 Block Diagram of a Compensatory Control Task.

designed to approximate this type of signal. The subject is simply told to keep the error as small as possible at all times, and is free to move the control stick in any manner he deems best[1].

Another type of tracking task, called pursuit tracking [13, 26][2], is quite similar to the compensatory tracking task described above. The only difference in the two tasks is that in pursuit tracking a dual-beam oscilloscope is used, and both the input and output signals are displayed, rather than the error between them. The objective in this case is to keep the output indicator on top of the input indicator, again by proper manipulation of the control stick. Pursuit tracking is considered to be an easier task than compensatory tracking. This is because the input signal is explicitly displayed on the oscilloscope and the subject can more readily determine its characteristics.

Research related to these two types of tracking tasks started during World War II when men in the armed forces were being trained to manually sight and fire automatic weapons [33]. The research continued in the 1950's and has been stimulated in recent years by the presence of manual control systems in space vehicles.

---

[1]Typical instructions for subjects can be found in Appendix A.

[2]Bracketed numbers are references to be found at the end of the report.

1.2 Performance Measures

In the earliest experiments, researchers concentrated on measuring gross indices of performance such as the mean square error

$$\frac{1}{T}\int_0^T \epsilon^2(t)\,dt \quad , \tag{1.2-1}$$

or the mean absolute value of error

$$\frac{1}{T}\int_0^T |\epsilon(t)|\,dt \quad , \tag{1.2-2}$$

where T was the length of the tracking task and $\epsilon(t)$ the error in the compensatory control loop. (See Fig. 1.1.1.) These scores were related to individual differences, input signals, controlled elements, control sticks, and number of practice sessions, to name but a few.

Most of these early tests were conducted by and for experimental psychologists. As time passed, however, more and more engineers became involved in compensatory tracking research. Engineers were interested in compensatory tracking for two main reasons: first, they were called upon to assist the psychologists in the development of better and more significant indices of performance; second, they themselves were interested in learning what types of systems a subject could and could not control. By carefully analyzing the manner in

which subjects handled controlled elements with transfer operators like

$$Y_C(p) = \frac{K_1}{p} \ , \ \frac{K_1}{p^2} \ , \ \frac{K_1}{T\,p + 1} \ , \ \text{or} \ \frac{K_1}{p(T\,p + 1)} \ , \qquad (1.2\text{-}3)$$

where

$$p = \frac{d}{dt} \ , \ . \ . \ . \ . \ , \ p^n = \frac{d^n}{dt^n} \ ,$$

engineers hoped to determine some pertinent human operator characteristics which would prove useful in manual control system design. By having more information on a human operator's capabilities, systems such as aircraft control systems can be designed more efficiently and with less fear of under or over estimating the operating range of a pilot.

For these reasons, research engineers started to look beyond the gross indices of performance given in Eqs. (1.2-1) and (1.2-2). The most important extension in this area has been the attempt to catalog the equations that describe the human as a controller. Referring to Fig. 1.1.1, the equations in question are those relating $c(t)$ to $\epsilon(t)$, assuming that the control stick dynamics are negligible.

1.3 Determining the Equations of Human Response

Many different methods have been proposed for the determination

of the equations that describe the human as a controller. Most of these methods are designed to identify only the linear action of the human operator. These methods include: parameter tracking [4, 6, 23, 29]; random input describing functions [27]; orthogonal filtering [16]; and measurement of the impulse response [38, 39]. The most significant attempt that has been made to include the nonlinear aspects of the human operator has been by direct analog simulation [18], although some nonlinearities have been proposed for addition into parameter tracking systems [7].

Only the first two of the methods discussed above have been applied in practice to any large extent. These two methods will be discussed very briefly at this point, since they are quite different in nature, and since both methods are directly related to the research to be discussed in this report.

1.4 Parameter Tracking

Parameter tracking will be discussed in detail in Chapter 3. The discussion here will be limited to the basic philosophy behind this type of system identification.

In this type of analysis, a basic equation for the human operator is assumed with the coefficients being unknown quantities. The assumed model of the human operator is simulated on an analog computer and driven in parallel with the subject, the model receiving exactly

the same signal as the subject. The coefficients of the model are adjusted, either continuously or iteratively, in such a manner that the model output gives a best fit to the actual subject output. The coefficient adjustment is generally made using a gradient technique, where the gradients are determined using sensitivity equations [30, 35].

The main advantage of this method lies in its use as an on-line device. It has been used extensively by Bekey [7], Todosiev [34], and others [2, 3, 15, 37]. A general block diagram of this type of system is given in Fig. 1.4.1.

1.5 Random Input Describing Functions

Since $\theta_i(t)$ is generally filtered Gaussian white noise, one natural method of analysis is the random input describing function approach. In this method, the block diagram of the compensatory control system is assumed to be that shown in Fig. 1.5.1. $Y_p(j\omega)$ is the random input describing function of the human operator. It is determined from recorded tracking data by using spectral analysis in the following manner. The cross-spectral density $\Phi_{ic}(j\omega)$ between the input signal and the control stick output, and the cross-spectral density $\Phi_{i\epsilon}(j\omega)$ between the input signal and the compensatory error are determined experimentally. $Y_p(j\omega)$ is then defined in the conventional manner as [27],

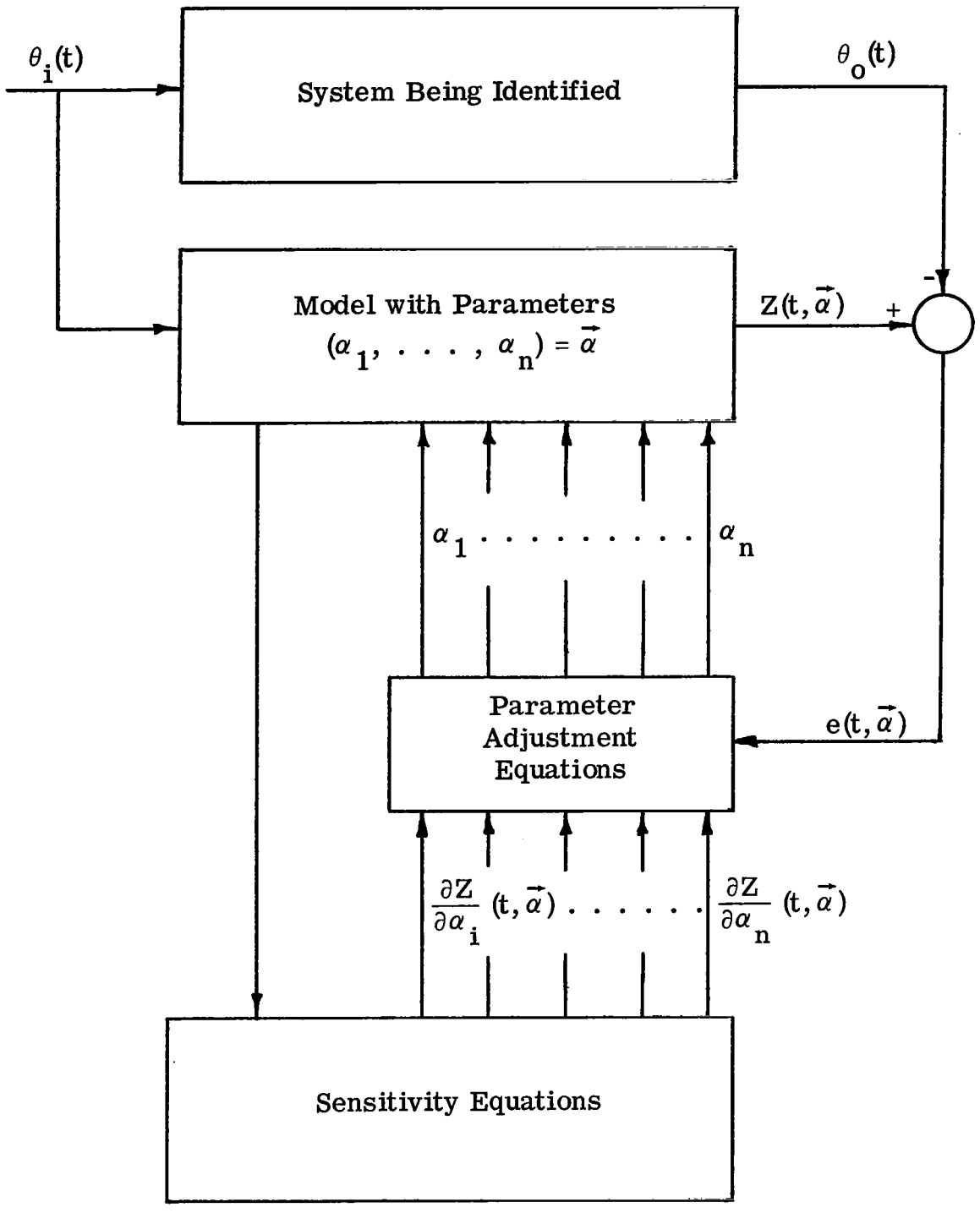

Figure 1.4.1 General Block Diagram of a Parameter Tracking System — Output Error Method

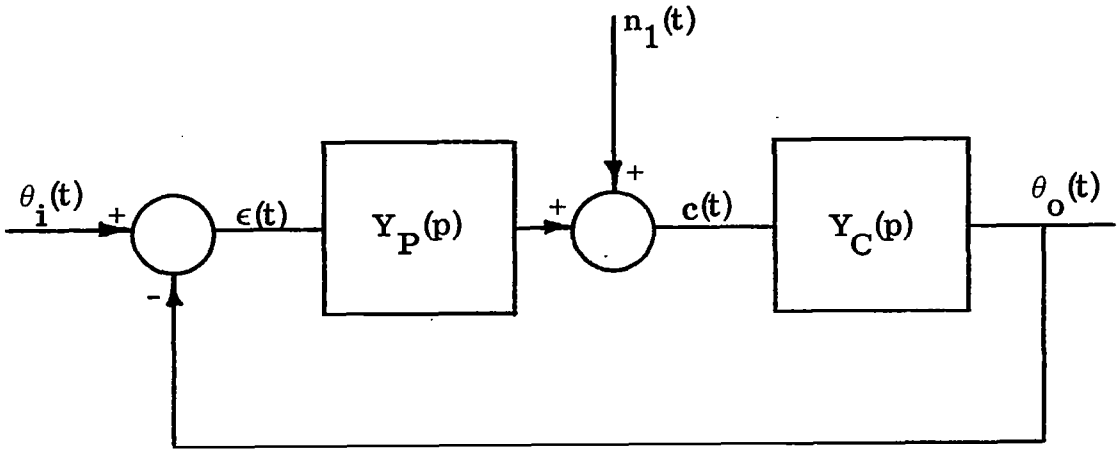

$Y_P(p)$ is the transfer operator of the subject. More exactly,

$$Y_P(j\omega,\ \theta_i,\ Y_C) = \frac{\Phi_{ic}(j\omega)}{\Phi_{i\epsilon}(j\omega)} \quad .$$

$n_1(t)$ is the uncorrelated portion of the subject output called the remnant.

Figure 1.5.1 Describing Function Block Diagram of the Compensatory Control System.

$$Y_P(j\omega) = \frac{\Phi_{ic}(j\omega)}{\Phi_{i\epsilon}(j\omega)} \qquad (1.5\text{-}1)$$

The magnitude and phase of this experimentally determined describing function can be plotted on standard semi-log paper. These plots give a graphical description of the average linear action of the subject in the particular task being evaluated.

If a more useable form of the describing function is desired, simple mathematical forms for $Y_P(j\omega)$ are assumed and the coefficients of the assumed form are varied until the approximate gain-phase plots closely match the experimental gain-phase plots. Several models may have to be tried before the curve fit is satisfactory.

Since $Y_P(j\omega)$ models only that portion of the human operator output that is linearly correlated with the input signal, a noise term $n_1(t)$ is added to represent the injection of that portion of the human output which is not correlated with the input signal. $n_1(t)$ is called the remnant.

The main advantage of this method is that it is amenable to rigorous mathematical analysis. Also, no pre-experimental assumption of the form of $Y_P(j\omega)$ needs to be made before developing the actual gain-phase curves. The main disadvantage is that it is a time consuming off-line method that requires a considerable amount of equipment for analysis.

1.6 A General Model

McRuer, Elkind and their respective associates are two groups of researchers who have made an extremely thorough analysis of many compensatory tracking tests using the random input describing function approach [13, 25, 26]. McRuer, especially, has calculated $Y_P(j\omega)$ for numerous combinations of controlled elements and input signals and has postulated a transfer function that can be adjusted to match the gain-phase curves of most subjects. This transfer function is

$$Y_P(j\omega) = \frac{K_1 (j\omega T_1 + 1) e^{-j\omega\tau}}{(j\omega T_2 + 1)(j\omega T_3 + 1)} \qquad (1.6\text{-}1)$$

where K_1, T_1, T_2, T_3, and τ all vary with $\theta_i(t)$ and $Y_C(p)$.

This form is the result of many tests and, having been averaged over many subjects, is an equation which should adequately represent the linear action of a typical subject in a compensatory control task. The general acceptance of this form is indicated by the number of researchers who continually compare their results with this transfer function.

1.7 The Crossover Model

One of the more interesting results of the McRuer work is the postulation of a "crossover model" [25]. It was discovered that for several first and second order controlled elements, the gain-phase

curves of the entire compensatory forward loop were of the same approximate form. This form, called the crossover model, was approximated by the transfer operator

$$Y_P\, Y_C(p) = \frac{K e^{-\tau p}}{p} \quad . \qquad (1.7\text{-}1)$$

The gain-phase plot of this equation fits experimental magnitude data better than experimental phase data, but is generally a good fit to both in the crossover region, the crossover region being defined as that portion of the frequency spectrum near which $|Y_P\, Y_C(j\omega)| = 1$.

1.8 Description of the Research

The purpose of the research described in this report is the evaluation of the crossover model in the following manner:

(1) To determine the feasibility of using the crossover model as the parameter tracking model of certain first and second order compensatory control systems.

(2) To determine whether the crossover model gain K and time-delay τ are good performance indices for measuring the differences between subjects, the difficulty of compensatory tracking tasks, and the learning rates of subjects.

In addition, the following proposed contributions to the general methodology of continuous parameter tracking will be analyzed:

(1) A limited parameter adjustment technique to give smoother, less erratic performance.

(2) A mathematical method for determining the convergence rate of the parameters, and the amount of parameter interaction, when the gradient gains are low and the input signal is a sinusoid.

(3) A performance index that indicates how well the parameter tracking model compares with the optimum linear time-invariant model of the compensatory system.

The presentation of this research is broken down in the following manner. Chapters 2 and 3 discuss the reasons for, and the development of, a continuous parameter tracking system utilizing the crossover model. Chapter 4 contains the theoretical and experimental analyses of the parameter tracking system when tracking a known model of the correct form. The limited gradient technique and the sinusoidal analysis based on the method of Kryloff and Bogoliuboff are also discussed in this chapter. Chapter 5 outlines the actual experimental work with human operators and presents the results of the tracking tests. Chapter 6 discusses the spectral tests that were run on the compensatory tracking data and gives the comparisons of these results with those obtained by the parameter tracking system.

The new performance index for evaluating the crossover model is also introduced at this point. Chapter 7 reviews the basic results of the research and lists areas where further study is needed.

Chapter 2

ADVANTAGES OF THE CROSSOVER MODEL

There are many reasons for using the crossover model as the parameter tracking model of a compensatory control system, the important ones being: (1) the simplicity of the model and the resulting improvement in parameter tracking stability; (2) the relatively small amount of equipment needed for implementation; (3) the fact that the gain-phase characteristics of the compensatory forward loop, as obtained by other researchers, can be matched very closely with the crossover model; (4) the fact that the crossover model output is most sensitive to parameter changes in the same region it most accurately describes human response; and (5) the fact that crossover frequency and gain-margin, two important control system characteristics, are located in the region of maximum model accuracy. These items will be discussed in this chapter.

2.1 Stability and Equipment Considerations

A basic problem with continuous parameter tracking systems, as with most gradient methods, is the problem of stability. Although the entire parameter tracking system is a nonlinear time-varying system that is very difficult to analyze, several general facts are known to be causes of concern. First, stability problems are known to arise from

the interaction that exists between the different parameter adjustment loops. Second, the time required for the parameters to converge to their final values from some set of initial conditions is dependent upon the number of parameters being identified. In fact, Bekey, et al. [7] have hypothesized that the settling, or convergence, time increases at a rate of 2^n, where "n" is the number of parameters being tracked.

It is quite evident that if a relatively stable system is desired, then every effort should be made to choose a model which not only models subject response, but also contains the smallest number of parameters. Previous parameter tracking models, such as those used by Adams and Bekey, have contained three or four parameters. Since the crossover model has only two parameters, the basic stability and convergence properties of the related tracking system should be noticably better than those used with the previously mentioned models.

Another problem inherent with continuous parameter tracking systems is the amount of analog equipment necessary for implementation. The computing capacity required increases at a faster rate than the number of parameters being tracked. This is especially true of multiplication circuits. Since many human performance researchers do not have large analog facilities, the two parameter model is again more desirable than the three or four parameter models.

If the parameter tracking were to be done digitally, either on-line or off-line, programming and solution time considerations would still favor the two parameter model.

2.2 Comparison of Crossover Model Gain-Phase Curves with Those from Other Models

The fact that the crossover model is desirable from stability and equipment viewpoints would be of little significance if the model gave a poor fit to experimental data. Fortunately, this does not appear to be the case, at least as far as the gross characteristics at frequencies near and below crossover are concerned. Examination of other researchers data shows that the gain-phase curves of the crossover model can be adjusted to match closely the curves that were found to represent the compensatory forward loop. This implies that K and τ should afford enough model adjustment to fit the compensatory tracking data nearly as well as models with more parameters. Two examples of this fact are given below.

Figure 2.2.1 gives a comparison of the average compensatory forward loop gain-phase curves as determined by Todosiev, et al. [34], with the crossover model gain-phase curves, with K and τ adjusted to give a best fit. Both perfect time-delay and first order Padé approximation phase data are given [36]. Referring to Fig. 1.1.1, the model configuration used by Todosiev was

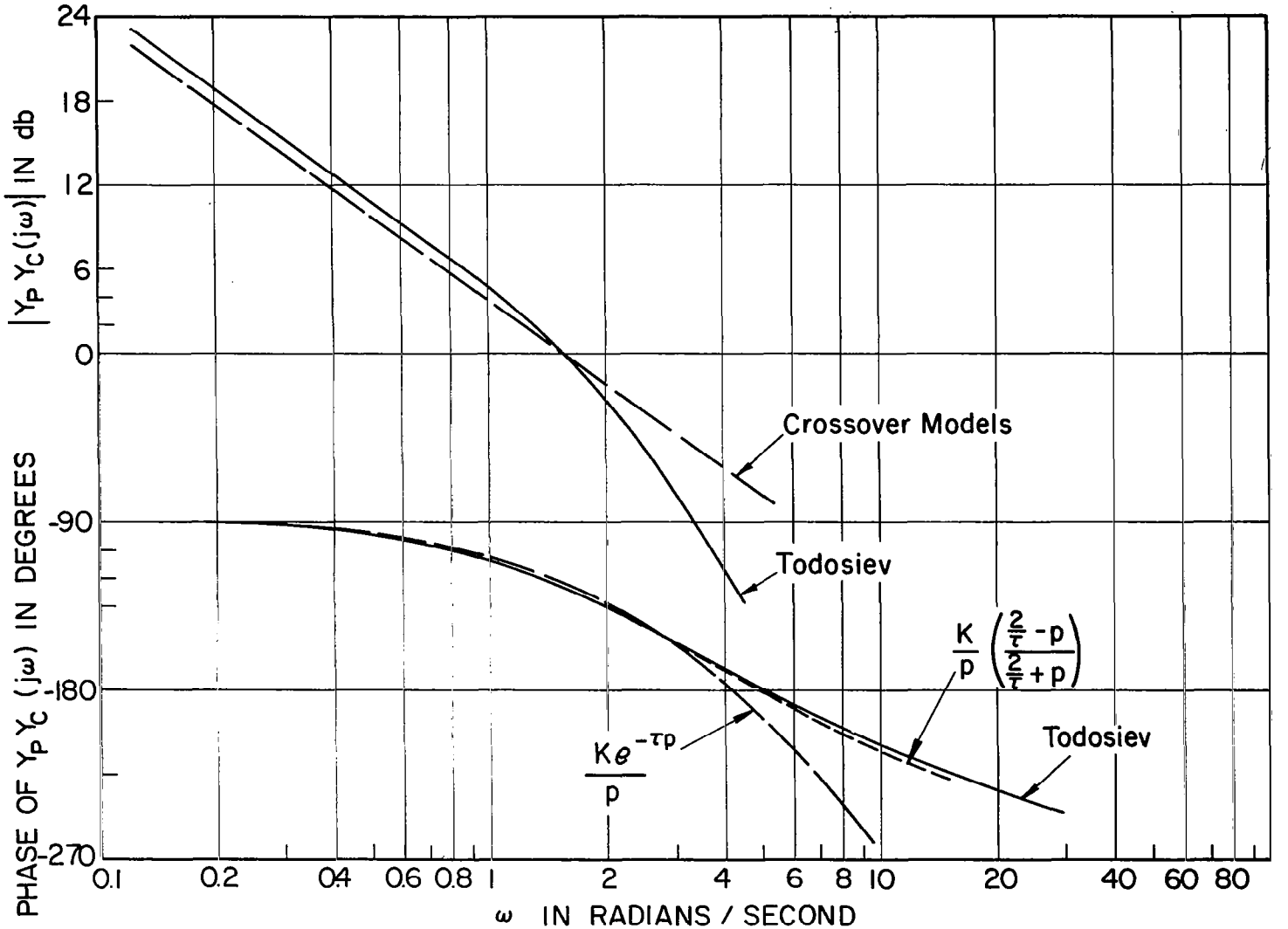

Figure 2.2.1 Comparison of Crossover Model Curves with Todosiev's Data, K = 1.7 and τ = 0.40.

$$\text{Subject Model} = \frac{c}{\epsilon}(p) = \frac{K_1 (T_1 p + 1)}{(T_2 p + 1)(T_3 p + 1)} \qquad (2.2\text{-}1)$$

with the controlled element

$$Y_C(p) = \frac{5.15}{p(3p + 1)} \quad . \qquad (2.2\text{-}2)$$

$\theta_i(t)$ was Gaussian white noise filtered by a low pass third order filter with a one radian per second cut-off frequency.

Figure 2.2.2 gives a comparison of the average compensatory forward loop gain-phase curves as determined by Adams and Bergeron[3], with the crossover model gain-phase curves, with K and τ again adjusted to give a best fit. The pertinent information in this case is

$$\text{Subject Model} = \frac{c}{\epsilon}(p) = \frac{K_1 T\left(1 + \frac{K_2}{T} p\right)}{(T + p)^2} \qquad (2.2\text{-}3)$$

and

$$Y_C(p) = \frac{2}{p} \quad . \qquad (2.2\text{-}4)$$

$\theta_i(t)$ was obtained by passing Gaussian white noise through a low pass second order filter with a one radian per second cut-off frequency.

In both Fig. 2.2.1 and Fig. 2.2.2 it is seen that the crossover model curves fit the experimental curves exceptionally well for

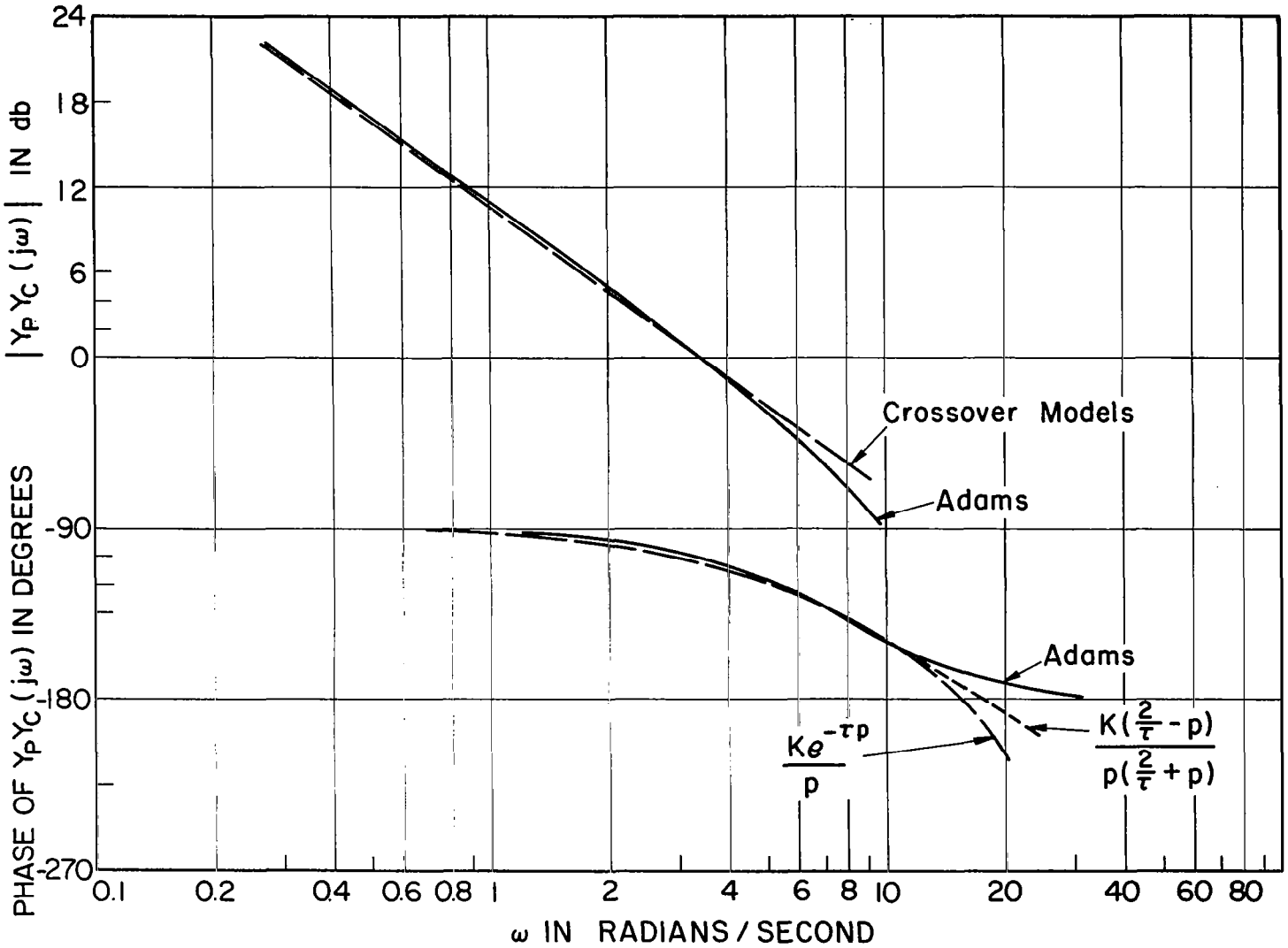

Figure 2.2.2 Comparison of Crossover Model Curves with Adam's and Bergeron's Data, K = 3.4 and τ = 0.11.

frequencies near and below crossover. At high frequencies the match is poorer. However, it should be remembered that the input power at frequencies above crossover is falling off at a rate of 12 or 18 db per octave, depending upon the filter being used. System identification in this region by any means is difficult due to the low power present. The important thing is that the crossover curves do match well in regions where there is appreciable input (and output) power.

2.3 Sensitivity of the Crossover Model Output to Changes in Crossover Model Parameters

From the comparison of the crossover model gain-phase curves with those obtained by other models, it can be concluded that the crossover model should be a reasonable model to use for certain systems. In light of the fact that McRuer's original data indicates that the crossover model fits experimental data best in the crossover region, it is of interest to see in what frequency range the model output is most sensitive to parameter changes. It would be desirable for the system to be most sensitive in the same region that the model most accurately describes subject response.

To investigate this area, sensitivity analysis will be used [30, 35]. This is a method which determines how the solution to a differential equation would vary if a small change was made in a parameter of the

differential equation at the start of the solution. For example, let $x(t, \lambda_o)$ be the solution to a differential equation for a specific equation forcing function. λ_o represents a specific value for an equation parameter λ.

To a first approximation, the solution related to the same forcing function with $\lambda = \lambda_1 = \lambda_o + \Delta\lambda$ is

$$x(t, \lambda_1) = x(t, \lambda_o) + \frac{\partial x}{\partial \lambda}(t, \lambda_o)\, \Delta\lambda \quad , \qquad (2.3\text{-}1)$$

where $\frac{\partial x}{\partial \lambda}(t, \lambda_o)$ is the sensitivity, or parameter influence, coefficient for λ evaluated at $\lambda = \lambda_o$. The equation for generating the sensitivity coefficient is derived under the assumption that all the parameters of the original equation are constant. Therefore, if any changes in the equation parameters are made during the course of a solution, the resulting transients must die out before the sensitivity coefficient is again accurate. This point will arise later in the report when sensitivity coefficients are used in the parameter tracking system.

As noted functionally above, the sensitivity coefficient is a time-varying quantity that depends upon both the differential equation and the equation forcing function. In the vicinity of a given solution it represents the gradient, in the λ direction, of the contour of the family of solutions obtained by using various values of λ with the same forcing function. In the case of the closed loop crossover model it

is of interest to see how the model output signal is effected by small changes in crossover model parameters in the vicinity of their nominal values.

The block diagram of the closed loop system containing the crossover model is shown in Fig. 2.3.1. The system output is denoted as $Z(t, K, \tau)$.

The transfer operator relating $Z(t, K, \tau)$ and $\theta_i(t)$ is

$$\frac{Z}{\theta_i}(p, K, \tau) = \frac{K e^{-\tau p}}{p + K e^{-\tau p}} \quad . \tag{2.3-2}$$

It follows then that

$$\frac{\partial Z}{\partial t}(t, K, \tau) + K Z(t - \tau, K, \tau) = K \theta_i(t - \tau) \tag{2.3-3}$$

or

$$\frac{\partial Z}{\partial t}(t, K, \tau) + K Z(t_o, K, \tau) = K \theta_i(t_o) \quad , \tag{2.3-4}$$

where $t_o \triangleq t - \tau$, so that $\theta_i(t_o)$ denotes $\theta_i(t)$ delayed τ seconds.

To find the sensitivity of $Z(t, K, \tau)$ to variations in K, Eq. (2.3-4) is differentiated with respect to K.

$$\frac{\partial^2 Z}{\partial K \, \partial t}(t, K, \tau) + K \frac{\partial Z}{\partial K}(t_o, K, \tau) = \theta_i(t_o) - Z(t_o, K, \tau) \tag{2.3-5}$$

or, by changing the order of differentiation,

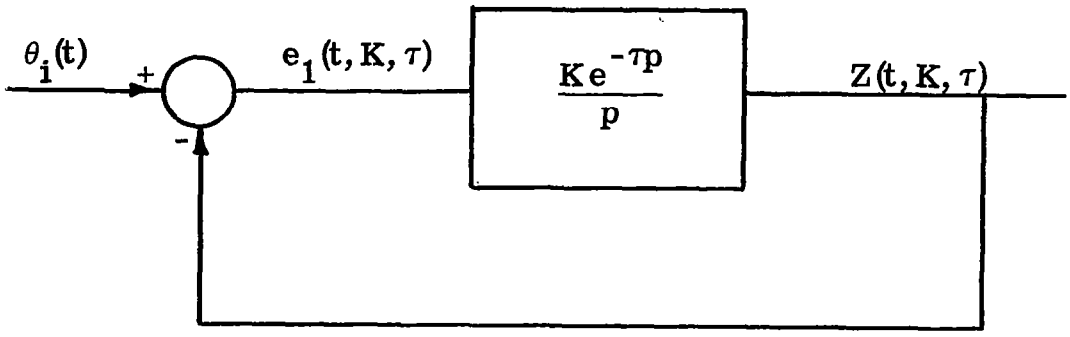

Figure 2.3.1 Closed Loop Crossover Model.

$$\frac{\partial}{\partial t}\left[\frac{\partial Z}{\partial K}(t, K, \tau)\right] + K\frac{\partial Z}{\partial K}(t_o, K, \tau) = e_1(t_o, K, \tau) \quad . \qquad (2.3\text{-}6)$$

By defining the sensitivity coefficient for K as

$$u_o(t, K, \tau) \triangleq \frac{\partial Z}{\partial K}(t, K, \tau) \qquad (2.3\text{-}7)$$

Eq. (2.3-6) becomes

$$\dot{u}_o(t, K, \tau) + K u_o(t_o, K, \tau) = e_1(t_o, K, \tau) \quad , \qquad (2.3\text{-}8)$$

where the dot signifies differentiation with respect to time t.

Equation (2.3-8) shows that $u_o(t, K, \tau)$, the sensitivity coefficient for K, is directly dependent upon the error signal in the crossover model control loop. The error signal is dependent not only on the parameters K and τ, but also on the characteristics of the input signal $\theta_i(t)$.

Before proceeding with the analysis of $u_o(t, K, \tau)$, the sensitivity equation for τ will be developed. To do this, Eq. (2.3-4) is differentiated with respect to τ, under the assumption that the derivative $\partial Z(t, K, \tau)/\partial \tau$ does exist. Cases can arise where the derivative will not exist, but these cases should not be encountered when using the type of input functions discussed in this report. The differentiation of Eq. (2.3-4) with respect to τ gives

$$\frac{\partial^2 Z(t, K, \tau)}{\partial \tau\, \partial t} + K\frac{\partial Z}{\partial \tau}(t_o, K, \tau) + K\frac{\partial Z(t_o, K, \tau)}{\partial t_o} \cdot \frac{\partial t_o}{\partial \tau} = K\frac{\partial \theta_i(t_o)}{\partial t_o} \cdot \frac{\partial t_o}{\partial \tau} \quad . \qquad (2.3\text{-}9)$$

Since

$$\frac{\partial t_o}{\partial \tau} = \frac{\partial}{\partial \tau}(t - \tau) = -1 \quad ,$$

and by noting that for any function $f(t_o, K, \tau)$

$$\frac{\partial}{\partial t}\left[f(t_o, K, \tau)\right] = \frac{\partial f(t_o, K, \tau)}{\partial t_o} \cdot \frac{\partial t_o}{\partial t} = \frac{\partial f(t_o, K, \tau)}{\partial t_o} \quad , \qquad (2.3\text{-}10)$$

it follows that Eq. (2.3-9) can be put in the form

$$\frac{\partial}{\partial t}\left[\frac{\partial Z}{\partial \tau}(t, K, \tau)\right] + K\left[\frac{\partial Z}{\partial \tau}(t_o, K, \tau)\right]$$

$$= -K\left[\frac{\partial \theta_i(t_o)}{\partial t_o} - \frac{\partial Z}{\partial t_o}(t_o, K, \tau)\right]$$

$$= -K\frac{\partial}{\partial t}\left[\theta_i(t_o) - Z(t_o, K, \tau)\right]$$

$$= -K\frac{\partial}{\partial t}\left[e_1(t_o, K, \tau)\right] \quad . \qquad (2.3\text{-}11)$$

If the sensitivity coefficient for τ is defined as

$$u_1(t, K, \tau) \triangleq \frac{\partial Z}{\partial \tau}(t, K, \tau) \quad , \qquad (2.3\text{-}12)$$

Eq. (2.3-11) becomes

$$\dot{u}_1(t, K, \tau) + K u_1(t_o, K, \tau) = -K\dot{e}_1(t_o, K, \tau) \quad , \qquad (2.3\text{-}13)$$

the dots again referring to differentiation with respect to time t.

Comparing Eq. (2.3-13) with Eq. (2.3-8) it is seen that

$$u_1(t, K, \tau) \cong -K\dot{u}_o(t, K, \tau) \quad , \qquad (2.3\text{-}14)$$

the approximation required since initial conditions are not being specified.

The block diagram showing the interrelationship between the crossover model, $u_o(t, K, \tau)$ and $u_1(t, K, \tau)$ is given in Fig. 2.3.2.

To investigate the frequency characteristics of $u_o(t, K, \tau)$ and $u_1(t, K, \tau)$, the transfer operators relating them to $\theta_i(t)$ are developed directly from Fig. 2.3.2.

$$\frac{e_1}{\theta_i}(p, K, \tau) = \frac{1}{1 + \frac{K e^{-\tau p}}{p}} \tag{2.3-15}$$

$$\frac{u_o}{e_1}(p, K, \tau) = e^{-\tau p}\left[\frac{\frac{1}{p}}{1 + \frac{K e^{-\tau p}}{p}}\right] \tag{2.3-16}$$

and

$$\frac{u_o}{\theta_i}(p, K, \tau) = \frac{p e^{-\tau p}}{\left[p + K e^{-\tau p}\right]^2} \quad . \tag{2.3-17}$$

From Eq. (2.3-14) it follows that

$$\frac{u_1}{\theta_i}(p, K, \tau) = \frac{-K p^2 e^{-\tau p}}{\left[p + K e^{-\tau p}\right]^2} \quad . \tag{2.3-18}$$

The absolute magnitudes of Eqs. (2.3-17) and (2.3-18) as functions of the real frequency ω are easily shown to be

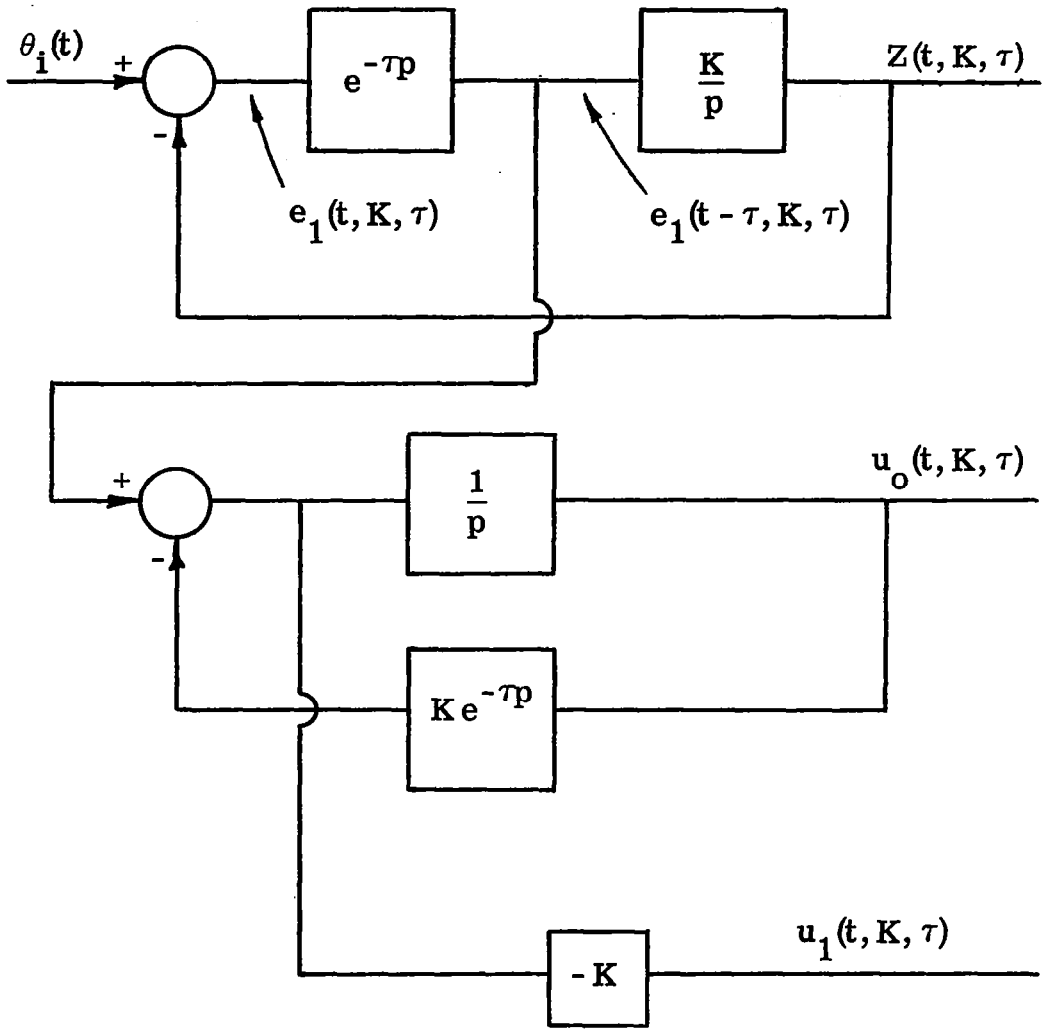

Figure 2.3.2 Relationship Between the Crossover Model and the Parameter Sensitivity Equations.

$$\left|\frac{u_o}{\theta_i}(j\omega, K, \tau)\right| = \frac{\omega}{K^2 \cos^2 \omega\tau + (\omega - K \sin \omega\tau)^2} \qquad (2.3\text{-}19)$$

and

$$\left|\frac{u_1}{\theta_i}(j\omega, K, \tau)\right| = \frac{K\omega^2}{K^2 \cos^2 \omega\tau + (\omega - K \sin \omega\tau)^2} \quad . \qquad (2.3\text{-}20)$$

In order to check the general characteristics of $u_o(j\omega, K, \tau)$ and $u_1(j\omega, K, \tau)$, the frequency can be normalized by letting

$$v = \omega\tau \quad . \qquad (2.3\text{-}21)$$

Using this substitution, Eqs. (2.3-19) and (2.3-20) can be reduced to the dimensionless equations below:

$$\frac{1}{\tau}\left|\frac{u_o}{\theta_i}(jv, K, \tau)\right| = \frac{v}{(K\tau)^2 \cos^2 v + (v - K\tau \sin v)^2} \qquad (2.3\text{-}22)$$

$$\frac{1}{K}\left|\frac{u_1}{\theta_i}(jv, K, \tau)\right| = \frac{v^2}{(K\tau)^2 \cos^2 v + (v - K\tau \sin v)^2} \quad . \qquad (2.3\text{-}23)$$

The denominators of these equations are identical and depend only upon the normalized frequency v and the dimensionless product $K\tau$. A review of other researchers data indicates that the variable $K\tau$ is fairly constant, usually falling in the range of 0.9 to 1.25. This is related to the fact that subjects generally adjust the compensatory system so that

the phase margin is fairly constant. For the crossover model, the phase margin in radians is $\pi - \frac{\pi}{2} - \omega\tau = \frac{\pi}{2} - \omega\tau$. However, at crossover, $|\omega| = |K|$ so that the phase margin is $\frac{\pi}{2} - K\tau$ radians. With $K\tau$ in the range given above the phase margin is 21 to 39 degrees. This is fairly constant considering that it is true for nearly all subjects in various low order compensatory control systems. It should also be noted that since the crossover frequency in the original system was at $|\omega| = |K|$, in the normalized system the crossover will be at $v = K\tau$, which as noted above is approximately one.

Figure 2.3.3 contains the plots of

$$\frac{1}{\tau}\left|\frac{u_o}{\theta_i}(jv, K, \tau)\right|$$

and

$$\frac{1}{K}\left|\frac{u_1}{\theta_i}(jv, K, \tau)\right|$$

evaluated at $K\tau = v_{crossover} = 1.25$. This is at the upper limit in terms of the normalized crossover frequency and, as such, represents a worst case in that the crossover model must represent the compensatory system over the widest probable frequency range. The curves in Fig. 2.3.3 also are the curves that would exist for $\frac{1}{\tau}\left|u_o(jv, K, \tau)\right|$ and $\frac{1}{K}|u_1(jv, K, \tau)|$ if $\theta_i(t)$ were white noise with a zero db power level and $K\tau = 1.25$.

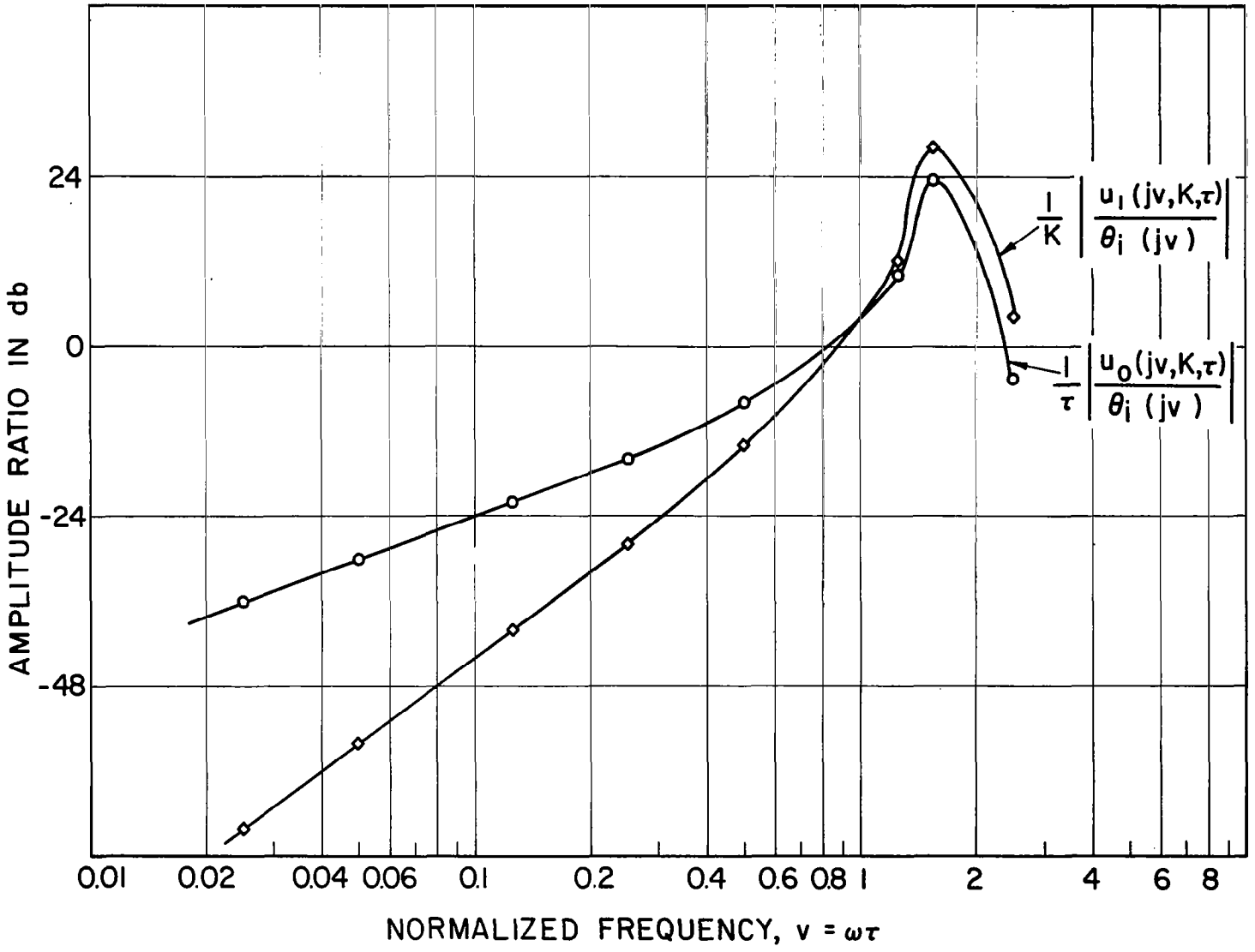

Figure 2.3.3 Magnitude Plots of the Sensitivity Coefficients, $K\tau = 1.25$.

It is seen that the sensitivity coefficients are maximum just above the crossover frequency. This fact is not surprising when one remembers that the closed loop crossover model responds somewhat like an underdamped second order system with a resonant peak near crossover frequency. Since the product $K\tau$ determines the phase margin of the system, and thus the characteristics of the system in the crossover region, one would expect the maximum sensitivity to be in this general section of the frequency spectrum. The important fact is that the crossover frequency is located in the region of high sensitivity.

Figure 2.3.4 shows the absolute magnitudes of the sensitivity coefficients under the same general conditions as above, with the exception that $\theta_i(t)$ is now bandwidth limited white noise. A third order filter of the form

$$\frac{1}{(T\,p + 1)^3} \qquad (2.3\text{-}24)$$

is chosen with $T = 1/2$ second. Assuming a nominal value of $\tau = 0.25$ seconds, the filter cut-off frequency is at

$$v = \left(\frac{2 \text{ radians}}{\text{second}}\right)(0.25 \text{ seconds}) = 0.5 \quad ,$$

which is four-tenths of the crossover frequency in the system discussed above. This relationship is commonly found in subject testing. In this case, the sensitivity coefficients have had the height of

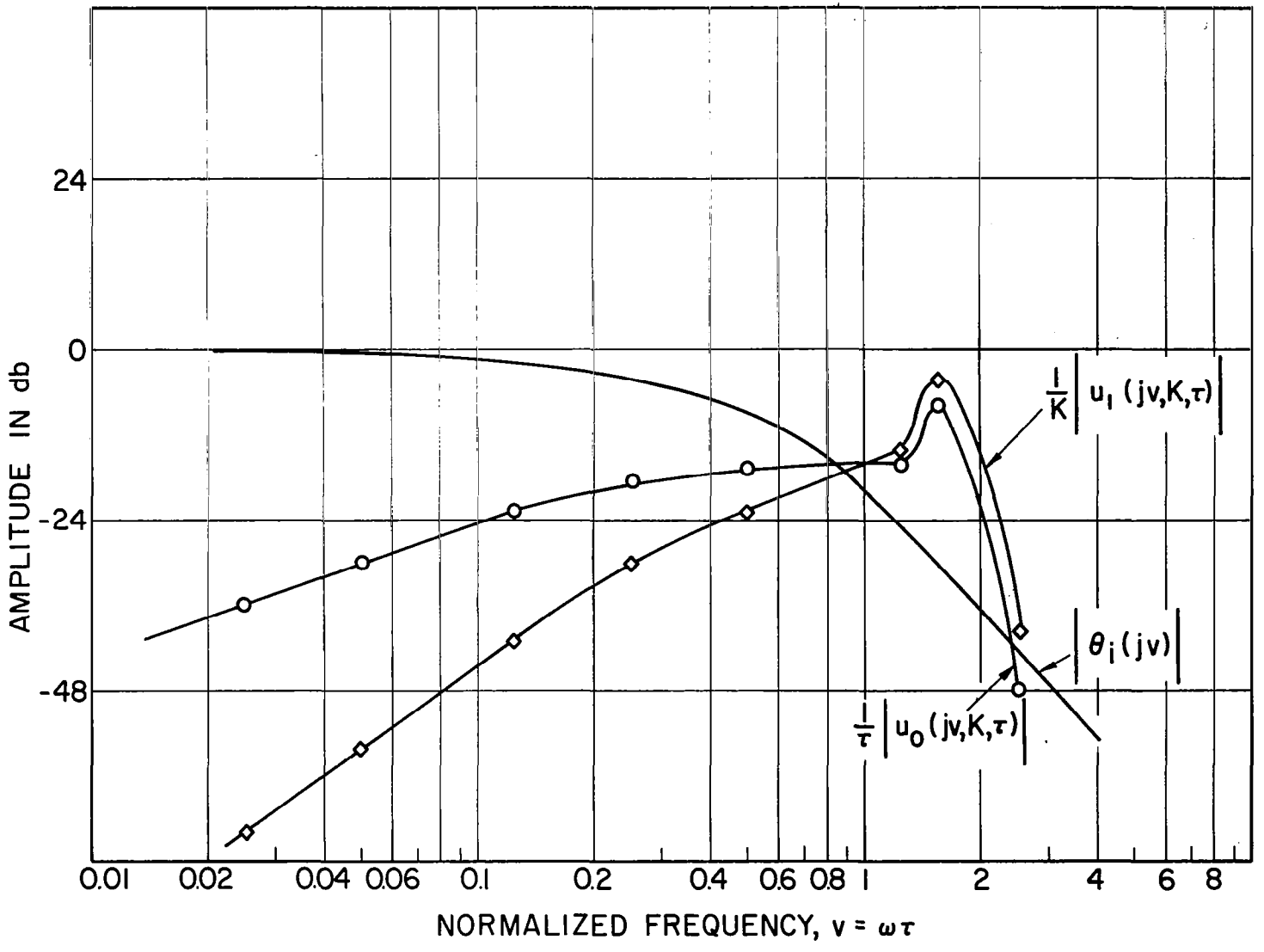

Figure 2.3.4 Magnitude Plots of the Sensitivity Coefficients with $\theta_i(t)$ Filtered, $K\tau = 1.25$.

their peaks reduced, although the location of maximum sensitivity is unchanged.

It can be visualized that a cut-off frequency chosen far below crossover would completely eliminate the peaks near crossover. This relationship between cut-off frequency and crossover frequency is quite important when parameter tracking is being used. If the crossover parameters are to be tracked with maximum accuracy, the sensitivity equations must be maximum in the region of crossover, and $\theta_i(j\omega)$ must have sufficient power at crossover. This indicates that care must be taken when choosing input spectral characteristics. This point will be discussed further in Chapter 6.

Another point of interest in Fig. 2.3.4 is that $u_1(jv, K, \tau)$ is less sensitive to low frequencies than is $u_o(jv, K, \tau)$. This point will arise in Chapter 4 when the convergence properties of the parameter tracking system are evaluated.

Later in the report the pure time-delays present in the crossover model and in the sensitivity equations will be replaced by the first order Padé approximation given in Eq. (2.3-25) [36].

$$e^{-\tau p} \cong \frac{\frac{2}{\tau} - p}{\frac{2}{\tau} + p} \quad . \tag{2.3-25}$$

When this approximation is evaluated with $p = j\omega$, the magnitude is

found to be unity at all frequencies, just like the pure time-delay. The phase characteristics of the approximation are equivalent to those of the pure time-delay at low frequencies, but differ markedly at higher frequencies. Fortunately, the phase characteristics of the approximation are quite close to those of the pure time-delay at frequencies near and below normal crossover frequencies. This is the same range of frequencies in which nearly all of the input and output power is located.

Figure 2.3.5 gives a comparison of the phase characteristics of the two sides of Eq. (2.3.25).

To check the effect of the Pade approximation on the sensitivity equations, Eq. (2.3-25) is used in Eqs. (2.3-17) and (2.3-18). The approximate sensitivity equation which result are as follows:

$$\frac{u_o}{\theta_i}(p, K, \tau) \cong \frac{p\left(\frac{\frac{2}{\tau} - p}{\frac{2}{\tau} + p}\right)}{\left[p + K\left(\frac{\frac{2}{\tau} - p}{\frac{2}{\tau} + p}\right)\right]^2}$$

$$= \frac{p\left(\frac{4}{\tau^2} - p^2\right)}{\left[p^2 + \left(\frac{2}{\tau} - K\right)p + \frac{2K}{\tau}\right]^2} \qquad (2.3\text{-}26)$$

and

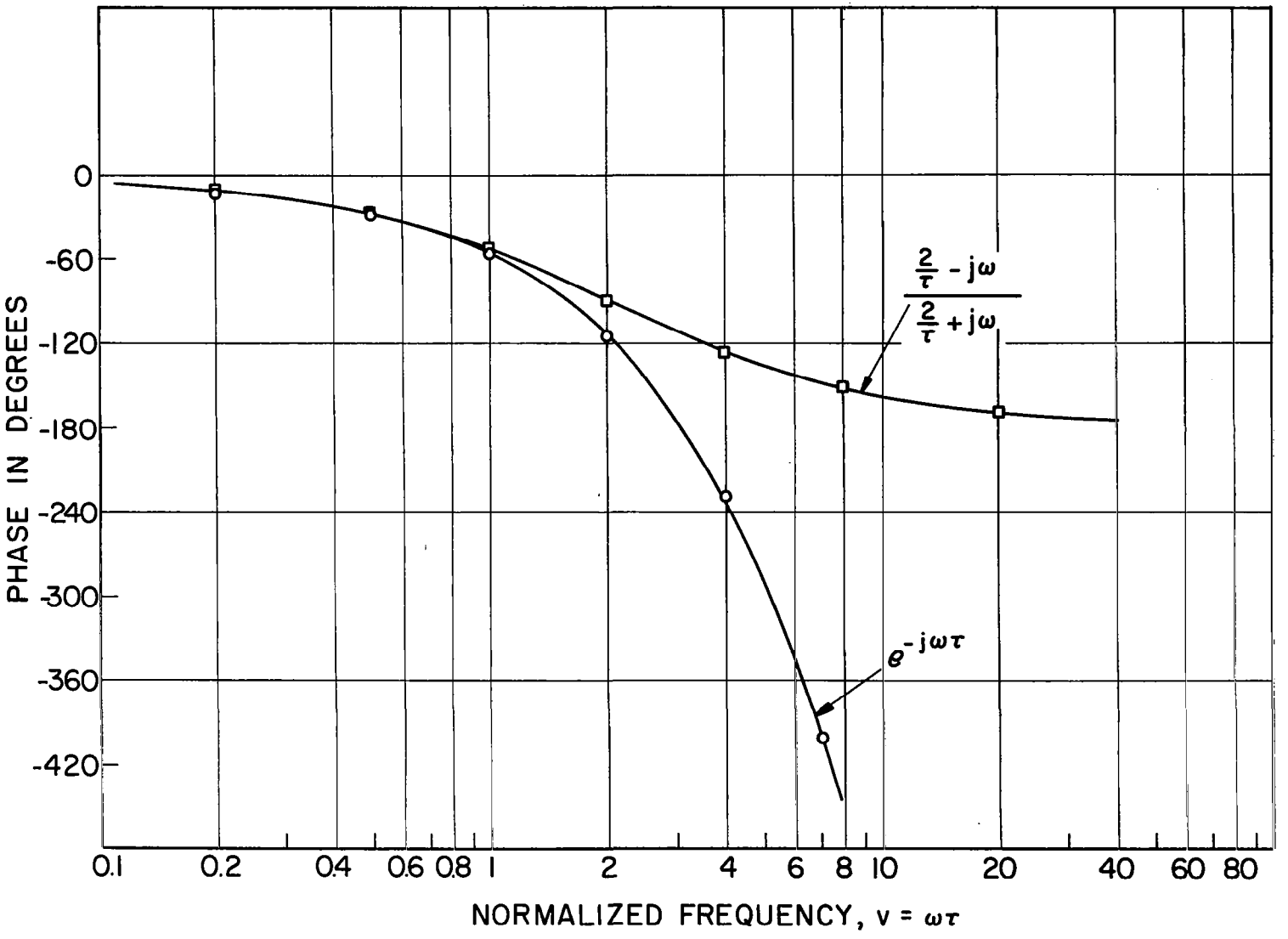

Figure 2.3.5 Phase Characteristics of Pure Time-Delay and the First Order Padé Approximation.

$$\frac{u_1}{\theta_i}(p, K, \tau) = \frac{-Kp^2\left(\frac{4}{\tau^2} - p^2\right)}{\left[p^2 + \left(\frac{2}{\tau} - K\right)p + \frac{2K}{\tau}\right]^2} \qquad (2.3\text{-}27)$$

The absolute magnitudes of these equations as a function of the real frequency ω are

$$\left|\frac{u_o}{\theta_i}(j\omega, K, \tau)\right| = \frac{\omega\left(\omega^2 + \frac{4}{\tau^2}\right)}{\left[\left(\frac{2K}{\tau} - \omega^2\right)^2 + \left(\frac{2}{\tau} - K\right)^2\omega^2\right]} \qquad (2.3\text{-}28)$$

and

$$\left|\frac{u_1}{\theta_i}(j\omega, K, \tau)\right| = \frac{K\omega^2\left(\omega^2 + \frac{4}{\tau^2}\right)}{\left[\left(\frac{2K}{\tau} - \omega^2\right)^2 + \left(\frac{2}{\tau} - K\right)^2\omega^2\right]} \qquad (2.3\text{-}29)$$

If the last two equations are normalized as before, by letting $v = \omega\tau$, the equations become

$$\frac{1}{\tau}\left|\frac{u_o}{\theta_i}(jv, K, \tau)\right| = \frac{v(v^2 + 4)}{(2K\tau - v^2)^2 + (2 - K\tau)^2 v^2} \qquad (2.3\text{-}30)$$

and

$$\frac{1}{K}\left|\frac{u_1}{\theta_i}(jv, K, \tau)\right| = \frac{v^2(v^2 + 4)}{(2K\tau - v^2)^2 + (2 - K\tau)^2 v^2} \qquad (2.3\text{-}31)$$

Evaluating Eqs. (2.3-30) and (2.3-31) at the nominal value of $K\tau = 1.25$ as before gives the curves of Figs. 2.3.6 and 2.3.7 for the

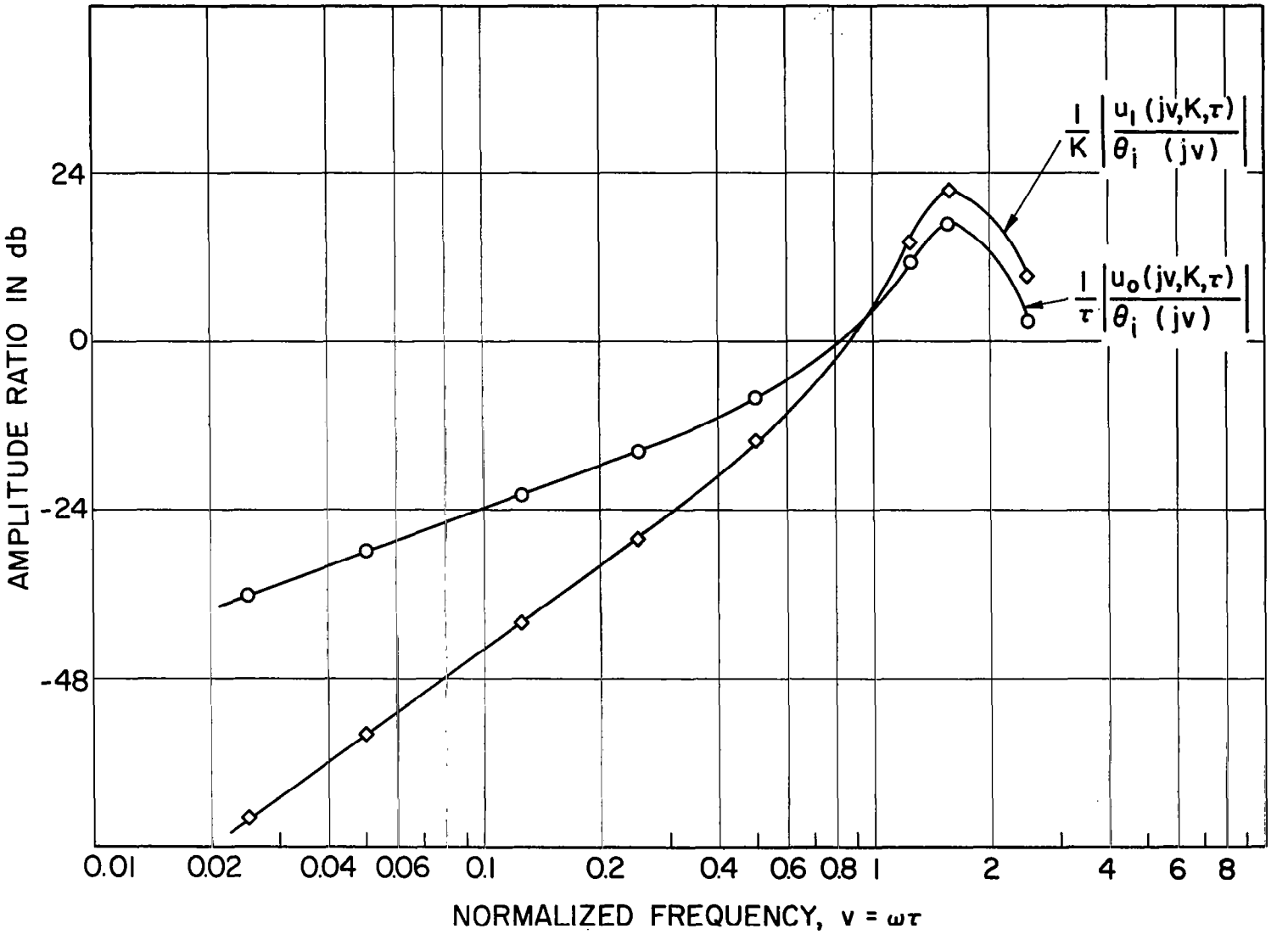

Figure 2.3.6 Magnitude Plots of the Approximate Sensitivity Coefficients, $K\tau = 1.25$.

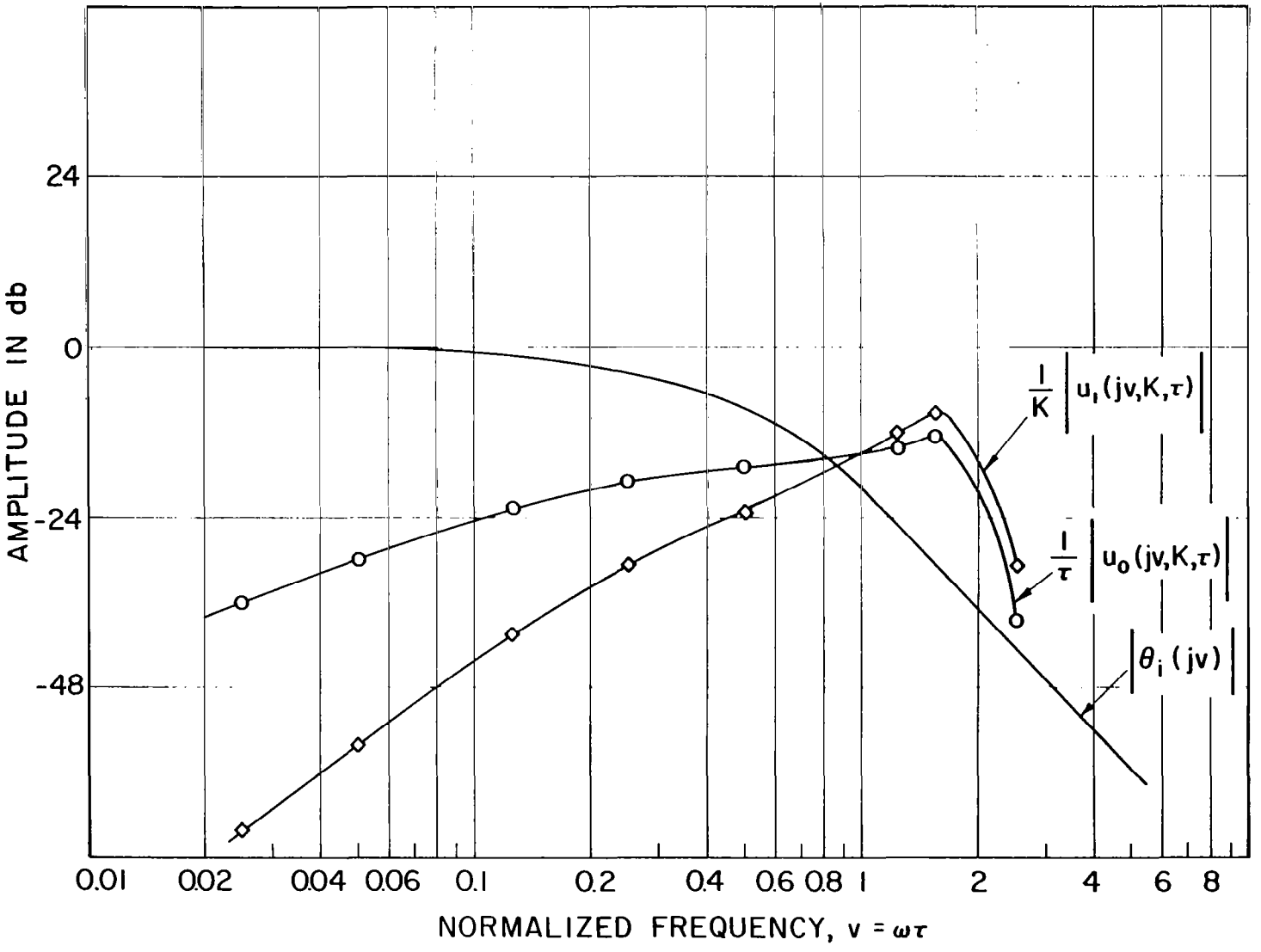

Figure 2.3.7 Magnitude Plots of the Approximate Sensitivity Coefficients with $\theta_i(t)$ Filtered, $K\tau = 1.25$.

unfiltered and filtered input cases, respectively. Comparing these figures with Figs. 2.3.3 and 2.3.4 it is seen that the approximation is quite good for frequencies at and below the crossover frequency of $v = 1.25$. In the bandwidth limited cases the magnitude of the error due to the approximation is 2 db at crossover with smaller errors below this frequency. The approximation is thus fairly good up to the point where the input is down 30 db. The crossover frequency in the Padé approximation case is still located in the region of maximum sensitivity.

Due to the additional amount of computing equipment needed to go from a first order Padé approximation to a more accurate second order approximation, plus the fact that input power above crossover is extremely low, it was decided to use a first order approximation in the crossover model.

2.4 General Conclusions on the Crossover Model

In light of the facts discussed in the first three sections of this chapter, it was concluded that the crossover model, or an approximate version of it, would be an excellent candidate for a parameter tracking model. The approximate model is simple, easy to implement, and appears to match other researchers data when the controlled element is of first or second order. The model output will also be most sensitive to parameter changes in the same region it most accurately describes human response, if the input is chosen properly.

For these reasons, the decision was made to evaluate a parameter tracking version of the crossover model in some detail.

Chapter 3

PARAMETER TRACKING CIRCUIT DEVELOPMENT

3.1 Basic Theory

In the development of the parameter tracking system it is assumed that the basic equation of the system being tested is known [7, 23, 35]. The coefficients of the differential equation are to be determined by the tracking system.

Let it be assumed that the system being identified—hereafter called the real system—is adequately described by the linear constant coefficient differential equation

$$\sum_{n=0}^{N} a_n \frac{d^n \theta_o(t)}{dt^n} = \sum_{m=0}^{M} b_m \frac{d^m \theta_i(t)}{dt^m} \quad , \qquad (3.1\text{-}1)$$

where $\theta_i(t)$ is the input and $\theta_o(t)$ the output of the real system.

Under the assumption that the form of Eq. (3.1-1) is known, the parameter tracking model—hereafter called the assumed model—can be defined by the equation

$$\sum_{n=0}^{N} \alpha_n \frac{\partial^n Z(t, \vec{\alpha}, \vec{\beta})}{\partial t} = \sum_{m=0}^{M} \beta_m \frac{\partial^m \theta_i(t)}{\partial t^m} \quad , \qquad (3.1\text{-}2)$$

where

$$\vec{\alpha} = \begin{bmatrix} \alpha_0 \\ \cdot \\ \cdot \\ \cdot \\ \cdot \\ \cdot \\ \alpha_N \end{bmatrix} \quad \text{and} \quad \vec{\beta} = \begin{bmatrix} \beta_0 \\ \cdot \\ \cdot \\ \cdot \\ \cdot \\ \cdot \\ \beta_M \end{bmatrix} .$$

Partial time derivatives are used in Eq. (3.1-2) since $\vec{\alpha}$ and $\vec{\beta}$ are free to be changed and will affect the assumed model output, $Z(t, \vec{\alpha}, \vec{\beta})$. The assumed model has the same form, and the same input, as the real system. The assumed model output $Z(t, \vec{\alpha}, \vec{\beta})$ may differ from the real system output $\theta_o(t)$, because $\vec{\alpha} \neq \vec{a}$ and/or $\vec{\beta} \neq \vec{b}$.

In order to force $\vec{\alpha} \rightarrow \vec{a}$ and $\vec{\beta} \rightarrow \vec{b}$, and thus $Z(t, \vec{\alpha}, \vec{\beta}) \rightarrow \theta_o(t)$, the coefficients of the assumed model are adjusted in some manner so as to force some function of the model error toward zero. The model error is defined as

$$Z(t, \vec{\alpha}, \vec{\beta}) - \theta_o(t) = e(t, \vec{\alpha}, \vec{\beta}) \qquad (3.1\text{-}3)$$

in the "output error" method used in this report [7][1].

---

[1] An alternate method called the "equation error" method uses an error defined as [19]

$$\sum_{n=0}^{N} \alpha_n \frac{\partial^n Z(t, \vec{\alpha}, \vec{\beta})}{\partial t^n} - \sum_{m=0}^{M} \beta_m \frac{\partial^m \theta_i(t)}{\partial t^m} = e(t, \vec{\alpha}, \vec{\beta}) .$$

One common method of parameter adjustment is obtained by defining the index of performance of the model as

$$I(t_1, \vec{\alpha}, \vec{\beta}) = \frac{1}{T} \int_{t_1 - T}^{t_1} \frac{e^2(t, \vec{\alpha}, \vec{\beta})\, dt}{2} \tag{3.1-4}$$

and determining

$$\frac{\partial I}{\partial \alpha_i}(t_1, \vec{\alpha}, \vec{\beta}) \quad , \quad i = 1, 2, \ldots, N$$

$$\frac{\partial I}{\partial \beta_j}(t_1, \vec{\alpha}, \vec{\beta}) \quad , \quad j = 1, 2, \ldots, M \ . \tag{3.1-5}$$

Once Eqs. (3.1-5) are known, the parameters $\vec{\alpha}$ and $\vec{\beta}$ can be step changed by an amount $\Delta\vec{\alpha}$ and $\Delta\vec{\beta}$ at time t_1 through the use of the gradient adjustment equations

$$\Delta\alpha_i(t_1, \vec{\alpha}, \vec{\beta}) = - k_i \frac{\partial I}{\partial \alpha_i}(t_1, \vec{\alpha}, \vec{\beta}) \quad , \quad i = 1, \ldots, N$$

$$\Delta\beta_j(t_1, \vec{\alpha}, \vec{\beta}) = - k_j \frac{\partial I}{\partial \beta_j}(t_1, \vec{\alpha}, \vec{\beta}) \quad , \quad j = 1, \ldots, M \ . \tag{3.1-6}$$

These step changes are made repeatedly each T seconds, and gradually drive the performance index, and the model error, toward zero. The size of each step, and hence the convergence of the process, is dependent upon the gradient gains k as well as the size of the components of the gradient.

Since the coefficients of the assumed model are constant during each performance measuring interval, the gradient equations can be evaluated in a straight forward manner.[2]

First it is noticed that

$$I(t_1, \vec{\alpha}, \vec{\beta}) = \frac{1}{T} \int_{t_1 - T}^{t_1} \frac{e^2(t, \vec{\alpha}, \vec{\beta})\, dt}{2} \qquad (3.1\text{-}7)$$

and

$$\frac{\partial I}{\partial \alpha_i}(t_1, \vec{\alpha}, \vec{\beta}) = \frac{1}{T} \int_{t_1 - T}^{t_1} e \frac{\partial e}{\partial \alpha_i}(t, \vec{\alpha}, \vec{\beta})\, dt \quad . \qquad (3.1\text{-}8)$$

However,

$$e(t, \vec{\alpha}, \vec{\beta}) = Z(t, \vec{\alpha}, \vec{\beta}) - \theta_o(t) \qquad (3.1\text{-}9)$$

and

$$\frac{\partial e(t, \vec{\alpha}, \vec{\beta})}{\partial \alpha_i} = \frac{\partial Z(t, \vec{\alpha}, \vec{\beta})}{\partial \alpha_i} \triangleq u_i(t, \vec{\alpha}, \vec{\beta}) \quad . \qquad (3.1\text{-}10)$$

It follows then that Eq. (3.1-8) reduces to

---

[2] See Appendix F for some observations on the iterative adjustment technique.

$$\frac{\partial I}{\partial \alpha_i}(t_1, \vec{\alpha}, \vec{\beta}) = \frac{1}{T} \int_{t_1 - T}^{t_1} e\, u_i(t, \vec{\alpha}, \vec{\beta})\, dt \quad . \qquad (3.1\text{-}11)$$

The gradients with respect to the α_i can thus be determined from Eq. (3.1-11) if $u_i(t, \vec{\alpha}, \vec{\beta}) \triangleq \frac{\partial Z}{\partial \alpha_i}(t, \vec{\alpha}, \vec{\beta})$ can be obtained. Similar results hold for $\frac{\partial I}{\partial \beta_i}(t_1, \vec{\alpha}, \vec{\beta})$.

To find $u_i(t, \vec{\alpha}, \vec{\beta})$ the partial derivative of Eq. (3.1-2) is taken with respect to α_i. This gives,

$$\sum_{n=0}^{N} \frac{\partial}{\partial \alpha_i}\left[\alpha_n \frac{\partial^n Z(t, \vec{\alpha}, \vec{\beta})}{\partial t^n}\right] = \sum_{m=0}^{M} \beta_m \frac{\partial^{(m+1)} \theta_i(t)}{\partial \alpha_i\, \partial t^m} \quad . \qquad (3.1\text{-}12)$$

Since $\theta_i(t)$ is not a function of $\vec{\alpha}$, the right side of Eq. (3.1-12) is zero. By interchanging the order of differentiation with respect to t and α_i, the left hand side of Eq. (3.1-12) becomes

$$\sum_{n=0}^{N} \alpha_n \frac{\partial^n}{\partial t^n}\left[\frac{\partial Z(t, \vec{\alpha}, \vec{\beta})}{\partial \alpha_i}\right] + \frac{\partial^i Z(t, \vec{\alpha}, \vec{\beta})}{\partial t^i} = 0 \quad . \qquad (3.1\text{-}13)$$

Using the identity in Eq. (3.1-10), Eq. (3.1-13) reduces to

$$\sum_{n=0}^{N} \alpha_n \frac{\partial^n u_i(t, \vec{\alpha}, \vec{\beta})}{\partial t^n} = - \frac{\partial^i Z(t, \vec{\alpha}, \vec{\beta})}{\partial t^i} \quad . \qquad (3.1\text{-}14)$$

Equation (3.1-14) is the sensitivity equation for α_i. $u_i(t, \vec{\alpha}, \vec{\beta})$ can be solved for continuously on an analog computer by solving the above equation. The characteristic equation of this system is exactly the same as for the real system. The forcing function, however, is a signal taken from the assumed model.

To determine the other gradient equations, a similar procedure is followed. To solve for all N + M gradient equations, N + M sensitivity equations of the form above must also be solved.

3.2 Continuous Parameter Tracking

In the continuous parameter tracking method the time interval over which the index of performance is measured is collapsed to zero. The index of performance then becomes an instantaneous index

$$I(t, \vec{\alpha}(t), \vec{\beta}(t)) = \frac{e^2}{2}(t, \vec{\alpha}(t), \vec{\beta}(t)) \quad . \qquad (3.2\text{-}1)$$

The functional notation $\vec{\alpha}(t)$ and $\vec{\beta}(t)$ denoting the fact that the coefficients of the assumed model may be varied continuously.

Although the coefficients of the assumed model are mechanized so that they can be adjusted continuously, the gradient and sensitivity equations are still derived under the tacit assumption that the coefficients of the assumed model are constant. The equations are consequently erroneous when coefficients are changing, but converge to the correct equations as $\vec{\alpha}(t) \longrightarrow \vec{a}$ and $\vec{\beta}(t) \longrightarrow \vec{b}$.

This method was used for the parameter tracking portion of the experimental work of this report. However, rather than developing a general approach of this method at this point, the mechanics of implementation will be introduced for the specific problem solved in Section 3.4.

The original thinking behind the continuous performance index was that sudden changes in the human describing function could be picked up quickly by the tracking system. In practice this has not been the case. The presence of uncorrelated signals in the system dictates low gradient gains and fairly slow convergence rates on the coefficients. Sudden changes are thus not tracked too effectively as will be shown in Appendix C.

3.3 Open vs. Closed Loop Tracking

The basic real system under test in this research is assumed to be the closed loop system given in Fig. 1.5.1 with

$$Y_P Y_C(p) = \frac{K^* e^{-\tau^* p}}{p} \quad . \tag{3.3-1}$$

This real system assumes that the best linear operator for the forward loop of the compensatory system is the crossover model.

If a parameter tracking model of this system is to be chosen, the choice must be made between:

(1) Picking an assumed model consisting of only the forward loop,

$$\frac{Z}{\epsilon}(p) = \frac{K e^{-\tau p}}{p} \qquad (3.3\text{-}2)$$

and driving the assumed model with $\epsilon(t)$, or

(2) Picking an assumed model consisting of the closed loop system

$$\frac{Z}{\theta_i}(p) = \frac{K e^{-\tau p}}{p + K e^{-\tau p}} \qquad (3.3\text{-}3)$$

and driving the assumed model with $\theta_i(t)$.

On the surface these two methods appear to be equivalent, but Elkind [11] and Jones [20] have both noted that the results of these two methods may not be the same. The reason for this difference is that in the forward loop case the assumed model input will contain human generated noise, while in the closed loop case the noise is not applied directly to the assumed model. Elkind and Jones show that the expected effect of the noise is zero in the closed loop case, while it will bias the coefficients obtained in the open loop case.

Since the original crossover model was developed from the ratio

$$Y_P\, Y_C(j\omega) = \frac{\Phi_{io}(j\omega)}{\Phi_{i\epsilon}(j\omega)} \quad , \qquad (3.3\text{-}4)$$

it should not have been influenced by noise and thus be compatible with the closed loop method. For this reason the closed loop method was used.

3.4 Development of the Crossover Model Parameter Tracking Equations

The closed loop equation of the real system using the McRuer crossover model for the forward loop is

$$\frac{d\,\theta_o(t)}{dt} + K^*\,\theta_o(t - \tau^*) = K^*\,\theta_i(t - \tau^*) \quad . \tag{3.4-1}$$

The assumed model is thus chosen to be

$$\frac{\partial Z(t, K, \tau)}{\partial t} + K\,Z(t - \tau,\ K, \tau) = K\,\theta_i(t - \tau) \quad . \tag{3.4-2}$$

If the index of performance is taken as

$$I(t, K, \tau) = \frac{e^2}{2}\,(t, K, \tau) \tag{3.4-3}$$

where

$$e(t, K, \tau) = Z(t, K, \tau) - \theta_o(t) \quad , \tag{3.4-4}$$

and if K and τ are assumed to be constant, then

$$\frac{\partial I}{\partial K} = e\,\frac{\partial e}{\partial K} = e\,\frac{\partial Z}{\partial K}\,(t, K, \tau) \tag{3.4-5}$$

and

$$\frac{\partial I}{\partial \tau} = e\,\frac{\partial e}{\partial \tau} = e\,\frac{\partial Z}{\partial \tau}\,(t, K, \tau) \quad . \tag{3.4-6}$$

By defining

$$u_o(t, K, \tau) \triangleq \frac{\partial Z}{\partial K}(t, K, \tau) \tag{3.4-7}$$

and

$$u_1(t, K, \tau) \triangleq \frac{\partial Z}{\partial \tau}(t, K, \tau) \tag{3.4-8}$$

it follows from Eqs. (3.4-5) and (3.4-6) that

$$\frac{\partial I}{\partial K}(t, K, \tau) = e\, u_o(t, K, \tau) \tag{3.4-9}$$

and

$$\frac{\partial I}{\partial \tau}(t, K, \tau) = e\, u_1(t, K, \tau) \quad . \tag{3.4-10}$$

The sensitivity equations needed for generating $u_o(t, K, \tau)$ and $u_1(t, K, \tau)$ are obtained by taking the partial derivatives of Eq. (3.4-2) with respect to K and τ, assuming again that K and τ are constants. These equations have already been developed in Chapter 2, as Eqs. (2.3-8) and (2.3-14). They are repeated here for convenience.

$$\frac{\partial u_o}{\partial t}(t, K, \tau) + K\, u_o(t - \tau, K, \tau) = e_1(t - \tau, K, \tau) \tag{3.4-11}$$

and

$$u_1(t, K, \tau) = - K \frac{\partial u_o(t, K, \tau)}{\partial t} \quad , \tag{3.4-12}$$

where

$$e_1(t, K, \tau) = Z(t, K, \tau) - \theta_i(t) \quad . \qquad (3.4\text{-}13)$$

3.5 The New Parameter Adjustment Equation

The conventional continuous parameter adjustment equation for the parameter K is [7, 23]

$$\dot{\Delta}K(t) = - k_K \frac{\partial I}{\partial K}(t, K, \tau) = - k_K \, e \, u_o(t, K, \tau) \quad . \qquad (3.5\text{-}1)$$

However, during the course of the experiment it was discovered that the uncorrelated portion of the model error $e(t, K, \tau)$ caused the calculated values of $K(t)$ and $\tau(t)$ to behave erratically at times. This was especially true in the cases where the subject task could be considered difficult.

In an effort to reduce large variations in $K(t)$ and $\tau(t)$ after and during convergence, a new parameter adjustment method was introduced. The new adjustment scheme limits and smooths the signal appearing on the right hand side of Eq. (3.5-1) before equating it to $\dot{\Delta}K(t)$. This is nothing more than a straightforward method of eliminating all rapid changes in the parameter.

The new adjustment equation is

$$\dot{\Delta K}(t) = \int_{-\infty}^{t} \text{sat}\left[-k_K \frac{\partial I}{\partial K}(\xi, K, \tau)\right] h(t-\xi)\, d\xi$$

$$= \int_{-\infty}^{t} \text{sat}\left[-k_K e u_o(\xi, K, \tau)\right] h(t-\xi)\, d\xi \qquad (3.5\text{-}2)$$

for K(t), with a similar one used for $\tau(t)$. h(t) is the impulse response of a smoothing filter and the sat$[\gamma]$ function is defined as

$$\text{sat}[\gamma] = \gamma \quad , \quad -L \leq \gamma \leq L$$

$$= L \operatorname{sgn} \gamma \quad , \quad |\gamma| > L \quad . \qquad (3.5\text{-}3)$$

In practice the value of L is chosen empirically, so that the limiting is not too severe. It will be shown in Section 4.8 that the limiter will not bias the results if certain conditions are met. In addition the sat function will be shown to have a general stabilizing influence on the tracking system. The smoothing filter used in all tests was of first order with a time constant of one second.

The net effect of the new parameter adjustment method is a non-linear smoothing of the values K(t) and $\tau(t)$ when large disturbances enter the system in the form of remnant signal.

3.6 Parameter Tracking Circuit

The equations necessary for the complete implementation of the continuous parameter tracking system are (3.4-2), (3.4-11), (3.4-12),

(3.5-2) and an equation equivalent to (3.5-2) for the adjustment of τ. The complete block diagram of the parameter tracking system is given in Fig. 3.6.1. The complete analog circuit diagram is given in Appendix A.

It should be noted in each diagram that the first order Padé approximation given in Eq. (2.3-25) has been used in place of pure time-delay. This has been done because of the ease of analog implementation. It will be shown in Chapter 4 that this substitution is equivalent to redefining the original crossover model as having first order Padé time-delay. The real system being identified is thus essentially redefined as having

$$Y_P Y_C (p) = \frac{K^* \left(\frac{2}{\tau^*} - p\right)}{p \left(\frac{2}{\tau^*} + p\right)} \qquad (3.6\text{-}1)$$

for the forward loop.

3.7 Modified Block Diagram of the Real System Being Identified

In addition to changing the pure time-delay to a first order Padé approximation, one other modification of the real system block diagram is useful. This pertains to the location of the injection of the remnant signal.

Since the effect of the remnant signal enters the parameter tracking system only through $\theta_o(t)$, there is no reason why the entire

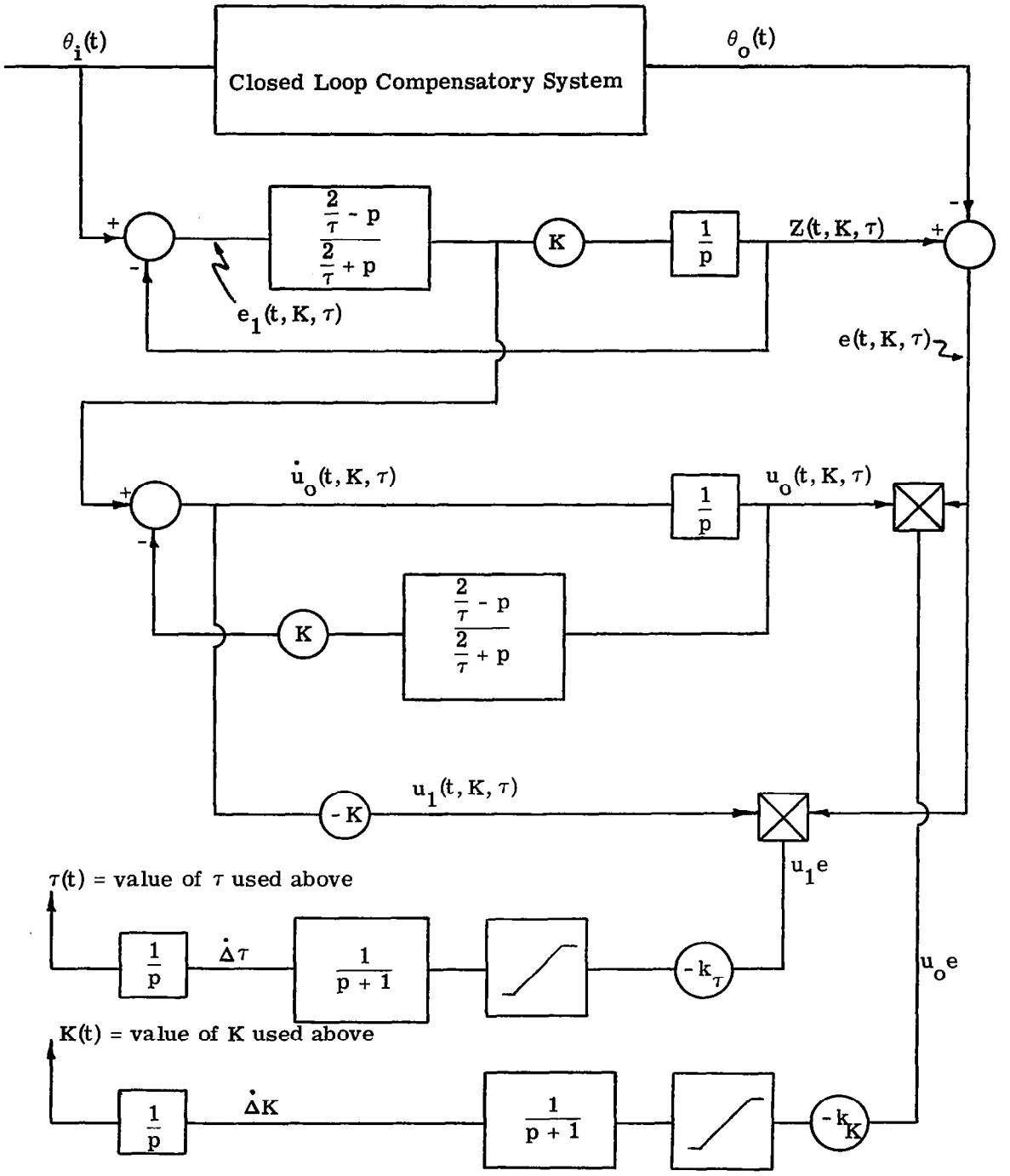

Figure 3.6.1 Block Diagram of the Parameter Tracking System.

remnant cannot be defined as being injected at the real system output. It will become evident in the following chapters that the mathematical notation is greatly simplified if this change is made. Fig. 3.7.1 gives the final block diagram of the real (compensatory) system being identified. The notation introduced in this figure will be used throughout the rest of the report.

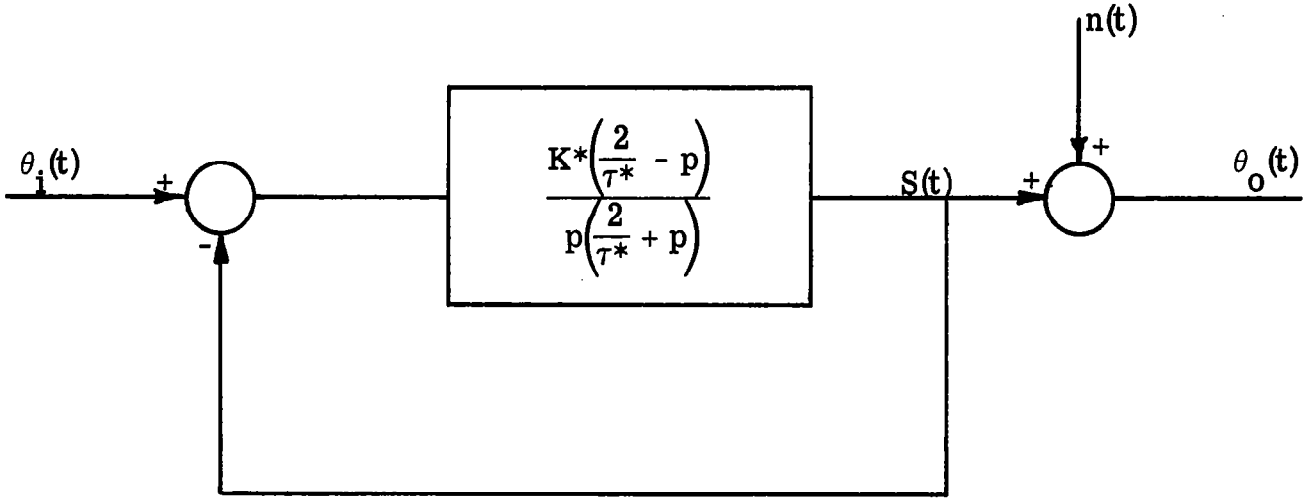

Figure 3.7.1 Final Block Diagram of the Compensatory System.

Chapter 4

PARAMETER TRACKING SYSTEM EVALUATION

The crossover model parameter tracking equations were developed in Chapter 3 under the assumptions that pure time-delay was present in the system, and that the parameters K and τ were constant. These equations were implemented, however, with a first order Padé approximation for time-delay and both parameters tracking continuously. The theoretical and experimental work of this chapter is intended to show that if the parameter tracking system is tracking a fixed real system whose form is the same as that of the implemented assumed model, then $K(t) \rightarrow K^*$ and $\tau(t) \rightarrow \tau^*$, providing the gradient gains and input signals are properly chosen.

4.1 Theoretical Stability Analysis

The general problem of stability in the large for output error continuous parameter tracking systems has not been solved. Margolis has analyzed stability in the small for systems tracking known models of first and second order with step, ramp, and acceleration inputs [23]. He also showed that when the input is a sinusoid, and the known model is of first order, then the linearized equations are transformable into a standard Mathieu equation. There is no evidence in the literature

that the stability in the small of output error continuous parameter tracking systems has been determined for sinusoidal inputs, when the system being tracked is of order greater than one. Needless to say, the random input case is also unsolved [19].

The theoretical analysis of the crossover model parameter tracking system used in the present research is composed of three main parts: (1) an investigation of the stability in the small for step, ramp, and acceleration inputs, where K(t) and τ(t) are being tracked singly and simultaneously; (2) an approximate method patterned after the method of Kryloff and Bogoliuboff for determining the dominant convergence time constants of the parameters. This is for the specific case of low gradient gains and sinusoidal inputs; (3) an investigation of the effect of the new limited gradient technique on parameter convergence.

The application of the method of Kryloff and Bogoliuboff is shown to be extendible to random inputs, and gives considerable insight into the problem of parameter tracking interaction.

4.2 The Basic State Variable Equations of Motion

Figure 4.2.1 is a simplified block diagram of the crossover model parameter tracking system when tracking a known real system of the correct form. The state variables $x_i(t)$, $i = 1, 2, \ldots, 10$ are defined as the integrator outputs. It will be noted that the limiters that were used at times in the gradient equations have not been included.

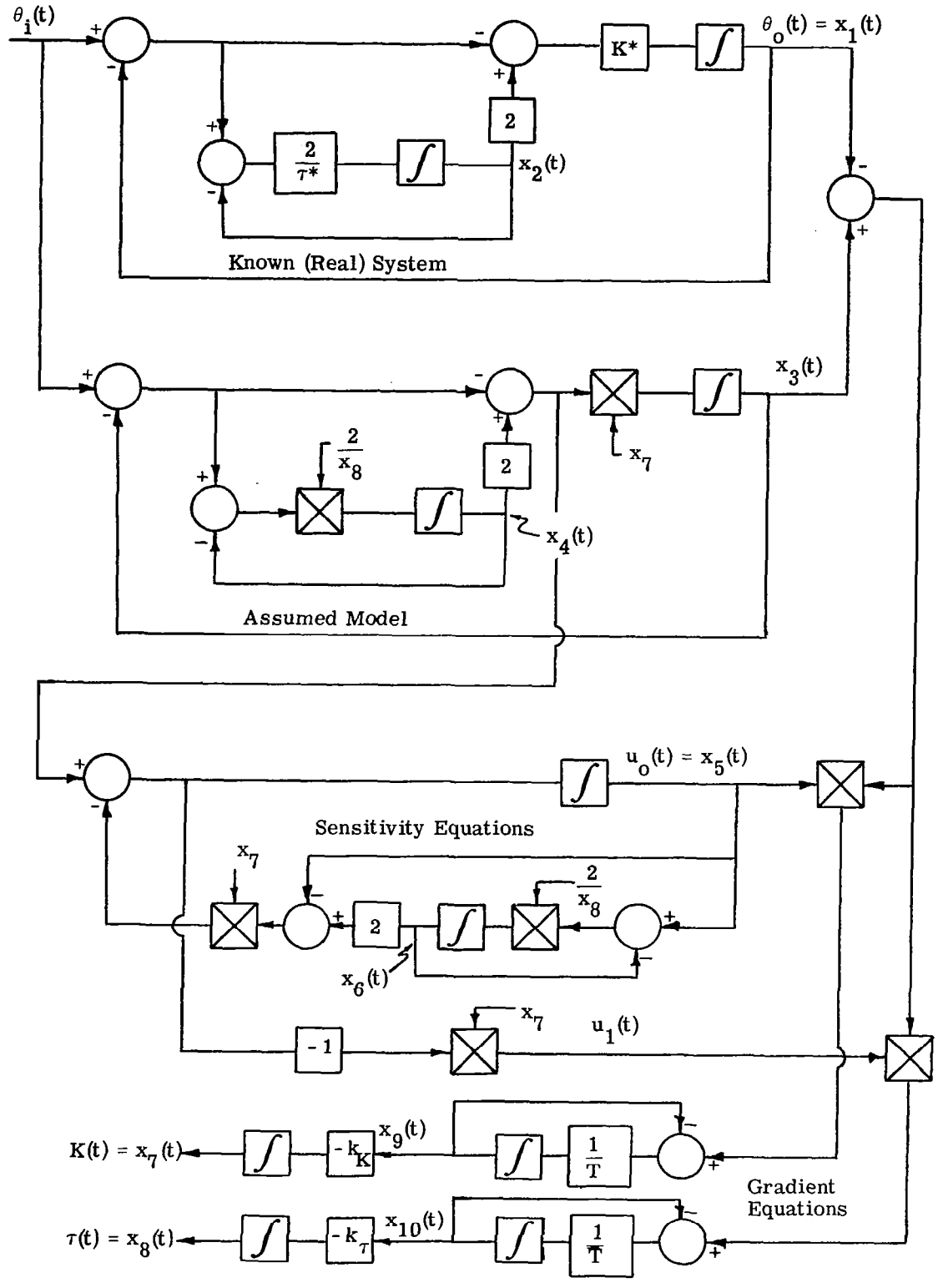

Figure 4.2.1 State Variable Block Diagram.

This is because all analyses will be made in the neighborhood of the desired solution with $e(t, K, \tau)$ small and the signals through the limiter assumed to be operating in the linear region. The case of limited action will be discussed in Section 4.8.

The equations of motion for the basic system are found to be

$$\dot{x}_1 = K^*[x_1 + 2x_2 - \theta_i]$$

$$\dot{x}_2 = \frac{2}{\tau^*}[-x_1 - x_2 + \theta_i]$$

$$\dot{x}_3 = x_7[x_3 + 2x_4 - \theta_i]$$

$$\dot{x}_4 = \frac{2}{x_8}[-x_3 - x_4 + \theta_i]$$

$$\dot{x}_5 = x_3 + 2x_4 + x_5 x_7 - 2x_6 x_7 - \theta_i \qquad (4.2\text{-}1)$$

$$\dot{x}_6 = \frac{2}{x_8}[x_5 - x_6]$$

$$\dot{x}_7 = -k_K x_9$$

$$\dot{x}_8 = -k_\tau x_{10}$$

$$\dot{x}_9 = \frac{1}{T}[(x_3 - x_1)x_5 - x_9]$$

$$\dot{x}_{10} = \frac{1}{T}[(x_3 - x_1)(-x_7)(x_3 + 2x_4 + x_5 x_7 - 2x_6 x_7 - \theta_i) - x_{10}]$$

4.3 Step Input Signals

The use of step functions as desirable input signals can be discounted with the following reasoning. If $\theta_i(t)$ is a step function and the system ever does reach steady state then $x_1(t) = x_3(t) \Rightarrow e(t, K, \tau) = 0$, even if $x_7(t) = K(t)$ is a constant other than K^* and $x_8(t) = \tau(t)$ is a constant other than τ^*. This is due to the fact that both the known model and the assumed model are type one control systems with zero steady state errors for step input signals. It can be concluded that a step input signal does not give the tracking system enough information for the determination of either parameter. A more "active" input is required.

4.4 Ramp Input Signal, Single Parameter Tracking

As a starting point, a single parameter tracking case will be analyzed. Let $x_8(t) = \tau(t) = \tau^*$ and $x_7(t) = K(t)$ be tracked alone. Equations (4.2-1) are still in effect with the exceptions that the $\dot{x}_8$ and $\dot{x}_{10}$ equations can be eliminated because x_8 is held constant. The new equations of motion are given in Eq. (4.4-1).

$$\dot{x}_1 = K^*[x_1 + 2x_2 - \theta_i]$$

$$\dot{x}_2 = \frac{2}{\tau^*}[-x_1 - x_2 + \theta_i]$$

$$\dot{x}_3 = x_7[x_3 + 2x_4 - \theta_i]$$

$$\dot{x}_4 = \frac{2}{\tau^*}[-x_3 - x_4 + \theta_i]$$

$$\dot{x}_5 = x_3 + 2x_4 + x_5 x_7 - 2x_6 x_7 - \theta_i \qquad (4.4\text{-}1)$$

$$\dot{x}_6 = \frac{2}{\tau^*}[x_5 - x_6]$$

$$\dot{x}_7 = -k_K x_9$$

$$\dot{x}_9 = \frac{1}{T}[(x_3 - x_1)x_5 - x_9]$$

If $\theta_i(t) = Vt$, a ramp input, the perturbation variables y_i, $i = 1, 2, \ldots, 7$ and 9, can be defined around the desired steady state solution as $x_i = x_{iss} + y_i$, where x_{iss} is the steady state solution. These equations are given in Eq. (4.4-2).

$$x_1 = V(t - \frac{1}{K^*}) + y_1$$

$$x_2 = \frac{V}{K^*} + y_2$$

$$x_3 = V(t - \frac{1}{K^*}) + y_3$$

$$x_4 = \frac{V}{K^*} + y_4$$

$$x_5 = \frac{V}{K^{*2}} + y_5 \qquad (4.4\text{-}2)$$

$$x_6 = \frac{V}{K^*} + y_6$$

$$x_7 = K^* + y_7$$

$$x_9 = y_9$$

By placing the perturbation equations (4.4-2) back into the equations of motion (4.4-1), and ignoring second order and higher terms, the linearized equations reduce to Eq. (4.4-3).

$$\dot{\vec{y}} = A\vec{y} \qquad (4.4\text{-}3)$$

where

$$\vec{y} = \begin{bmatrix} y_1 \\ \cdot \\ \cdot \\ \cdot \\ \cdot \\ y_7 \\ y_9 \end{bmatrix} \quad , \quad \dot{\vec{y}} = \frac{d}{dt}[\vec{y}] \quad ,$$

and

$$A = \begin{bmatrix} K^* & 2K^* & 0 & 0 & 0 & 0 & 0 & 0 \\ -\frac{2}{\tau^*} & -\frac{2}{\tau^*} & 0 & 0 & 0 & 0 & 0 & 0 \\ 0 & 0 & K^* & 2K^* & 0 & 0 & \frac{V}{K^*} & 0 \\ 0 & 0 & -\frac{2}{\tau^*} & -\frac{2}{\tau^*} & 0 & 0 & 0 & 0 \\ 0 & 0 & 1 & 2 & K^* & -2K^* & -\frac{V}{K^{*2}} & 0 \\ 0 & 0 & 0 & 0 & \frac{2}{\tau^*} & -\frac{2}{\tau^*} & 0 & 0 \\ 0 & 0 & 0 & 0 & 0 & 0 & 0 & -k_K \\ -\frac{V}{K^{*2}T} & 0 & \frac{V}{K^{*2}T} & 0 & 0 & 0 & 0 & -\frac{1}{T} \end{bmatrix} . \quad (4.4\text{-}4)$$

To determine the stability of Eq. (4.4-3), the eight eigenvalues of matrix A are solved for in the usual manner by setting

$$\det [A - \lambda I] = 0 \quad . \quad (4.4\text{-}5)$$

This equation is found, after some manipulation, to be factorable into the three equations given below.

$$\lambda^2 + \left(\frac{2}{\tau^*} - K^*\right)\lambda + \frac{2K^*}{\tau^*} = 0 \quad (4.4\text{-}6)$$

$$\lambda^2 + \left(\frac{2}{\tau^*} - K^*\right)\lambda + \frac{2K^*}{\tau^*} = 0 \quad (4.4\text{-}7)$$

$$- (K^* - \lambda)\left(\frac{2}{\tau^*} + \lambda\right)(\lambda)\left(\frac{1}{T} + \lambda\right) + \frac{4K^*}{\tau^*}(\lambda)\left(\frac{1}{T} + \lambda\right) + \frac{k_K V^2}{TK^{*3}}\left(\frac{2}{\tau^*} + \lambda\right) = 0 \quad (4.4\text{-}8)$$

It is seen that four of the eigenvalues of A are fixed by K^* and τ^* and consist of two pairs of equal roots. As was found by Margolis, each pair of these roots is identical with the roots of the known model. In fact, one pair belongs to the known model and the other pair to the assumed model. If the known model is stable, these four roots will automatically have negative real parts and thus be stable.

The four roots defined by Eq. (4.4-8) are functions of the gradient gain k_K and the slope of the input ramp, V. These roots are easily analyzed by drawing their root locus plot. Equation (4.4-8) is, therefore, rearranged into Eq. (4.4-9).

$$\frac{\lambda + \frac{2}{\tau^*}}{\lambda\left(\lambda + \frac{1}{T}\right)\left[\lambda^2 + \left(\frac{2}{\tau^*} - K^*\right)\lambda + \frac{2K^*}{\tau^*}\right]} = -\frac{TK^{*3}}{k_K V^2} \qquad (4.4\text{-}9)$$

The root locus plot of this equation is given in Fig. 4.4.1 with the gain variable being $V^2 k_K / TK^{*3}$.

The open loop, or zero gain, poles of Eq. (4.4-9) are readily identifiable. One real pole is due to the gradient filter and the other due to the gradient integrator. The complex poles are the same as the closed loop poles of the known model.

By referring to Fig. 4.4.1 it can be seen that the four gradient

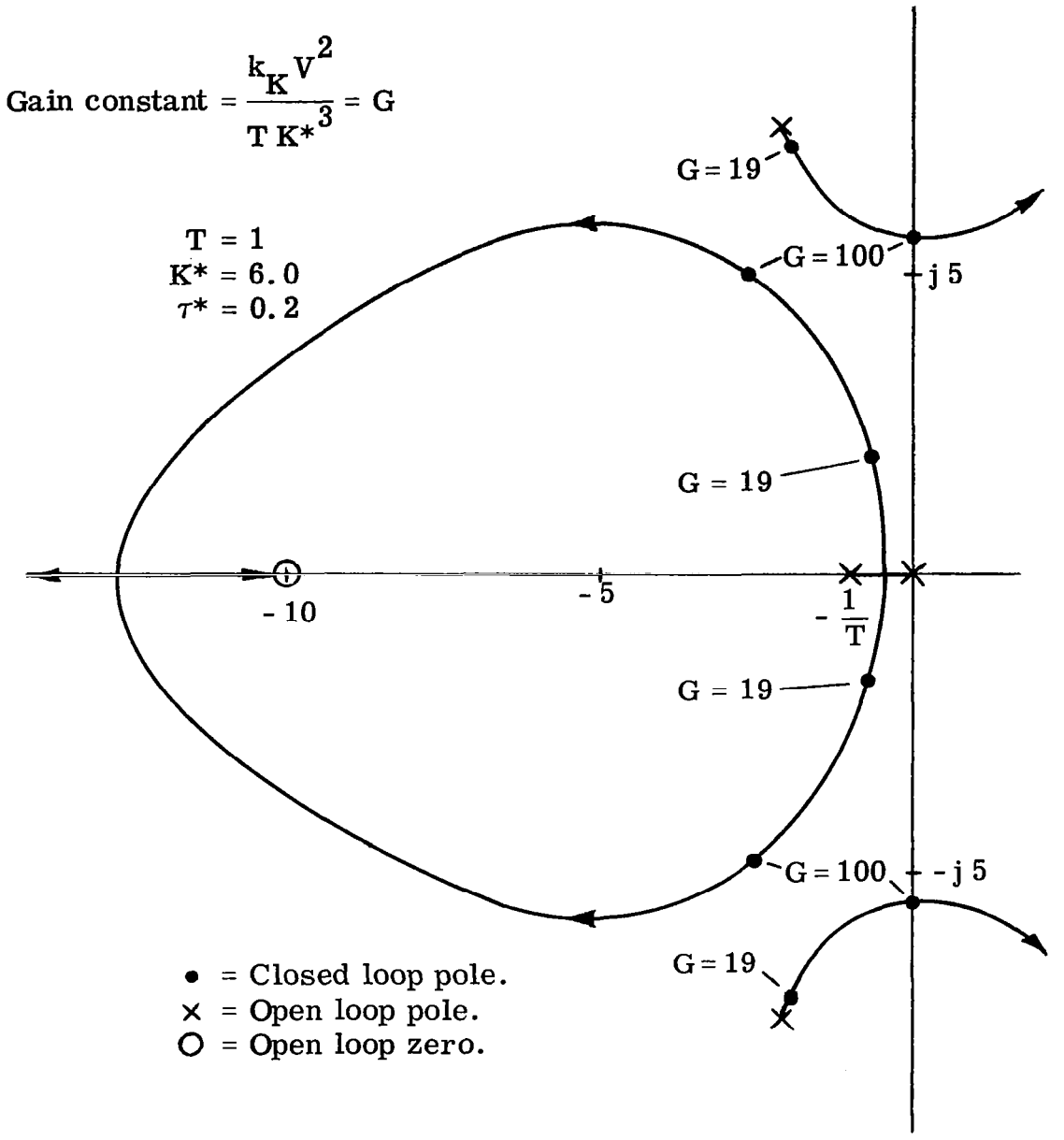

Figure 4.4.1 Root Locus Plot of Gradient Gain Dependent Roots — $\theta_i(t) = Vt$ — K(t) Tracking Alone.

gain dependent roots will all have negative real parts if k_K is chosen properly. Therefore, all eight of the characteristic roots of A will have negative real parts if: (1) the known model is stable; and (2) k_K is chosen properly. It is evident that the system can be made stable and $\lim_{t \to \infty} x_7(t) = K^*$ [8].

Several items are important to note with respect to Eq. (4.4-9). First, the effective gain variable for this portion of the system is $k_K V^2 / T K^{*3}$, which indicates that stability is directly effected by the input slope. Second, the effect of changes in the input slope can be offset by a suitable change in gradient gain. Third, by referring to Fig. 4.4.1, it is seen that for low values of k_K, the dominant root is a single real root located near the origin. The basic response for low gradient gains should therefore be first order. This result will be found to be present with all types of inputs.

If $x_7(t) = K(t)$ is held constant at K^*, and $\tau(t) = x_8(t)$ is tracked alone, the basic equations of motion are

$$\dot{x}_1 = K^* [x_1 + 2x_2 - \theta_i]$$

$$\dot{x}_2 = \frac{2}{x_8} [- x_1 - x_2 + \theta_i]$$

$$\dot{x}_3 = K^* [x_3 + 2x_4 - \theta_i]$$

$$\dot{x}_4 = \frac{2}{x_8} [- x_3 - x_4 + \theta_i]$$

$$\dot{x}_5 = x_3 + 2x_4 + K^* x_5 - 2K^* x_6 - \theta_i \qquad (4.4\text{-}10)$$

$$\dot{x}_6 = \frac{2}{x_8} [x_5 - x_6]$$

$$\dot{x}_8 = - k_\tau x_{10}$$

$$\dot{x}_{10} = \frac{1}{T} [(x_3 - x_1)(- K^*)(x_3 + 2x_4 + x_5 K^* - 2x_6 K^* - \theta_i) - x_{10}]$$

These are obtained from the general case given in Eq. (4.2-1) by merely eliminating $\dot{x}_7$ and $\dot{x}_9$, which are not relevant since x_7 is being held constant at K^*.

If $\theta_i(t) = Vt$, the perturbation variables can be defined as

$$
\begin{aligned}
x_1 &= V\left(t - \frac{1}{K^*}\right) + y_1 \\
x_2 &= \frac{V}{K^*} + y_2 \\
x_3 &= V\left(t - \frac{1}{K^*}\right) + y_3 \\
x_4 &= \frac{V}{K^*} + y_4 \\
x_5 &= \frac{V}{K^{*2}} + y_5 \\
x_6 &= \frac{V}{K^{*2}} + y_6 \\
x_8 &= \tau^* + y_8 \\
x_{10} &= y_{10}
\end{aligned}
\qquad (4.4\text{-}11)
$$

and the perturbed equations of motion reduced to

$$
\begin{aligned}
\dot{\vec{y}} &= B\vec{y} + \vec{f}(\vec{y}, y_8) \\
\dot{y}_8 &= -k_\tau y_{10} \\
\dot{y}_{10} &= -\frac{1}{T} y_{10} + g(\vec{y})
\end{aligned}
\qquad (4.4\text{-}12)
$$

where

$$\vec{y} = \begin{bmatrix} y_1 \\ \cdot \\ \cdot \\ \cdot \\ y_6 \end{bmatrix}$$

$$B = \begin{bmatrix} K^* & 2K^* & 0 & 0 & 0 & 0 \\ -\frac{2}{\tau^*} & -\frac{2}{\tau^*} & 0 & 0 & 0 & 0 \\ 0 & 0 & K^* & 2K^* & 0 & 0 \\ 0 & 0 & -\frac{2}{\tau^*} & -\frac{2}{\tau^*} & 0 & 0 \\ 0 & 0 & 1 & 2 & K^* & -2K^* \\ 0 & 0 & 0 & 0 & \frac{2}{\tau^*} & -\frac{2}{\tau^*} \end{bmatrix}, \qquad (4.4\text{-}13)$$

and $\vec{f}(\vec{y}, y_8)$ and $g(\vec{y})$ contain only second and higher order terms of the perturbation variables.

The additional approximation required to get Eq. (4.4-12) from Eq. (4.4-11) is

$$\frac{1}{\tau^* + y_8} = \frac{1}{\tau^*}\left[\frac{1}{1 + \frac{y_8}{\tau^*}}\right] \cong \frac{1}{\tau^*}\left[1 - \frac{y_8}{\tau^*}\right] \quad . \qquad (4.4\text{-}14)$$

Matrix B can be shown to have all stable roots. Equation (4.4-12) is thus stable, but not asymptotically stable [23]. $y_8(t)$ will approach a constant with increasing time, but this constant may not be zero.

This implies that $x_8(t)$ will also approach a constant, but this constant will not be τ^*.

This can be explained by examining the steady state signals in the block diagram of Fig. 4.2.1. Since $x_3(t)$ is a ramp, $\dot{x}_3(t)$ is a constant. The signal through the Padé time-delay unit in the steady state must also be a constant. The value of τ is therefore unimportant in the steady state when $\theta_i(t)$ is a ramp. This is another situation in which the input signal is not active enough to enable determination of the parameter being tracked.

The fact that a ramp input is sufficient to determine K*, but not τ^*, is the first indication that more active inputs are required for determining time-delay than for determining gain. However, it has already been noted in Chapter 2 that for low frequency inputs the output of the crossover model is more sensitive to changes in crossover model gain, than to changes in crossover time-delay. (See Fig. 2.3.3). This low sensitivity at low frequencies is directly related to the difficulty of tracking $\tau(t)$ with a ramp input.

4.5 Acceleration Input, Single Parameter Tracking

In order to evaluate the convergence of $\tau(t)$, assume again that $x_7 = K^*$, but let $\theta_i(t) = at^2/2$. Equations (4.4-10) are still the basic equations of motion, but the perturbation variables y_i are now defined as

$$x_1 = a\left[\frac{t^2}{2} - \frac{t}{K^*} + \frac{1}{K^{*2}} - \frac{\tau^*}{K^*}\right] + y_1$$

$$x_2 = a\left[\frac{t}{K^*} - \frac{1}{K^{*2}} + \frac{\tau^*}{2K^*}\right] + y_2$$

$$x_3 = a\left[\frac{t^2}{2} - \frac{t}{K^*} + \frac{1}{K^{*2}} - \frac{\tau^*}{K^*}\right] + y_3$$

$$x_4 = a\left[\frac{t}{K^*} - \frac{1}{K^{*2}} + \frac{\tau^*}{2K^*}\right] + y_4$$

$$x_5 = a\left[\frac{t}{K^{*2}} - \frac{2}{K^{*3}} + \frac{\tau^*}{K^{*2}}\right] + y_5 \qquad (4.5\text{-}1)$$

$$x_6 = a\left[\frac{t}{K^{*2}} + \frac{\tau^*}{2K^{*2}} - \frac{2}{K^{*3}}\right] + y_6$$

$$x_8 = \tau^* + y_8$$

$$x_{10} = y_{10}$$

By placing Eq. (4.5-1) back into Eq. (4.4-10), the following linearized equation can be obtained.

$$\dot{\vec{y}} = C\vec{y} \qquad (4.5\text{-}2)$$

where

$$\vec{y} = \begin{bmatrix} y_1 \\ \cdot \\ \cdot \\ \cdot \\ y_6 \\ y_8 \\ y_{10} \end{bmatrix} \quad ,$$

and

$$C = \begin{bmatrix} K^* & 2K^* & 0 & 0 & 0 & 0 & 0 & 0 \\ -\frac{2}{\tau^*} & -\frac{2}{\tau^*} & 0 & 0 & 0 & 0 & 0 & 0 \\ 0 & 0 & K^* & 2K^* & 0 & 0 & 0 & 0 \\ 0 & 0 & -\frac{2}{\tau^*} & -\frac{2}{\tau^*} & 0 & 0 & \frac{-a}{\tau^* K^*} & 0 \\ 0 & 0 & 1 & 2 & K^* & -2K^* & 0 & 0 \\ 0 & 0 & 0 & 0 & \frac{2}{\tau^*} & -\frac{2}{\tau^*} & \frac{-a}{\tau^* K^{*2}} & 0 \\ 0 & 0 & 0 & 0 & 0 & 0 & 0 & -k_\tau \\ +\frac{a}{TK^*} & 0 & -\frac{a}{TK^*} & 0 & 0 & 0 & 0 & -\frac{1}{T} \end{bmatrix} . \quad (4.5\text{-}3)$$

To determine the stability of Eq. (4.5-2), the eigenvalues of the matrix C are determined by solving

$$\det [C - \lambda I] = 0 \quad . \quad (4.5\text{-}4)$$

This equation can be factored into the three equations given below:

$$\lambda^2 + \left(\frac{2}{\tau^*} - K^*\right)\lambda + \frac{2K^*}{\tau^*} = 0 \qquad (4.5\text{-}5)$$

$$\lambda^2 + \left(\frac{2}{\tau^*} - K^*\right)\lambda + \frac{2K^*}{\tau^*} = 0 \qquad (4.5\text{-}6)$$

$$-\lambda\left(\lambda + \frac{1}{T}\right)\left(\lambda + \frac{2}{\tau^*}\right)(K^* - \lambda) + \left(\lambda + \frac{1}{T}\right)\left(\frac{4K^*}{\tau^*}\right) + \frac{2a^2 k_\tau}{\tau^* K^* T} = 0 \quad . \qquad (4.5\text{-}7)$$

The situation is similar to that found when tracking K(t) when the input was a ramp. Four of the eigenvalues are determined completely by the values of K^* and τ^*, and coincide with the closed loop roots of the known model. The other four eigenvalues are functions of the gradient gain and the input signal.

The eigenvalues that are functions of gradient gain will again be analyzed through the root locus approach. Equation (4.5-7) is therefore rearranged into the correct form given in Eq. (4.5-8).

$$\frac{1}{\lambda\left(\lambda + \frac{1}{T}\right)\left[\lambda^2 + \left(\frac{2}{\tau^*} - K^*\right)\lambda + \frac{2K^*}{\tau^*}\right]} = \frac{-TK^*\tau^*}{2a^2 k_\tau} \qquad (4.5\text{-}8)$$

The root locus plot associated with this equation is given in Fig. 4.5.1. It is seen that all four roots will be stable if k_τ is chosen properly.

The entire system defined by Eq. (4.5-2) will thus be stable if: (1) the known model is stable; and (2) k_τ is chosen properly through the use of Fig. 4.5.1.

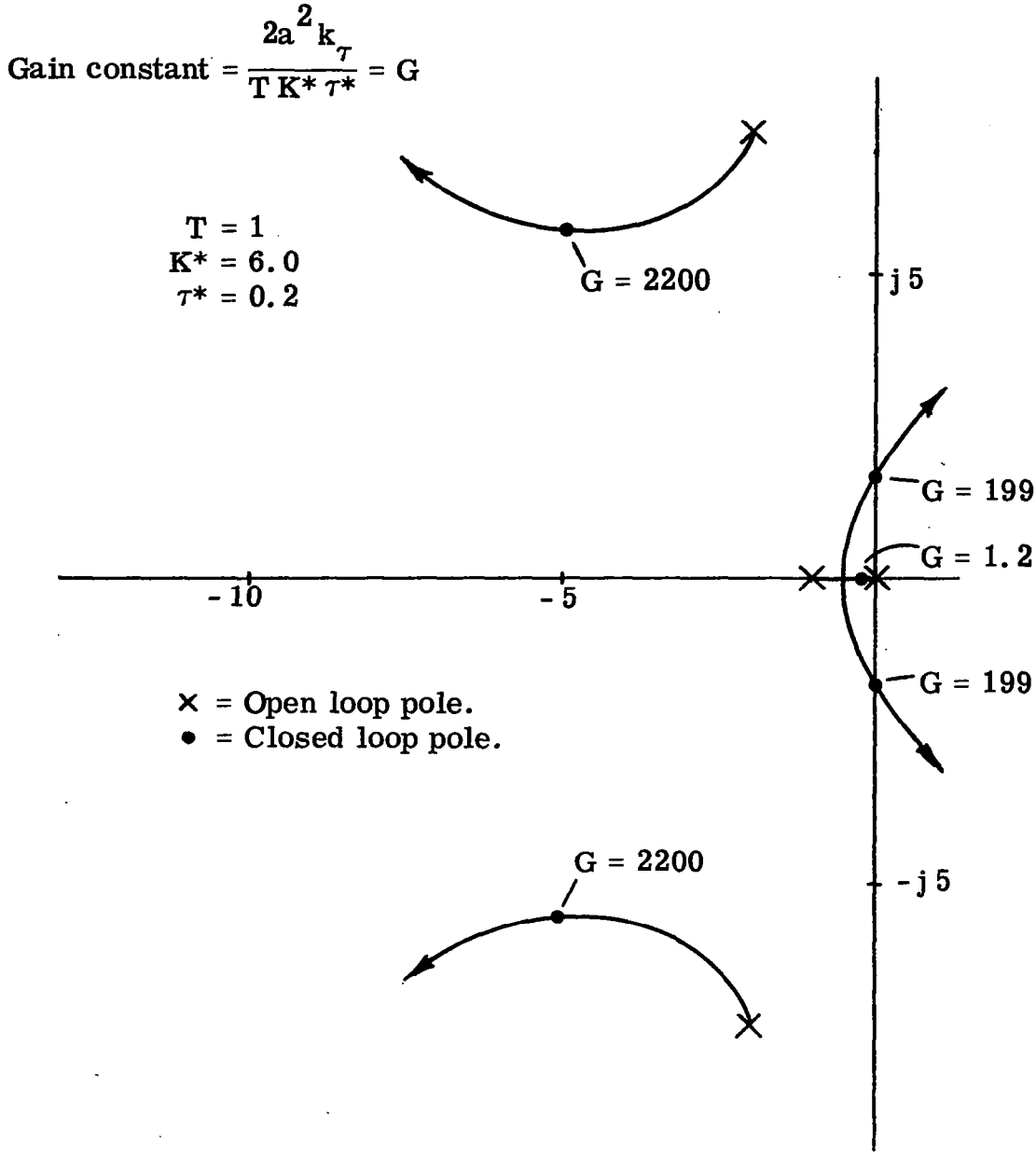

Figure 4. 5. 1 Root Locus Plot of Gradient Gain Dependent Roots — $\theta_i(t) = at^2/2$ — $\tau(t)$ Tracking Alone.

The zero gain poles of Fig. 4. 5. 1 are again identifiable. The real poles correspond to the gradient integrator and the gradient filter, while the complex poles are the same as the closed loop poles of the known model.

4.6 Ramp and Acceleration Inputs, Both Parameters Tracking

If an attempt is made to analyze the stability of the system with both parameters tracking and $\theta_i(t)$ a ramp, the linearized equations are stable, but not asymptotically stable. This is the same type of condition that existed with a ramp input when $\tau(t)$ was being tracked alone.

It can be deduced that the two parameter tracking case calls for an input of higher order than a ramp. However, if a higher order input such as an acceleration or a sinusoid is used, the linearized equations are time-varying and appear to be difficult to solve analytically.

Rather than proceeding further with a conventional linearized stability analysis, which presents considerable difficulties, a new approach was adopted. This method is discussed in the next section.

4.7 Sinusoidal Stability Analysis Using the Method of Kryloff and Bogoliuboff

The sinusoidal stability analysis of the parameter tracking system is based on the following conditions:

(1) The tracking system is tracking a known real system of the correct form with crossover gain K* and first order Padé time-delay τ^*.

(2) The input signal is a single sinusoid with a frequency in the general region of crossover. The exact frequency is arbitrary, but must be in a region where the assumed model output is sensitive to parameter variation.

(3) The convergence properties will be investigated only in the neighborhood of the desired solution $K = K^*$ and $\tau = \tau^*$.

(4) The gradient gains k_K and k_τ are low.

Under these conditions the convergence (or divergence) rates of $K(t)$ and $\tau(t)$ can be made as slow as desired by reducing the gradient gains. The rates of change of $K(t)$ and $\tau(t)$ can be made slow with respect to the decay rates of the dominant transients of the assumed model, the sensitivity equations, and the gradient filters.

In the neighborhood of the desired solution the signals $Z(t, K, \tau)$, $u_o(t, K, \tau)$, $u_1(t, K, \tau)$, $\dot{\Delta}K(t, K, \tau)$ and $\dot{\Delta}\tau(t, K, \tau)$ are all assumed to be in a quasi-steady state condition, with their amplitudes and phases being slowly modulated by the changes in $K(t)$ and $\tau(t)$. In particular, it is assumed that when

$$\theta_i(t) = D \sin \omega t \qquad (4.7\text{-}1)$$

then

$$\theta_o(t) = A^* \sin(\omega t + \psi_1^*)$$

$$Z(t, K, \tau) = [A^* + \Delta A(t)] \sin(\omega t + \psi_1^* + \Delta\psi_1(t))$$

$$u_o(t, K, \tau) = [B^* + \Delta B(t)] \sin(\omega t + \psi_1^* + \psi_2^* + \Delta\psi_2(t))$$

$$u_1(t, K, \tau) = - K\dot{u}_o(t, K, \tau) = - [K^* + \Delta K(t)] \dot{u}_o(t, K, \tau) \qquad (4.7\text{-}2)$$

$$= - \omega \Big\{ [K^* B^* + K^* \Delta B(t) + B^* \Delta K(t)] \cos(\omega t + \psi_1^* + \psi_2^*)$$

$$- K^* B^* \Delta\psi_2(t) \sin(\omega t + \psi_1^* + \psi_2^*) \Big\}$$

The last equation was developed under the assumption that $\frac{d}{dt}[B^* + \Delta B(t)] \sin \omega t \cong [B^* + \Delta B(t)] \omega \cos \omega t$. The (*) values in Eq. (4.7-2) are steady state amplitudes and phases at the desired solution point. $A^* = A(\omega, D, K, \tau)\big|_{K^*, \tau^*}$ and $B^* = B(\omega, D, K, \tau)\big|_{K^*, \tau^*}$ are the desired steady state amplitudes of the assumed model and the sensitivity equation for K. $\psi_1^* = \psi_1(\omega, K, \tau)\big|_{K^*, \tau^*}$ is the steady state phase shift through the assumed model. $\psi_2^* = \psi_2(\omega K, \tau)\big|_{K^*, \tau^*}$ is the steady state phase difference between the assumed model output and the output of the sensitivity equation for K.

A block diagram of this system is given in Fig. 4.7.1.

Using Eqs. (4.7-2) the outputs of the two gradient multipliers can be shown to be

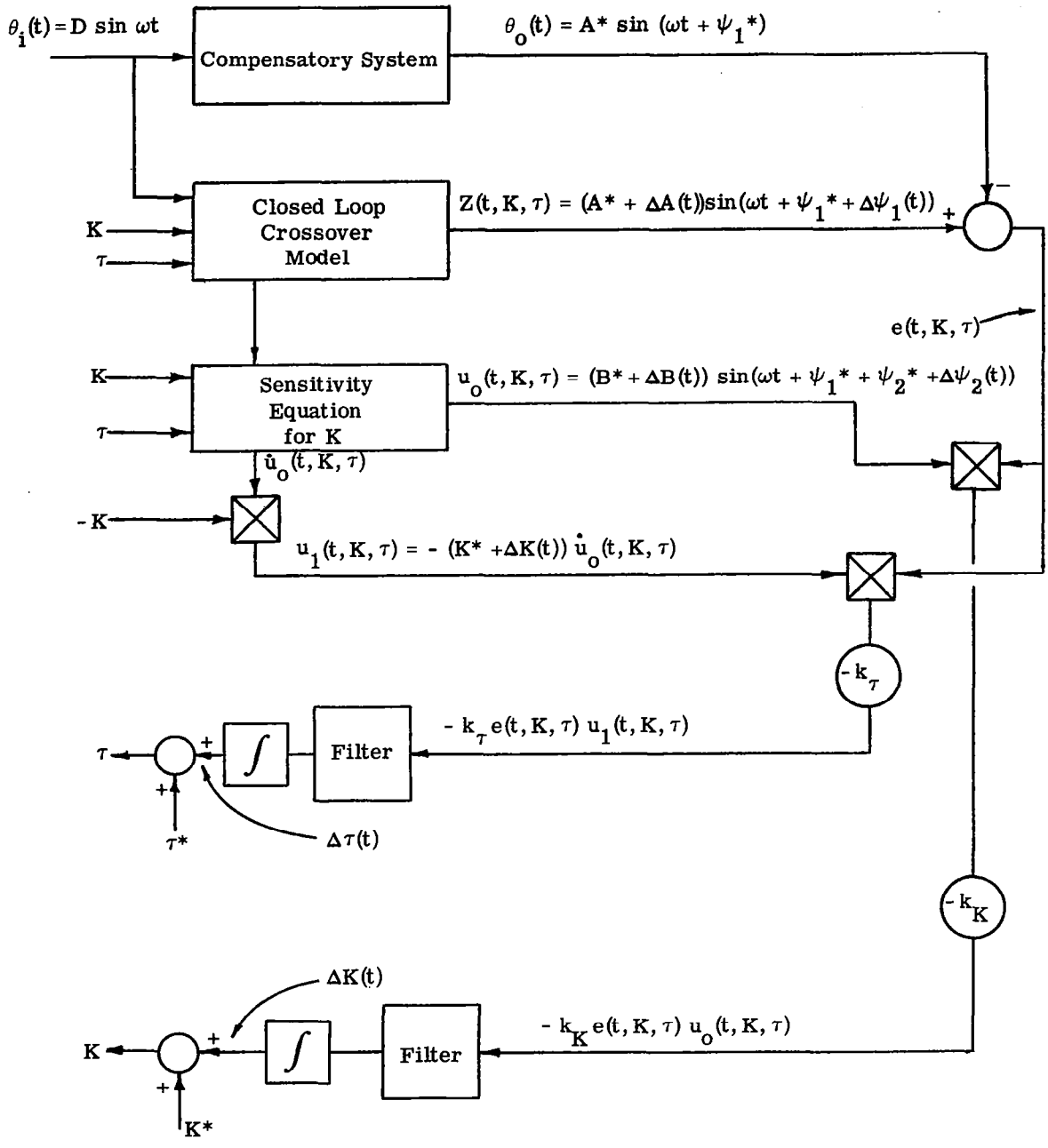

Figure 4.7.1 Block Diagram for Sinusoidal Input Stability Analysis.

$$e(t,K,\tau)\,u_o(t,K,\tau) = \frac{B^*\Delta A(t)}{2}\left[\cos\psi_2^* - \cos(2\omega t + 2\psi_1^* + \psi_2^*)\right]$$

$$+\frac{B^*A^*\Delta\psi_1(t)}{2}\left[\sin\psi_2^* + \sin(2\omega t + 2\psi_1^* + \psi_2^*)\right] \tag{4.7-3}$$

and

$$e(t,K,\tau)\,u_1(t,K,\tau) = -\frac{\omega K^* B^*\Delta A(t)}{2}\left[-\sin\psi_2^* + \sin(2\omega t + 2\psi_1^* + \psi_2^*)\right]$$

$$-\frac{\omega K^* B^* A^*\Delta\psi_1(t)}{2}\left[\cos\psi_2^* + \cos(2\omega t + 2\psi_1^* + \psi_2^*)\right]. \tag{4.7-4}$$

Equations (4.7-3) and (4.7-4) are developed with the aid of the identities

$$\sin x \sin y = \frac{1}{2}\cos(x - y) - \frac{1}{2}\cos(x + y)$$

$$\sin x \cos y = \frac{1}{2}\sin(x + y) + \frac{1}{2}\sin(x - y) \quad , \tag{4.7-5}$$

and the standard first order approximations

$$\sin\Delta \cong \Delta$$

$$\cos\Delta \cong 1 \tag{4.7-6}$$

$$\Delta\cdot\Delta \cong 0 \quad .$$

The signals represented by Eqs. (4.7-3) and (4.7-4) are multiplied by the gradient gains k_K and k_τ, respectively, and passed through the gradient filters to give the parameter adjustment rate equations $\dot{\Delta}K(t,K,\tau)$ and $\dot{\Delta}\tau(t,K,\tau)$. (See Fig. 4.7.1) The filter outputs are

$$\dot{\Delta K}(t, K, \tau) = - k_K \left\{ \frac{B^* \Delta A(t)}{2} \left[\cos \psi_2^* - M_f \cos(2\omega t + 2\psi_1^* + \psi_2^* + \psi_f) \right] \right.$$

$$\left. + \frac{B^* \Delta \psi_1(t)}{2} \left[\sin \psi_2^* + M_f \sin(2\omega t + 2\psi_1^* + \psi_2^* + \psi_f) \right] \right\} \qquad (4.7\text{-}7)$$

and

$$\dot{\Delta \tau}(t, K, \tau) = \frac{k_\tau K^* B^* \omega}{2} \left\{ \Delta A(t) \left[- \sin \psi_2^* + M_f \sin(2\omega t + 2\psi_1^* + \psi_2^* + \psi_f) \right] \right.$$

$$\left. + A \, \Delta \psi_1(t) \left[\cos \psi_2^* + M_f \cos(2\omega t + 2\psi_1^* + \psi_2^* + \psi_f) \right] \right\} , \qquad (4.7\text{-}8)$$

where $\psi_f = \psi_f(\omega, T)$ is the phase shift and $M_f = M_f(\omega, T)$ the magnitude attenuation introduced by the gradient filters. The filters are assumed to be equal for this discussion.

It is now remembered that $\Delta A(t)$ and $\Delta \psi_1(t)$ are modulating functions caused by the slowly varying changes in $K(t)$ and $\tau(t)$. In the neighborhood of the desired solution these modulating terms are approximately

$$\Delta A(t) = \left. \frac{\partial A}{\partial K} \right|_{K^*, \tau^*} \Delta K(t) + \left. \frac{\partial A}{\partial \tau} \right|_{K^*, \tau^*} \Delta \tau(t) \qquad (4.7\text{-}9)$$

and

$$\Delta \psi_1(t) = \left. \frac{\partial \psi_1}{\partial K} \right|_{K^*, \tau^*} \Delta K(t) + \left. \frac{\partial \psi_1}{\partial \tau} \right|_{K^*, \tau^*} \Delta \tau(t) \quad . \qquad (4.7\text{-}10)$$

Placing Eqs. (4.7-9) and (4.7-10) back into (4.7-7) and (4.7-8), the desired forms for the method of Kryloff and Bogoliuboff are obtained [21].

$$\dot{\Delta K}(t, K, \tau) = -\frac{k_K B^*}{2}\left\{\left[\cos\psi_2 \frac{\partial A}{\partial K} + A \sin\psi_2 \frac{\partial \psi_1}{\partial K}\right]_{K^*, \tau^*} \Delta K(t)\right.$$

$$\left. + \left[\cos\psi_2 \frac{\partial A}{\partial \tau} + A \sin\psi_2 \frac{\partial \psi_1}{\partial \tau}\right]_{K^*, \tau^*} \Delta\tau(t)\right\} \qquad (4.7\text{-}11)$$

$$+ k_K f_1(\Delta K(t),\ \Delta\tau(t)) \cdot (\text{Sinusoid of } 2\omega t) \ .$$

and

$$\dot{\Delta\tau}(t, K, \tau) = \frac{k_\tau K^* B^* \omega}{2}\left\{\left[-\sin\psi_2 \frac{\partial A}{\partial K} + A\cos\psi_2 \frac{\partial \psi_1}{\partial K}\right]_{K^*, \tau^*} \Delta K(t)\right.$$

$$\left. + \left[-\sin\psi_2 \frac{\partial A}{\partial \tau} + A\cos\psi_2 \frac{\partial \psi_1}{\partial \tau}\right]_{K^*, \tau^*} \Delta\tau(t)\right\} \qquad (4.7\text{-}12)$$

$$+ k_\tau f_2(\Delta K(t),\ \Delta\tau(t)) \cdot (\text{Sinusoid of } 2\omega t) \ .$$

It should be emphasized that since their introduction $\Delta A(t)$ and $\Delta\psi_1(t)$ have been taken as constant in all calculations. This is in line with the basic method as proposed by Kryloff and Bogoliuboff, and is continued for one more calculation. This additional calculation is the integration with respect to time of both sides of Eqs. (4.7-11) and (4.7-12) from t to $t + \frac{\pi}{\omega}$. This eliminates the sinusoidal terms on the right hand sides of both equations since the sinusoids are integrated over exactly one cycle.

The resulting equations are

$$\frac{\Delta K\left(t + \frac{\pi}{\omega}\right) - \Delta K(t)}{\frac{\pi}{\omega}} = -\frac{k_K B^*}{2}\left\{\left[\cos\psi_2 \frac{\partial A}{\partial K} + A \sin\psi_2 \frac{\partial \psi_1}{\partial K}\right]_{K^*, \tau^*} \Delta K(t)\right.$$

$$\left. + \left[\cos\psi_2 \frac{\partial A}{\partial \tau} + A \sin\psi_2 \frac{\partial \psi_1}{\partial \tau}\right]_{K^*, \tau^*} \Delta\tau(t)\right\} \qquad (4.7\text{-}13)$$

and

$$\frac{\Delta\tau\left(t + \frac{\pi}{\omega}\right) - \Delta\tau(t)}{\frac{\pi}{\omega}} = \frac{k_\tau K^* B^* \omega}{2}\left\{\left[-\sin\psi_2 \frac{\partial A}{\partial K} + A\cos\psi_2 \frac{\partial \psi_1}{\partial K}\right]_{K^*, \tau^*} \Delta K(t)\right.$$

$$\left. + \left[-\sin\psi_2 \frac{\partial A}{\partial \tau} + A\cos\psi_2 \frac{\partial \psi_1}{\partial \tau}\right]_{K^*, \tau^*} \Delta\tau(t)\right\}. \qquad (4.7\text{-}14)$$

In keeping with the method of Kryloff and Bogoliuboff, the terms on the left sides of Eqs. (4.7-13) and (4.7-14) are taken as the approximate derivatives of $\Delta K(t)$ and $\Delta\tau(t)$ with respect to time.

$$\frac{\Delta K\left(t + \frac{\pi}{\omega}\right) - \Delta K(t)}{\frac{\pi}{\omega}} = \frac{d}{dt}(\Delta K(t)) \cong \dot{\Delta K}(t) \qquad (4.7\text{-}15)$$

and

$$\frac{\Delta\tau\left(t + \frac{\pi}{\omega}\right) - \Delta\tau(t)}{\frac{\pi}{\omega}} = \frac{d}{dt}(\Delta\tau(t)) \cong \dot{\Delta\tau}(t) \quad . \qquad (4.7\text{-}16)$$

Placing these approximations back into Eqs. (4.7-13) and (4.7-14), the desired equations of motion are obtained.

$$\begin{bmatrix} \dot{\Delta K}(t) \\ \dot{\Delta \tau}(t) \end{bmatrix} = \left[\begin{array}{c|c} -\frac{k_K B}{2}\left[\cos\psi_2 \frac{\partial A}{\partial K} + A \sin\psi_2 \frac{\partial \psi_1}{\partial K}\right] & -\frac{k_K B}{2}\left[\cos\psi_2 \frac{\partial A}{\partial \tau} + A \sin\psi_2 \frac{\partial \psi_1}{\partial \tau}\right] \\ \hline -\frac{k_\tau K B \omega}{2}\left[\sin\psi_2 \frac{\partial A}{\partial K} - A \cos\psi_2 \frac{\partial \psi_1}{\partial K}\right] & -\frac{k_\tau K B \omega}{2}\left[\sin\psi_2 \frac{\partial A}{\partial \tau} - A \cos\psi_2 \frac{\partial \psi_1}{\partial \tau}\right] \end{array}\right]_{K^*, \tau^*} \begin{bmatrix} \Delta K(t) \\ \Delta \tau(t) \end{bmatrix} \tag{4.7-17}$$

Equation (4.7-17) describes the motion of the perturbed parameters $\Delta K(t)$ and $\Delta\tau(t)$ in the neighborhood of the desired solution $\Delta K(t) = \Delta\tau(t) = 0$. Several facts are apparent from an inspection of the coefficient matrix of Eq. (4.7-17).

(1) The parameter adjustments are coupled in a rather complicated manner, with the amount of coupling depending upon six variables: D, ω, K^*, τ^*, k_K and k_τ.

(2) If coupling is to be eliminated the off-diagonal terms must be zero. A sufficient condition for zero coupling can be developed by merely setting the off-diagonal terms equal to zero. These equations are

$$-\frac{k_K B^*}{2}\left[\cos\psi_2\frac{\partial A}{\partial\tau}+A\sin\psi_2\frac{\partial\psi_1}{\partial\tau}\right]_{K^*,\tau^*}=0 \qquad (4.7\text{-}18)$$

and

$$-\frac{k_K K^* B^*\omega}{2}\left[\sin\psi_2\frac{\partial A}{\partial K}-A\cos\psi_2\frac{\partial\psi_1}{\partial K}\right]_{K^*,\tau^*}=0\ . \qquad (4.7\text{-}19)$$

Since k_K, k_τ, K^*, B^*, and ω are all non-zero in the non-trivial case, Eqs. (4.7-18) and (4.7-19) can be reduced to

$$\cos\psi_2\frac{\partial A}{\partial\tau}\bigg|_{K^*,\tau^*}=-A\sin\psi_2\frac{\partial\psi_1}{\partial\tau}\bigg|_{K^*,\tau^*} \qquad (4.7\text{-}20)$$

and

$$A\cos\psi_2\frac{\partial\psi_1}{\partial K}\bigg|_{K^*,\tau^*}=\sin\psi_2\frac{\partial A}{\partial K}\bigg|_{K^*,\tau^*}\ . \qquad (4.7\text{-}21)$$

By dividing Eq. (4.7-20) by (4.7-21), the transcendental functions can be eliminated.

$$\frac{\left.\frac{\partial A}{\partial \tau}\right|_{K^*, \tau^*}}{A \left.\frac{\partial \psi_1}{\partial K}\right|_{K^*, \tau^*}} = \frac{-A \left.\frac{\partial \psi_1}{\partial \tau}\right|_{K^*, \tau^*}}{\left.\frac{\partial A}{\partial K}\right|_{K^*, \tau^*}} \qquad (4.7\text{-}22)$$

or,

$$\frac{\partial A}{\partial \tau} \cdot \left.\frac{\partial A}{\partial K}\right|_{K^*, \tau^*} = -A^2 \frac{\partial \psi_1}{\partial \tau} \cdot \left.\frac{\partial \psi_1}{\partial K}\right|_{K^*, \tau^*} . \qquad (4.7\text{-}23)$$

It can be seen that one cannot force this equality to occur without complete a priori knowledge of the system. Even then, the equality may not occur if ω is the only free variable. Since the coefficients K* and τ^* are assumed unknown, the coupling cannot in general be eliminated using the present tracking configuration.

(3) Each term in the coefficient matrix of Eq. (4.7-17) is proportional to both $(A^*)^2$ and either k_K or k_τ. Since A* is directly proportional to D, the input amplitude, it follows that the effect of changes in D can be offset by changes in k_τ and k_K. This fact was also found to be true in the ramp and acceleration input cases.

(4) If $\Delta\tau(t) \equiv \dot{\Delta}\tau(t) \equiv 0$, the time constant of the convergence of $\Delta K(t)$ is the reciprocal of the upper left hand term in the coefficient matrix. Likewise, if $\Delta K(t) \equiv \dot{\Delta}K(t) \equiv 0$, the time constant of $\Delta\tau(t)$ convergence is the reciprocal of the lower right hand term.

(5) Due to the number of variables contained in the coefficient matrix of Eq. (4.7-17), no attempt was made to determine stability regions in terms of the parameters involved. However, if nominal values for K^*, τ^*, ω and D are assumed, Eq. (4.7-17) is found to be asymptotically stable.

Examples of some of these characteristics are given in Appendix C.

4.8 Applying the Method of Kryloff and Bogoliuboff to the Random Input Case

In the practical application of parameter tracking systems the input signal is filtered Gaussian white noise, or a sum of sinusoids that produces an apparently random signal. The purpose of this section is the investigation of the general convergence properties of the parameter tracking system associated with the random input case. This must be approached somewhat differently than the sinusoidal input case.

The method will be developed using a two parameter model system. The extension to higher order systems can be deduced from this example.

The notation for this method is given in Fig. 4.8.1. The input is assumed to be filtered Gaussian white noise, with the assumptions and conditions of Section 4.7 still in effect. The gradient filters have been eliminated for ease of presentation.

In the neighborhood of the solution point,

$$Z(t,K,\tau) = Z(t,K^*,\tau^*) + \frac{\partial Z}{\partial K}(t,K,\tau)\Big|_{K^*,\tau^*} \Delta K(t)$$

$$+ \frac{\partial Z}{\partial \tau}(t,K,\tau)\Big|_{K^*,\tau^*} \Delta\tau(t) \quad , \tag{4.8-1}$$

$$u_o(t,K,\tau) = u_o(t,K^*,\tau^*) + \frac{\partial u_o}{\partial K}(t,K,\tau)\Big|_{K^*,\tau^*} \Delta K(t)$$

$$+ \frac{\partial u_o}{\partial \tau}(t,K,\tau)\Big|_{K^*,\tau^*} \Delta\tau(t) \tag{4.8-2}$$

and

$$u_1(t,K,\tau) = u_1(t,K^*,\tau^*) + \frac{\partial u_1}{\partial K}(t,K,\tau)\Big|_{K^*,\tau^*} \Delta K(t)$$

$$+ \frac{\partial u_1}{\partial \tau}(t,K,\tau)\Big|_{K^*,\tau^*} \Delta\tau(t) \quad . \tag{4.8-3}$$

But

$$\frac{\partial Z}{\partial K}(t,K,\tau)\Big|_{K^*,\tau^*} = u_o(t,K^*,\tau^*) \quad , \tag{4.8-4}$$

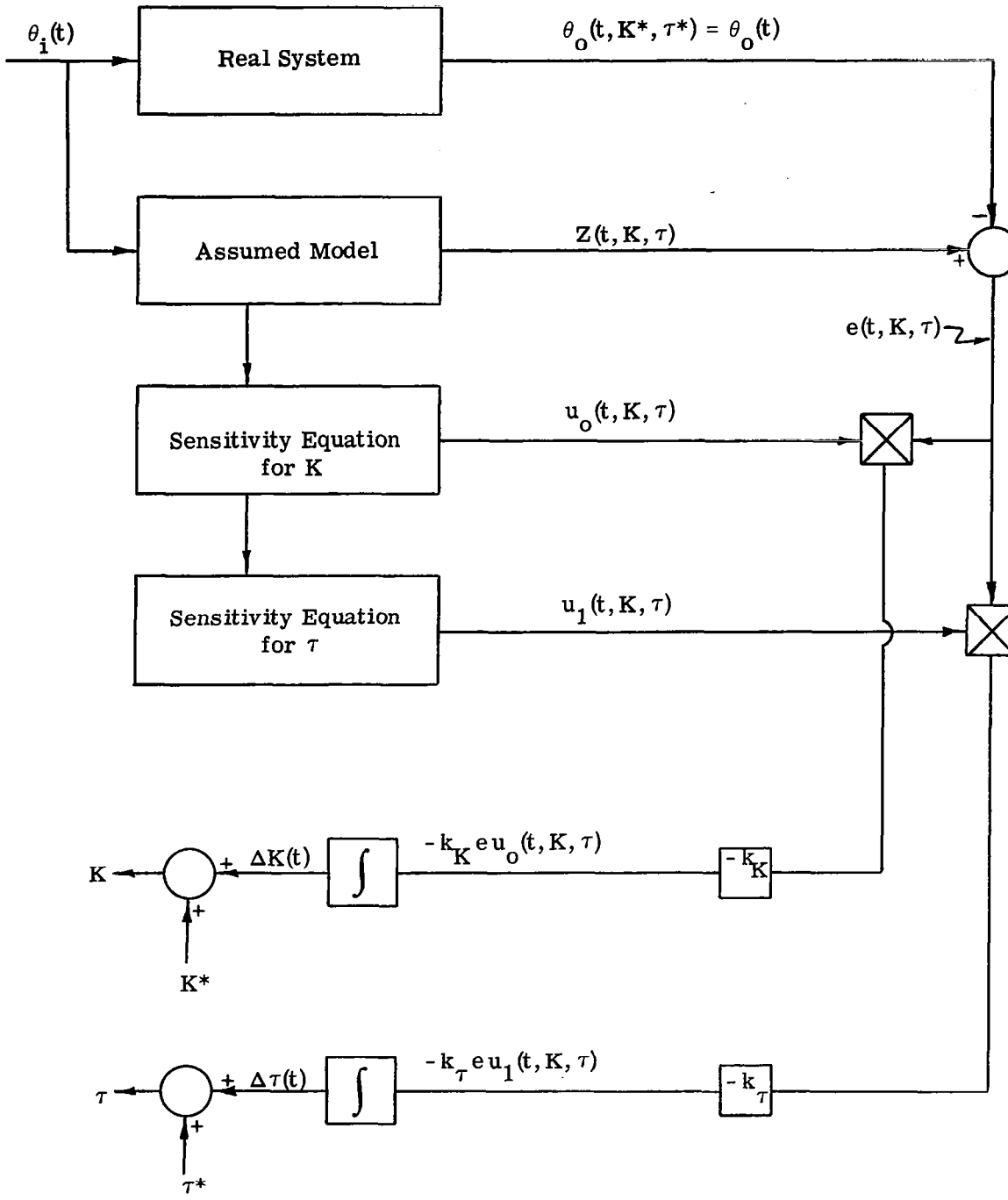

Figure 4.8.1 Block Diagram for Random Input Stability Analysis.

$$\left.\frac{\partial Z}{\partial \tau}(t, K, \tau)\right|_{K^*, \tau^*} = u_1(t, K^*, \tau^*) \quad , \tag{4.8-5}$$

and

$$\theta_o(t) = Z(t, K^*, \tau^*) \quad . \tag{4.8-6}$$

Therefore,

$$Z(t, K, \tau) = \theta_o(t) + u_o(t, K^*, \tau^*)\,\Delta K(t) + u_1(t, K^*, \tau^*)\,\Delta\tau(t) \tag{4.8-7}$$

and

$$e(t, K, \tau) = u_o(t, K^*, \tau^*)\,\Delta K(t) + u_1(t, K^*, \tau^*)\,\Delta\tau(t) \quad . \tag{4.8-8}$$

By using Eqs. (4.8-2), (4.8-3) and (4.8-8), and neglecting the Δ^2 terms generated in the multipliers, the inputs to the gradient integrators are found to be

$$\begin{aligned}
\dot{\Delta}K(t, K, \tau) &= -k_K\, e(t, K, \tau)\, u_o(t, K, \tau) \\
&= -k_K u_o^2(t, K^*, \tau^*)\Delta K(t) - k_K u_o(t, K^*, \tau^*)\, u_1(t, K^*, \tau^*)\Delta\tau(t) \\
\dot{\Delta}\tau(t, K, \tau) &= -k_\tau\, e(t, K, \tau)\, u_1(t, K, \tau) \\
&= -k_\tau u_1(t, K^*, \tau^*)\, u_o(t, K^*, \tau^*)\Delta K(t) - k_\tau u_1^2(t, K^*, \tau^*)\Delta\tau(t) .
\end{aligned} \tag{4.8-9}$$

If the input was a single sinusoid, Eqs. (4.8-9) could be integrated with respect to time over one cycle of the sinusoid to generate the

"average" differential equations for $\dot{\Delta K}(t)$ and $\dot{\Delta \tau}(t)$. This averaging would be done with $\Delta K(t)$ and $\Delta \tau(t)$ held constant on the right hand sides of the equations.

In Eq. (4.8-9) the u_o and u_1 terms are not sinusoids, but sample functions from random processes. They cannot be averaged over "one period", since an infinite number of frequencies are present. However, if most of the power in the $u_1(t, K^*, \tau^*)$ terms is located at frequencies such that $\Delta K(t)$ and $\Delta \tau(t)$ are essentially constant over one cycle of the lowest frequency present, then a meaningful average value for $\dot{\Delta K}(t)$ and $\dot{\Delta \tau}(t)$ can still be obtained, while keeping with the intent of the basic method of Kryloff and Bogoliuboff. It should be remembered that in Chapter 2 the maximum power in $u_o(t, K^*, \tau^*)$ and $u_1(t, K^*, \tau^*)$ was shown to be near crossover, with the power falling off toward zero on both sides of this region.

With these facts in mind, the average or expected values for $\dot{\Delta K}(t)$ and $\dot{\Delta \tau}(t)$ at any particular time can be determined by taking the statistical expectation of the right hand sides of Eq. (4.8-9), under the assumption that $\Delta K(t)$ and $\Delta \tau(t)$ are constant.

The "averaged" differential equations are then

$$\begin{bmatrix} \dot{\Delta K} \\ \dot{\Delta \tau} \end{bmatrix} = \begin{bmatrix} -k_K & 0 \\ 0 & -k_\tau \end{bmatrix} R \begin{bmatrix} \Delta K(t) \\ \Delta \tau(t) \end{bmatrix} \qquad (4.8\text{-}10)$$

where

$$R = \begin{bmatrix} E\left\{u_o^2(t, K^*, \tau^*)\right\} & E\left\{u_o(t, K^*, \tau^*)\, u_1(t, K^*, \tau^*)\right\} \\ E\left\{u_1(t, K^*, \tau^*)\, u_o(t, K^*, \tau^*)\right\} & E\left\{u_1^2(t, K^*, \tau^*)\right\} \end{bmatrix}$$

R is a moment matrix and is positive definite. Equation (4.8-10) is therefore stable and the system should "on the average" converge.

Equation (4.8-10) indicates the futility of trying to predict a priori the convergence rates for a given model. The coefficient matrix is a function of all the variables encountered in the sinusoidal case, plus being dependent upon the characteristics of the input filter. In addition, the short-term characteristics of convergence may differ drastically from that predicted by Eq. (4.8-10), due to the statistical variation of the coefficients in matrix R. This variation is not present in the sinusoidal input case.

Although they were developed from an entirely different point of view, the results of this and the last section are compatible with previous results obtained by Meissinger and Bekey [7, 29].

4.9 Theoretical Analysis of the Limited Gradient

During actual subject testing a problem with the somewhat erratic action of the parameters K(t) and τ(t) was encountered. These parameters would converge to a fairly stable value, stay there for a period

of time, and then, on occasion, jump away from the convergent point in one sudden movement. An extremely bad case of this is shown in Fig. C.4.1 in Appendix C. This result occurs in cases where the subject is operating in a fairly nonlinear manner.

The fact that the disturbed parameter would start converging back toward the original stable point indicated that the jump was due to a momentary lapse in effort on the part of the subject, rather than a planned increase or decrease in the parameter. This lapse shows up in the tracking network as a large increase in $e(t, K, \tau)$, and thus in $\dot{\Delta}K(t, K, \tau)$ and $\dot{\Delta}\tau(t, K, \tau)$. In extreme cases, like the one cited above, the average value of the parameter over a short sample period can be greatly affected. This condition is not peculiar to the particular tracking system used, but is evident in the records of other researchers.

One way to reduce the magnitude of these sudden changes in parameter values is to reduce the gradient gain. This effectively increases the filtering action inherent in the tracking system and tends to smooth out all disturbances. The difficulty in this approach is that lowering the gradient gain also increases the convergence time. Todosiev and Bekey have tried to circumvent this problem in at least two different ways:

(1) they instructed their subjects not to use sudden control stick movement; and

(2) they systematically dropped all gradient gains by a factor of 10, after a suitable convergence interval.

In order to reduce the magnitude of the problem during the experimental work of this research, a new parameter adjustment technique was used. The adjustment equation has already been introduced in Chapter 3 as Eq. (3.5-2).

Equation (3.5-2) shows that $\Delta K(t)$ is nothing more than the limited and filtered value of the conventional gradient integrator input $-k_K e u_o$. The practical reasoning behind this type of system is quite simple. In the conventional adjustment scheme the crossover gain K would be adjusted according to the equation

$$\dot{\Delta}K(t, K, \tau) = -k_K \frac{\partial I}{\partial K}(t, K, \tau) = -k_K e\, u_o(t, K, \tau)$$

$$= -k_K[Z(t, K, \tau) - \theta_o(t)]\, u_o(t, K, \tau)$$

$$= -k_K[Z(t, K, \tau) - S(t) - n(t)]\, u_o(t, K, \tau) \quad . \qquad (4.9\text{-}1)$$

Large increases in n(t), the remnant signal out of the human system, are immediately felt in $\dot{\Delta}K(t, K, \tau)$. These disturbances in n(t) will show up as disturbances in K(t), providing $u_o \neq 0$.

By introducing the sat function, the maximum rate of change of K(t) is directly limited. This means that K(t) will depend mainly on

the average value of $- k_K e u_o$, and will be fairly insensitive to large short duration disturbances. The linear filter was added for additional smoothing, but is not essential for good operation.

To determine the net effect of the limiter on the average value of the gradient, the limiter output will be analyzed in two ways:

(1) At the true optimum $K = K^*$ and $\tau = \tau^*$, to see if the expected value of the limiter output is zero.

(2) In the vicinity of K^*, τ^* when the input is sinusoidal and n(t) is present, to see if the parameters will still converge.

With noise present in the system

$$e(t, K, \tau) = Z(t, K, \tau) - \theta_o(t) \qquad (4.9\text{-}2)$$

$$= Z(t, K, \tau) - S(t) - n(t) \quad . \qquad (4.9\text{-}3)$$

At the desired convergence point

$$Z(t, K^*, \tau^*) = S(t) \qquad (4.9\text{-}4)$$

and

$$e(t, K^*, \tau^*) = - n(t) \quad . \qquad (4.9\text{-}5)$$

Under these conditions the gradient for the parameter K is

$$\frac{\partial I}{\partial K}(t, K^*, \tau^*) = e\, u_o(t, K^*, \tau^*)$$

$$= - n(t)\, u_o(t, K^*, \tau^*) \quad , \qquad (4.9\text{-}6)$$

and the limiter output is

$$\text{sat}\left[-k_K \frac{\partial I}{\partial K}(t, K^*, \tau^*)\right] = \text{sat}\left[k_K\, n(t)\, u_o(t, K^*, \tau^*)\right] \quad . \quad (4.9\text{-}7)$$

The expected value of the limited gradient is

$$E\left\{\text{sat}\left[k_K n(t)\, u_o(t, K^*, \tau^*)\right]\right\} = -L\left\{\Pr\left[k_K n u_o \leq -L\right]\right\}$$

$$+ k_K \int_{-L/k_K}^{L/k_K} \alpha\, p_{n u_o}(\alpha)\, d\alpha + L\left\{\Pr\left[k_K n u_o \geq L\right]\right\}. \quad (4.9\text{-}8)$$

It is desired that the expectation in Eq. (4.9-8) be zero so that the true convergence point will not be biased due to the nonlinear action of the filter. A sufficient condition for Eq. (4.9-8) to be zero is that $p_{n u_o}(\alpha)$, the probability density function of $n(\alpha)\, u_o(\alpha, K^*, \tau^*)$, be symmetric. In addition, sufficient conditions for the random variable $n(\alpha)\, u_o(\alpha, K^*, \tau^*)$ to have a symmetric probability density function are:

(1) $n(\alpha)$ and $u_o(\alpha, K^*, \tau^*)$ are independent, or Gaussian and uncorrelated.

(2) At least one of the two random variables $n(\alpha)$ or $u_o(\alpha, K^*, \tau^*)$ must have a symmetric probability density function.

These conditions are proven in Appendix B.

If $\theta_i(t)$ is chosen to be filtered Gaussian white noise with zero mean, then:

(1) $u_o(\alpha, K^*, \tau^*)$ is Gaussian with zero mean, and thus symmetric. This follows directly from the fact that $\theta_i(t)$ is Gaussian with zero mean.

(2) $n(\alpha)$ and $u_o(\alpha, K^*, \tau^*)$ are not correlated. This follows from the fact that $n(\alpha)$ is not correlated with $\theta_i(\alpha)$, while $u_o(\alpha, K^*, \tau^*)$ is linearly related to $\theta_i(\alpha)$.

(3) $n(\alpha)$ may be Gaussian, but it is doubtful that it is completely independent of $u_o(\alpha, K^*, \tau^*)$.

If $n(\alpha)$ is either Gaussian or independent of $u_o(\alpha, K^*, \tau^*)$, then the conditions on $n(\alpha)$ and $u_o(\alpha, K^*, \tau^*)$ are sufficient to make Eq. (4.9-8) equal to zero. This will insure that the limiter will not bias the point of convergence in actual compensatory testing. If $n(\alpha)$ does not meet either one of these conditions, then the possibility exists that the final values of K and τ could be biased.

The limited gradient was actually used on all parameter tracking runs in the K_2/p^2 experiment described in Chapter 5. Limiting in some cases was quite severe. In spite of this, it will be shown in Chapter 6 that the limiting did not apparently bias the final parameter values. This tends to support the assumption that $n(\alpha)\, u_o(\alpha, K^*, \tau^*)$ is a symmetric random variable, or at least close enough so as not to bias the results. This assumption will be made throughout the rest of the discussion.

To check the qualitative effect of the new parameter adjustment method on the average speed of convergence, a sinusoidal input together with the method of Section 4.7 will be used. One parameter convergence will be investigated with the other parameter held constant at the desired value.

Assume first of all that $n(t) = 0$ and $\theta_i(t) = D \sin \omega t$. If k_K is small, as it must be in actual operation, then the equations developed in Section 4.7 hold when $K(t) \cong K^*$ and $\tau = \tau^*$. From Eq. (4.7-11) with $\Delta\tau = 0$,

$$\dot{\Delta K}(t, K, \tau^*) = -\frac{k_K B^*}{2}\left[\cos \psi_2 \frac{\partial A}{\partial K} + A \sin \psi_2 \frac{\partial \psi_1}{\partial K}\right]_{K^*, \tau^*} \Delta K(t) + k_K f(\Delta K) \cdot (\text{Sinusoid of } 2\omega t) \quad . \tag{4.9-9}$$

In the unlimited case discussed in Section 4.7, the sinusoidal term is filtered out and the average convergence rate is determined solely by the term

$$-\frac{k_K B^*}{2}\left[\cos \psi_2 \frac{\partial A}{\partial K} + A \sin \psi_2 \frac{\partial \psi_1}{\partial K}\right]_{K^*, \tau^*} \Delta K(t) \quad . \tag{4.9-10}$$

As described earlier, this term is assumed constant over time intervals $\frac{\pi}{\omega}$ in length.

If the limits L are lowered to the point where the waveform of Eq. (4.9-9) is clipped, then the situation shown in Fig. 4.9.1 is encountered.

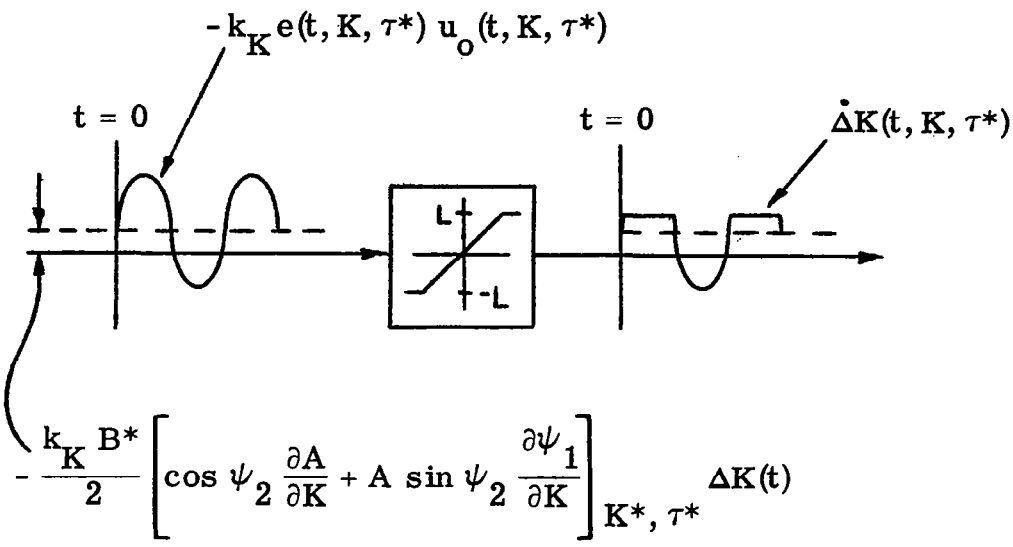

Figure 4.9.1 Parameter Adjustment Limiting—Sinusoidal Input

It is seen by inspection that the average value of the limiter output will be lower than the average value of the limiter input. Since this average value represents the new value of $\dot{\Delta}K(t, K, \tau^*)$, it can be concluded that the limiter will reduce the average rate of convergence once limiting occurs. The convergence is still in the same direction, however.

By injecting an uncorrelated Gaussian signal n(t) into the compensatory system output, Eq. (4.9-9) is changed to

$$\dot{\Delta K}(t, K, \tau^*) = -\frac{k_K B^*}{2}\left[\cos\psi_2 \frac{\partial A}{\partial K} + A \sin\psi_2 \frac{\partial \psi_1}{\partial K}\right]_{K^*, \tau^*} \Delta K(t)$$

$$+ k_K f(\Delta K) \cdot (\text{Sinusoid of } 2\omega t) + k_K n(t) u_o(t, K, \tau^*) \quad . \tag{4.9-11}$$

At any instant of time t_1, the product of the remnant $n(t_1)$ and the quasi-steady state sinusoid $u_o(t_1, K, \tau^*)$ will be a symmetric random variable if $\theta_i(t)$ is Gaussian with zero mean. The sum

$$k_K f(\Delta K) \cdot (\text{Sinusoid of } 2\omega t) + k_K\, n(t)\, u_o(t, K, \tau^*) \tag{4.9-12}$$

will also be symmetric.

When this sum is super-imposed on the biasing term given by Eq. (4.9-10), and passed through the limiter, the limiting will on the average by most severe on the side determined by the sign of Eq. (4.9-10). Due to the symmetry involved the average value of the output of the limiter will again be lower than the average value of the input to the limiter. $\dot{\Delta K}(t, K, \tau^*)$ will again be reduced on the average when limiting occurs.

If the limits L are made too small, or if n(t) is very large, the condition can be reached where extreme limiting occurs on both sides of the limiter. The average output in this case approaches zero and the parameter will not converge at all. An example of this will be constructed in Appendix C.

4.10 Experimental Convergence Tests

A series of experimental tests were run to check the parameter tracking system while tracking a real system of the correct form, (i.e., a real system as given in Fig. 3.7.1). Since Margolis [23] had verified the action of continuous parameter tracking systems as predicted by root locus plots when the input was a step, ramp, or acceleration, the experimental analysis was designed to evaluate three things:

(1) The general convergence properties of the parameter tracking system when the input was bandwidth limited white noise. The purpose here was to show that $K(t) \rightarrow K^*$ and $\tau(t) \rightarrow \tau^*$ from various values of $K(0)$ and $\tau(0)$.

(2) The convergence properties when the input was sinusoidal and no gradient limiting was occurring. This was to check the sinusoidal results predicted by Eq. (4.4-17).

(3) The convergence properties when the input was sinusoidal and gradient limiting was occurring. This was to evaluate the action of the limiter.

In addition, the effectiveness of the limiter in reducing parameter disturbances is shown graphically by comparing some actual compensatory test runs with and without the limiters in use.

A detailed description of the tests and some sample time histories are given in Appendix C. It is sufficient to state at this point that all theoretical points were verified, and that the parameter tracking system performed as predicted.

Chapter 5

COMPENSATORY TESTS AND TEST RESULTS

In order to check the crossover model parameter tracking system in actual operation, two separate compensatory tracking tests were run. A complete outline of the test conditions and instructions to the subjects are given in Appendix A. A summary of the actual tests conducted is given below.

5.1 Description of the Compensatory Tracking Tests

In the first compensatory tracking test three subjects were trained for ten days on a system containing a K_1/p controlled element. The input was Gaussian pseudo-white noise filtered with a simple 3rd order filter of the form

$$\frac{1}{(Tp + 1)^3} \quad .$$

Filter cut-off frequencies of 1, 2 and 4 radians per second were used. The control stick used required horizontal movement of the entire forearm and had light spring loading and essentially no damping. Stick inertia was small in comparison with the inertia of the arm.

The subject was comfortably seated in a straight backed chair with his right arm resting on the control stick, and the oscilloscope located approximately 28 inches directly in front of him. The

oscilloscope had a 5 inch green tinted face that was coated with P-31, a very low persistence phosphor. A vertical cursor was located in the center of the oscilloscope with the error displayed as a dot moving horizontally.

All of the subjects were right handed males with no known physical abnormalities that would affect their tracking capability. None of them had previous tracking experience of any kind. Subject testing was conducted in a quiet test booth. A picture taken inside of the test booth is given in Fig. 5.1.1.

On each day, each subject completed 5 two minute trials at each of the cut-off frequencies for a total of 15 two minute trials per day. The blocks of 5 trials at each frequency were randomly ordered each day in order to minimize the effects of training transfer from one test condition to the other.

In the second compensatory test three different subjects were trained in the same manner as above, with the exception that $Y_C(p)$ was K_2/p^2. In addition, after 10 days of training the arm control stick was replaced by a force stick, and three additional days of training were given on this stick. Although the force stick data was not completely analyzed, its quantitative effects on K, τ and the parameter tracking system in general were of interest.

During each trial completed by each subject the input signal $\theta_i(t)$,

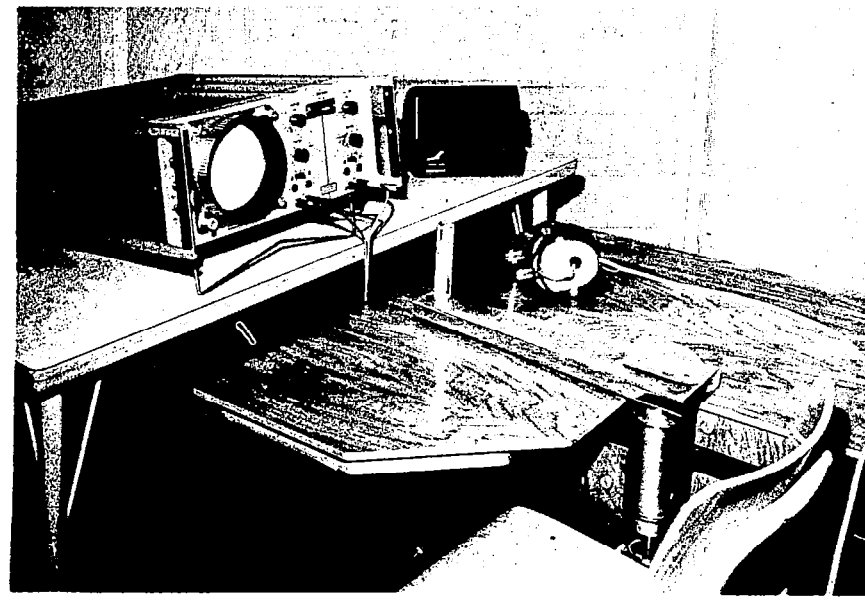

Figure 5.1.1 The Subject Test Booth.

the compensatory output signal $\theta_o(t)$, and the control stick output signal c(t) were all recorded on magnetic tape. $\theta_i(t)$ and $\theta_o(t)$ were then played back into the parameter tracking system and K and τ determined. c(t) was not used in the parameter tracking system. The bandwidth of the tape recorder was 175 cycles per second.

In addition to the signals recorded the conventional index of performance given in Eq. (1.2-2) was calculated for each trial. The equation is repeated here for convenience.

$$\text{Compensatory Tracking Index} = \int_0^{120\ \text{sec}} |\epsilon(t)|\, dt = \text{IAE}. \quad (5.1\text{-}1)$$

This index was averaged over the 5 trials at each frequency, normalized by the average value of

$$\int_0^{120\ \text{sec}} |\theta_i(t)|\, dt \quad , \quad (5.1\text{-}2)$$

and plotted as the normalized integral of the absolute error. These graphs are presented in Figs. 5.1.2 and 5.1.3. The only data plotted on these graphs are those which were analyzed in one manner or another later in the research. Data for days not included appeared quite consistent with that given.

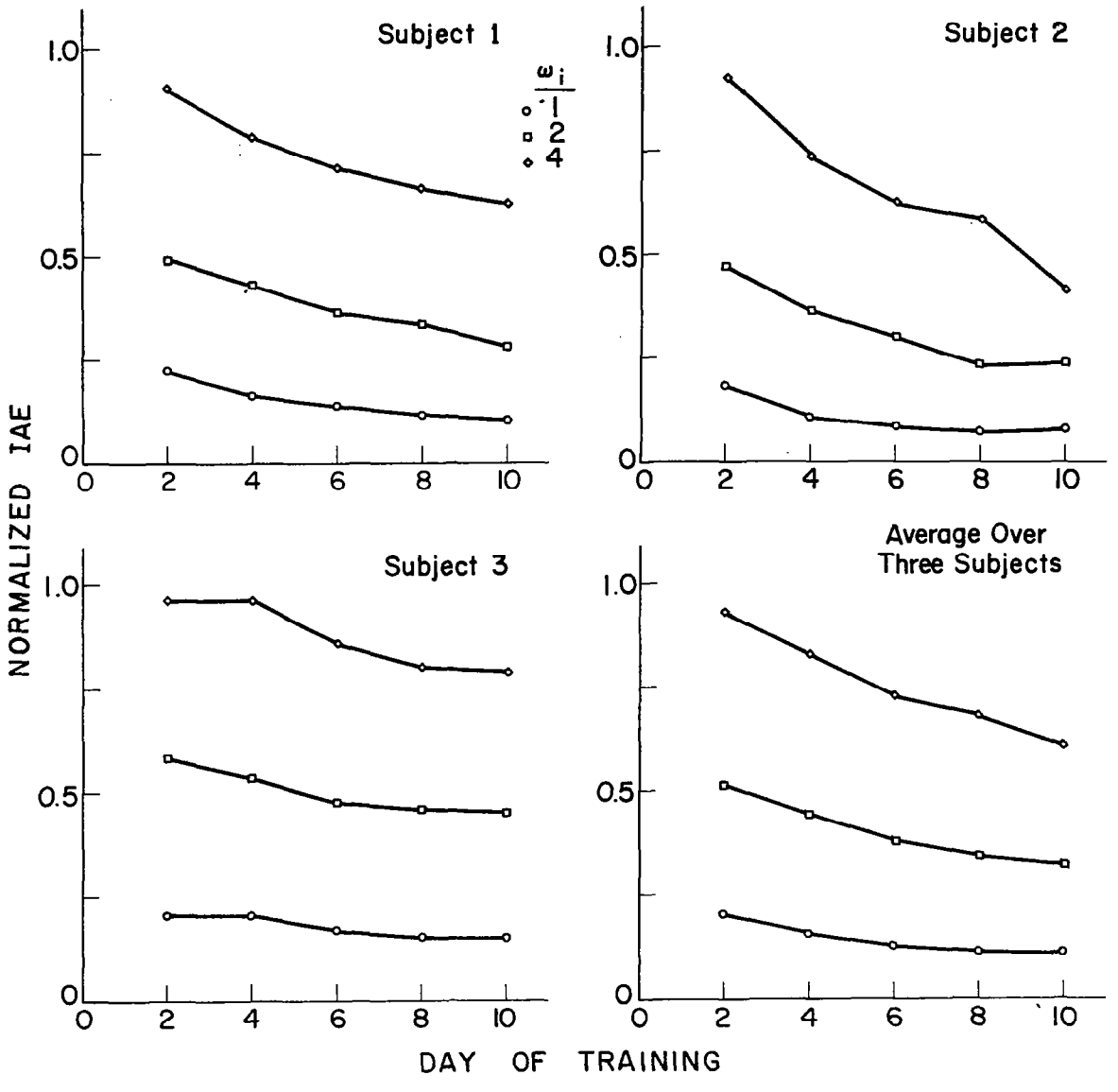

Figure 5.1.2 Normalized IAE—$Y_C(p) = K_1/p$.

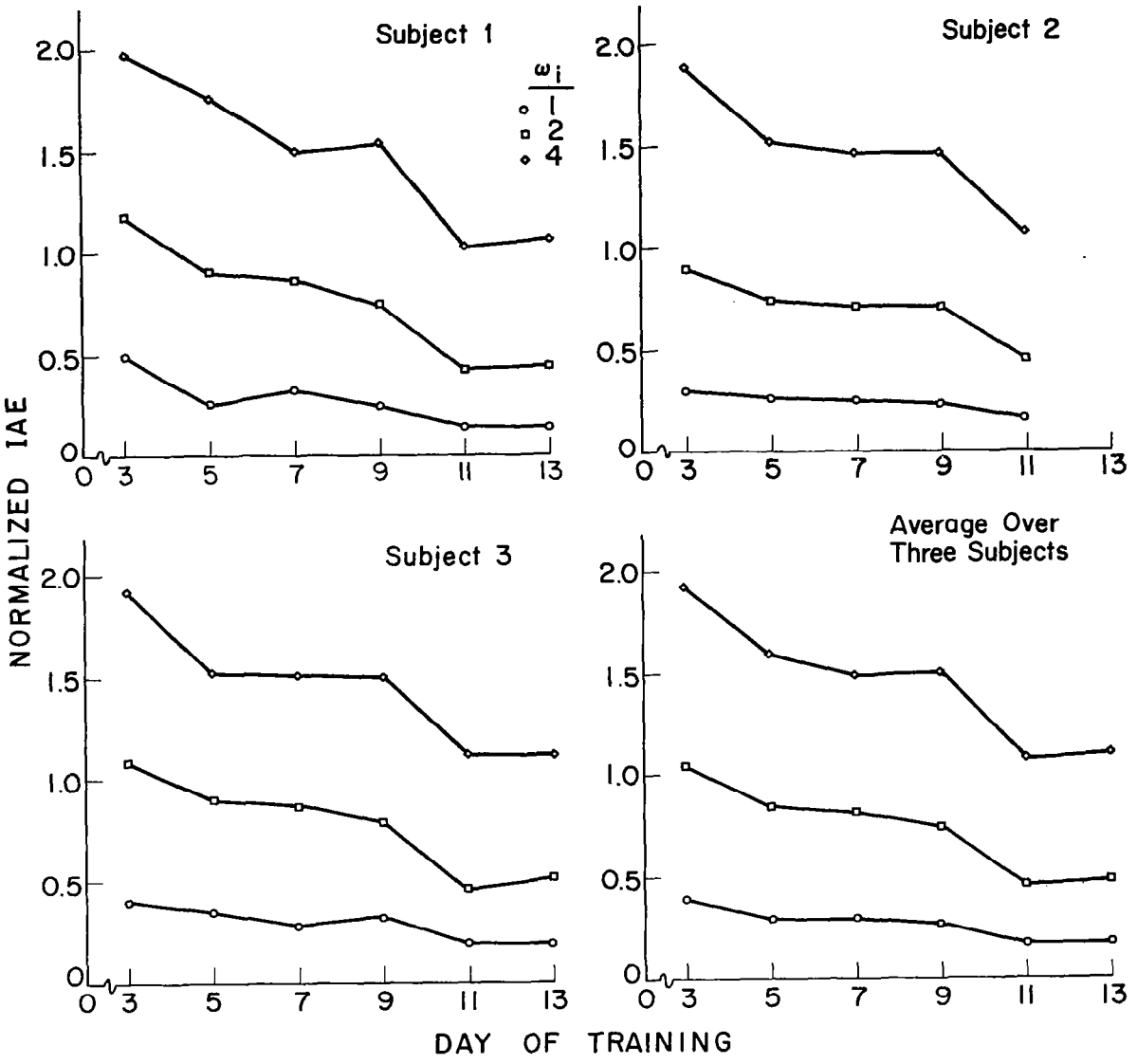

Figure 5.1.3 Normalized IAE—$Y_C(p) = K_2/p^2$

5.2 Analysis of Variance on Normalized IAE Data

An inspection of the normalized IAE curves shows that there are apparent differences between subjects and between tasks, plus a tendency to reduce the error score with training. To check the statistical significance of the apparent changes in the normalized IAE due to training and cut-off frequency, an analysis of variance was run on the error score data from each experiment [40].

The sources of variation were cut-off frequency and days of training. In both analyses the cut-off frequencies were 1, 2 and 4 radians per second. For the first experiment, $Y_C(p) = K_1/p$, the days considered were 2, 4, 6, 8, and 10. For the second experiment, $Y_C(p) = K_2/p^2$, the days considered were 3, 5, 7 and 9. These conditions all used the position control stick.

The results of these two analyses are given in Table 5.2.1. It is seen that in both cases there are significant effects on the normalized IAE due to both training and cut-off frequency. The interaction between these two sources of variation is greater in the K_1/p case than in the K_2/p^2 case. This last point is best understood by looking at the average IAE values given in Figs. 5.1.2 and 5.1.3. In the K_1/p case the curves have more of a tendency to converge with training, than they do in the K_2/p^2 case.

TABLE 5.2.1

ANALYSIS OF VARIANCE OF NORMALIZED IAE

$Y_C(p) = K_1/p$

Source of Variation	Sum of Squares	Degrees of Freedom	Mean Square	F Ratio
Cut-Off Frequency-A	28,622	2	14,311	1076***
Day of Training-B	2,294	4	574	45.15***
A x B	2,693	8	337	25.33***
Within Cell	399	30	13.3	

$Y_C(p) = K_2/p^2$

Source of Variation	Sum of Squares	Degrees of Freedom	Mean Square	F Ratio
Cut-Off Frequency-A	105,684	2	52,842	840***
Day of Training-B	4,537	3	1,512	24***
A x B	991	6	165.2	2.62**
Within Cell	1,509	24	62.9	

*** Significant at 0.01 Level

** Significant at 0.05 Level

5.3 Parameter Tracking Method and Results

To determine the average values of K and τ for each subject at each test condition, the recorded values of $\theta_i(t)$ and $\theta_o(t)$ were played into the parameter tracking system. The gradient gains k_K and k_τ were adjusted empirically so that K(t) and $\tau(t)$ converged exponentially with time constants of about 15-20 seconds. This meant that after the first sixty seconds of each two minute run the parameters K(t) and $\tau(t)$ had fairly well lined out at their final values. At this point in each run an averaging network was automatically activated and the values of K and τ for each run were calculated as

$$K = \frac{1}{60}\int_{60}^{120} K(t)\,dt \qquad (5.3\text{-}1)$$

and

$$\tau = \frac{1}{60}\int_{60}^{120} \tau(t)\,dt \quad . \qquad (5.3\text{-}2)$$

By averaging the results of Eqs. (5.3-1) and (5.3-2) over the five runs at each frequency, the values of K and τ for that frequency, for that subject, for that day were determined. The results of these tests are given in Figs. 5.3.1 to 5.3.6. Typical time histories of K(t) and $\tau(t)$ for different test conditions are given in Appendix D.

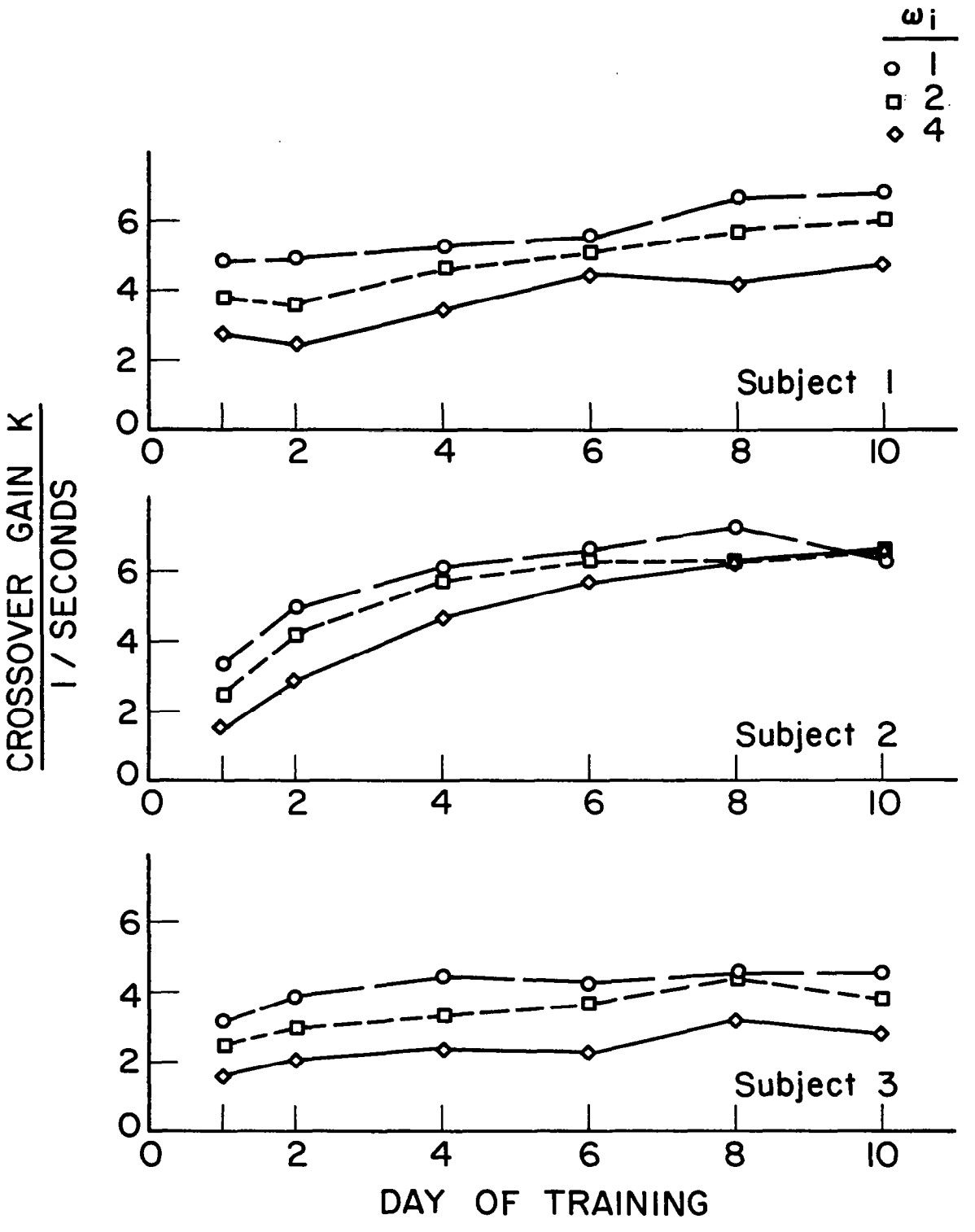

Figure 5.3.1 Individual Crossover Gain Values — $Y_C(p) = K_1/p$.

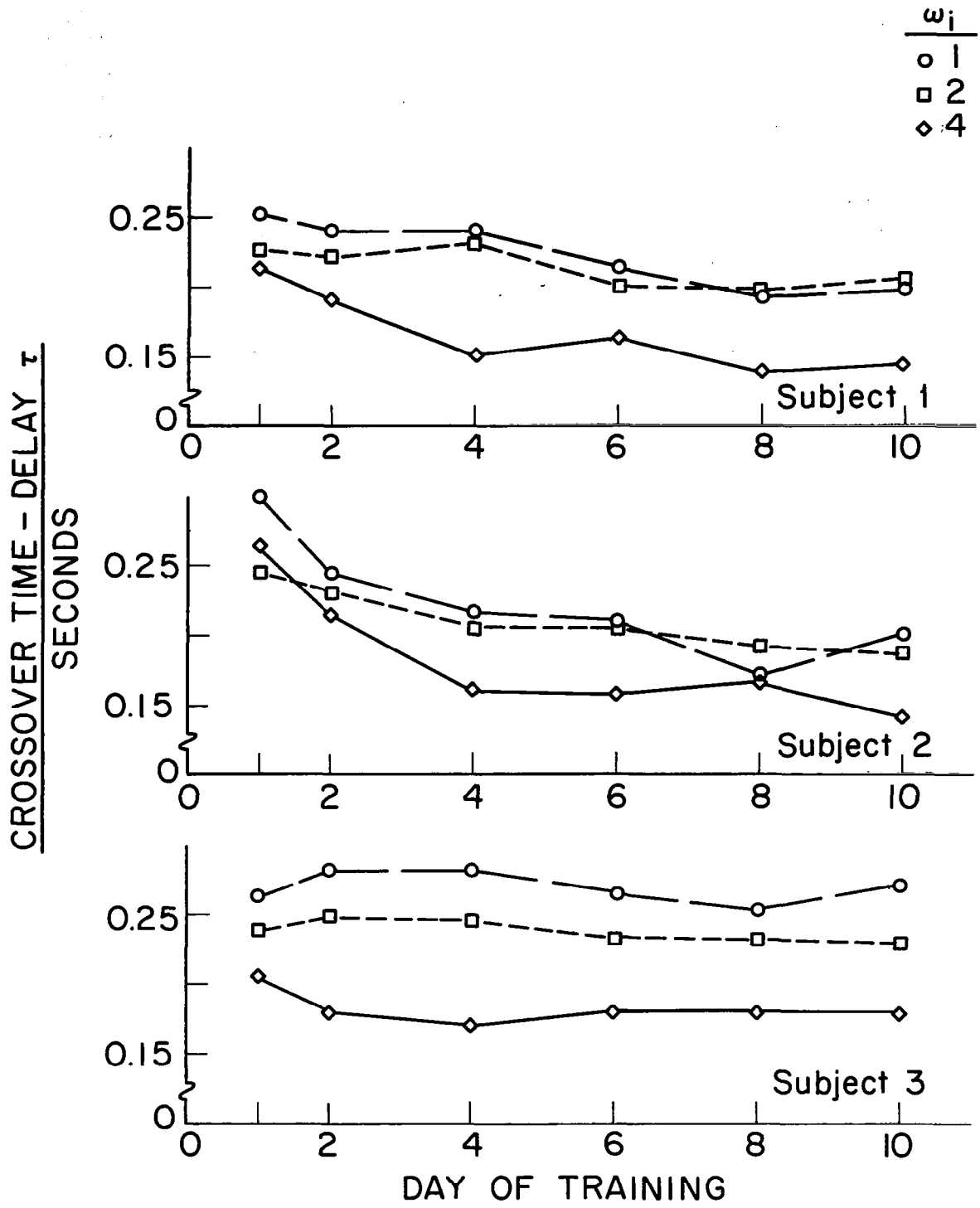

Figure 5.3.2 Individual Crossover Time-Delay Values—
$Y_C(p) = K_1/p$.

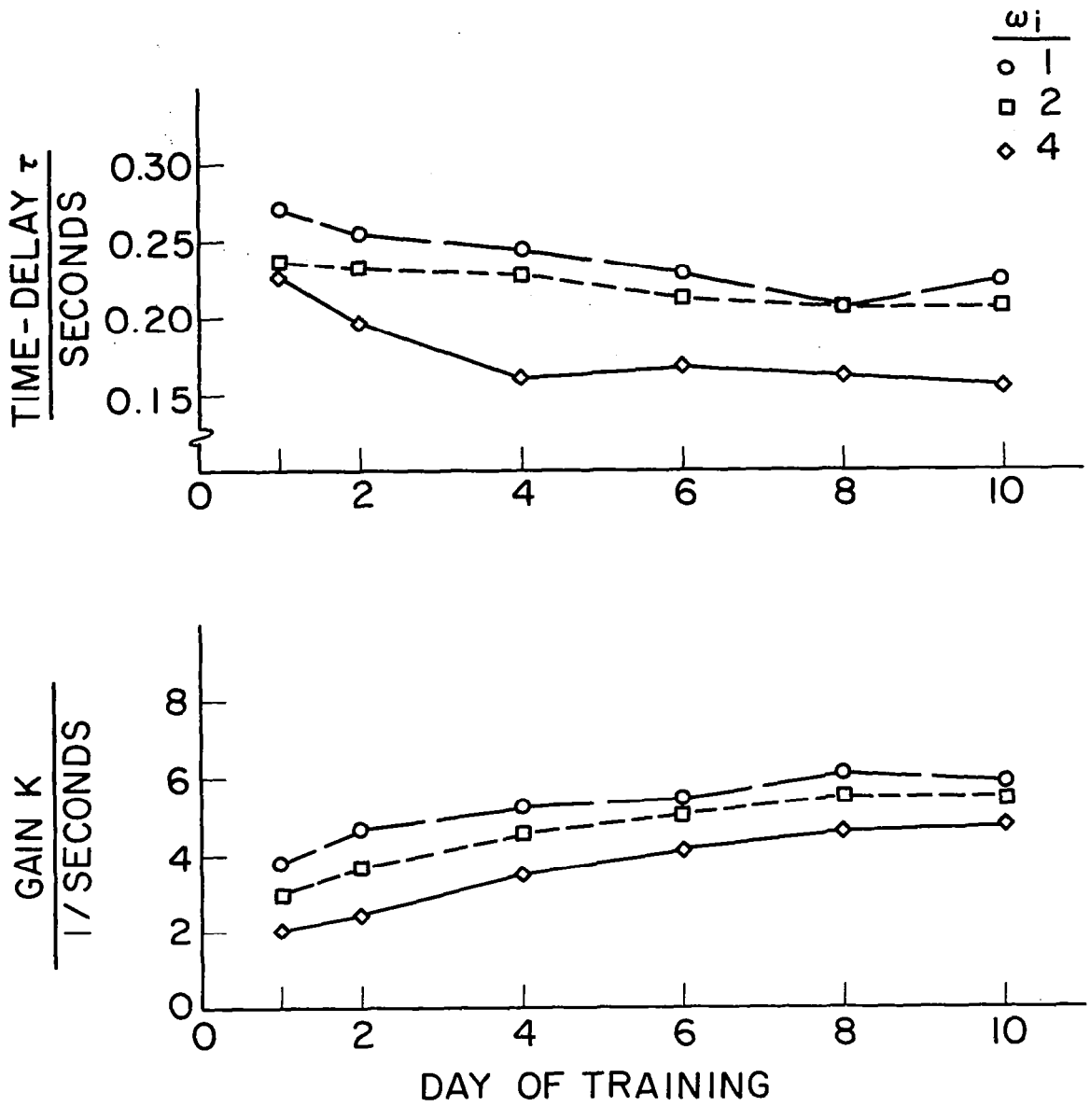

Figure 5.3.3 Crossover Gain and Time-Delay—Average Over Three Subjects—$Y_C(p) = K_1/p$.

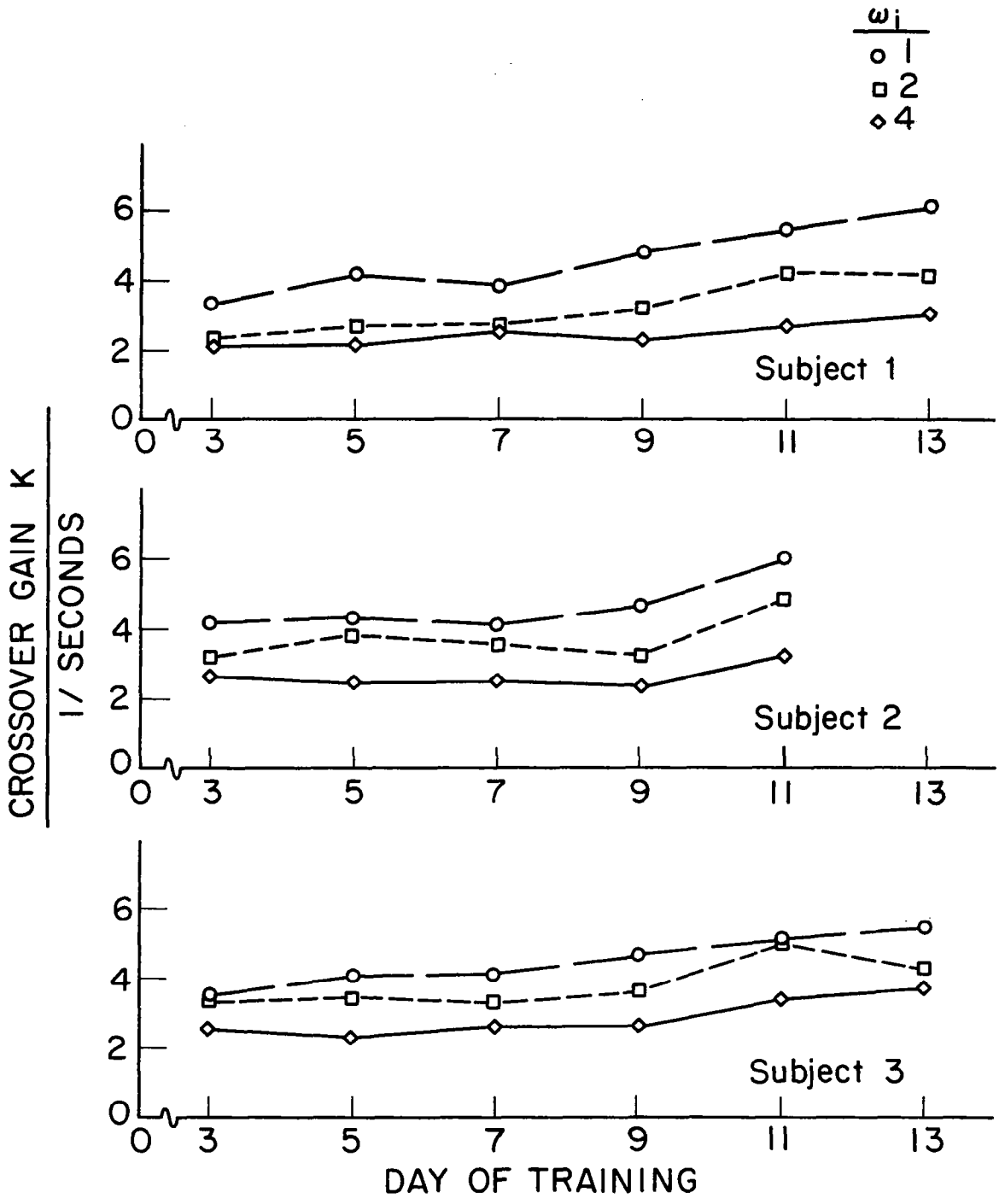

Figure 5.3.4 Individual Crossover Gain Values—$Y_C(p) = K_2/p^2$.

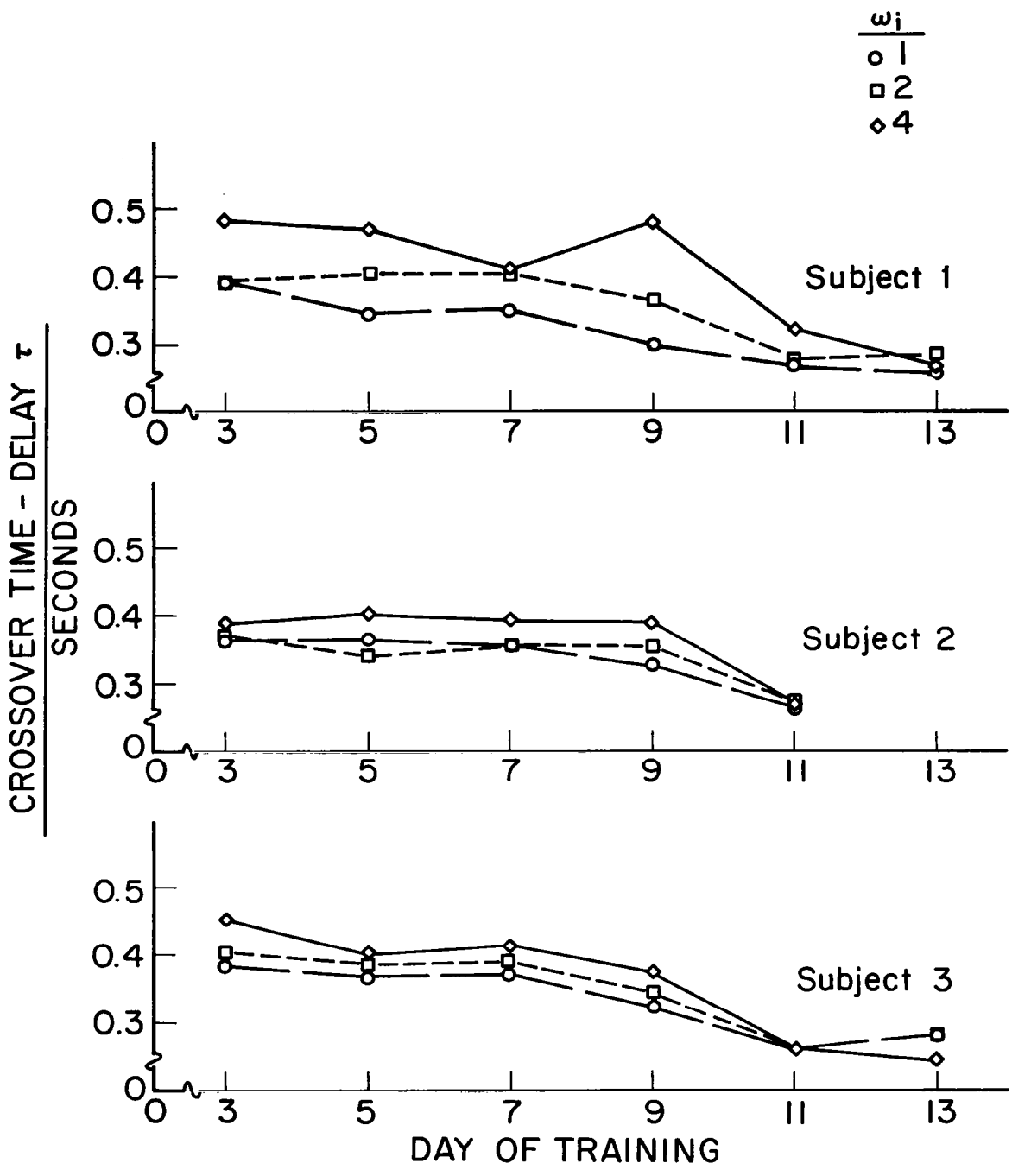

Figure 5.3.5 Individual Crossover Time-Delay Values— $Y_C(p) = K_2/p^2$.

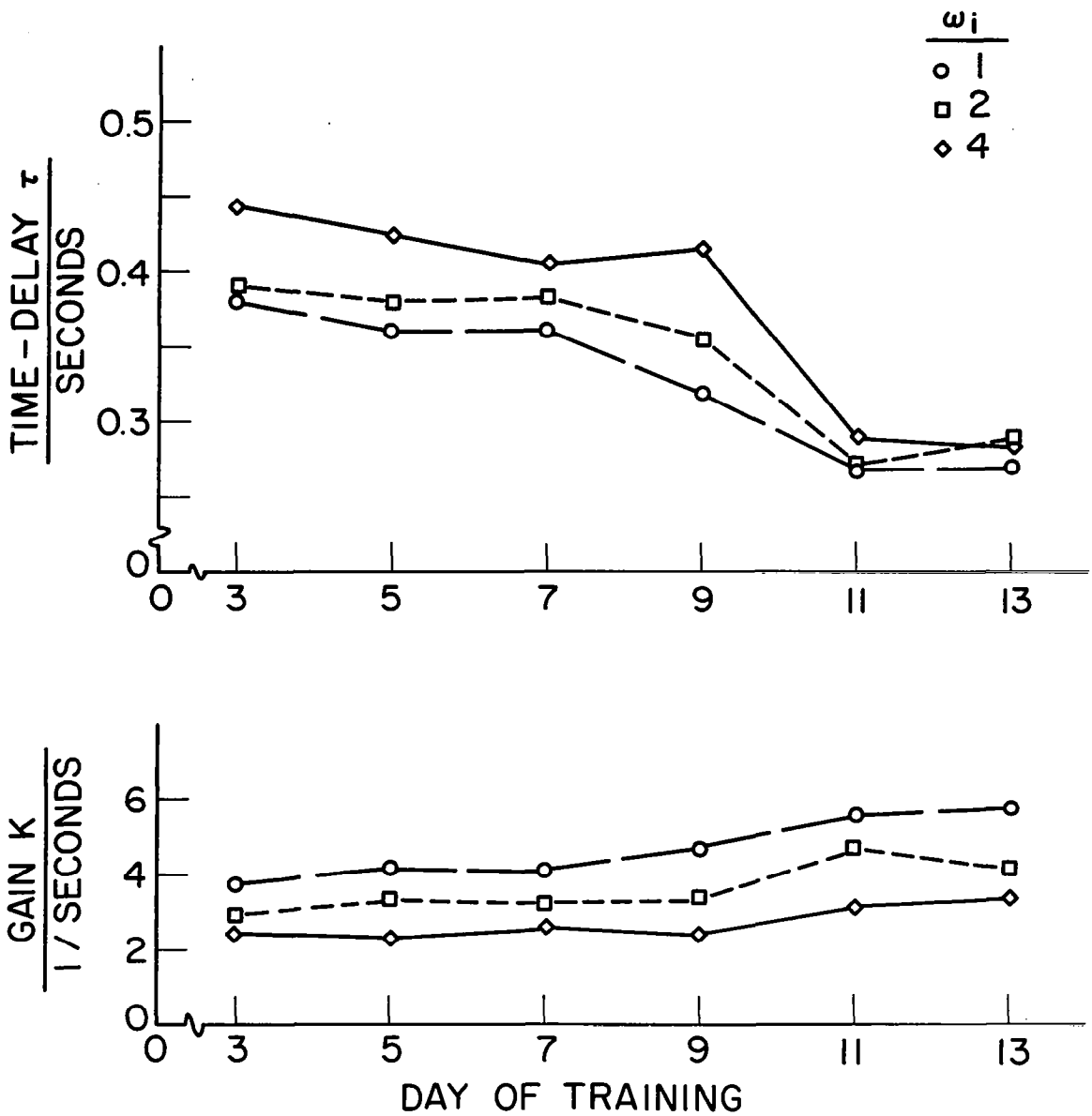

Figure 5.3.6 Crossover Gain and Time-Delay—Average Over Three Subjects—$Y_C(p) = K_2/p^2$.

The subjects tested all exhibit the same general characteristics.

(1) K increases with training.

(2) τ decreases with training.

(3) K decreases with ω_i.

(4) τ decreases with ω_i when $Y_C(p) = K_1/p$, but increases with ω_i when $Y_C(p) = K_2/p^2$.

(5) The differences in the characteristics of the position control stick and the force stick used on days 11-13 on the $Y_C(p) = K_2/p^2$ experiment appear to have a marked effect on K and τ. K is seen to increase and τ to decrease when the force stick is used. (See Fig. 5.3.6)

All these points are evident by inspecting the individual subject data, and also from the data averaged over three subjects. It should be noted that although all subjects had the same general characteristics, the specific values for K and τ at any point in training varied widely between subjects. Also, the rate of change of K and τ with training was greater in some subjects than in others.

By comparing Figs. 5.3.1 to 5.3.6 with Figs. 5.1.2 and 5.1.3, it is found that high gain and low time-delay are associated with low normalized IAE, as might be expected. From a control point of view this merely says that better control exists when K is high and τ is low.

To determine the statistical significance of the apparent changes in K and τ with cut-off frequency and training, two analyses of variance were run on the data from each experiment. The sources of variation were taken as cut-off frequency and training. The cut-off frequencies were 1, 2 and 4 radians per second. In the K_1/p experiment the days taken were 2, 4, 6, 8 and 10. In the K_2/p^2 experiment the days taken were 3, 5, 7 and 9. The results of these analyses are given in Tables 5.3.1 and 5.3.2.

The changes in K and τ due to changes in ω_i are significant at the 0.01 level in all four cases. The effect of training on K is significant at the 0.05 level in experiment one and at the 0.01 level in experiment two. The effect of training on τ is significant at only the 0.1 level in the first experiment, but to the 0.05 level in the second experiment.

The fact that the changes in K and τ are significant at the levels given is a valuable piece of information. This tends to confirm the hypothesis that the crossover model parameters can be used as indices for measuring task difficulty and subject learning rates.

5.4 Comparison of Parameter Tracking Data with McRuer's Data

As was mentioned in Chapter 1, McRuer collected extensive data in the process of arriving at the crossover model. Since McRuer's data [25] is for trained subjects, the only direct comparison that can be made with his data is with the present subjects after training.

TABLE 5.3.1

ANALYSIS OF VARIANCE: $Y_C(p) = \frac{K_1}{p}$

CROSSOVER GAIN, K

Source of Variation	Sum of Squares	Degrees of Freedom	Mean Square	F Ratio
Cut-Off Frequency-A	18.21	2	9.11	5.91***
Day of Training-B	21.13	4	5.28	3.43**
A x B	3.61	8	0.45	< 1
Within Cell	46.22	30	1.54	

CROSSOVER TIME-DELAY, τ

Source of Variation	Sum of Squares	Degrees of Freedom	Mean Square	F Ratio
Cut-Off Frequency-A	0.034	2	0.017	24.286***
Day of Training-B	0.007	4	0.00175	2.50*
A x B	0	8	0	< 1
Within Cell	0.021	30	0.0007	

*** Significant at 0.01 Level

** Significant at 0.05 Level

* Significant at 0.10 Level

TABLE 5.3.2

ANALYSIS OF VARIANCE: $Y_C(p) = \frac{K_2}{p^2}$

CROSSOVER GAIN, K

Source of Variation	Sum of Squares	Degrees of Freedom	Mean Square	F Ratio
Cut-Off Frequency-A	17.55	2	8.78	79.82***
Day of Training-B	1.39	3	0.46	4.81***
A x B	0.57	6	0.09	< 1
Within Cell	2.54	24	0.11	

CROSSOVER TIME-DELAY, τ

Source of Variation	Sum of Squares	Degrees of Freedom	Mean Square	F Ratio
Cut-Off Frequency-A	0.028	2	0.014	16.8***
Day of Training-B	0.008	3	0.0027	3.2**
A x B	0.003	6	0.0005	< 1
Within Cell	0.020	24	0.00083	

*** Significant at 0.01 Level

** Significant at 0.05 Level

In the K_1/p experiment the values of K and τ averaged over the three subjects for day 10 were used. In the K_2/p^2 experiment the values of K and τ averaged over the three subjects on day 9 were used. These were all position control stick runs.

Table 5.4.1 gives the comparison of these two sets of data with McRuer's data. It should be noted that two of McRuer's cut-off frequencies differ by 1/2 radian per second from those used in the present research. In addition, the control sticks and system gains differed in the two sets of data. Also, McRuer used a sum of sinusoids rather than filtered white noise as an input. However, it is still interesting to compare the results.

Considering the small number of subjects, plus the differences in test conditions, no firm statements can be made from a comparison of the two sets of data. There are, however, two apparent differences.

(1) K was found to decrease with an increase in ω_i in the present research. McRuer did not in general find this result, although it was previously noted by Elkind [13].

(2) τ was found to increase with ω_i in the K_2/p^2 experiment in the present research, while McRuer found it to decrease.

Whether these discrepancies are due to individual subject differences or to differences in test conditions, is open to conjecture.

TABLE 5.4.1

AVERAGE CROSSOVER GAIN AND TIME-DELAY VALUES FOR TRAINED SUBJECTS

McRUER'S DATA

$Y_C(p)$	ω_i = 1.5 rad/sec		ω_i = 2.5 rad/sec		ω_i = 4 rad/sec	
	K	τ	K	τ	K	τ
$\frac{K_1}{p}$	4.6	0.24	4.7	0.18	5.0	0.12
$\frac{K_2}{p^2}$	3.2	0.385	3.3	0.335	1.8	0.260

DATA FROM PRESENT RESEARCH

$Y_C(p)$	ω_i = 1 rad/sec		ω_i = 2 rad/sec		ω_i = 4 rad/sec	
	K	τ	K	τ	K	τ
$\frac{K_1}{p}$	5.88	0.224	5.5	0.208	4.78	0.155
$\frac{K_2}{p^2}$	4.7	0.318	3.37	0.356	2.14	0.416

It is believed, however, that the parameter tracking system used in this research gives valid results. These results will be cross-checked in Chapter 6 and shown to be confirmed by spectral analysis.

The data from the present experiments tend to confirm Elkind's position that K does decrease with an increase in ω_i. The change of τ with ω_i appears to depend on $Y_C(p)$ and cannot be simply defined from the two cases studied here.

5.5 Calculation of Power Match

Todosiev has defined an index called Power Match (PM)[34], which he uses to evaluate the assumed model under test. Using the notation of this research, the Power Match for a given run is

$$PM = 1 - \frac{\int_{60}^{120} e^2(t)\,dt}{\int_{60}^{120} \theta_o{}^2(t)\,dt} \quad . \qquad (5.5\text{-}1)$$

A PM = 1.0 means that the assumed model output perfectly matches the compensatory system output. Numbers differ from 1.0 by the power in the model mismatch as a fraction of the output power of the compensatory system.

During the parameter tracking tests, PM was calculated for each

run and the PM values were then averaged over the five runs at each test condition. This gave the average PM value for a particular subject, on a given day, at a given test condition. These values are plotted in Figs. 5.5.1 and 5.5.2.

In most cases the PM values were found to increase with training. This apparently indicates that the model accounts for more output power later in training than it does early in training. It will be shown in Chapter 6 that the subjects act in a more nearly linear manner later in training, and therefore PM values should increase with training. Due to differences in tasks between this research and that conducted by Todosiev, a comparison of PM values would not be very meaningful. It is sufficient to note that the PM values are in the same range, namely $0.6 \leq PM < 1.0$.

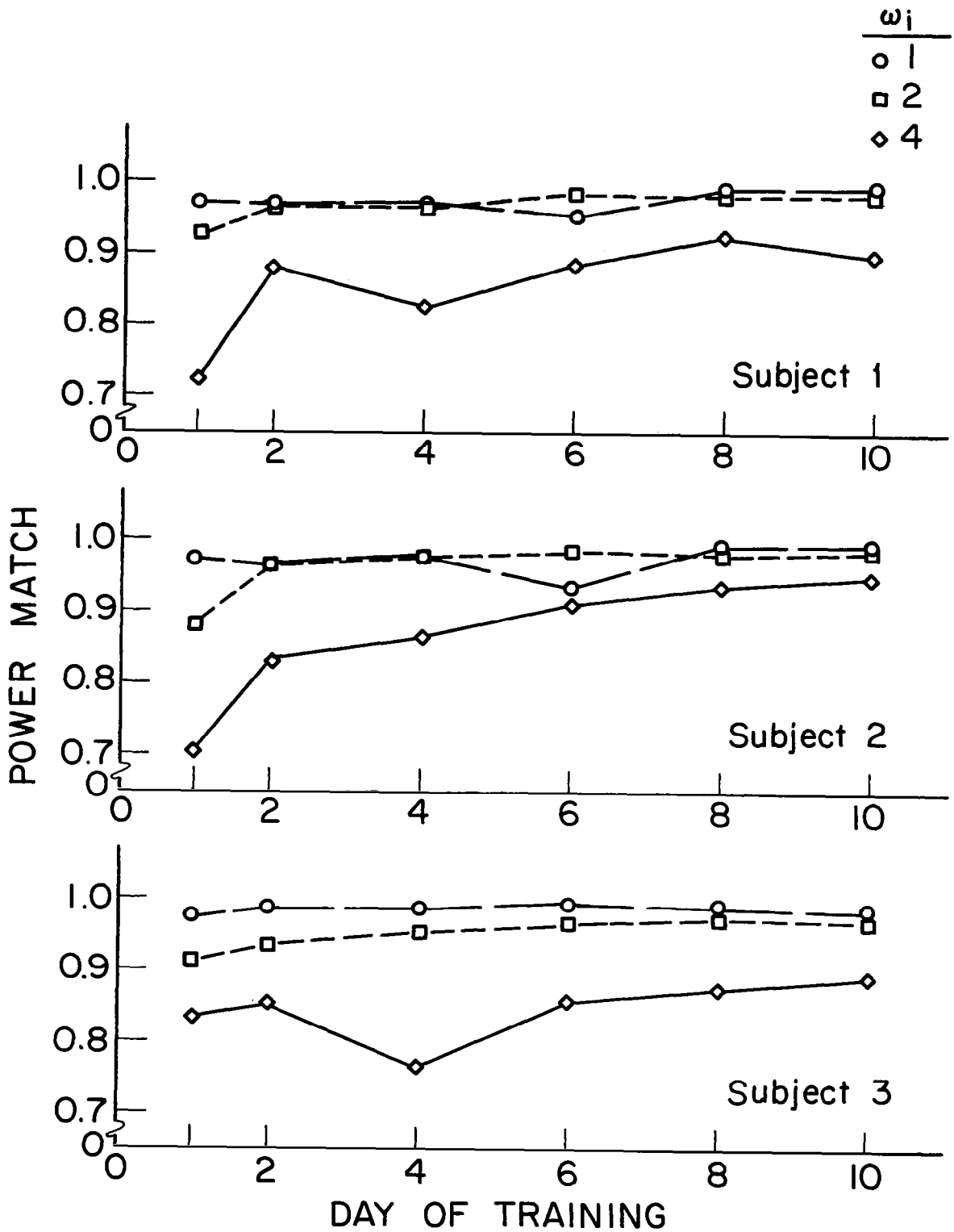

Figure 5.5.1 Individual Power Match Values—$Y_C(p) = K_1/p$.

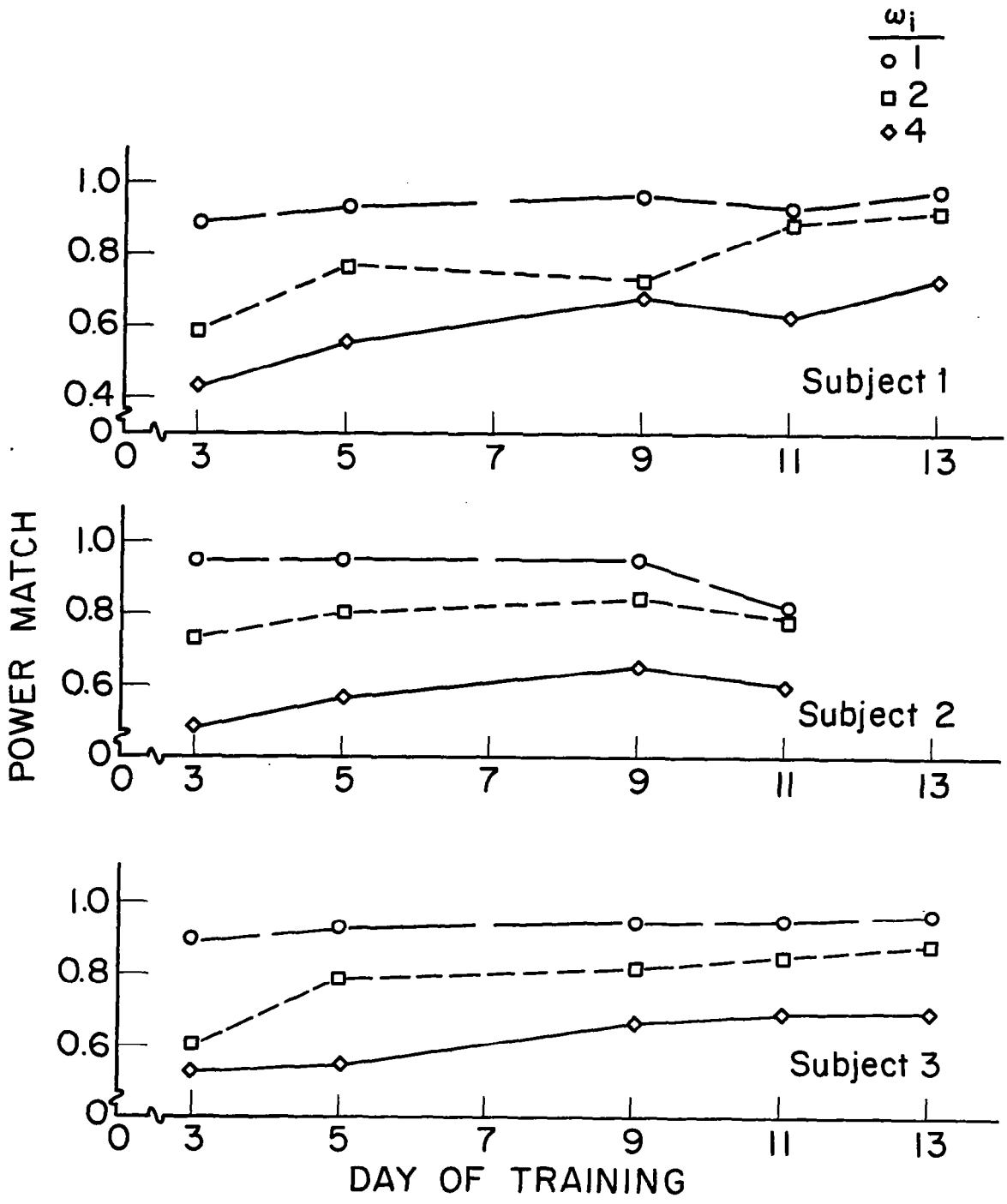

Figure 5.5.2 Individual Power Match Values—$Y_C(p) = K_2/p^2$.

Chapter 6

VERIFICATION OF THE PARAMETER TRACKING RESULTS

The experimental results of Chapter 5 were shown to compare favorably with the average crossover model data determined by McRuer with the notable exceptions that: (1) τ increased with ω_i when $Y_C(p) = K_2/p^2$, rather than decreased as McRuer stated, and (2) K was found to decrease with increases in ω_i, rather than hold constant.

Due to the great variation existing between subjects, a more accurate cross check on the parameter tracking data was desired. This was especially true early in training, since nearly all published data was for trained subjects, with very little information available on the effects of practice on model coefficients [28, 34]. Also, the validity of the crossover model early in training was suspect due to the increases in power match values found in Chapter 5.

To clarify these points, and to verify the parameter values determined by the parameter tracking system, selected data were analyzed using spectral analysis. The verification tests were made on specific subjects, on specific days, and on given test conditions to allow direct comparison with the parameter tracking results.

6.1 Determining $Y_P\, Y_C(j\omega)$ With Spectral Data

In order to properly define the experimental analysis used to determine $Y_P\, Y_C(j\omega)$ with spectral data, the following assumptions and notation are defined:

(1) The compensatory system signals $\theta_i(t)$, $\theta_o(t)$ and $\epsilon(t)$ are assumed to be sample functions of random processes.

(2) For a given subject, on a given day, with a given input frequency and a given controlled element, the random processes from which the sample functions are taken are assumed to be stationary and ergodic [10, 28].

Under these conditions the auto- and cross-correlation and spectral and cross-spectral density functions related to the processes can be defined in a standard manner. The time auto-correlation of $\theta_o(t)$ is

$$R_{oo}(\alpha) = \lim_{T \to \infty} \frac{1}{2T} \int_{-T}^{T} \theta_o(t)\, \theta_o(t + \alpha)\, dt \qquad (6.1\text{-}1)$$

and the spectral density of $\theta_o(t)$ is

$$\Phi_{oo}(j\omega) = \int_{-\infty}^{\infty} R_{oo}(\alpha)\, e^{-j\omega\alpha}\, d\alpha \quad . \qquad (6.1\text{-}2)$$

Similar equations would give $R_{ii}(\alpha)$ and $\Phi_{ii}(j\omega)$ for $\theta_i(t)$.

The cross-correlation function between $\theta_i(t)$ and $\theta_o(t)$ is

$$R_{io}(\alpha) = \lim_{T \to \infty} \frac{1}{2T} \int_{-T}^{T} \theta_i(t)\, \theta_o(t + \alpha)\, dt \qquad (6.1\text{-}3)$$

and the associated cross-spectral density is

$$\Phi_{io}(j\omega) = \int_{-\infty}^{\infty} R_{io}(\alpha)\, e^{-j\omega\alpha}\, d\alpha \quad . \qquad (6.1\text{-}4)$$

Similar equations would give $R_{i\epsilon}(\alpha)$ and $\Phi_{i\epsilon}(j\omega)$.

Using the compensatory system model shown in Fig. 6.1.1, the random input describing function $Y_P\, Y_C(j\omega)$ is by definition [27]

$$Y_P\, Y_C(j\omega) = \frac{\Phi_{is}(j\omega)}{\Phi_{i\epsilon}(j\omega)} \quad . \qquad (6.1\text{-}5)$$

However, since n(t) and S(t) are uncorrelated,

$$\Phi_{is}(j\omega) = \Phi_{io}(j\omega) \quad , \qquad (6.1\text{-}6)$$

$$\Phi_{i\epsilon}(j\omega) = \Phi_{ii}(j\omega) - \Phi_{io}(j\omega) \quad ,$$

and

$$Y_P\, Y_C(j\omega) = \frac{\Phi_{io}(j\omega)}{\Phi_{ii}(j\omega) - \Phi_{io}(j\omega)} \quad . \qquad (6.1\text{-}7)$$

This is the computational form that was used.

In the ideal case where all of the spectral densities are known

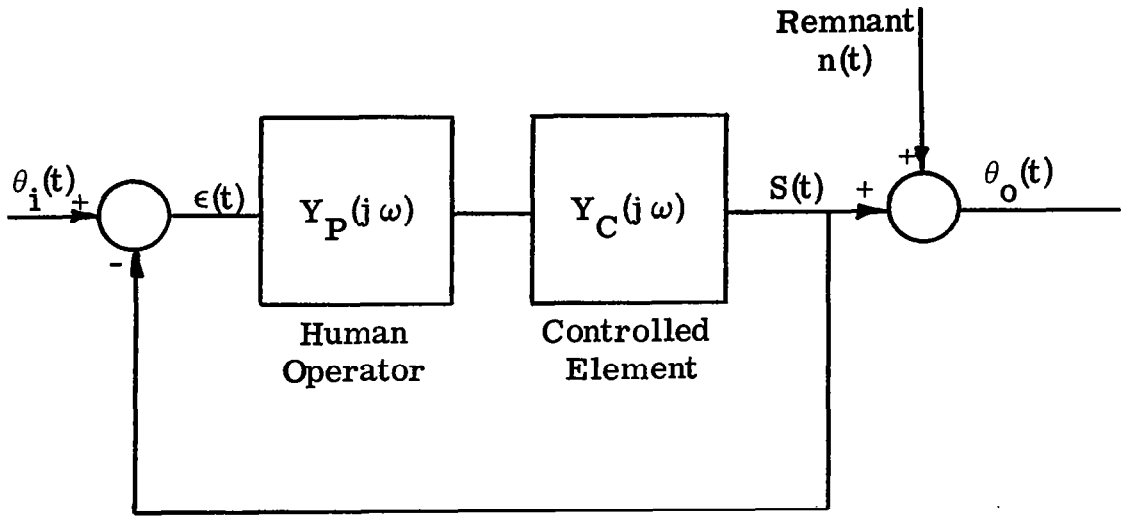

$$Y_P(j\omega) = Y_P(j\omega,\ Y_C,\ \theta_i)$$

= Human operator describing function.

Figure 6.1.1 Modified Describing Function Block Diagram of the Compensatory System.

exactly, Eq. (6.1-7) can be solved directly to determine $Y_P\, Y_C(j\omega)$. In practice the desired densities must be estimated using finite length sample functions from the random processes involved. The estimation procedures used in this report are explained below.

During each two minute compensatory tracking run $\theta_i(t)$ and $\theta_o(t)$ were recorded for every subject. The two signals were recorded simultaneously on magnetic tape in analog form. The five pairs of samples taken each day at each test condition were identified as

$$\theta_{iq}(t) \text{ and } \theta_{oq}(t), \qquad q = 1, \ldots, 5 \quad . \tag{6.1-8}$$

From each pair of these sample functions the approximate autocorrelation and spectral density functions were defined as [9]

$$C_{ooq}(\alpha) = \frac{W(\alpha)}{T_n - \alpha} \int_0^{T_n - \alpha} \theta_{oq}(t)\, \theta_{oq}(t + \alpha)\, dt \quad , \tag{6.1-9}$$

and

$$\phi_{ooq}(j\omega) = 2 \int_0^{T_m} C_{ooq}(\alpha)\, e^{-j\omega\alpha}\, d\alpha \tag{6.1-10}$$

$$2 \text{ min} \geq T_n > T_m \geq \alpha \geq 0$$

where $W(\alpha)$ is a smoothing function described in Appendix E. Similar equations were used to find $C_{iiq}(\alpha)$ and $\phi_{iiq}(j\omega)$. Also, the approximate

cross-correlation and cross-spectral density functions are defined as

$$C_{ioq}(\alpha) = \frac{W(\alpha)}{2(T_n - |\alpha|)} \int_{-T_n + |\alpha|}^{T_n - |\alpha|} \theta_{iq}(t)\, \theta_{oq}(t + \alpha)\, dt \quad (6.1\text{-}11)$$

and

$$\phi_{ioq}(j\omega) = \int_{-T_m}^{T_m} C_{ioq}(\alpha)\, e^{-j\omega\alpha}\, d\alpha \quad . \quad (6.1\text{-}12)$$

$$2 \min \geq T_n > T_m \geq |\alpha| \geq 0$$

The average values of the approximate density functions over the five samples were used as the estimators of the true densities for that condition.

$$\hat{\Phi}_{ii}(j\omega) = \frac{1}{5} \sum_{q=1}^{5} \phi_{iiq}(j\omega)$$

$$\hat{\Phi}_{oo}(j\omega) = \frac{1}{5} \sum_{q=1}^{5} \phi_{ooq}(j\omega) \quad (6.1\text{-}13)$$

$$\hat{\Phi}_{io}(j\omega) = \frac{1}{5} \sum_{q=1}^{5} \phi_{ioq}(j\omega) \quad .$$

These values were in turn used to estimate Eq. (6.1-7).

$$\widehat{Y_P\, Y_C}(j\omega) = \frac{\hat{\Phi}_{io}(j\omega)}{\hat{\Phi}_{ii}(j\omega) - \hat{\Phi}_{io}(j\omega)} \quad . \qquad (6.1\text{-}14)$$

It should be noted that all of the spectral calculations were done numerically with integrations replaced by the appropriate summations. The programmed equations are given in Appendix E.

Due to the amount of computer time needed for complete spectral analysis, only a limited amount of the compensatory tracking data was analyzed spectrally. From the K_1/p experiment, data from Subject 1 on days 1, 2, 6 and 10 were analyzed. From the K_2/p^2 experiment, data from Subject 3 on days 3, 5, 9 and 13 were analyzed. These subjects were chosen simply because their parameter tracking data were considered "typical".

For each day $\left|Y_P\, Y_C(j\omega)\right|$ and arg $Y_P\, Y_C(j\omega)$ were calculated for each input frequency. These values were then plotted in the standard manner as gain-phase plots on semi-log paper. On the same graphs the forward loop gain and phase curves of the assumed crossover model were plotted with K and τ set at the average values determined by the parameter tracking system. This provides a direct visual comparison of the same data analyzed by the two entirely different methods.

As mentioned previously, all spectral calculations were made

numerically. It was discovered that when ω_i was one radian per second the spectral densities in the crossover region could not be calculated accurately. The compensatory system input power was so low in this region that the computer program could not accurately perform the desired calculations. The input power in these cases was down well over 30db. For this reason only the 2 and 4 radians per second data are presented. These results are given in Figs. 6.1.2 through 6.1.17.

In all but two instances the match between the spectral and parameter tracking data is exceptionally good in the region of crossover. In most cases a better fit to the spectral data could not have been obtained if a manual curve fitting of the data had been made. These results lend confidence to the validity of the parameter tracking system and the form of the crossover model being used.

There are only two cases where there is a questionable discrepancy between the two methods. These are in the phase curves of Figs. 6.1.4 and 6.1.5.

The discrepancies in the phase curves of these two cases can be attributed to the fact that the input power in the region of crossover is too low to allow accurate parameter tracking. In Fig. 6.1.4 $|\theta_i(j\omega)|$ is down 24db at crossover, while in Fig. 6.1.5 it is down 28db at crossover. These are the only two cases where the input power at

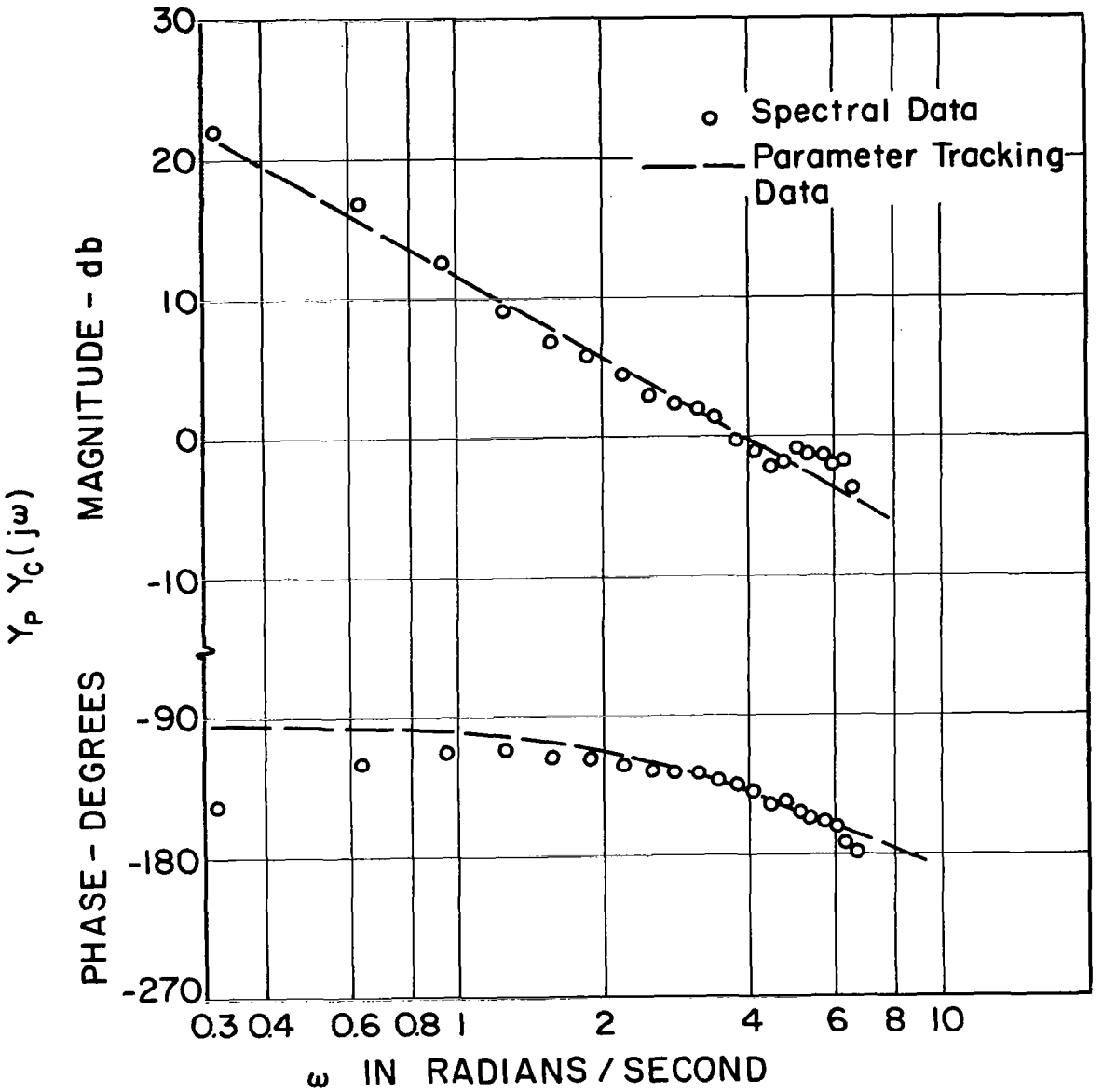

Figure 6.1.2 Comparison of Spectral and Parameter Tracking Tests. Subject 1—Day 1—$Y_C(p) = K_1/p$—ω_i = 2 radians/second.

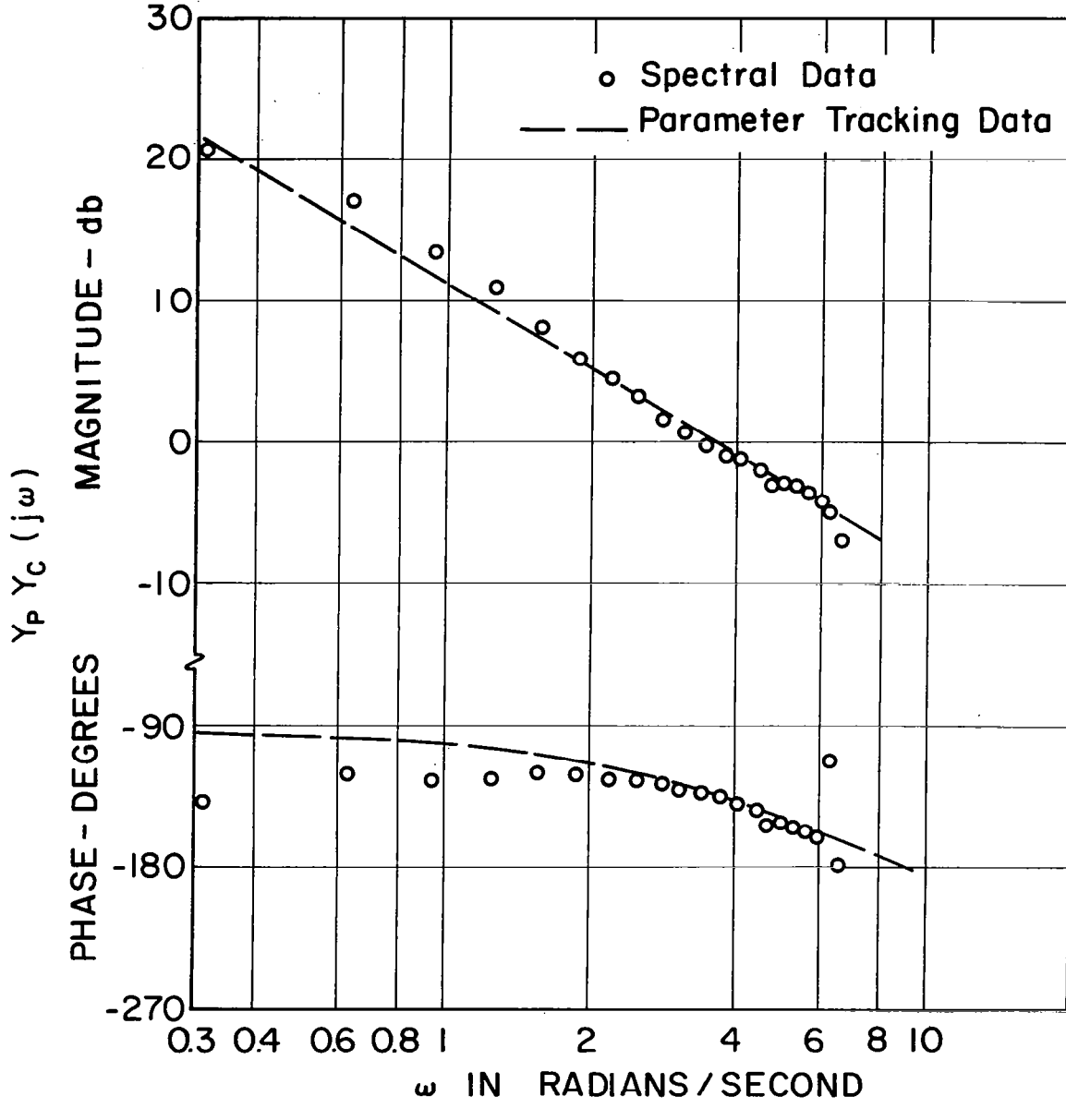

Figure 6.1.3 Comparison of Spectral and Parameter Tracking Tests. Subject 1—Day 2—$Y_C(p) = K_1/p$—ω_i = 2 radians/second.

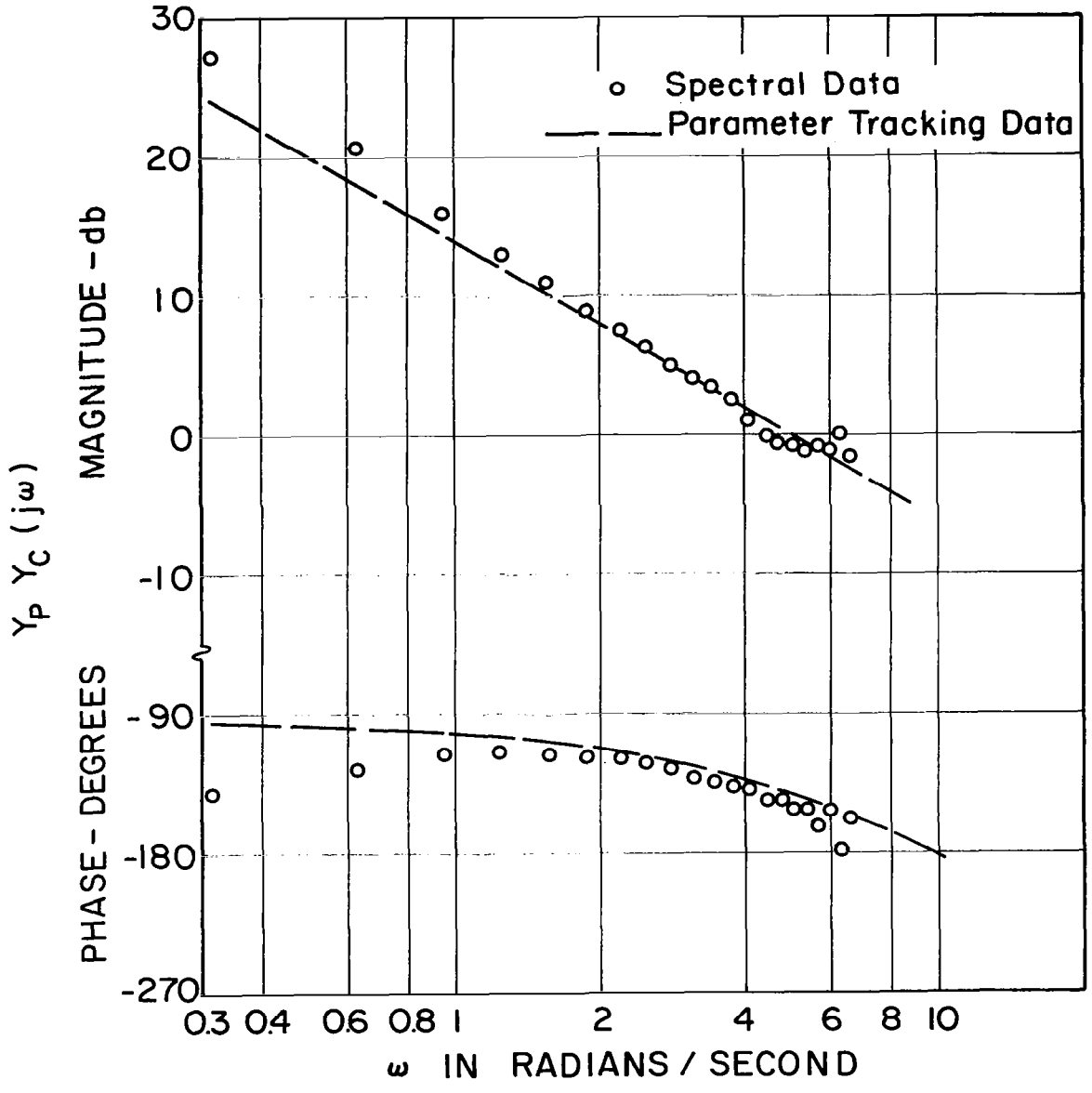

Figure 6.1.4 Comparison of Spectral and Parameter Tracking Tests. Subject 1—Day 6—$Y_C(p) = K_1/p$—$\omega_i = 2$ radians/second.

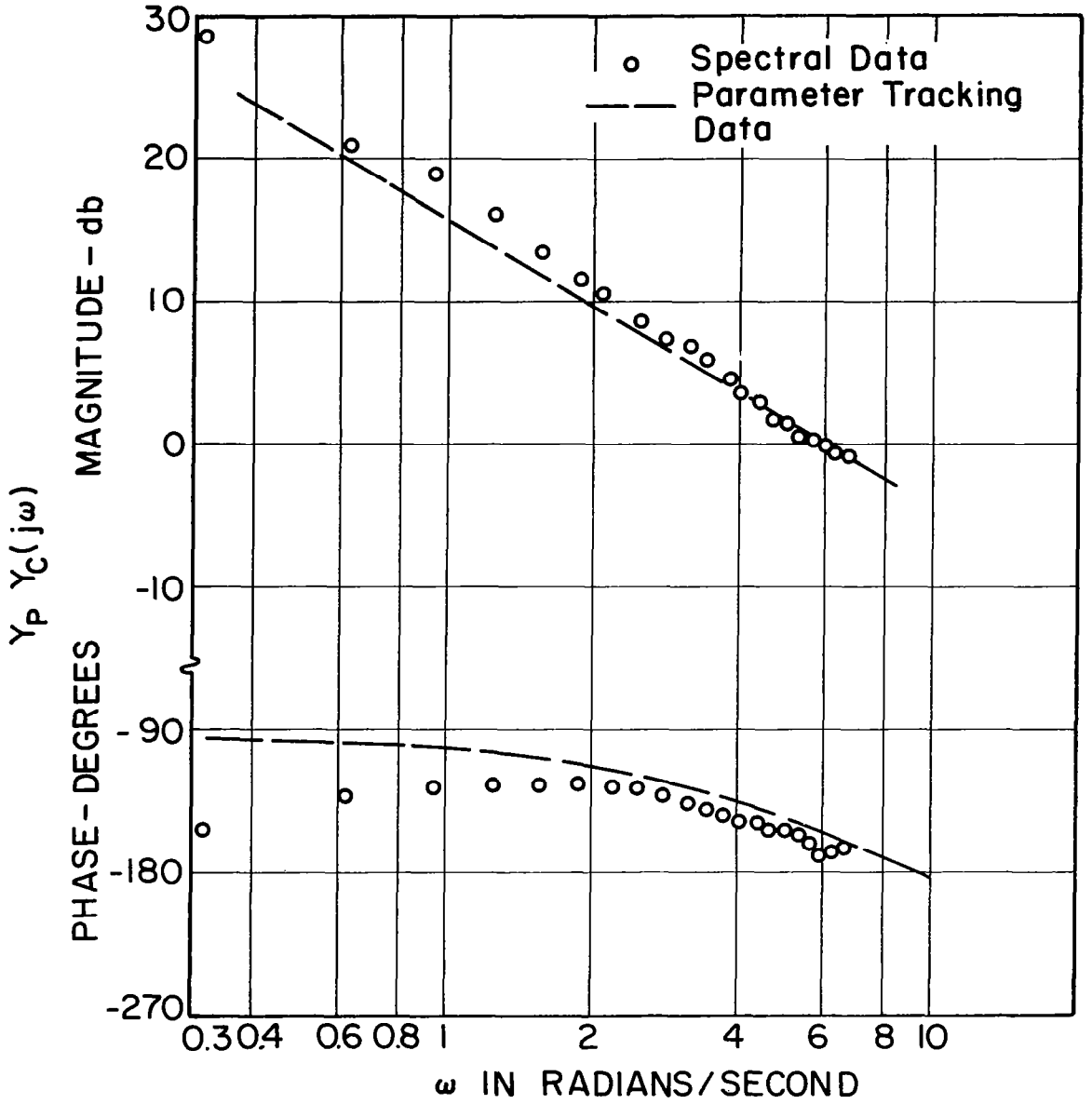

Figure 6.1.5 Comparison of Spectral and Parameter Tracking Tests. Subject 1—Day 10—$Y_C(p) = K_1/p$—ω_i = 2 radians/second.

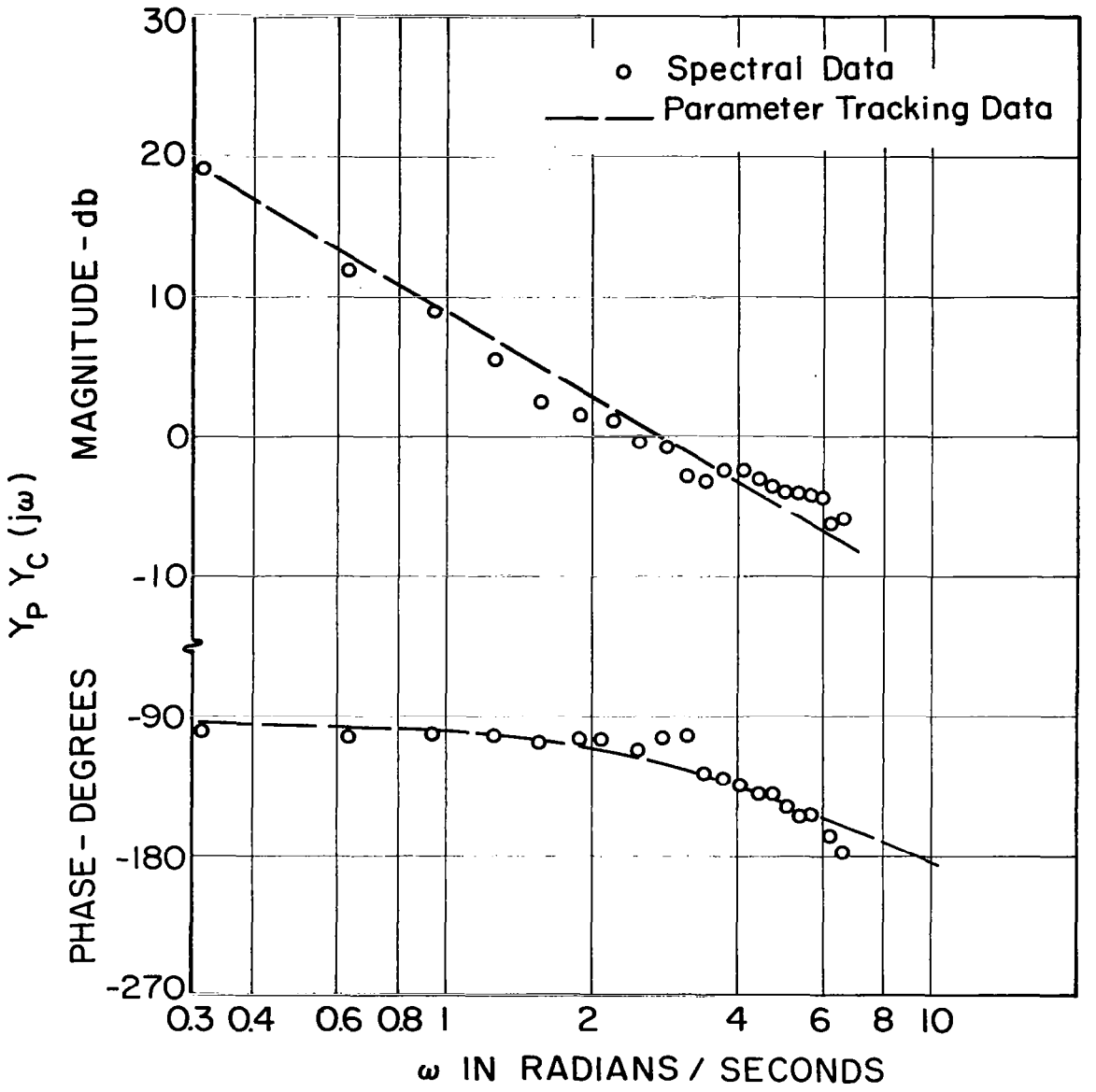

Figure 6.1.6 Comparison of Spectral and Parameter Tracking Tests. Subject 1—Day 1—$Y_C(p) = K_1/p$—ω_i = 4 radians/second.

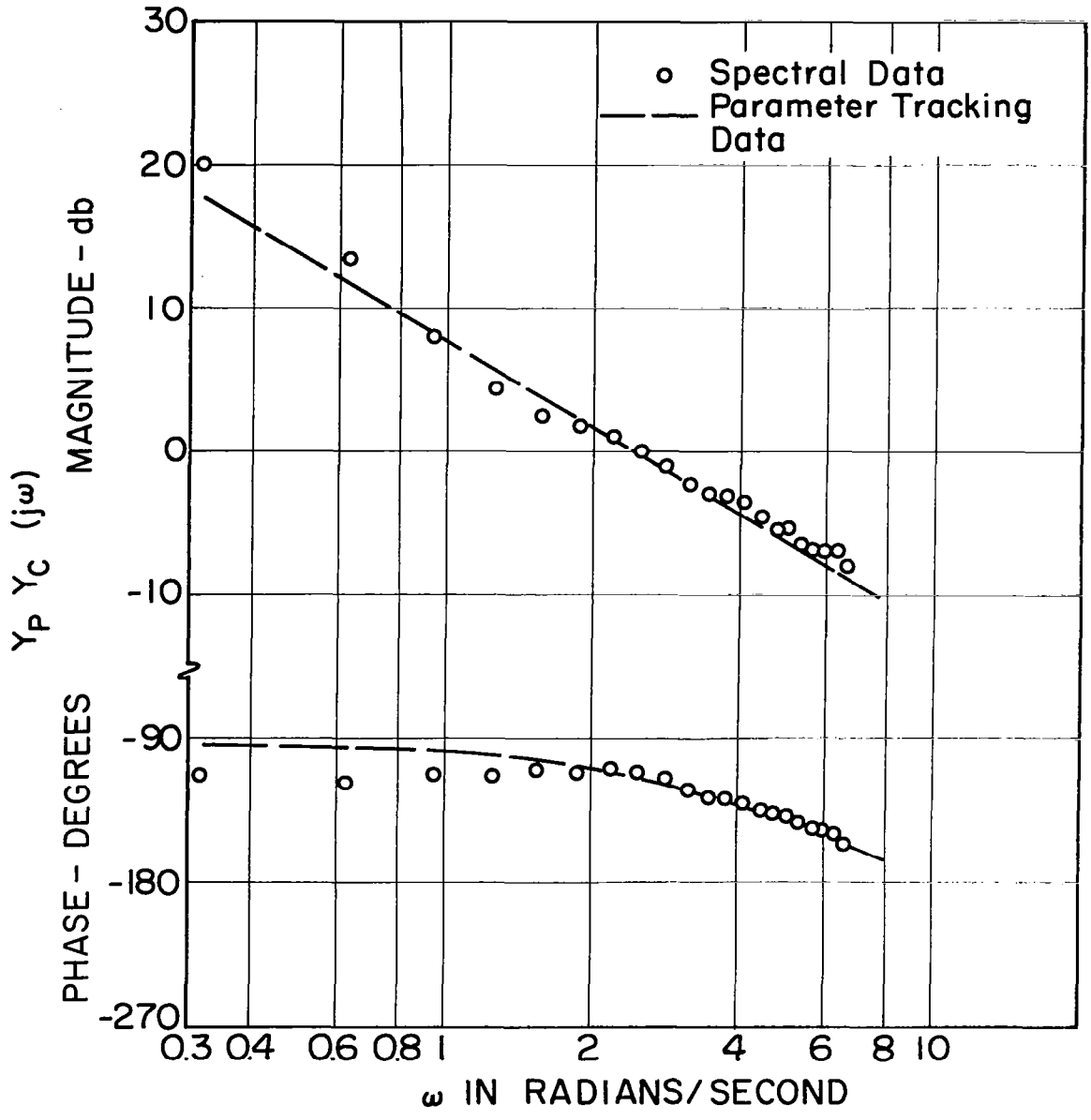

Figure 6.1.7 Comparison of Spectral and Parameter Tracking Tests. Subject 1—Day 2—$Y_C(p) = K_1/p$—ω_i = 4 radians/second.

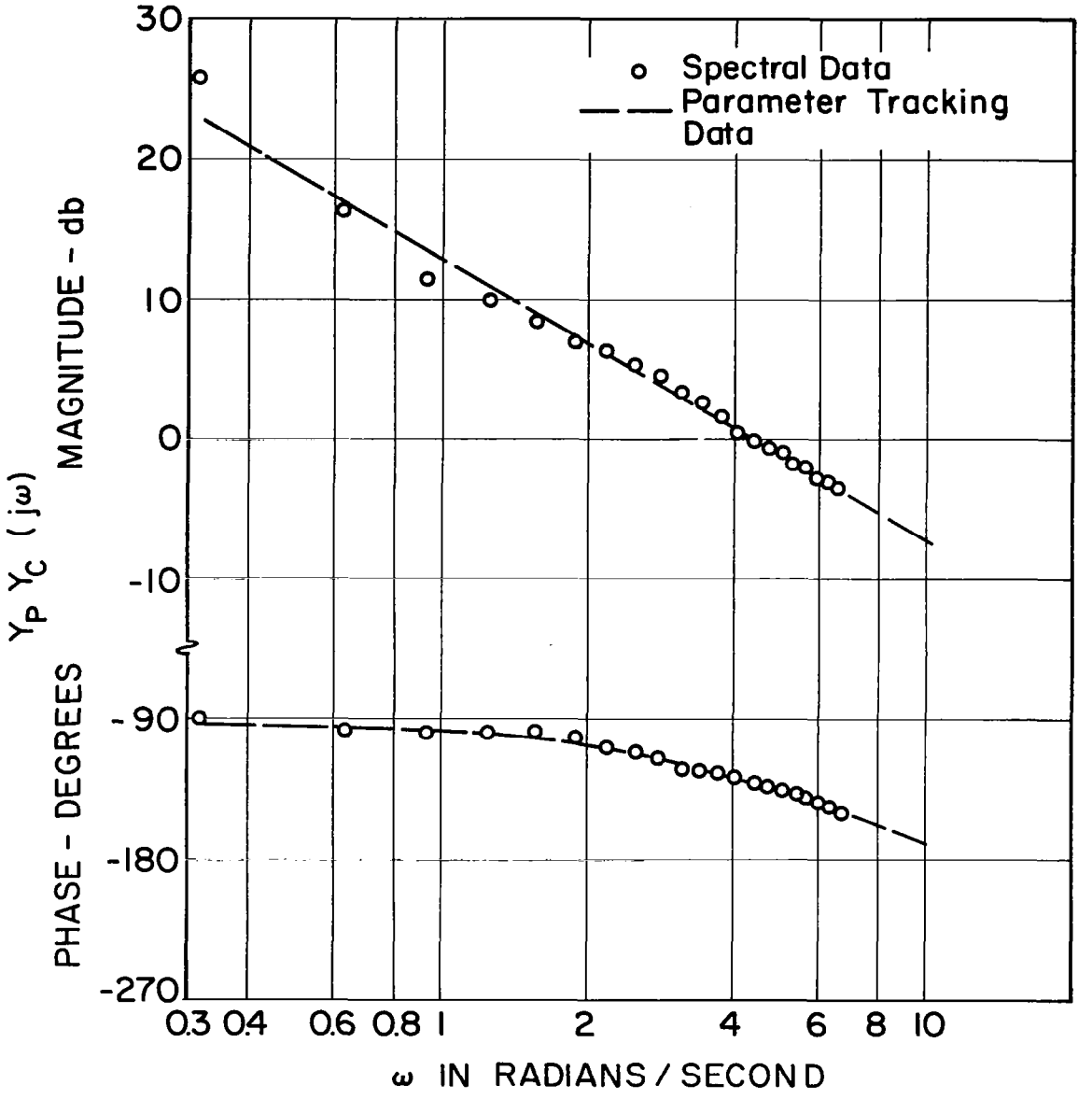

Figure 6.1.8 Comparison of Spectral and Parameter Tracking Tests. Subject 1—Day 6—$Y_C(p) = K_1/p$—ω_i = 4 radians/second.

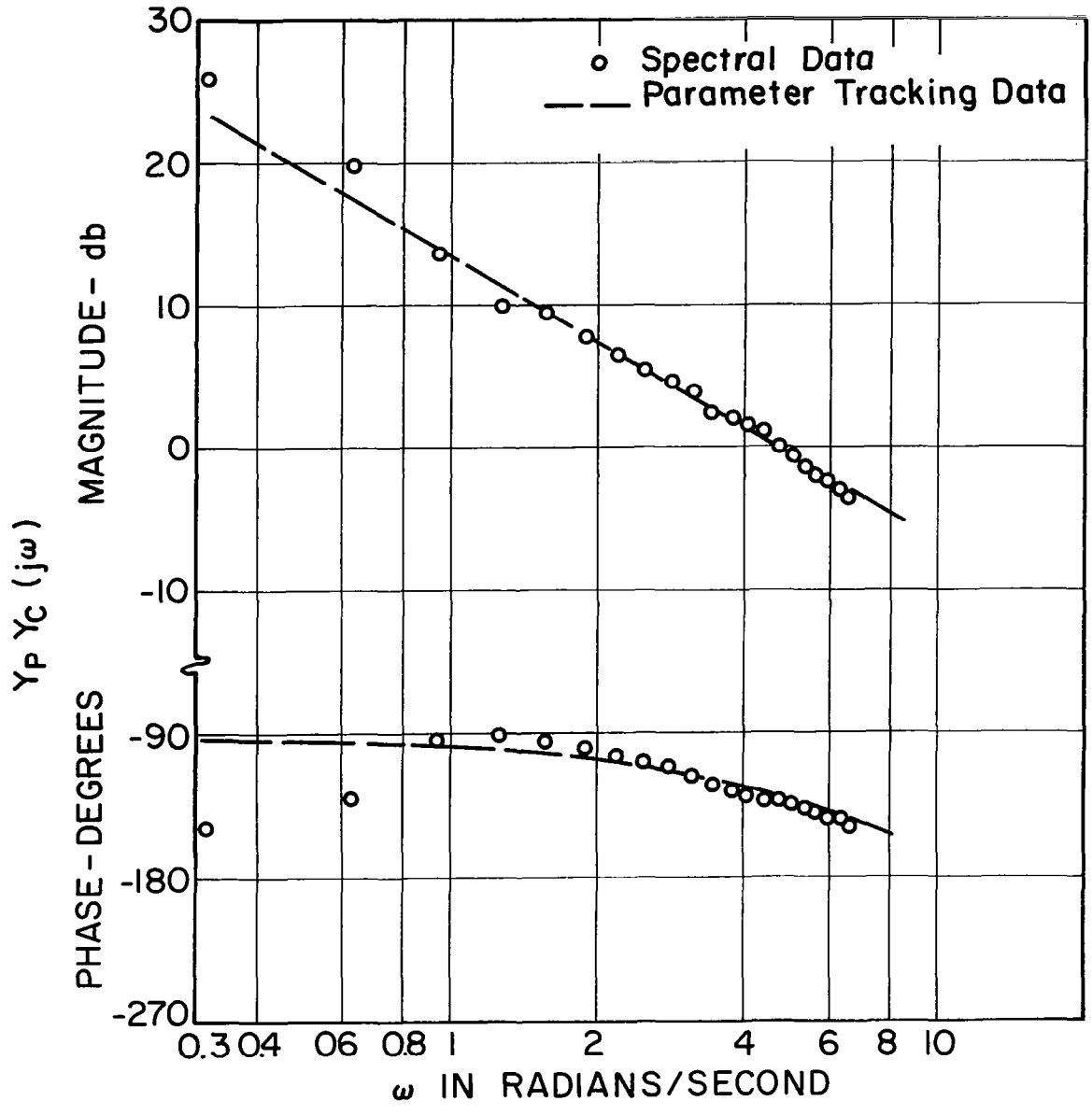

Figure 6.1.9 Comparison of Spectral and Parameter Tracking Tests. Subject 1—Day 10—$Y_C(p) = K_1/p$—ω_i = 4 radians/second.

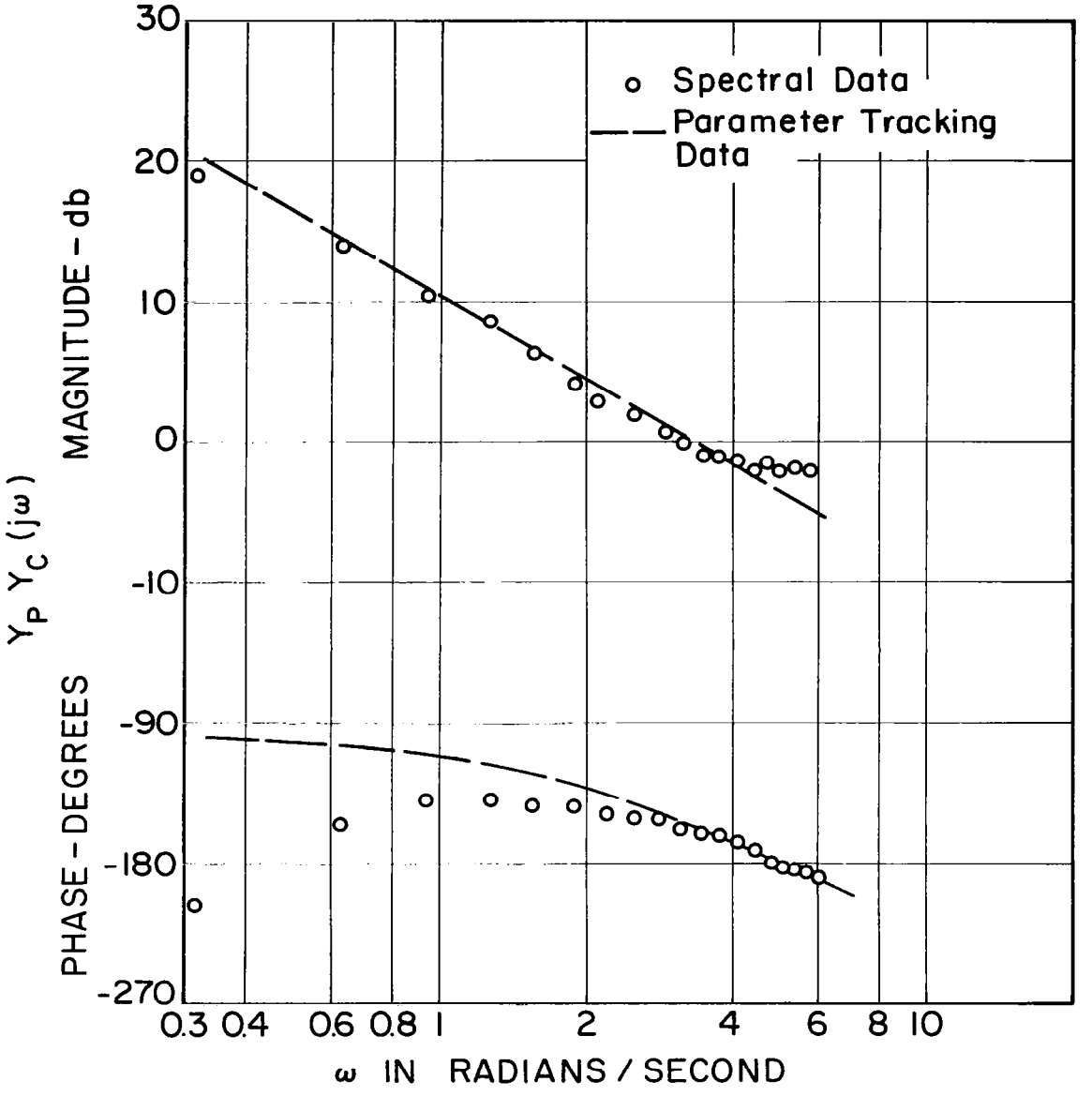

Figure 6.1.10 Comparison of Spectral and Parameter Tracking Tests. Subject 3—Day 3—$Y_C(p) = K_2/p^2$—ω_i = 2 radians/second.

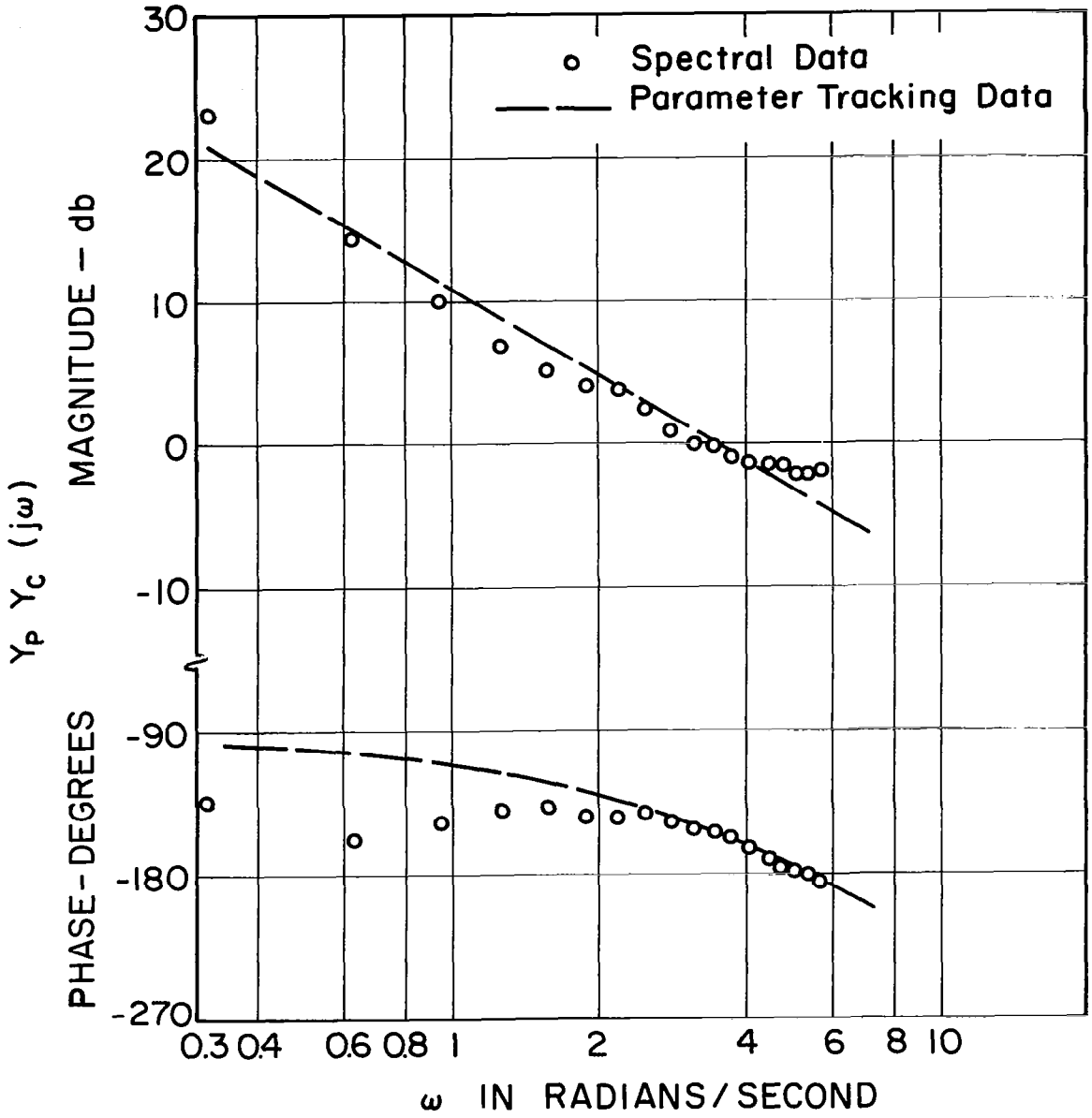

Figure 6.1.11 Comparison of Spectral and Parameter Tracking Tests. Subject 3 — Day 5 — $Y_C(p) = K_2/p^2$ — ω_i = 2 radians/second.

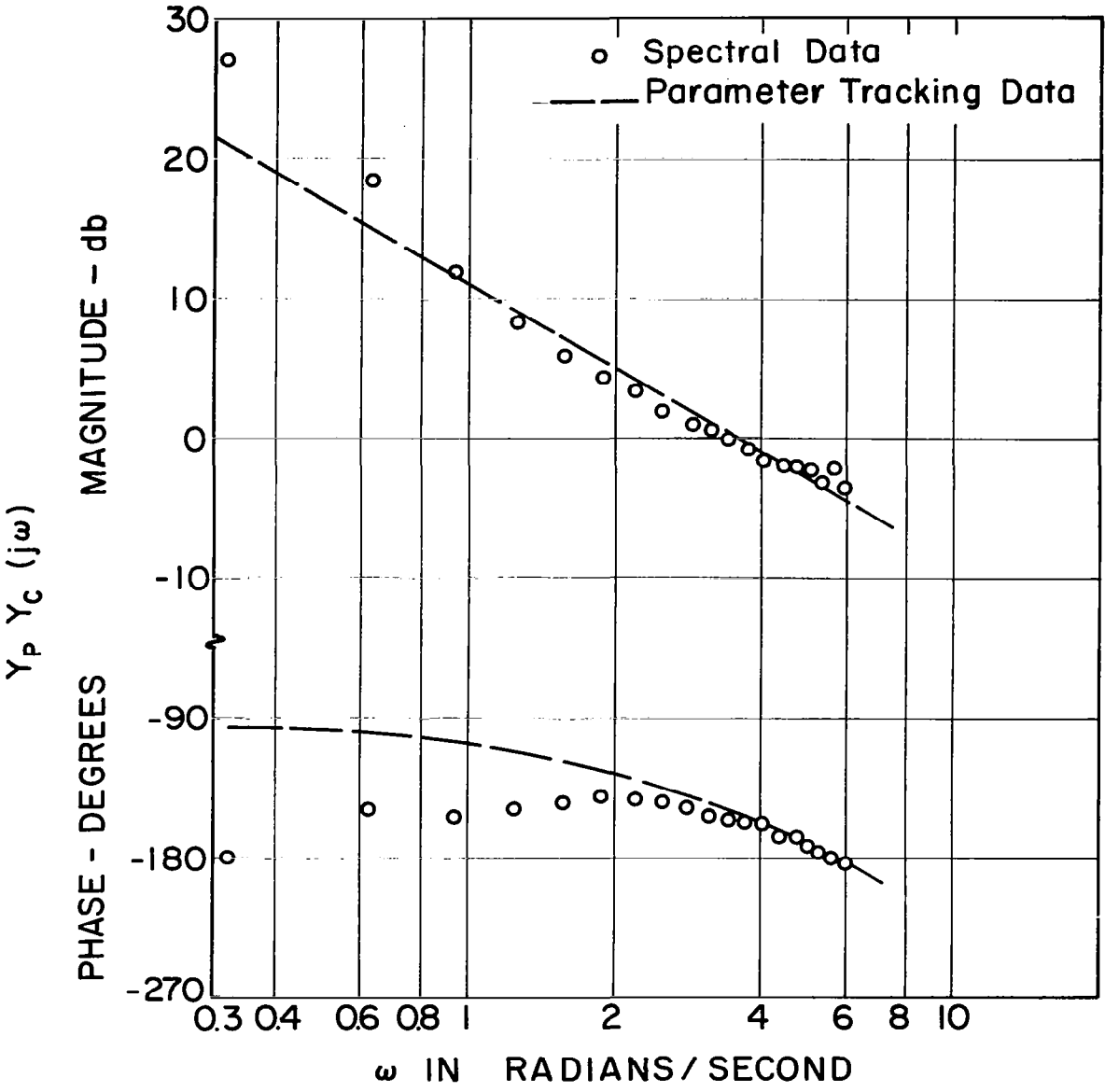

Figure 6.1.12 Comparison of Spectral and Parameter Tracking Tests. Subject 3—Day 9—$Y_C(p) = K_2/p^2$—ω_i = 2 radians/second.

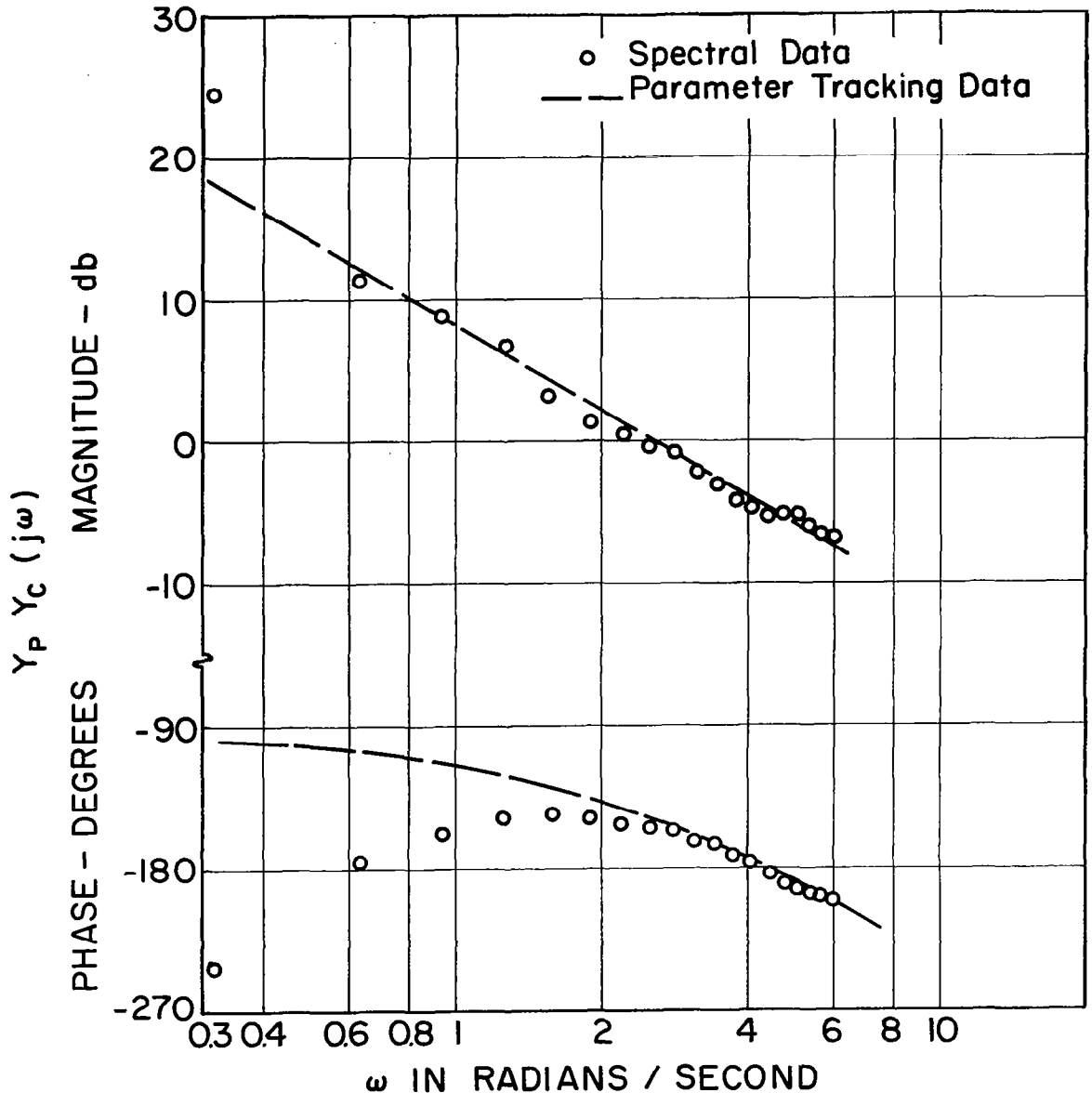

Figure 6.1.13 Comparison of Spectral and Parameter Tracking Tests. Subject 3—Day 3—$Y_C(p) = K_2/p^2$—ω_i = 4 radians/second.

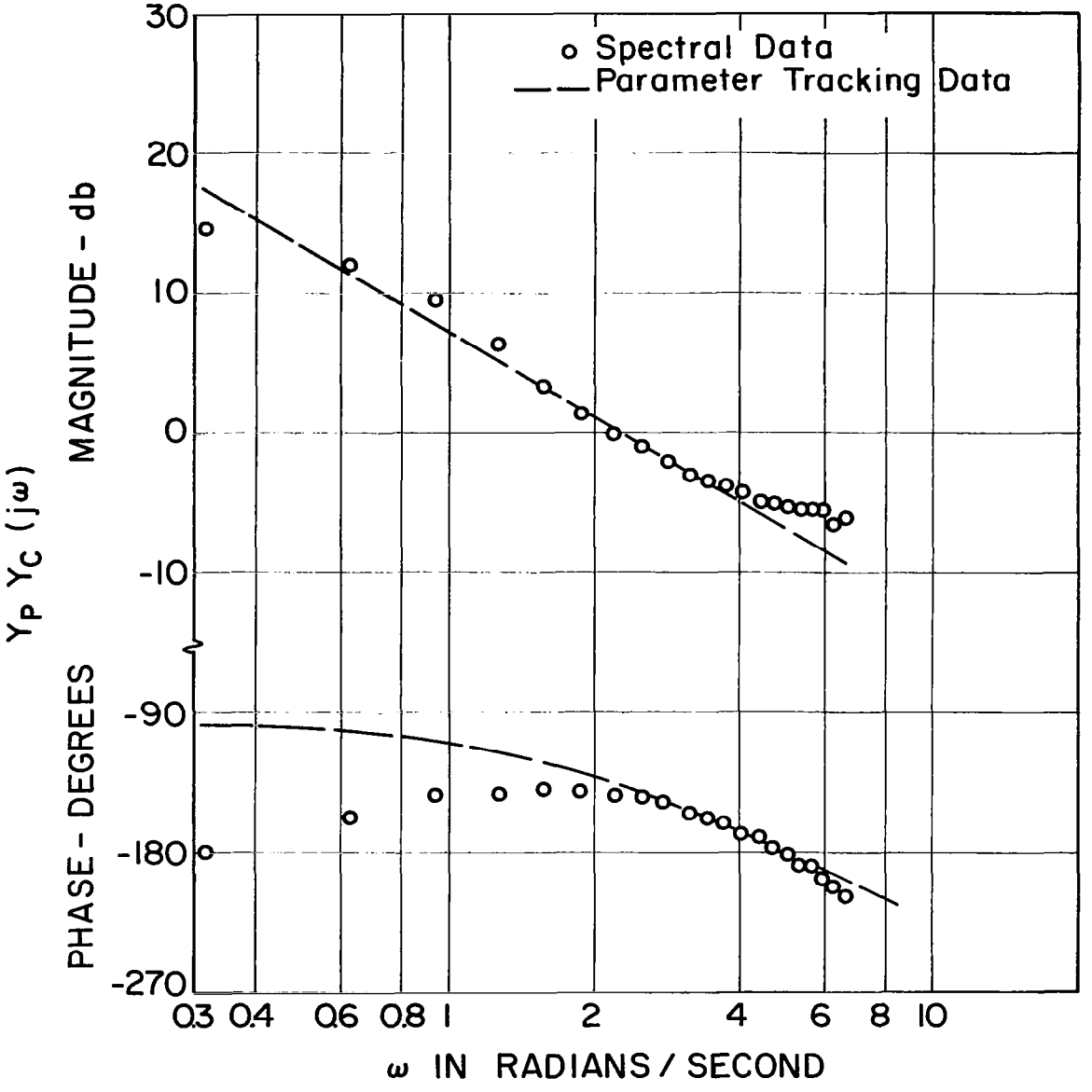

Figure 6.1.14 Comparison of Spectral and Parameter Tracking Tests. Subject 3—Day 5—$Y_C(p) = K_2/p^2$—ω_i = 4 radians/second.

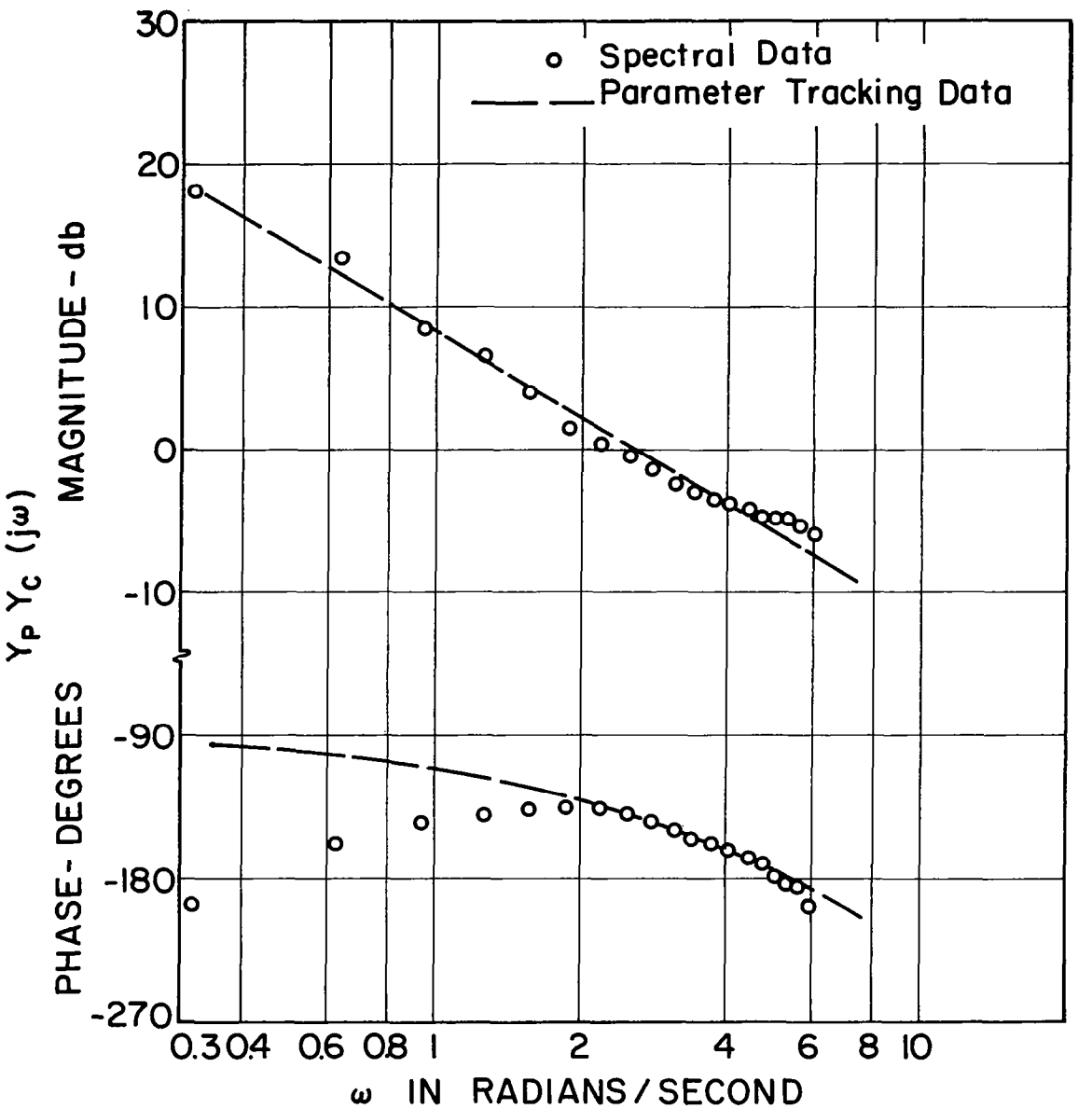

Figure 6.1.15 Comparison of Spectral and Parameter Tracking Tests. Subject 3—Day 9—$Y_C(p) = K_2/p^2$—ω_i = 4 radians/second.

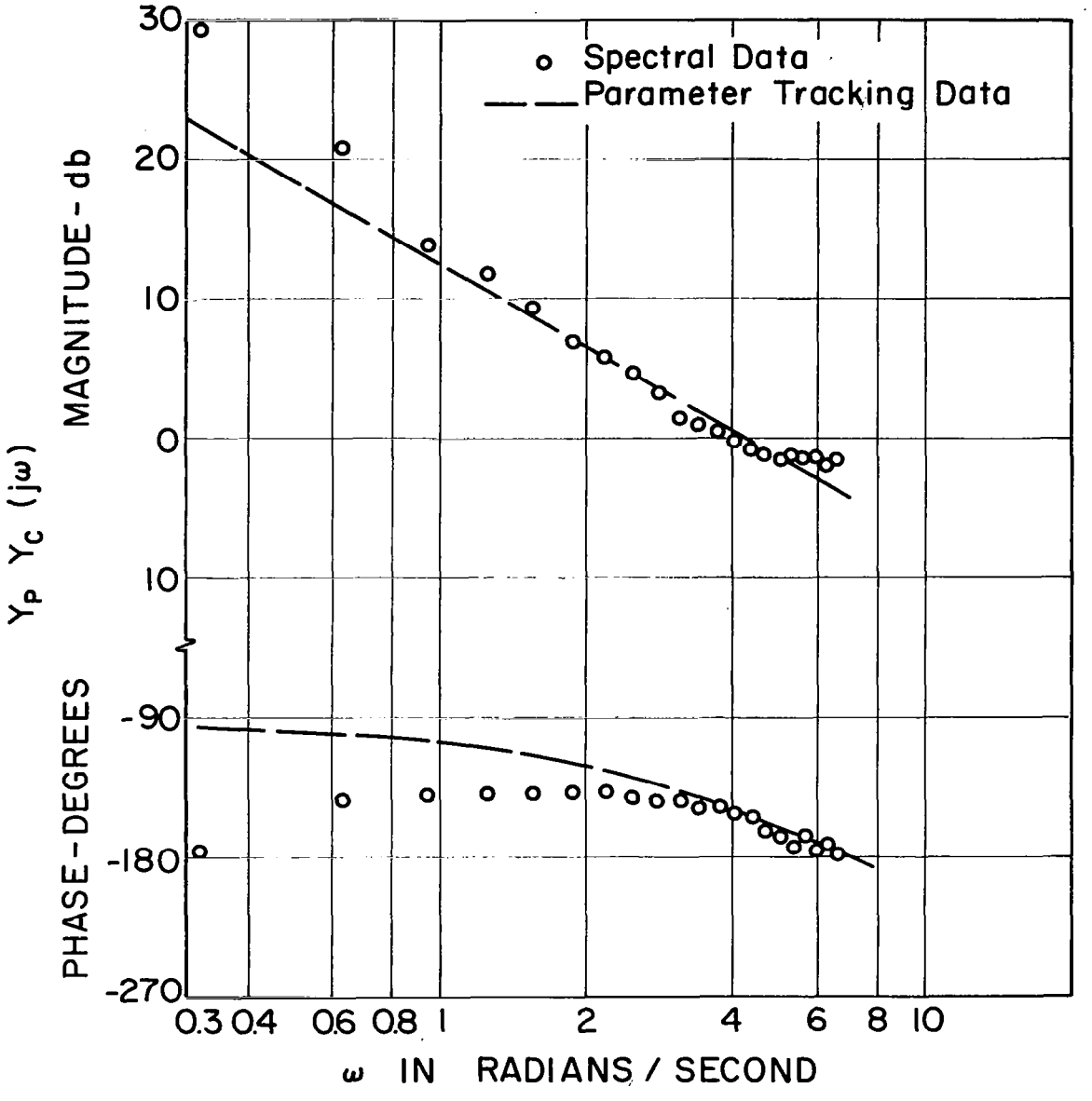

Figure 6.1.16 Comparison of Spectral and Parameter Tracking Tests. Subject 3—Day 13 (Force Stick)— $Y_C(p) = K_2/p^2$—ω_i = 2 radians/second.

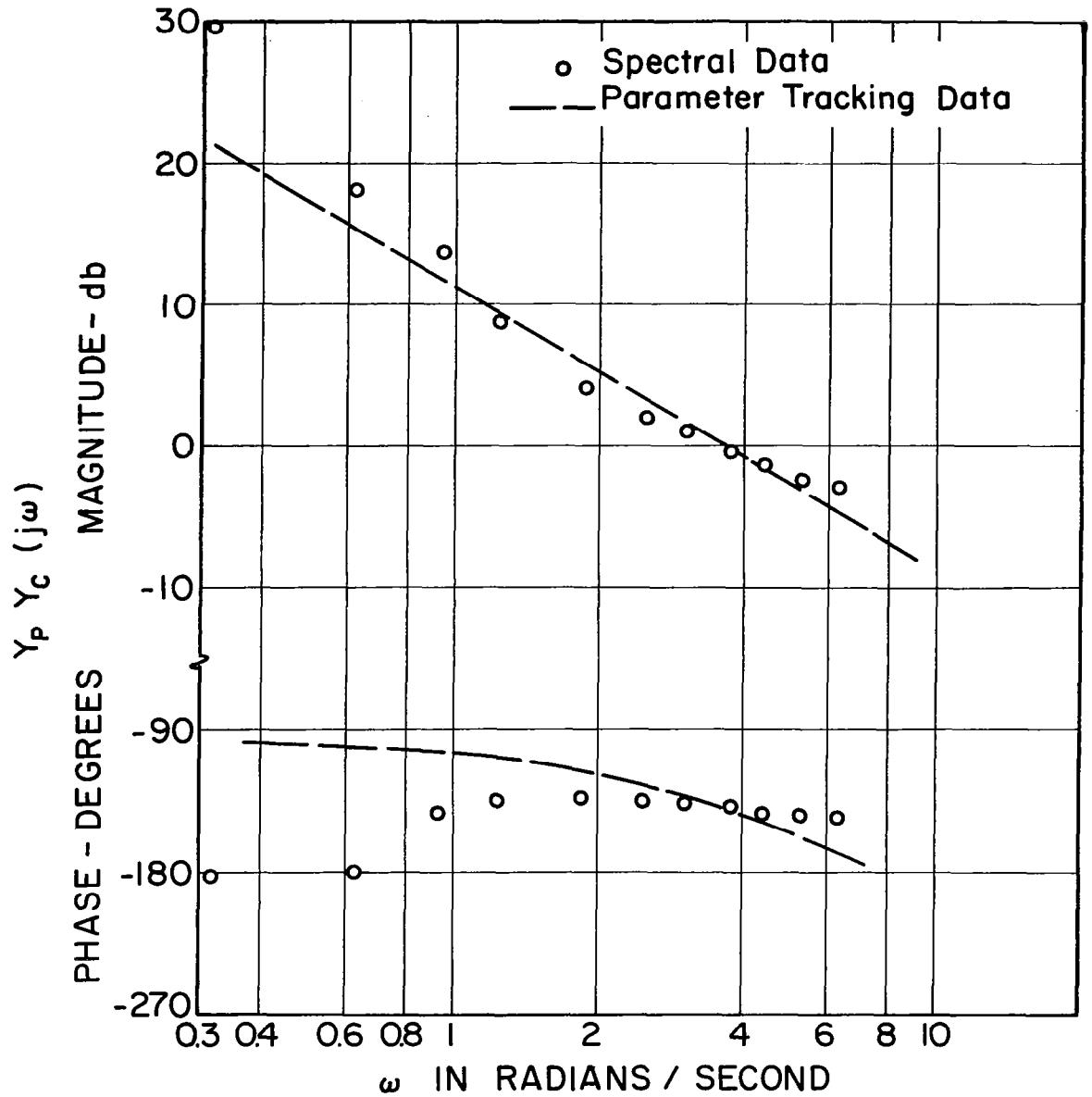

Figure 6.1.17 Comparison of Spectral and Parameter Tracking Tests. Subject 3—Day 13 (Force Stick)—
$Y_C(p) = K_2/p^2$—ω_i = 4 radians/second.

crossover is this low, and is undoubtedly the reason for poor parameter tracking values.

The parameter adjustment driving force, as given by Eq. (4. 9-1), is -keu. As the input power at a given frequency is decreased, the power present in -keu at that frequency is decreased at an even faster rate, and at some point it will become too small to be effective. This point appears to be when $\left|\theta_i(j\omega)\right|$ at crossover is down 20 to 25db.

Evidently some care must be exercised in choosing an input filter when parameter tracking is used. The results of these experiments indicate that if a third order filter is used the cut-off frequency should not be lower than 3 radians per second. If a second order filter is used then the cut-off frequency could be dropped back to 2 radians per second. These frequencies may be reduced somewhat when the controlled element is difficult to control, since the subject tends to reduce the system bandwidth as the task gets more difficult.

As long as the input filter is chosen so that $\left|\theta_i(j\omega)\right|$ is down less than 20db at crossover, the parameter tracking system should be sufficiently accurate.

6.2 The Relative Remnant

In Fig. 6.1.1 the output signal from the closed loop compensatory system is expressed as the sum of two signals

$$\theta_o(t) = S(t) + n(t) \quad . \qquad (6.2\text{-}1)$$

S(t) is that portion of the output signal that is correlated with the input signal. Equivalently, S(t) is that portion of the compensatory system output which can be reproduced by passing the input signal through a linear time-invariant system. The system needed to generate S(t) from $\theta_i(t)$ is described by the transfer operator

$$\frac{S}{\theta_i}(p) = \frac{Y_P\, Y_C(p)}{1 + Y_P\, Y_C(p)} \quad , \tag{6.2-2}$$

where $Y_P\, Y_C(j\omega)$ is defined by Eq. (6.1-5). n(t), on the other hand, is that portion of the compensatory system output that cannot be related to $\theta_i(t)$ by a linear time-invariant element. It represents the uncorrelated portion of the output signal, and is caused by the nonlinear and time-varying operation of the subject.

Using frequency domain descriptions of S(t) and n(t), the ratio of correlated power to total power out of the human system can be defined as

$$\rho_o^2 = 1 - \frac{\int_0^\infty \Phi_{nn}(j\omega_1)\, d\omega_1}{\int_0^\infty \Phi_{oo}(j\omega_2)\, d\omega_2} = \frac{\int_0^\infty \Phi_{ss}(j\omega_1)\, d\omega_1}{\int_0^\infty \Phi_{oo}(j\omega_2)\, d\omega_2} \tag{6.2-3}$$

ρ_o is called the relative remnant by McRuer [25]. If the signals S(t)

and n(t) are assumed to have negligible power present above frequency ω_d, Eq. (6.2-3) can be rewritten as

$$\rho_o^2 = 1 - \frac{\int_o^{\omega_d} \Phi_{nn}(j\omega_1)\, d\omega_1}{\int_o^{\omega_d} \Phi_{oo}(j\omega_2)\, d\omega_2} = \frac{\int_o^{\omega_d} \Phi_{ss}(j\omega_1)\, d\omega_1}{\int_o^{\omega_d} \Phi_{oo}(j\omega_2)\, d\omega_2} \quad . \quad (6.2\text{-}4)$$

Using the notation established in Eq. (6.1-13), the straightforward method of estimating ρ_o^2 would be

$$\hat{\rho}_o^2 = 1 - \frac{\int_o^{\omega_d} \hat{\Phi}_{nn}(j\omega_1)\, d\omega_1}{\int_o^{\omega_d} \hat{\Phi}_{oo}(j\omega_2)\, d\omega_2} \quad . \quad (6.2\text{-}5)$$

Because n(t) is not directly measurable, Eq. (6.2-4) must be rearranged.

Since the standard linear correlation is defined as [27]

$$\frac{\Phi_{ss}(j\omega)}{\Phi_{oo}(j\omega)} = \frac{\left|\Phi_{io}(j\omega)\right|^2}{\Phi_{ii}(j\omega)\, \Phi_{oo}(j\omega)} \quad , \quad (6.2\text{-}6)$$

it follows that

$$\Phi_{ss}(j\omega) = \frac{\left|\Phi_{io}(j\omega)\right|^2}{\Phi_{ii}(j\omega)} \quad . \tag{6.2-7}$$

ρ_o^2 as defined in Eq. (6.2-4) is seen to be equivalent to

$$\rho_o^2 = \frac{\int_o^{\omega_d} \frac{\left|\Phi_{io}(j\omega_1)\right|^2}{\Phi_{ii}(j\omega_1)} d\omega_1}{\int_o^{\omega_d} \Phi_{oo}(j\omega_2)\, d\omega_2} \quad . \tag{6.2-8}$$

Equation (6.2-8) can be estimated directly using Eqs. (6.1-13). The basic equation used for the calculation of $\hat{\rho}_o^2$ was

$$\hat{\rho}_o^2 = \frac{\int_o^{\omega_d} \frac{\left|\hat{\Phi}_{io}(j\omega_1)\right|^2}{\hat{\Phi}_{ii}(j\omega_1)} d\omega_1}{\int_o^{\omega_d} \hat{\Phi}_{oo}(j\omega_2)\, d\omega_2} \quad , \tag{6.2-9}$$

which was solved numerically.

Figure 6.2.1 contains plots of $\hat{\rho}_o^2$ versus day of training for one subject from each experiment. These subjects are the same ones that were analyzed in Section 6.1.

These graphs show that both subjects became more linear and time-invariant with training, and less linear and time-invariant with an increase in ω_i. This is exactly what one would expect.

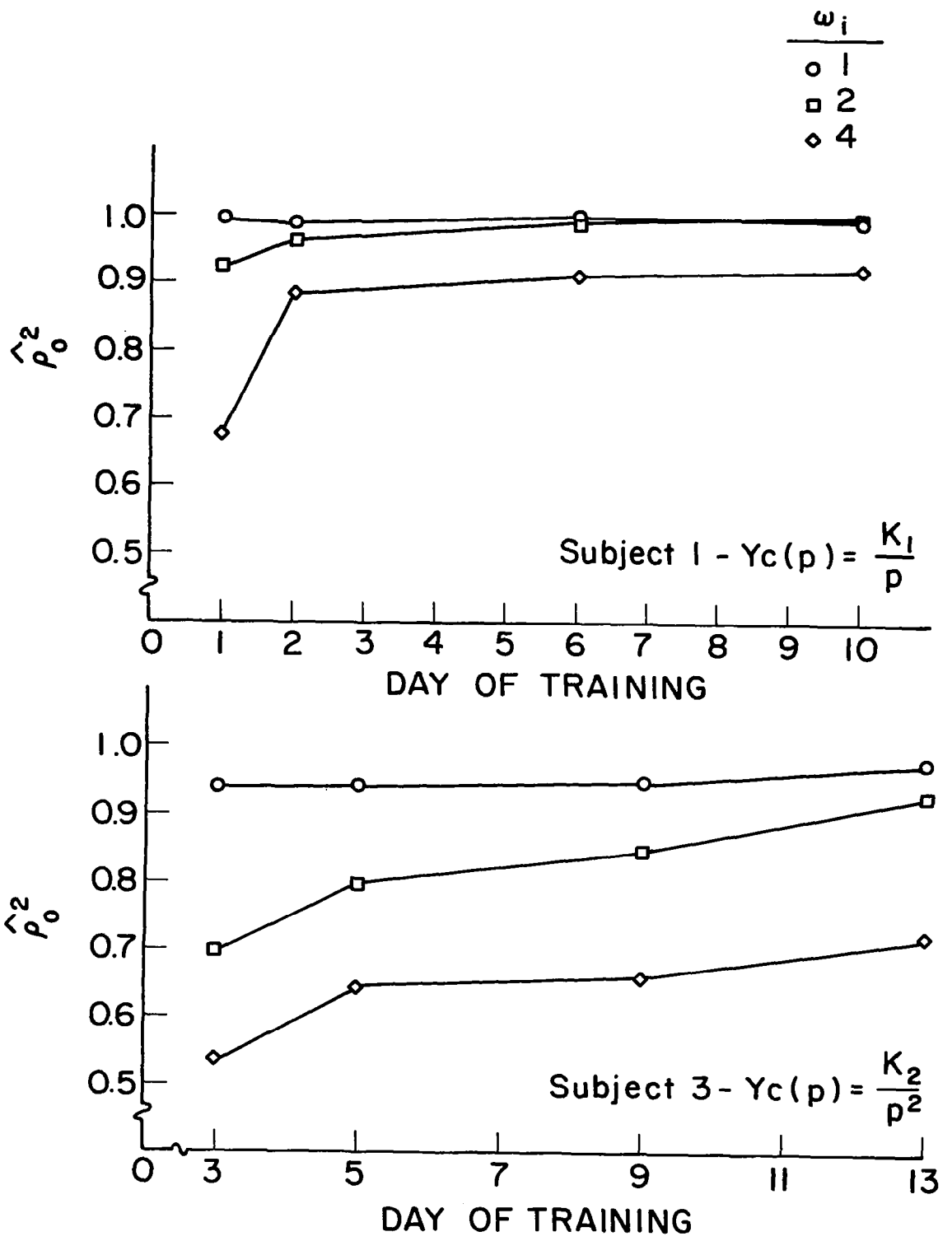

Figure 6.2.1 $\hat{\rho}_o^2$ vs. Training.

The $\hat{\rho}_o^2$ values for the subject from the K_1/p experiment are considerably higher than those for the subject from the K_2/p^2 experiment. This is because subjects are generally more consistent on easier tasks, and should therefore have higher $\hat{\rho}_o^2$ values on lower order systems [41]. Since the comparison of these two sets of curves represents a comparison of only two subjects, no definite statements can be made other than the results appear to be consistent with previous data [25].

The major importance of measuring $\hat{\rho}_o^2$ is given in the next section.

6.3 Comparing the Crossover Model with the Best Linear Time-Invariant Model

Let it be assumed that K(t) and $\tau(t)$ are constant at their optimum values, i.e., they are set at the values determined by the parameter tracking network.

From the basic definition of the time auto-correlation function

$$R_{ee}(0) = \lim_{T \to \infty} \frac{1}{2T} \int_{-T}^{T} e^2(t)\, dt \triangleq \overbrace{e^2(t)} \qquad (6.3\text{-}1)$$

where $\overbrace{e^2(t)}$ is the average energy in the error that exists between the outputs of the compensatory system and the assumed model. Likewise,

$$R_{oo}(0) = \lim_{T \to \infty} \frac{1}{2T} \int_{-T}^{T} \theta_o^2(t)\, dt = \overbrace{\theta_o^2(t)} \qquad (6.3\text{-}2)$$

where $\overbrace{\theta_o^2(t)}$ is the average energy in the output of the compensatory system.

Since

$$e(t) = Z(t) - \theta_o(t)$$

$$= [Z(t) - S(t)] - n(t) \qquad (6.3\text{-}3)$$

and

$$e^2(t) = [Z(t) - S(t)]^2 - 2n(t)[Z(t) - S(t)] \qquad (6.3\text{-}4)$$

$$+ n^2(t) \quad ,$$

it follows that

$$\overbrace{e^2(t)} = \overbrace{[Z(t) - S(t)]^2} + \overbrace{n^2(t)} \quad . \qquad (6.3\text{-}5)$$

This is because n(t) and S(t) are not correlated by definition. Since Z(t) and S(t) are both fully correlated with $\theta_i(t)$, they are fully correlated with each other. This means that Z(t) and n(t) must be uncorrelated and

$$\overbrace{2n(t)\,[Z(t) - S(t)]} = 0 \quad . \qquad (6.3\text{-}6)$$

Using this equation, Eq. (6.3-5) follows directly from Eq. (6.3-4).

Using Eqs. (6.3-1) and (6.3-2) an Ideal Power Match (PM_I) can be defined as

$$PM_I = 1 - \frac{\overbrace{e^2(t)}}{\theta_o^2(t)} \tag{6.3-7}$$

$$= 1 - \frac{\overbrace{[Z(t) - S(t)]^2} + \overbrace{n^2(t)}}{\theta_o^2(t)} \quad . \tag{6.3-8}$$

By subtracting Eq. (6.3-8) from (6.2-3) it is seen that

$$\rho_o^2 - PM_I = 1 - \frac{\int_o^\infty \Phi_{nn}(j\omega)\, d\omega}{\int_o^\infty \Phi_{oo}(j\omega)\, d\omega} - 1 + \frac{\overbrace{[Z(t) - S(t)]^2} + \overbrace{n^2(t)}}{\theta_o^2(t)} \tag{6.3-9}$$

or

$$\rho_o^2 - PM_I = \frac{\overbrace{[Z(t) - S(t)]^2}}{\theta_o^2(t)} \quad . \tag{6.3-10}$$

This follows from the fact that

$$\overbrace{\theta_o^2(t)} = \frac{1}{\pi} \int_o^\infty \Phi_{oo}(j\omega)\, d\omega \tag{6.3-11}$$

and

$$\overbrace{n^2(t)}^{\sim\sim} = \frac{1}{\pi} \int_0^\infty \Phi_{nn}(j\omega)\, d\omega \quad , \qquad (6.3\text{-}12)$$

since the average energies as computed in the time and frequency domains for the same signal must be the same.

Several important facts should be noted at this point. From Eq. (6.3-8) it can be seen that the maximum power match is obtained when $Z(t) = S(t)$, or when the assumed model perfectly represents the linear portion of the compensatory system. It should also be noted that the maximum possible PM_I will not be 1.0. The maximum PM_I is only ρ_o^2, which could be well below 1.0 if the compensatory system is very nonlinear or time variable. This implies that a low power match does not in itself indicate a poor linear model. In fact it indicates nothing at all, unless it can be compared with ρ_o^2. This fact has not been emphasized by any researcher doing parameter tracking studies.

As was discussed in Section 6.2, since only finite length samples of the various sample functions are available, ρ_o^2 can only be estimated. The same holds true for PM_I. For the experimental work of this report PM_I was estimated by

$$\widehat{PM_I} = 1 - \frac{\overbrace{e^2(t)}^{\sim\sim}}{\overbrace{\theta_o^2(t)}^{\sim\sim}} \qquad (6.3\text{-}13)$$

where

$$\widetilde{e^2}(t) = \frac{1}{5}\sum_{q=1}^{5}\frac{1}{60}\int_{60\,sec}^{120\,sec} e^2_q(t)\,dt \qquad (6.3\text{-}14)$$

and

$$\widetilde{\theta_o^2}(t) = \frac{1}{5}\sum_{q=1}^{5}\frac{1}{60}\int_{60\,sec}^{120\,sec} \theta_{oq}^2(t)\,dt \quad . \qquad (6.3\text{-}15)$$

The estimations of $\widetilde{e^2}(t)$ and $\widetilde{\theta_o^2}(t)$ are thus made over the maximum length of time during which K(t) and $\tau(t)$ were essentially constant. (K(t) and $\tau(t)$ were allowed to converge for the first 60 seconds of each two minute run, and time averages were computed over the second 60 seconds.)

Using the previous estimate for ρ_o^2 given in Eq. (6.2-9) together with the estimate for PM_I given in Eq. (6.3-13), the "quality" of the assumed model can be estimated by

$$\hat{\rho}_o^2 - \widehat{PM}_I = \left[\frac{\widetilde{[Z(t) - S(t)]^2}}{\widetilde{\theta_o^2}(t)}\right]^{\wedge} \quad . \qquad (6.3\text{-}16)$$

The difference $\hat{\rho}_o^2 - \widehat{PM}_I$ provides an index for the evaluation of the effectiveness of the assumed linear model. If the assumed model is a good one $\hat{\rho}_o^2 - \widehat{PM}_I$ will be small, going to zero if the assumed

model is perfect. $\hat{\rho}_o^2 - \widehat{PM}_I$ actually indicates how much can be gained by going from the present assumed model to the best linear time-invariant model of the subject under the particular test condition.

Figures 6.3.1 and 6.3.2 give plots of $\hat{\rho}_o^2 - \widehat{PM}_I$ for the two subjects analyzed spectrally.

In both cases the differences are quite small, with one or two exceptions. This indicates that for many purposes the gains to be made by going to a more complicated model are probably not worth the added expense in parameter tracking equipment, or the additional stability problems caused by adjusting more parameters.

In Fig. 6.3.1 two values of $\hat{\rho}_o^2 - \widehat{PM}_I$ are found to be slightly less than zero. This would be impossible with perfect experimental data. This discrepancy can be attributed to one of two things, or a combination of both: (1) the values were calculated from a limited amount of data and the natural variation of the data could be of the same order of magnitude as the true difference between ρ_o^2 and PM_I; and (2) $\hat{\rho}_o^2$ and $\widehat{PM}_I$ were not calculated from exactly the same length of data. $\hat{\rho}_o^2$ was calculated from 110 seconds of data from each two minute run, while $\widehat{PM}_I$ used only 60 seconds from each run.

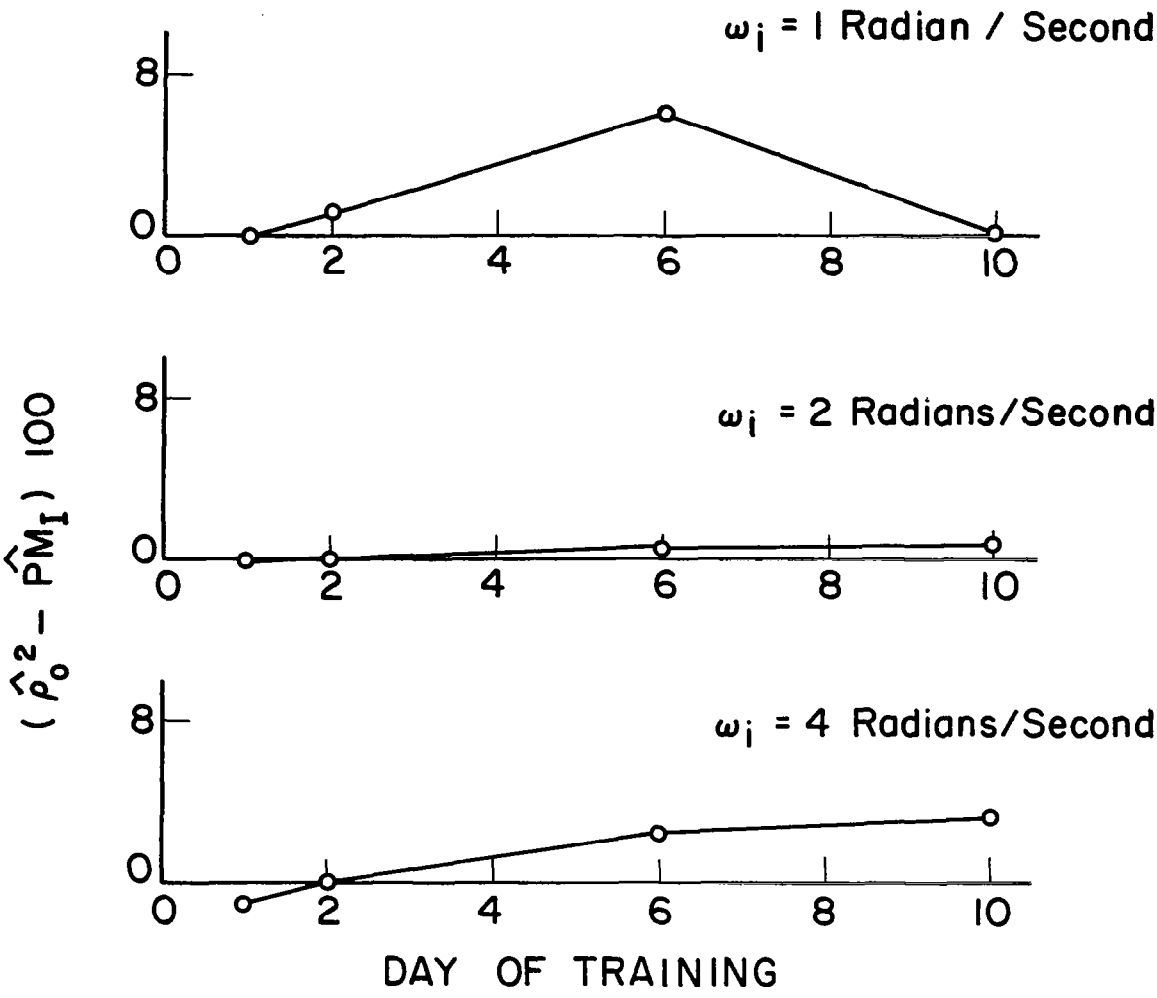

Figure 6.3.1 Comparison of the Crossover Model with the Best Linear Time-Invariant Model—Subject 1—
$Y_C(p) = K_1/p$.

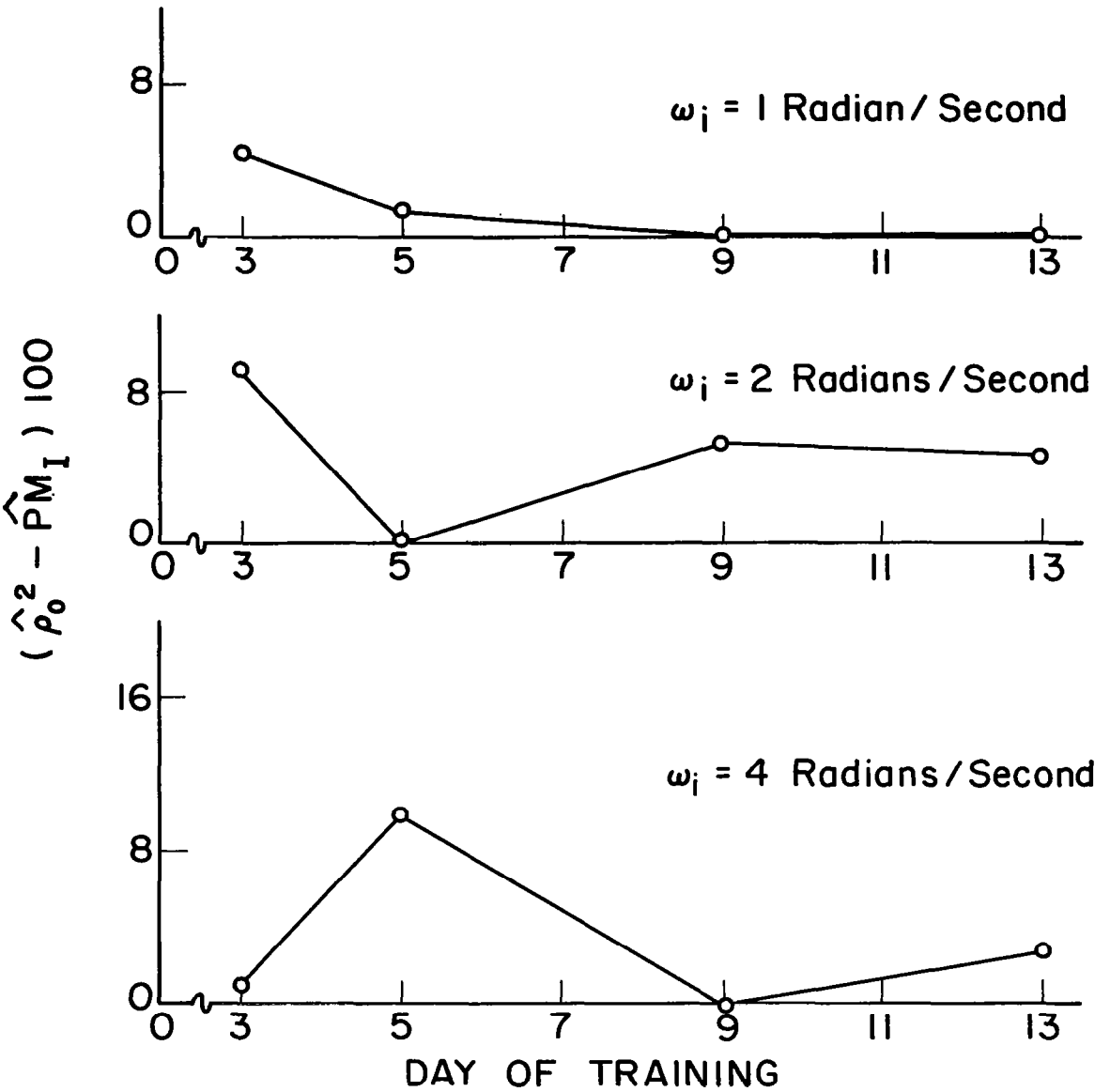

Figure 6.3.2 Comparison of the Crossover Model with the Best Linear Time-Invariant Model—Subject 3—
$Y_C(p) = K_2/p^2$.

Chapter 7

CONCLUSIONS

7.1 On the Value of the Crossover Model

The original purpose of this research was the evaluation of the crossover model as the parameter tracking model for certain compensatory control systems. The evaluation was performed on subjects controlling single and double integrator plants.

The choice of these two specific plants was not at all arbitrary. From McRuer's original work it was known that the crossover model gain-phase curves fit experimental data very well when the plant was a single integrator, but only moderately well when the plant was a double integrator. For first and second order plants such as $1/(Tp + 1)$ and $1/p(Tp + 1)$, the crossover model is probably "poorer" than in the single integrator case, but "better" than in the double integrator case.

The pre-test reasoning was that the value of the crossover model parameter tracking system would be minimal if the system did well on the single integrator tests, but poorly on the double integrator tests. Alternately, if the system performed well on both tests its value would be established, since this would imply its application to plants like $1/(Tp + 1)$ and $1/p(Tp + 1)$, in addition to the two plants tested.

The comparison tests of Chapter 6 indicated that on both tests the

values of K and τ were accurate, providing ω_i had been chosen properly. For the reasons given above, this indicates the system's usefulness on a large class of first and second order controlled elements. The particular elements contained in this class of controlled elements still needs to be determined.

7.2 On the Input Characteristics for Parameter Tracking Systems

When parameter tracking is being used in conjunction with the crossover model, sufficient power must be present in the crossover region if accurate parameter identification is to be made. The experimental results indicate that the input power must not be down more than 20db at the crossover frequency for accurate parameter tracking to take place.

Since the crossover frequency is a function of both the cut-off frequency and the controlled element, the input characteristics are difficult to specify exactly. However, for a K_1/p controlled element and an input filter of the form $1/(Tp + 1)^2$, cut-off frequencies of 2, 3 and 4 radians per second should be acceptable. If a $1/(Tp + 1)^3$ filter is used then only 3 and 4 radians per second should be used for cut-off frequencies. For K_2/p^2 controlled elements, a $1/(Tp + 1)^3$ filter can be used with cut-off frequencies of 2, 3 and 4 radians per second. These cut-off frequencies assume that the signal being filtered is Gaussian white noise.

A cut-off frequency of one radian per second appears to be too low for most applications, and should be avoided if possible.

7.3 On the Limited Gradient Parameter Adjustment Technique

The limited gradient adjustment technique was found experimentally to give far smoother parameter tracking performance than the conventional linear adjustment technique. Although the possibility of parameter biasing cannot be completely discounted, the biasing (if it existed at all) was so small that it was not apparent on the tests conducted.

This technique should prove valuable in future parameter tracking tests.

7.4 On the Evaluation of Linear Parameter Tracking Models of Human Operators

After convergence, a linear parameter tracking model is basically a time-invariant system, providing the gradient gains are low. Since the system is linear, it cannot be expected to account for any of the uncorrelated signals generated by the human. The method of comparing ideal power match with the relative remnant given in Chapter 6 represents one way that the quality of the parameter tracking model can be evaluated by direct measurement. This method admittedly requires rather extensive calculations, but should be performed on selected data to give a good evaluation of the particular model being tested.

Since the simple parameter tracking version of the crossover model accounts for such a large portion of the total linear compensatory output, the value of more complex linear models for the systems tested must be questioned. The correlated output power not accounted for by the crossover model is in general much less than the uncorrelated output power, which is being completely ignored by the linear model. It would appear that there is more to gain from an investigation of the uncorrelated signals, than from looking for further refinements in linear models.

7.5 On the Applications of the Crossover Model Parameter Tracking System

The values of K and τ determined by the crossover model were found to change significantly with training and with cut-off frequency. K and τ also varied widely between subjects, and indications were that K and τ would change for a given subject, if the controlled element were changed.

These factors provide the basis for using K and τ to:

(1) Classify subjects.

(2) Measure task difficulty.

(3) Determine subject learning rates.

In short, the crossover model parameter tracking system should be a valuable tool for measuring human performance. One area for future research is the application of the system to the type of problems listed above.

7.6 On the Effect of Training on the Form of the Human Transfer Operator

One side-light of the experiments was the observation that the subjects did not appreciably change the basic form of their transfer operators during training. The forms of the gain-phase curves were established during the first training sessions, and only the relative position of these curves changed with training. This change in curve position is associated with a change in equation coefficients, rather than a change in the basic equation. This is the prime reason why the parameter tracking system gives consistent results throughout testing. If the subjects had actually changed the form of their equations, the crossover model might have proven invalid early in training.

7.7 On the Measurement of Remnant

The crossover model was shown to account for all but a few percent of the correlated power out of the compensatory system. In the experiments where $\hat{\rho}_o^2$ was low, the model matching error was due mostly to remnant.

$$\begin{aligned} e(t) &= Z(t, K, \tau) - \theta_o(t) \\ &= Z(t, K, \tau) - S(t) - n(t) \qquad (7.4\text{-}1) \\ &\cong - n(t) \quad . \end{aligned}$$

This provides a method for obtaining the remnant as a time function from which on-line analysis of the remnant can be performed.

The analysis of n(t) deserves considerable attention, especially how it changes during training. The crossover model provides an on-line method for obtaining pertinent information.

7.8 Nonlinear Modifications of the Crossover Model

Another area open for study is the addition of nonlinear elements into the parameter tracking crossover model. It is entirely possible that the addition of simple nonlinearities, such as position or velocity limiting, would enable the model to account for a sizeable portion of the remnant. This area could be investigated jointly with an investigation of the remnant itself.

7.9 Concluding Remarks

The major contribution of this research has been the development of a usable tool for the on-line measurement of human performance. The method has been shown to be both accurate and stable in actual operation. It also requires a modest amount of analog equipment for implementation and should be readily available to a large number of researchers.

It is hoped that other researchers will be able to use this system to their advantage.

Appendix A

COMPENSATORY TEST CONSTANTS

The general test procedure for the compensatory tracking task is outlined in Section 5.1. This appendix is included for the presentation of various details involved in setting up the test program.

A.1 Instructions to Subjects

Prior to testing each subject was given the chance to read and ask questions about the instructions given below. In addition, the subject was allowed to test the control stick action and "feel", but no trial runs were made.

The printed instructions given to the subject were as follows:

"This experiment has been designed to gain information on the manner in which a person learns to control a particular system, and how learning is related to the characteristics of the signal being used as an input to the control system.

"Before I describe exactly what you will do, I want to explain the task in a general way.

"On the screen you see a dot. That dot represents the error of the system you are controlling, and will move back and forth horizontally in a random fashion. You will find that by moving the control stick you can force the dot to stay near the vertical center

line on the scope. Your task is to move the stick in such a manner that the dot stays on the center line, or as near to it as possible. During any one run you will find that the highest speed at which the dot tries to move will not change. However, the highest speed of the dot will be different during various blocks of runs. You will be told prior to each run whether to expect relatively 'fast', 'medium', or 'slow' movement.

"The graph below shows how close to the centerline a typical subject was able to hold the dot during a portion of a run.

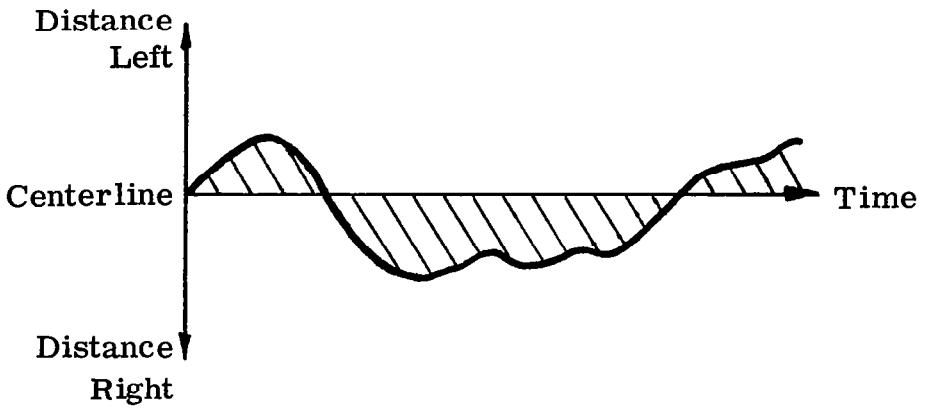

Figure A.1.1 Typical Subject Error and Subject Scoring Method.

During each run that you make, the shaded area for your run will be measured electronically. This area will add up to a positive number which is an indication of how well you performed your task. A lower score, or a smaller area, means you performed better than if the score is higher. You will find that your score

will be dependent upon whether the dot is moving in the fast, medium, or slow mode, with the fast mode having the larger score. However, you should strive to reduce your score on each run.

"Please be seated. Place your right arm on the control stick, grasping the bar so that your elbow is in the same plane as your shoulders and body. Make yourself comfortable and remain in this position during the tests. You will wear these earphones, through which you will hear a 'waterfall-like' noise. This noise will mask out room noise which might otherwise disturb you. I can interrupt the noise to speak to you, and there is an intercom connected to the outside of the booth so that I will be able to hear you easily.

"Here is what will happen.

"Before the beginning of each run the dot will be stationary in the center of the scope. You should also have the control stick in the center position. You will hear the noise in the earphones. I will then interrupt the noise to see if you are ready, and tell you whether the run will be fast, medium, or slow. You will then hear a click in the earphones which acts as a warning that 10 seconds later the target dot will begin moving back and forth

across the screen in a random manner. You must then begin moving the control stick to keep the dot in the center of the scope. In general, if you want the dot to move left, you must move the control stick to the left, and move the control stick to the right, if you want the dot to move to the right.

"Each run will last 2 minutes. You will have 5 runs at one average speed. The speed will then be changed and 5 more runs made. The speed will be changed again and 5 more runs made. Thus you will make a total of 15 two-minute runs. You will have half-minute rest periods between each run, with a five minute rest after each group of five. I will also give you your score after each run.

"Are there any questions?"

A.2 Compensatory System Gains

The basic compensatory system block diagram is given in Fig. 1.1.1. The system gain constants used in the two experiments discussed in this report are given below.

Element	Gain		Units
	K_1/p Exp.	K_2/p^2 Exp.	
5 inch diameter oscilloscope (Fairchild Model 700)	0.133	0.0625	$\frac{\text{cm deflection}}{\text{volt error}}$
Control stick	2.5	2.2	$\frac{\text{volts output}}{\text{degree rotation}}$
K_1	5.0		$\frac{\text{volts}}{\text{volt}}$
K_2		5.0	$\frac{\text{volts}}{\text{volt}}$

The control stick was of the arm movement type, pivoted at the position of the elbow. Maximum stick deflection was ± 45 degrees, although deflections of only half this value were generally not exceeded in actual test conditions. The control stick was spring loaded with a linear spring with a restraining force of 0.0235 pounds per degree rotation, measured at the hand location point on the stick.

In both experiments the input signals were filtered Gaussian pseudo-white noise. A $1/(Tp + 1)^3$ filter was used with the cut-off frequency adjustable to 1, 2 and 4 radians per second. The filter gains were set empirically so that the peak values of $\theta_i(t)$ were approximately 75 volts. The filter gains were set prior to testing and were not changed during the experiment.

A.3 Analog Diagram of the Parameter Tracking System

The analog circuit used in the actual parameter tracking tests is given in Figs. A.3.1 through A.3.4. The potentiometer settings required to give the scaled variables noted on the diagram are given in the next section in conjunction with a static test procedure.

The total equipment needed to implement the parameter tracking circuit given in these figures is:

28 summers and inverters

8 integrators

7 multipliers

17 potentiometers.

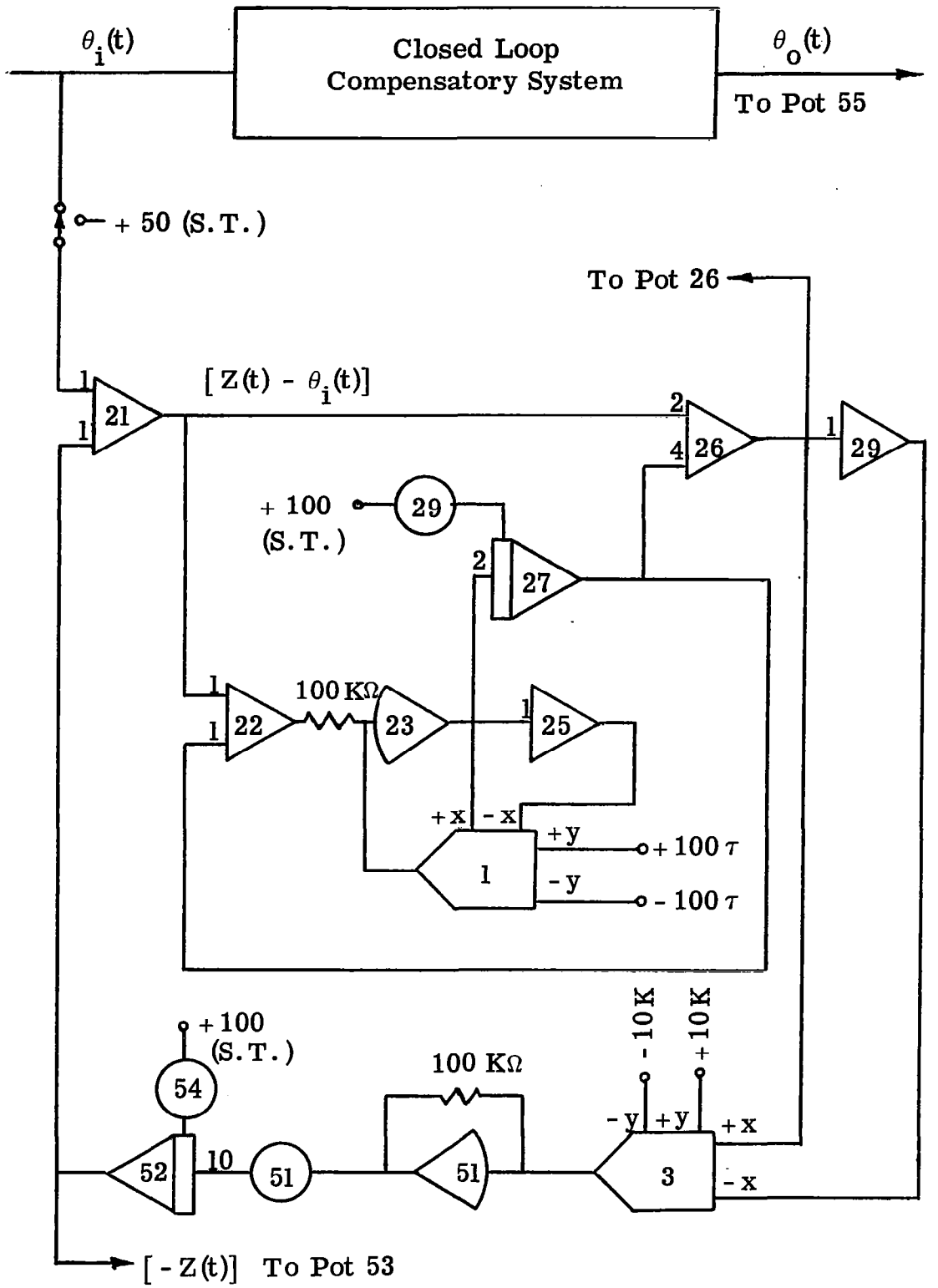

Figure A. 3. 1 Assumed Model Portion of the Parameter Tracking Circuit.

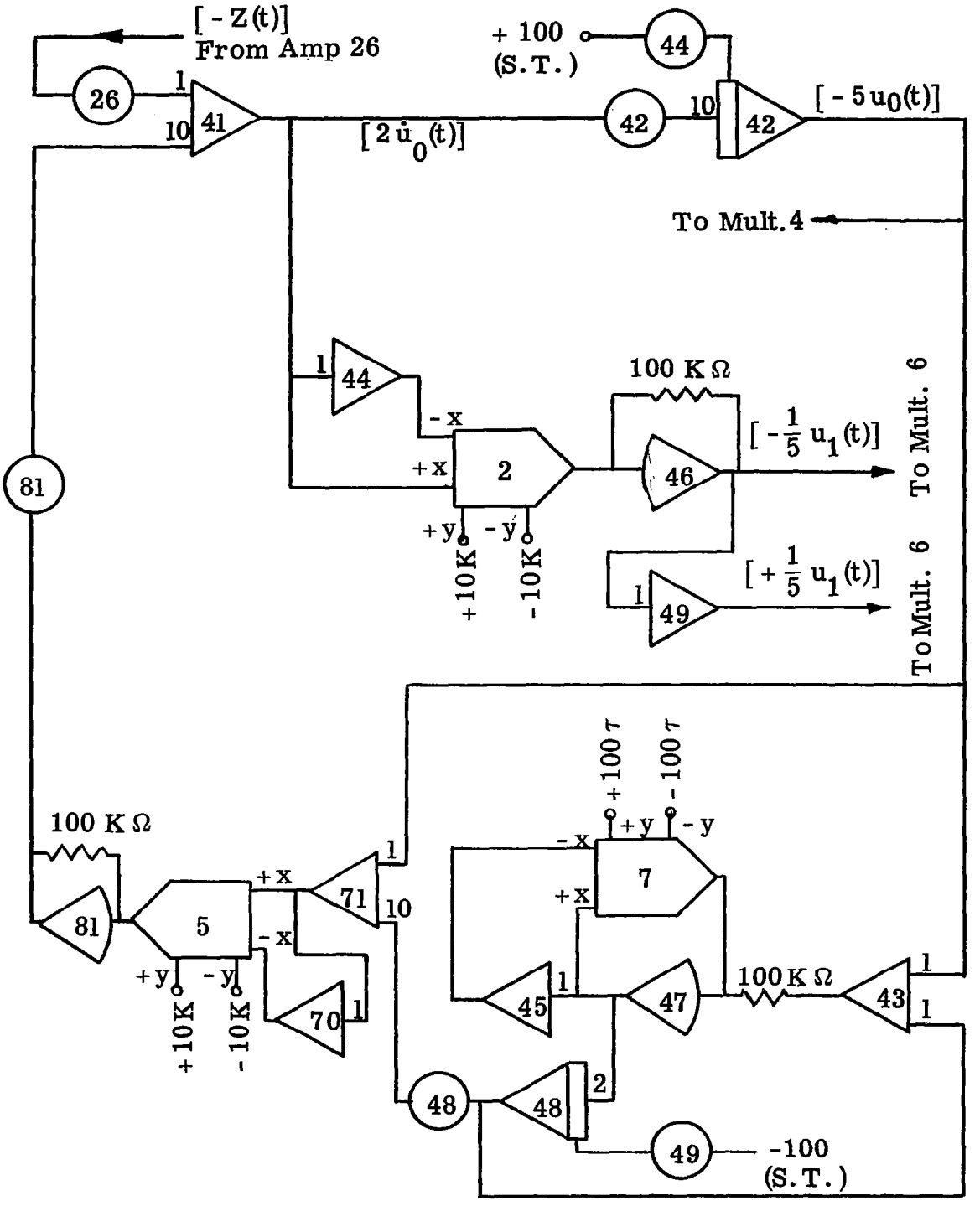

Figure A. 3. 2 Sensitivity Equation Portion of the Parameter Tracking Circuit.

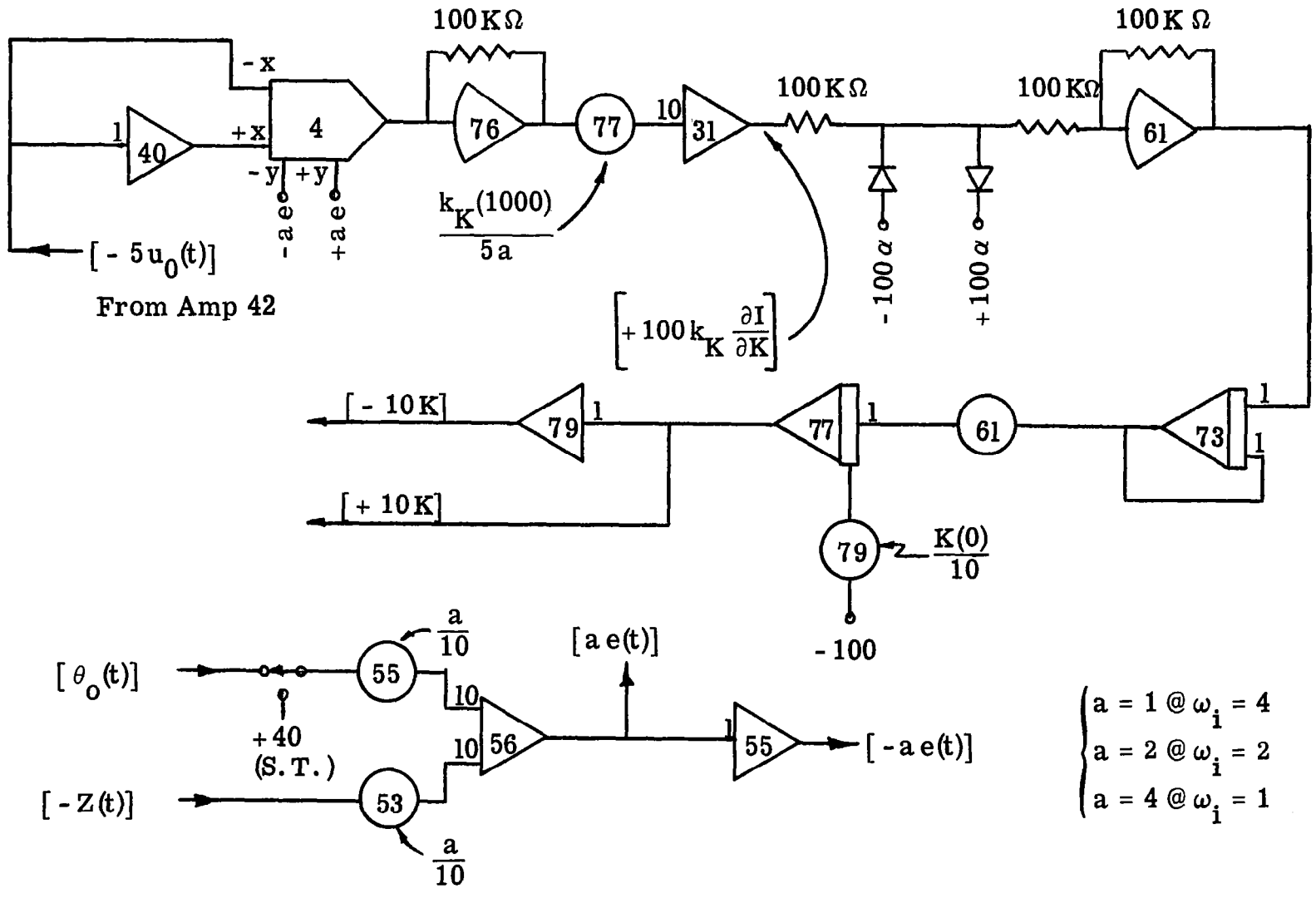

Figure A. 3. 3 Parameter Adjustment Circuit for K(t), and the Model Error Circuit.

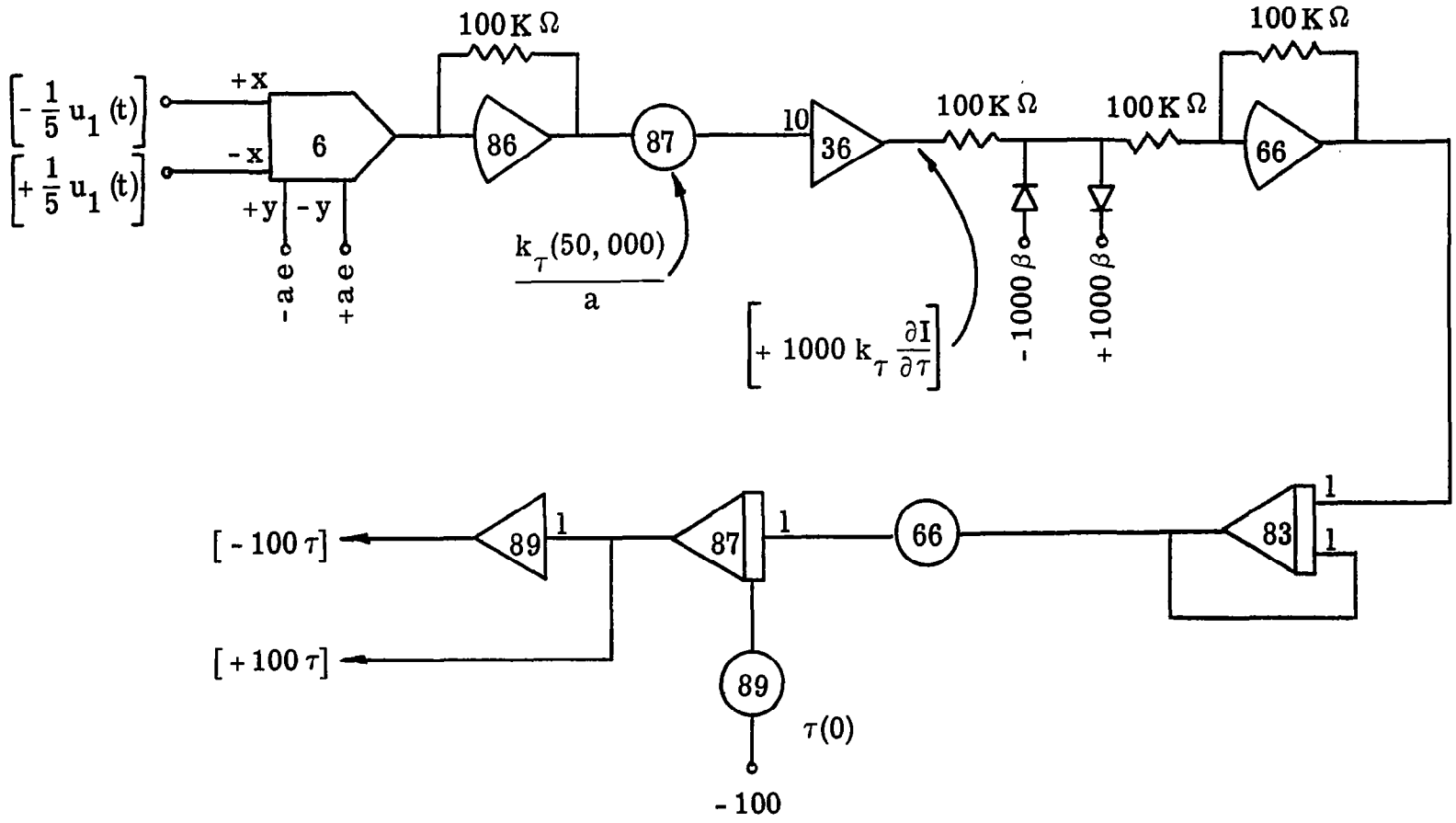

Figure A.3.4 Parameter Adjustment Circuit for $\tau(t)$.

A.4 Static Test Sheet

The following static test sheet is included for those desiring to implement the analog circuit given in Figs. A.3.1 through A.3.4.

Pot	Pot Setting	Amp.	Amplifier Output	Int.	Integrator Output	Additional Items
26	0.5000	21	+ 10.00	27	- 25.00	(1) $\theta_i(t) = +50.00$
29	0.2500	22	+ 15.00	42	- 45.00	
42	0.2500	23	- 37.50	48	+55.00	(2) $\theta_o(t) = +40.00$
44	0.4500	25	+ 37.50	52	- 60.00	
48	0.2000	26	+ 80.00	53	———	(3) $\pm 100\alpha = \pm 100$
49	0.5500	29	- 80.00	77	+40.00	
51	0.5000	31	+ 45.00	83	———	
53	0.5000	36	+ 26.40	87	+40.00	$\pm 1000\beta = \pm 100$
54	0.6000	40	+ 45.00			
55	0.5000	41	- 66.00			
61	0.2000	43	- 10.00			
66	0.2000	44	+ 66.00			
77	0.1000	45	- 25.00			
79	0.4000	46	+ 26.40			
81	0.1000	47	+ 25.00			
87	0.1000	49	- 26.40			
89	0.4000	51	- 32.00			
		55	-100.00			
		56	+100.00			
		61	- 22.50			
		66	- 13.20			
		70	+ 65.00			
		71	- 65.00			
		76	- 45.00			
		79	- 40.00			
		81	+ 26.00			
		86	- 26.40			
		89	- 40.00			

In actual operation with ω_i = 1 or 2 radians per second, the same pot settings given on the static test sheet were used except for pots 26, 53, 55, and 81. Pots 26 and 81 must be changed to 1.000 and 0.4000, respectively. Pot settings for 53 and 55 are given on Fig. A.3.3. The scaled variables given on the figures assume these pot settings exist. When ω_i = 4 radians per second, pot 26 should be reduced to 0.5000.

If limiting is desired in the parameter adjustment loops, the voltages $\pm 100\alpha$ and $\pm 1000\beta$ must be reduced to give the desired limiting. As mentioned in Chapter 4, this is done empirically, by observing the outputs of amplifiers 61 and 66 on Figs. A.3.3 and A.3.4. The limits are lowered until only the largest peaks of voltage occurring at the outputs of these amplifiers are limited.

A.5 k_K and k_τ Values for Actual Operation

When the input signal is random, the values of k_K and k_τ needed to give a desired convergence rate are directly dependent upon both the input filter characteristics and the point of convergence. As was pointed out in Chapter 4, trying to specify k_K and k_τ exactly a priori is a futile task.

However, for the analog circuit given in Figs. A.3.1 through A.3.4 and with $\theta_i(t)$ Gaussian pseudo-white noise filtered in the 1-4 radians per second range, the k_K and k_τ potentiometers are scaled

in the range necessary for practical convergence rates. This assumes that the peak values of $\theta_i(t)$ are approximately 75 volts. Typical values used for k_K and k_τ are given on the time history curves of Appendix D.

It should be noted that the variation in input characteristics from one 2 minute run to the next can give appreciable changes in the convergence properties. This is true even when a known system is being tracked using a random input signal.

Appendix B

THE RANDOM VARIABLE $n(\alpha)\, u_o(\alpha, K^*, \tau^*)$

In Chapter 4 the random variable $n(\alpha)\, u_o(\alpha, K^*, \tau^*)$ was encountered. Sufficient conditions for this random variable to have a symmetric probability density function will be derived in this appendix.

B.1 Derivation of the Sufficiency Conditions

Let $X = n(\alpha)$, $Y = u_o(\alpha, K^*, \tau^*)$ and $Z = XY$ be the random variables with the related density functions $p_X(x)$, $p_Y(y)$, $p_Z(z)$ and $p_{X,Y}(x,y)$.

It is first noted that if the characteristic function of Z [10], as given in Eq. (B.1-1), is real, then $p_Z(z)$ must be symmetric.

$$M_Z(\omega) = \int_{-\infty}^{\infty} p_Z(z)\, e^{j\omega z}\, dz$$

$$= \int_{-\infty}^{\infty} \int_{-\infty}^{\infty} p_{X,Y}(x,y)\, e^{j\omega xy}\, dx\, dy \qquad \text{(B.1-1)}$$

If X and Y are independent, or if they are Gaussian and uncorrelated, then

$$p_{X,Y}(x,y) = p_X(x)\, p_Y(y) \qquad \text{(B.1-2)}$$

and

$$M_Z(\omega) = \int_{-\infty}^{\infty} p_X(x)\,dx \int_{-\infty}^{\infty} p_Y(y)\, e^{j\omega xy}\,dy$$

$$= \int_{-\infty}^{\infty} p_X(x)\,dx \int_{-\infty}^{\infty} p_Y(y) \left\{\cos \omega xy + j \sin \omega xy\right\} dy \ . \quad \text{(B.1-3)}$$

If $p_Y(y)$ is symmetric, and therefore an even function of y,

$$j \int_{-\infty}^{\infty} p_Y(y) \sin \omega xy\, dy \equiv 0 \quad \text{(B.1-4)}$$

for all values of x. This insures that $M_Z(\omega)$ will be real and that $p_Z(z)$ will have a symmetric density function.

It should be noted that Eq. (B.1-3) could have been arranged into the form

$$M_Z(\omega) = \int_{-\infty}^{\infty} p_Y(y)\,dy \int_{-\infty}^{\infty} p_X(x)\, e^{-j\omega yx}\,dx \ . \quad \text{(B.1-5)}$$

Using this form, $p_X(x)$ being an even function insures that $M_Z(\omega)$ is real and that $p_Z(z)$ has a symmetric density function.

The sufficient conditions for $p_Z(z)$ to have a symmetric probability density function are:

(1) $n(\alpha)$ and $u_o(\alpha, K^*, \tau^*)$ are independent, or Gaussian and uncorrelated; and

(2) either $n(\alpha)$ or $u_o(\alpha, K^*, \tau^*)$ must have a symmetric probability density function.

Appendix C

EXPERIMENTAL CONVERGENCE TESTS

C.1 Sinusoidal Input Signal—No Limiting in the Parameter Adjustment

In Chapter 4 the convergence properties of K(t) and $\tau(t)$ were discussed and expressions were developed for the time constants of convergence of K(t) and $\tau(t)$ when $\theta_i(t)$ is a sinusoid. From Eq. (4.7-17), if $\Delta\tau(t) \equiv 0$ then the time constant of convergence of K(t) is

$$\text{Time Constant of } K(t) = \frac{2}{k_K K^* \left[\cos \psi_2 \frac{\partial A}{\partial K} + A \sin \psi_2 \frac{\partial \psi_1}{\partial K}\right]_{K^*, \tau^*}} . \quad \text{(C.1-1)}$$

If $\Delta K(t) \equiv 0$, then the time constant of convergence of $\tau(t)$ is

$$\text{Time Constant of } \tau(t) = \frac{2}{k_\tau K^* B^* \omega \left[\sin \psi_2 \frac{\partial A}{\partial \tau} - A \cos \psi_2 \frac{\partial \psi_1}{\partial \tau}\right]_{K^*, \tau^*}} . \quad \text{(C.1-2)}$$

To check the accuracy of these equations, a test point was arbitrarily chosen as: $K^* = 4.0$, $\tau^* = 0.35$, $\omega = 3$ radians per second, and $\theta_i(t) = 20 \sin 3t$ volts.

Under these conditions, and after considerable computational effort, Eqs. (C.1-1) and (C.1-2) reduce to

$$\text{Time Constant of } K(t) = \frac{1.52 \times 10^{-2}}{k_K} \qquad \text{(C.1-3)}$$

and

$$\text{Time Constant of } \tau(t) = \frac{1.345 \times 10^{-4}}{k_\tau} \; . \qquad \text{(C.1-4)}$$

The intermediate calculations between these two sets of equations have been omitted since they are straightforward, but fairly lengthy.

For a time constant of sixteen seconds, again chosen arbitrarily, k_K is found to be 9.5×10^{-4} and k_τ to be 8.4×10^{-6}. Figures C.1.1 and C.1.2 show the convergence of K(t) when K* is being tracked alone, and all of the above conditions are being applied. Convergence properties from both above and below K* are given. Figures C.1.3 and C.1.4 show the convergence of $\tau(t)$ when τ^* is being tracked alone, with all of the above conditions being applied. Again, convergence properties from both above and below the correct value are given. In all four figures the apparent time constant is seen to be approximately sixteen seconds.

Figure C.1.5 gives the convergence of K(t) and $\tau(t)$ when $|\theta_i(t)|$ has been doubled over the value used in Figs. C.1.1 through C.1.4. From the work of Chapter 4 this should cause the time constants to be reduced by a factor of four. In both cases the time constants are close to the theoretical values of four seconds. The four second time

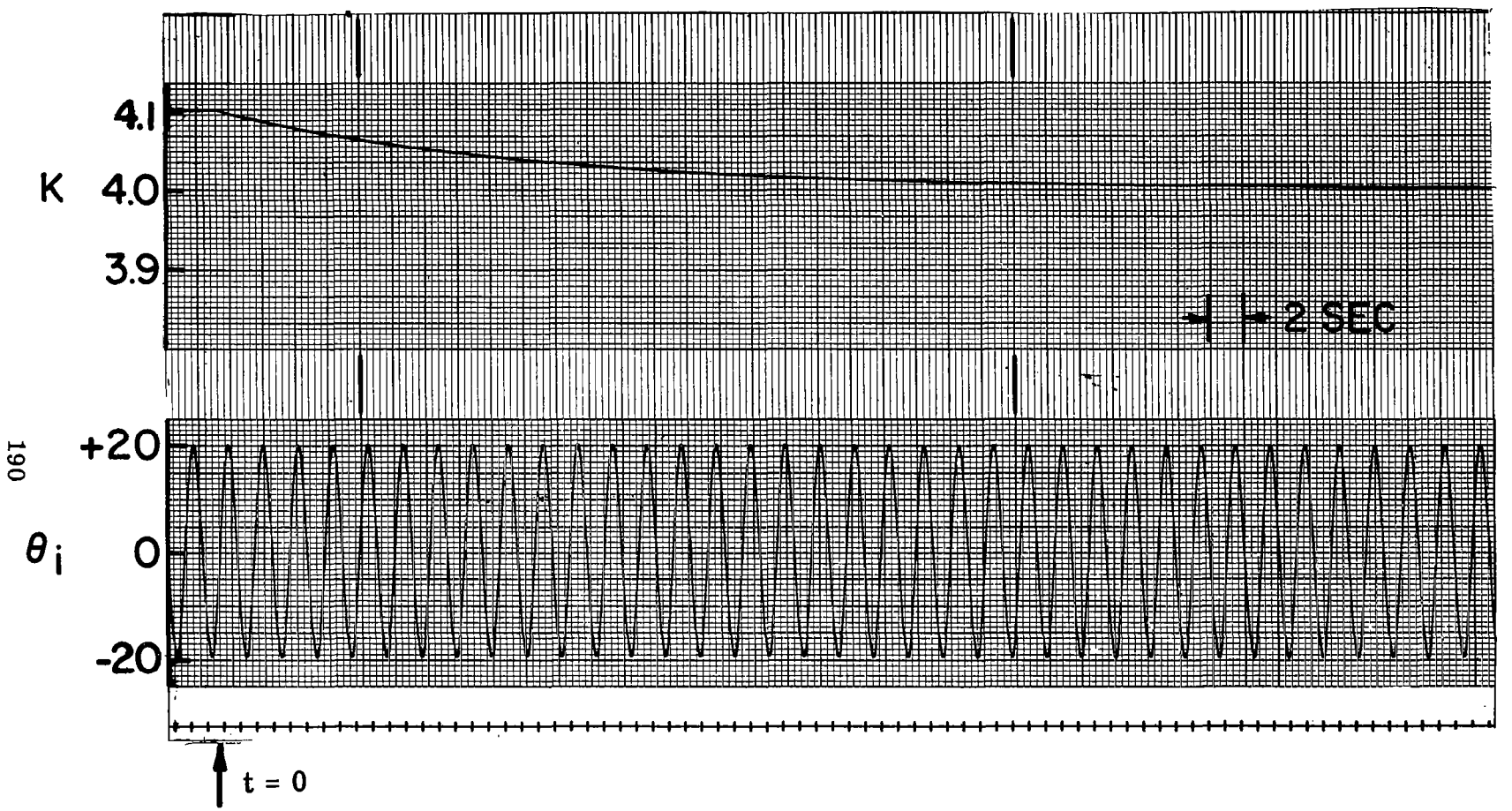

Figure C.1.1 Convergence of K(t) from Below K* = 4.0. Sinusoidal Input Signal. Theoretical Time Constant of 16 Seconds.

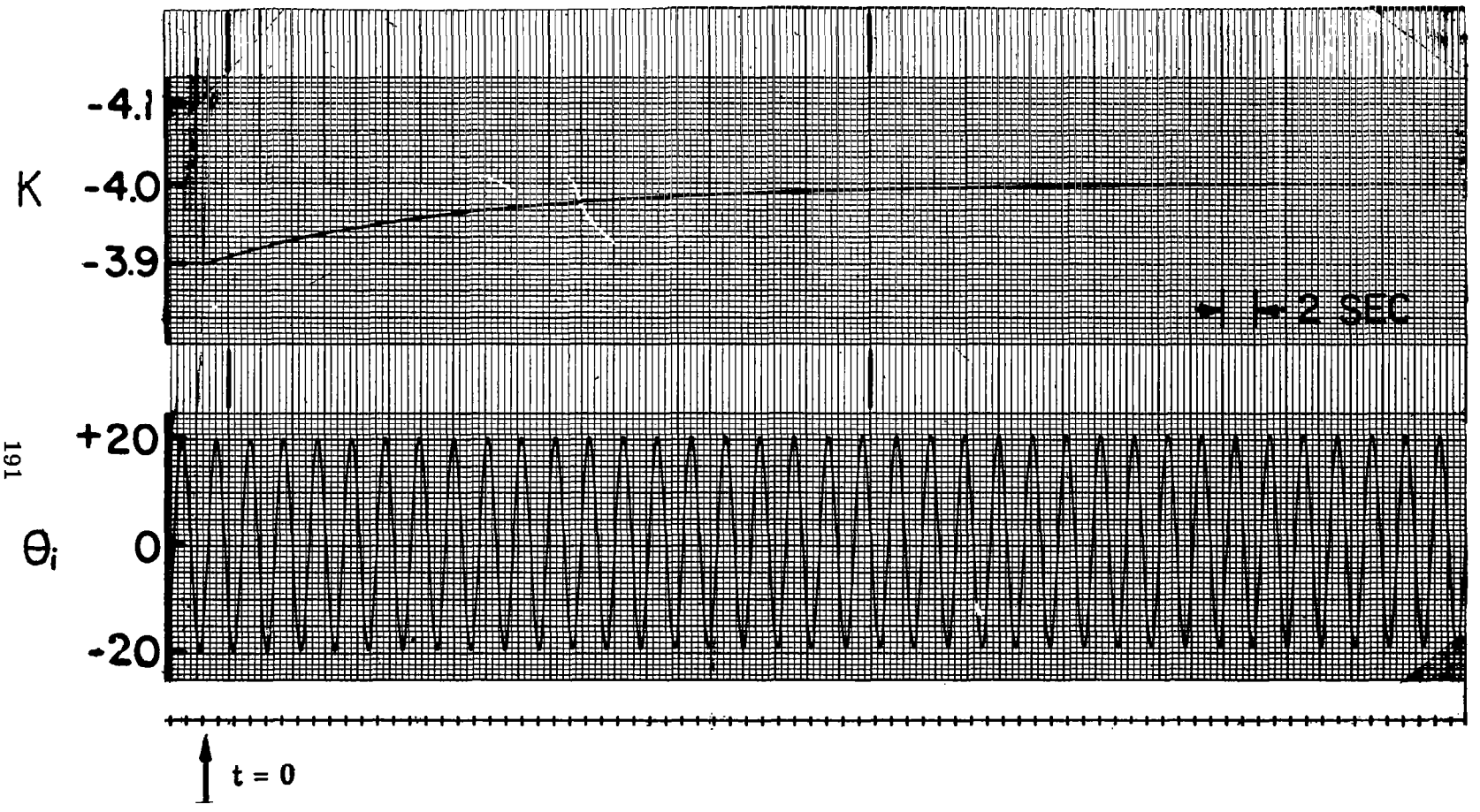

Figure C.1.2 Convergence of K(t) from Above K* = 4.0. Sinusoidal Input Signal. Theoretical Time Constant of 16 Seconds.

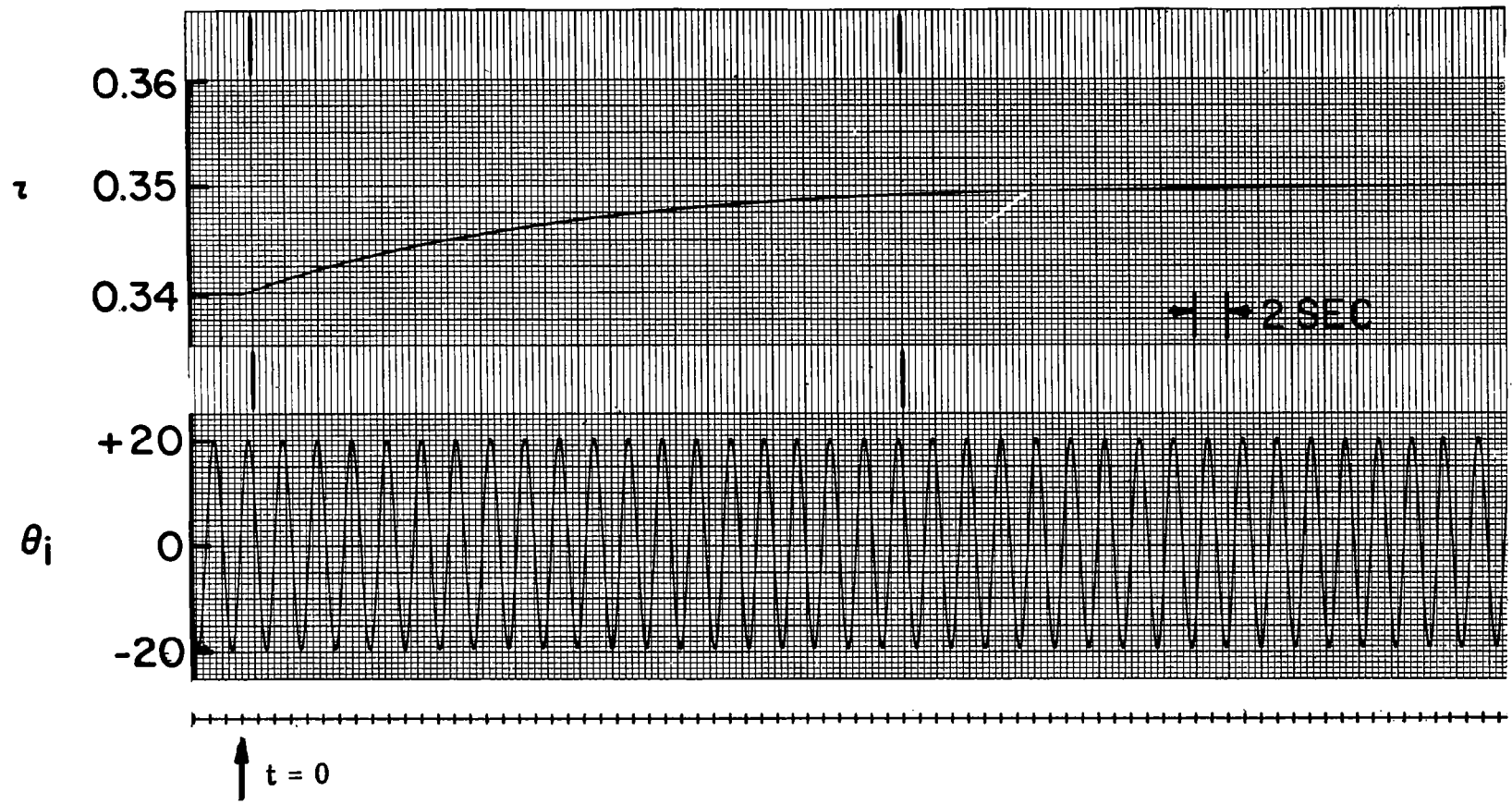

Figure C. 1. 3 Convergence of $\tau(t)$ from Below $\tau^* = 0.35$. Sinusoidal Input Signal. Theoretical Time Constant of 16 Seconds.

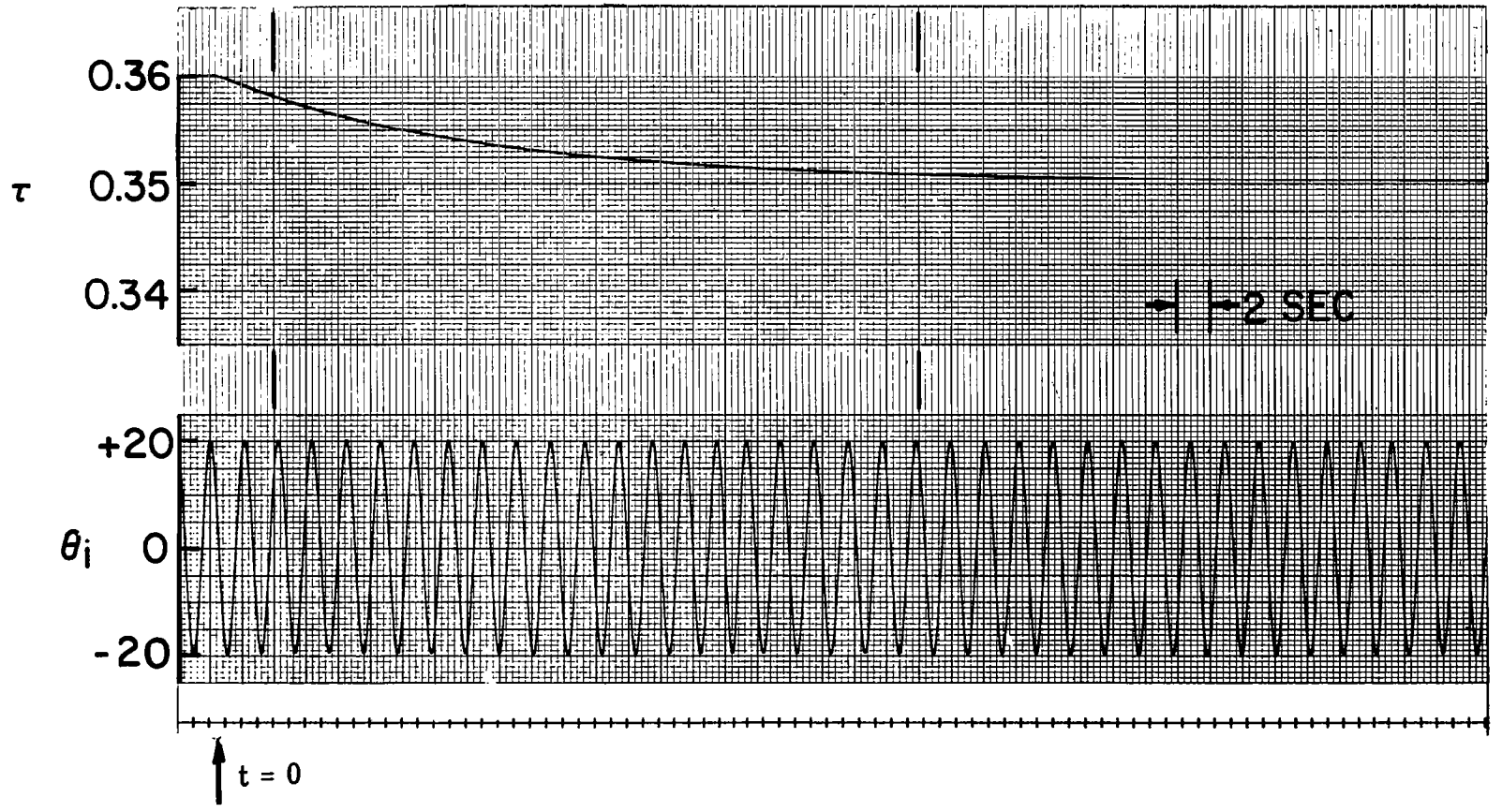

Figure C.1.4 Convergence of $\tau(t)$ from Above $\tau^* = 0.35$. Sinusoidal Input Signal. Theoretical Time Constant of 16 Seconds.

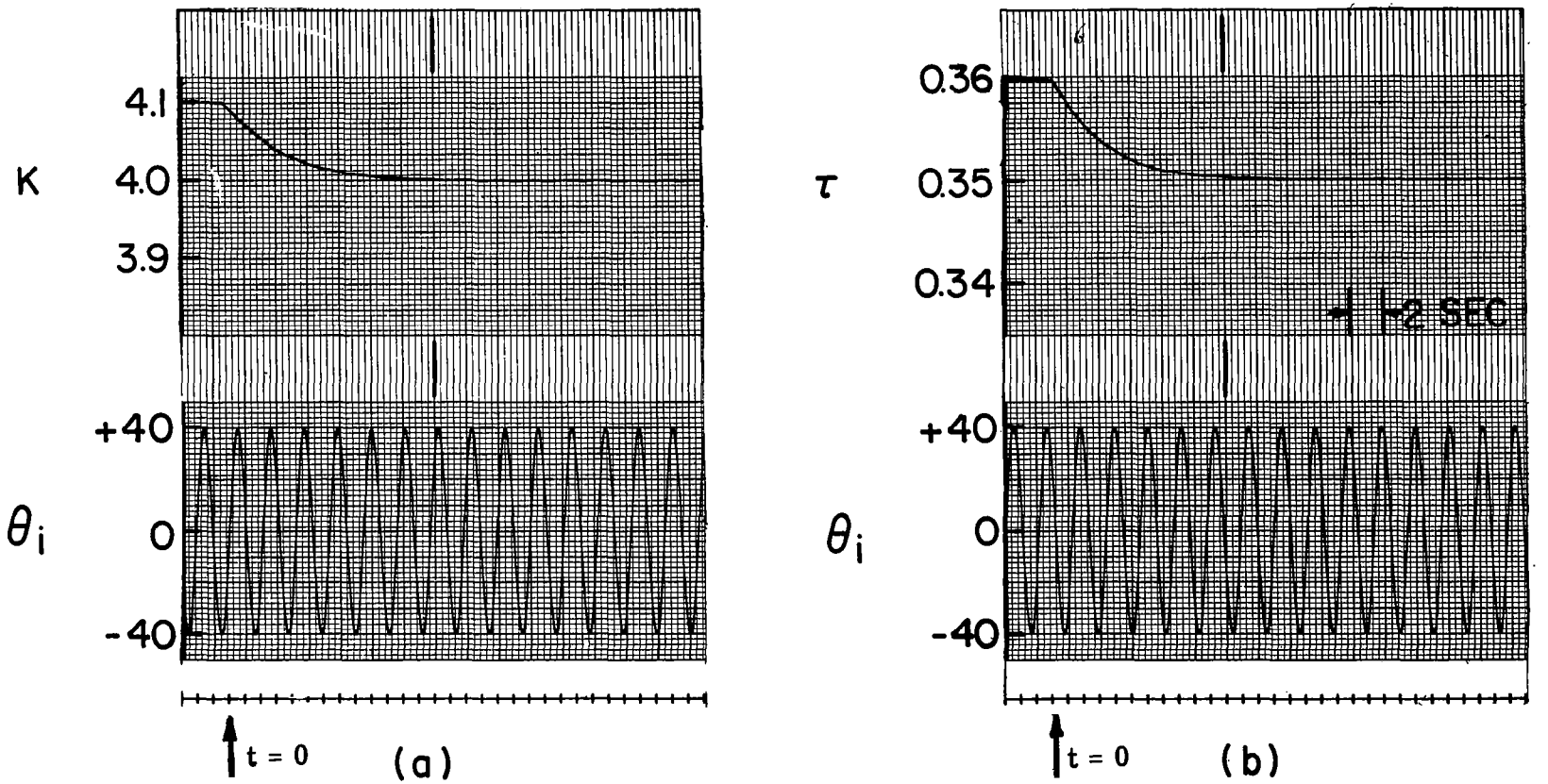

Figure C.1.5 Convergence of K(t) and τ(t) from Above K* = 4.0 and τ* = 0.35. Sinusoidal Input Signal. Theoretical Time Constant of 4 seconds in Each Case.

constants are actually pushing the limits on the use of Eqs. (C.1-1) and (C.1-2), since K(t) and $\tau(t)$ are no longer changing "slowly" with respect to the transients in the approximate crossover model. This is shown by noting that the characteristic equation of the approximate crossover model is

$$\lambda^2 + \left(\frac{2}{\tau^*} - K^*\right)\lambda + \frac{2K^*}{\tau^*} = 0$$

Comparing this equation with the standard form

$$\lambda^2 + 2\xi\omega_n\lambda + \omega_n^2 = 0$$

it follows that

$$2\xi\omega_n = \left(\frac{2}{\tau^*} - K^*\right) = \left(\frac{2}{0.35} - 4\right)$$

$$= 1.71$$

and

$$\xi\omega_n \cong 0.85.$$

The time constant of the transient decay envelope in the standard underdamped second order system is

$$\frac{1}{\xi\omega_n} \cong \frac{1}{0.85} \cong 1.18 \text{ seconds} \quad .$$

This is close to the value of 4 seconds found above in the convergence

rates of K(t) and τ(t), and indicates that Eq. (4.7-17) is good even when changes in K(t) and τ(t) are relatively fast.

To determine the stability of the parameter tracking system when both K(t) and τ(t) are being tracked and θ_i(t) is a sinusoid, Eq. (4.7-17) must be analyzed.

Equation (4.7-17) is of the form

$$\begin{bmatrix} \dot{K}(t) \\ \dot{\tau}(t) \end{bmatrix} = B \begin{bmatrix} K(t) \\ \tau(t) \end{bmatrix} \quad , \qquad \text{(C.1-4)}$$

where B is a 2x2 coefficient matrix. Using the same conditions on K*, τ*, and θ_i(t) as discussed above, the matrix B reduces to

$$B = \begin{bmatrix} -65.9\, k_K & -3.42\, k_K \\ +5.31\, k_\tau & -7440\, k_\tau \end{bmatrix} \quad . \qquad \text{(C.1-5)}$$

Evaluating det[B - λI] = 0, it is found that

$$\lambda^2 + (7440\, k_\tau + 65.9\, k_K)\lambda + 491,058\, k_K\, k_\tau = 0 \quad . \qquad \text{(C.1-6)}$$

As long as $k_K > 0$ and $k_\tau > 0$, Eq. (C.1-6) will yield two roots with negative real parts and the system is asymptotically stable. This will be verified in the next section, even when K(0) and τ(0) are far different from K* and τ*.

C. 2 Sinusoidal Input Signal—Limited Parameter Adjustment

Figures C. 2. 1 and C. 2. 2 indicate how the limited parameter adjustment technique affects the convergence rates of K(t) and τ(t) when both parameters are being tracked against a known model with a sinusoidal input signal. Figure C. 2. 1 has no limiting in either parameter adjustment loop. Figure C. 2. 2 has rather severe limiting in both parameter adjustment loops.

The input signal, gradient gains, and K* and τ* values are the same ones used in Fig. C. 1. 5 where K(t) and τ(t) were being tracked alone. It is evident that when limiting is not present, the new initial conditions on K(t) and τ(t), combined with dual parameter tracking, have drastically changed the convergence rates from those found in Fig. C. 1. 5. The parameters do converge asymptotically, as predicted by Eq. (C. 1-6).

In the limited case, the parameters still converge asymptotically although the rates are much slower. This point was evaluated in Section 4. 9.

C. 3 Random Input—Two Parameters Tracking a Known Model of the Correct Form

Figures C. 3. 1 to C. 3. 4 are typical convergence curves found when tracking a known model of the correct form. Figures C. 3. 1 and C. 3. 2 have ω_i = 2 radians/second and Figs. C. 3. 3 and C. 3. 4 have

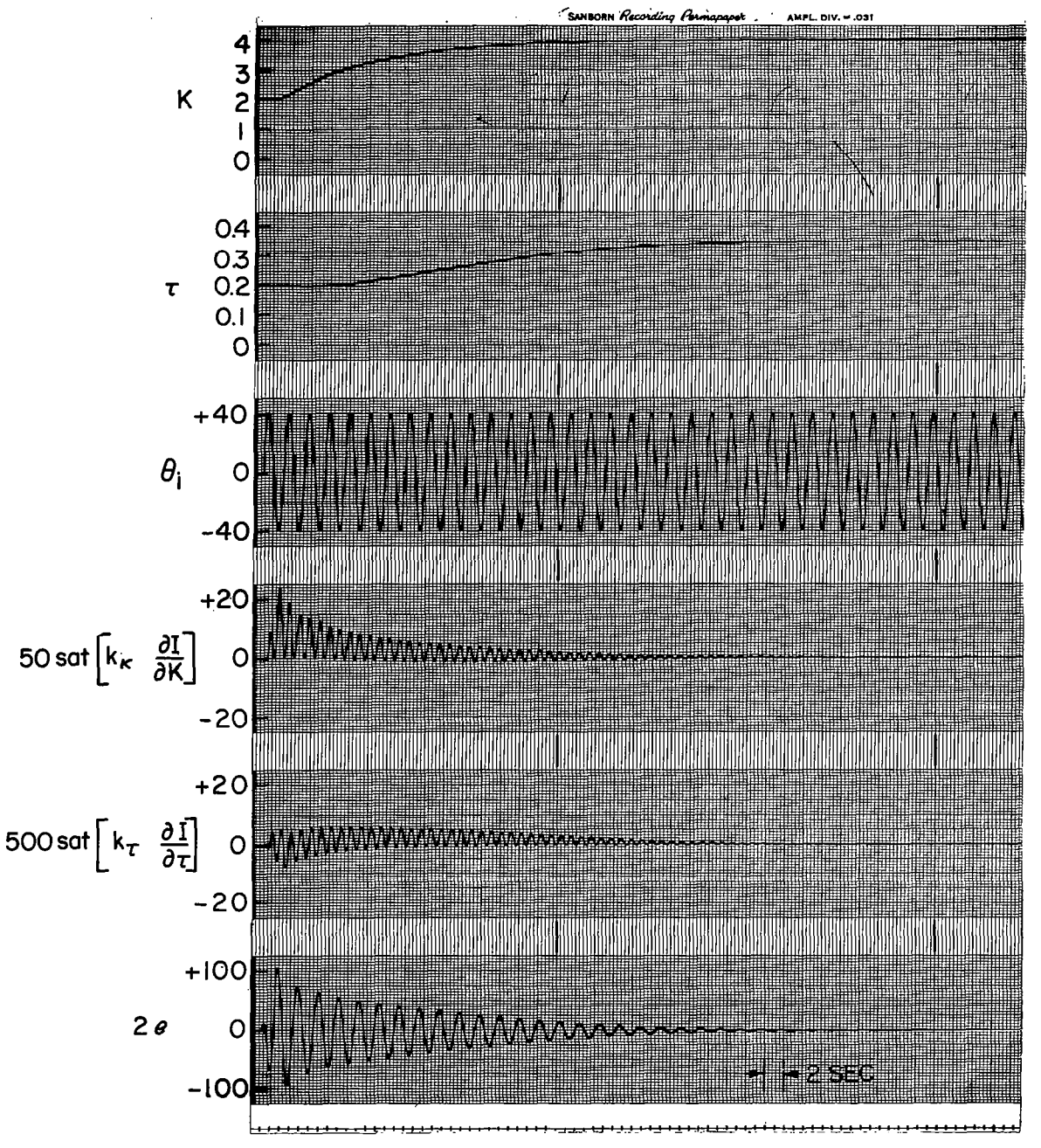

Figure C.2.1 Convergence of K(t) and τ(t) When Tracking Both Parameters. Sinusoidal Input Signal. $K^* = 4.0$ and $\tau^* = 0.35$. $k_K = 9.5 \times 10^{-4}$ and $k_\tau = 8.4 \times 10^{-6}$. No Parameter Adjustment Limiting.

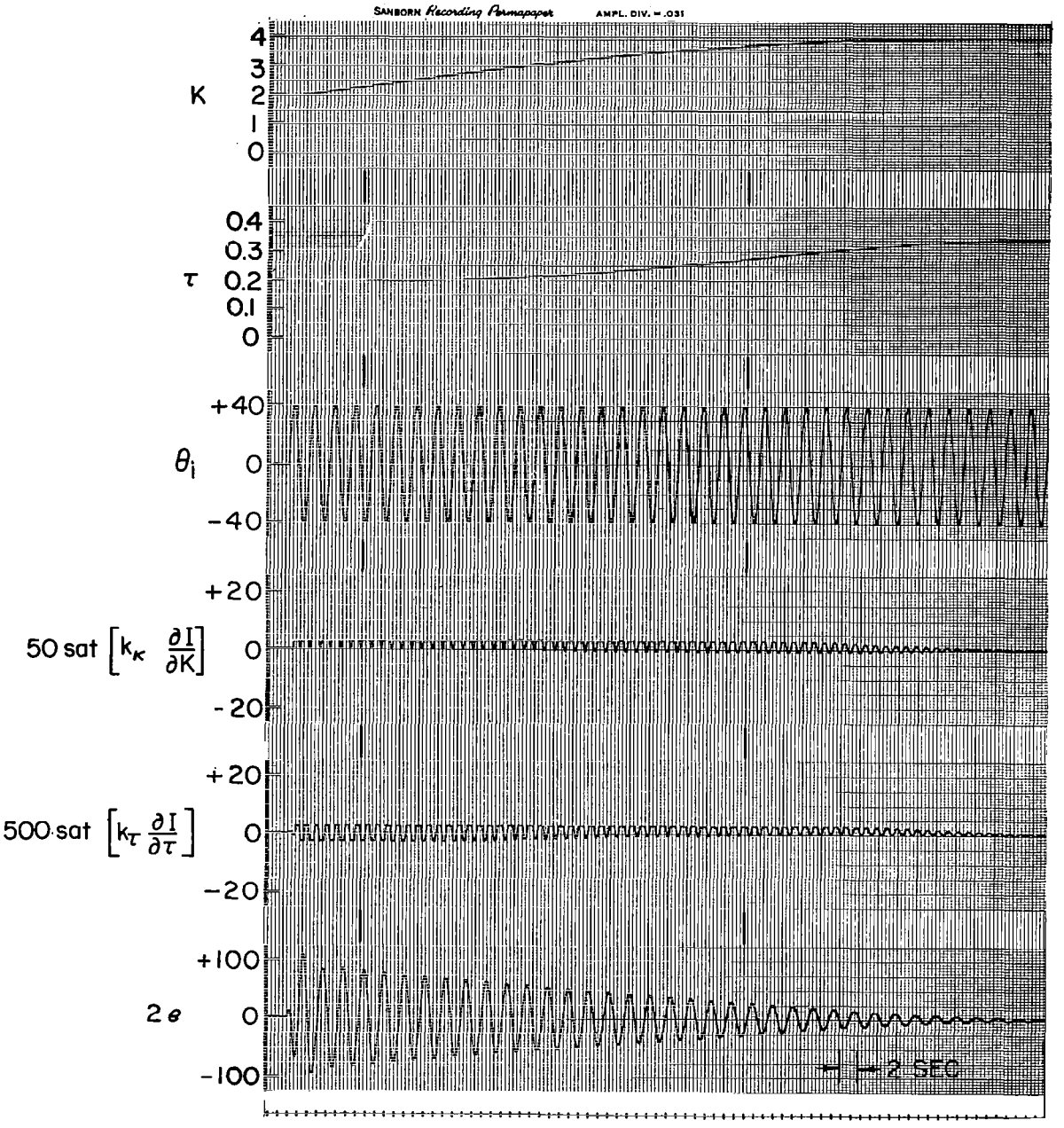

Figure C.2.2 Convergence of K(t) and τ(t) when Tracking Both Parameters. Sinusoidal Input Signal. $K^* = 4.0$ and $\tau^* = 0.35$. $k_K = 9.5 \times 10^{-4}$ and $k_\tau = 8.4 \times 10^{-6}$. Severe Parameter Adjustment Limiting.

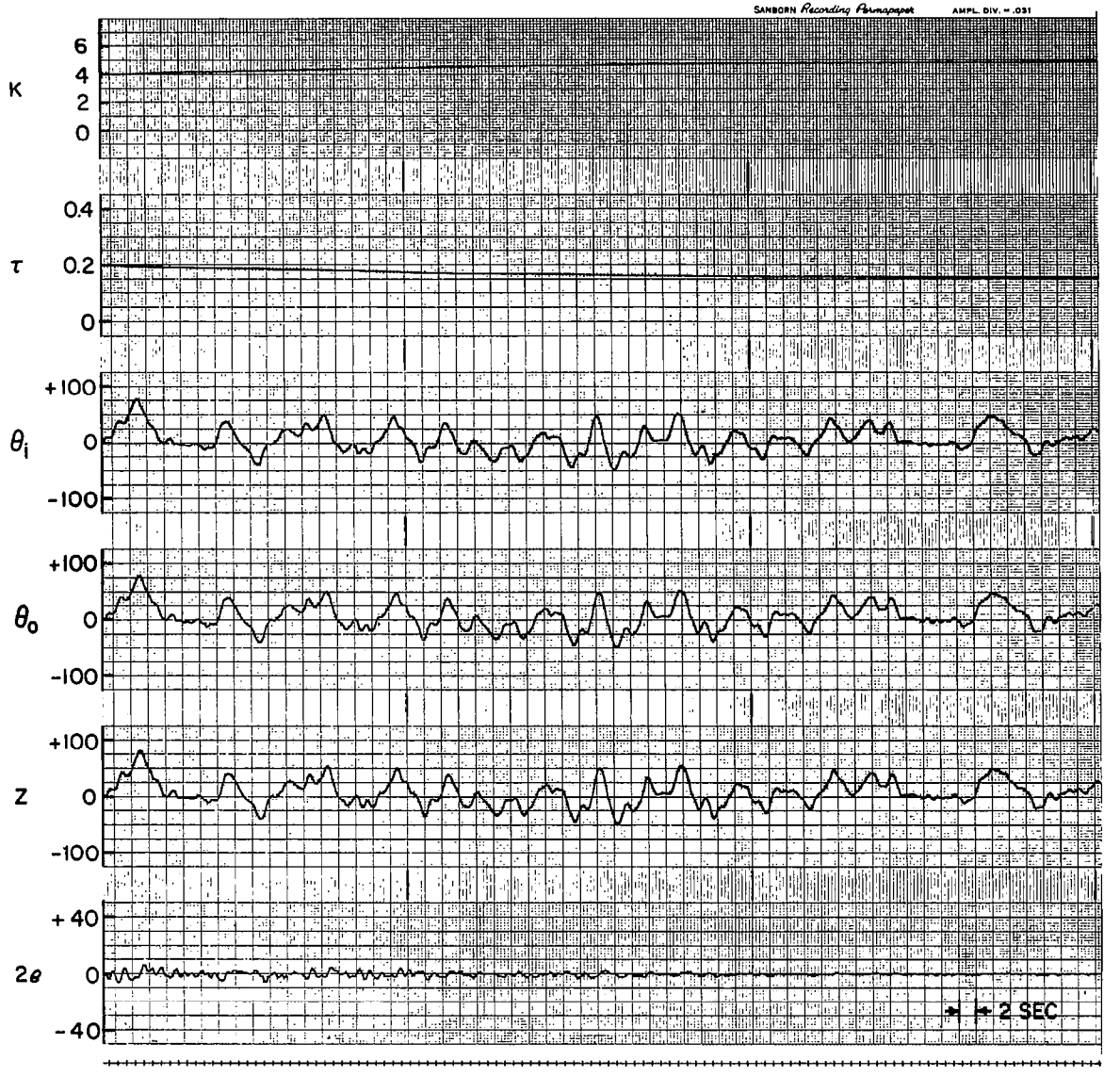

Figure C. 3. 1 Convergence on a Known Approximate Crossover Model. $K^* = 5.0$ and $\tau^* = 0.15$. Random Input Signal with $\omega_i = 2$ radians/second. $k_K = 2.5 \times 10^{-3}$ and $k_\tau = 10 \times 10^{-6}$.

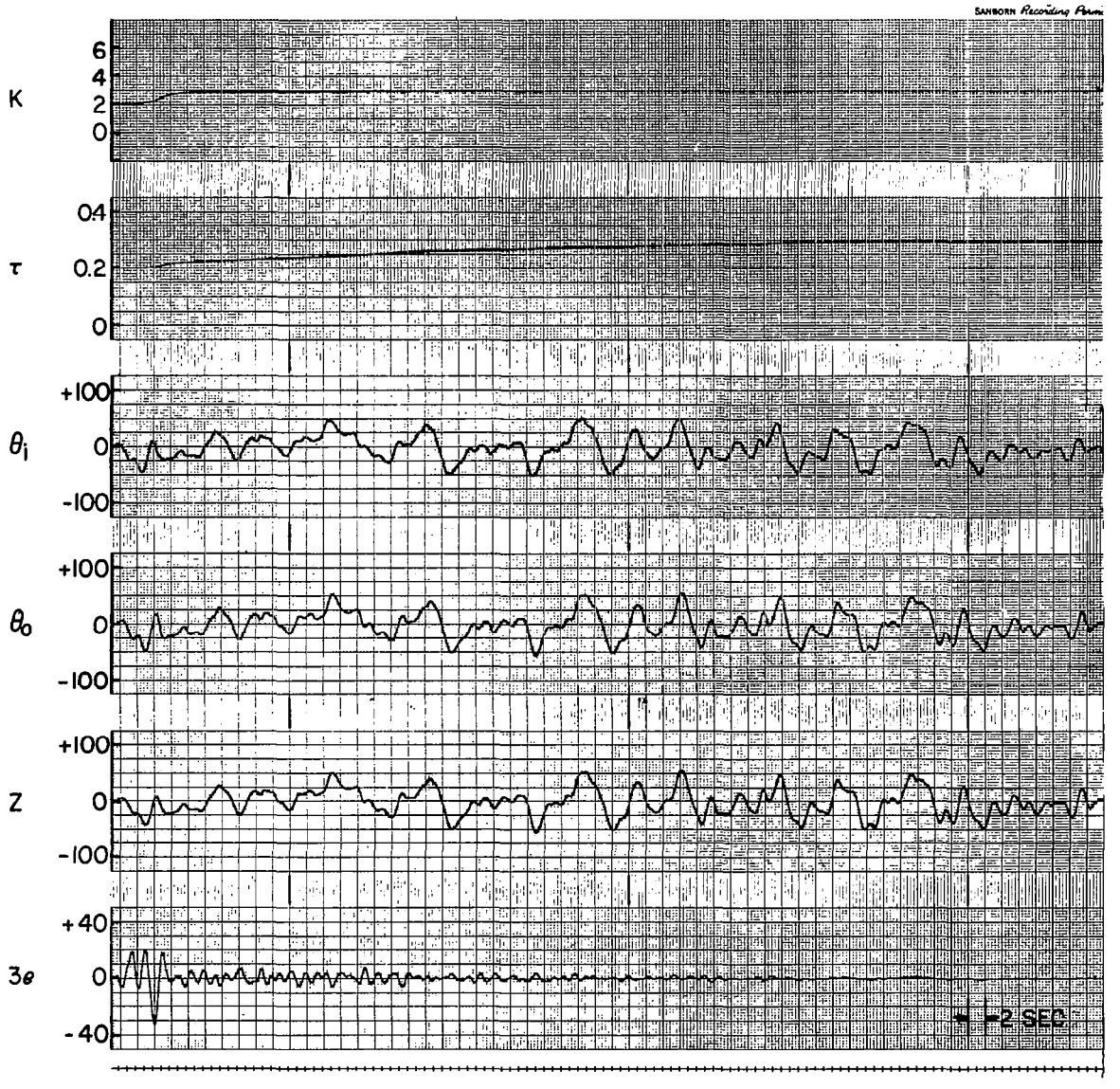

Figure C. 3.2 Convergence on a Known Approximate Crossover Model. $K^* = 3.0$ and $\tau^* = 0.30$. Random Input Signal with $\omega_i = 2$ radians/second. $k_K = 7.5 \times 10^{-3}$ and $k_\tau = 6 \times 10^{-5}$.

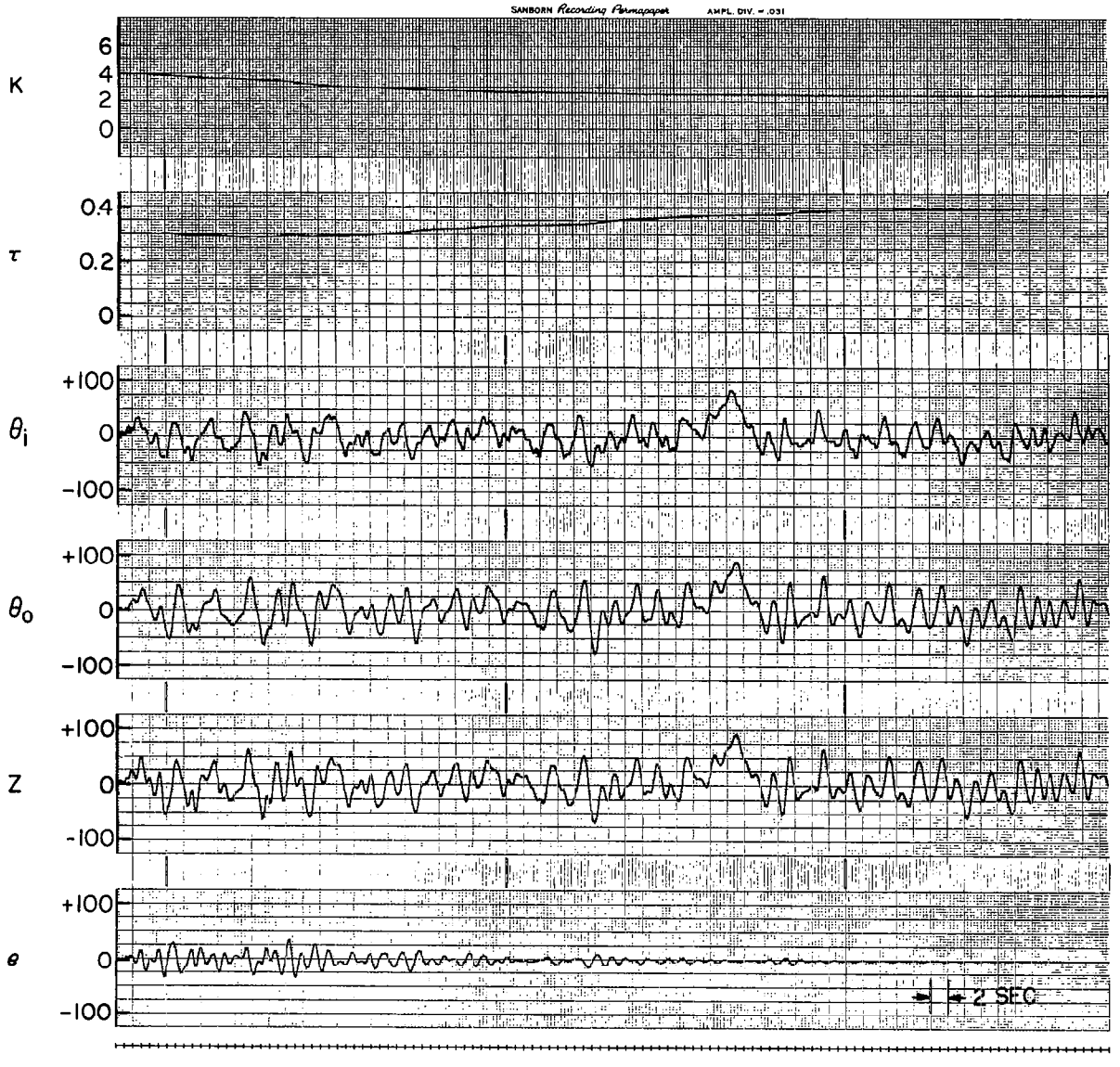

Figure C. 3. 3 Convergence on a Known Approximate Crossover Model. $K^* = 2.5$ and $\tau^* = 0.40$. Random Input Signal with $\omega_i = 4$ radians/second. $k_K = 3.1 \times 10^{-4}$ and $k_\tau = 5 \times 10^{-6}$.

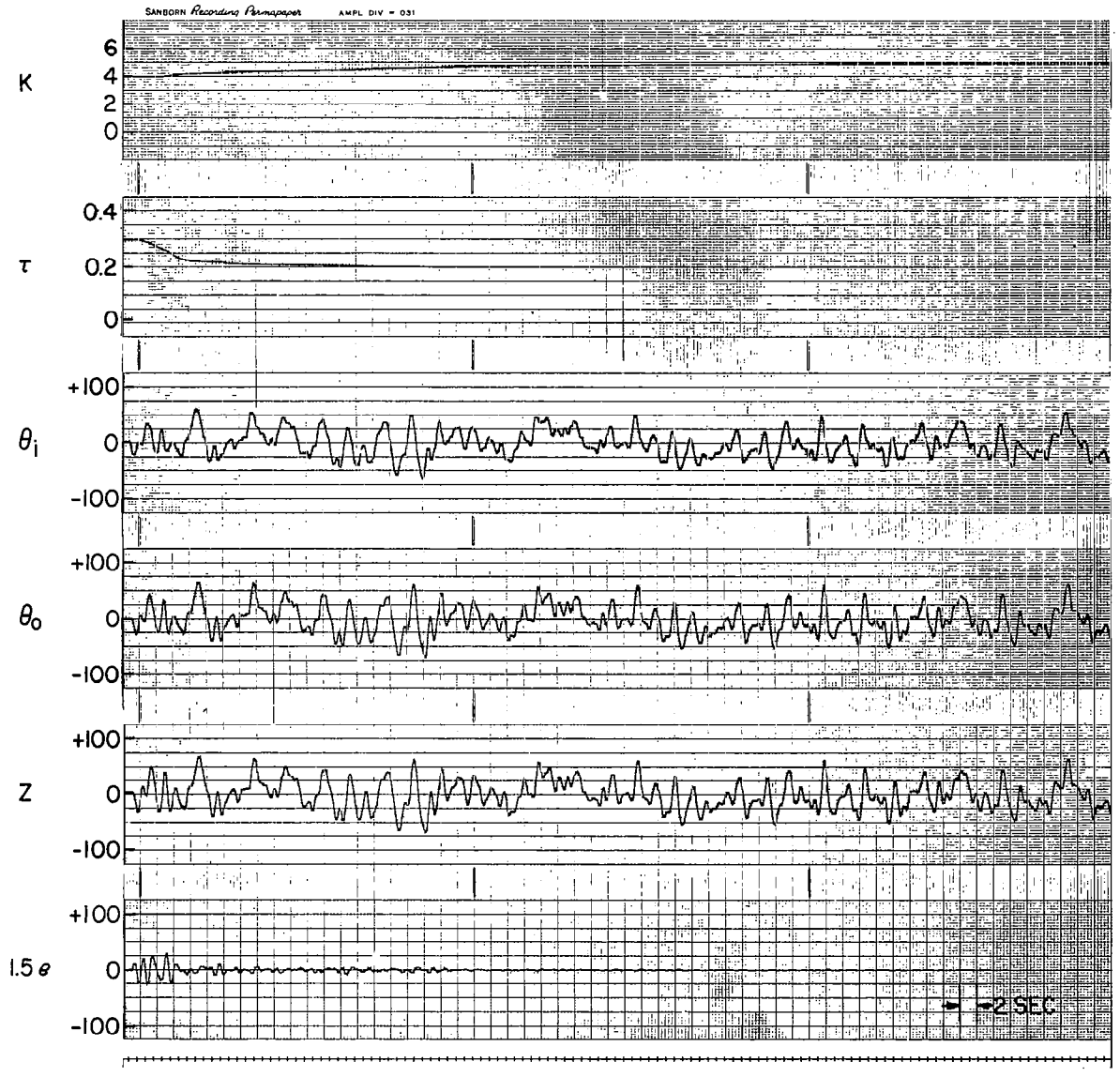

Figure C. 3. 4 Convergence on a Known Approximate Crossover Model. $K^* = 5.0$ and $\tau^* = 0.20$. Random Input Signal with $\omega_i = 4$ radians/second. $k_K = 4.65 \times 10^{-4}$ and $k_\tau = 30 \times 10^{-6}$.

ω_i = 4 radians/second. In each case different K* and τ* values were used. The k_K and k_τ values are typical of those used in actual subject testing. In each figure K(t) and τ(t) are found to converge asymptotically.

The response times shown in the figures above can be made considerably shorter by increasing the gradient gains. Complete convergence can be obtained in only three or four seconds, when no remnant is present in the model error signal e(t, K, τ). However, once remnant is present, convergence rates similar to those found in Figs. C.3.1 to C.3.4 must be used in order to give smooth parameter adjustment. The curves above are intended to show that even when the gradient gains are low, and convergence is slow, the convergence is still asymptotic.

The parameter responses given above indicate how well the tracking system is able to follow simultaneous step changes in K* and τ* with step magnitudes of $|K^* - K(0)|$ and $|\tau^* - \tau(0)|$. The slowness of the responses indicates that in actual practice the tracking system would accurately follow only very slow trends in K* and τ*. This fact has been well documented by both Bekey [7] and Hoffman [19]. Fortunately, it has been shown that, on the average, the human operator is fairly stationary for periods of 10-12 minutes or even longer [28].

C.4 Effect of Parameter Adjustment Limiting on Convergence in Actual Operation

The spectral and parameter tracking comparisons made in Chapter 6 indicated that for the cases evaluated the limited gradient did not bias the parameter values. The time histories included in this section are intended to emphasize the desirability, from and experimental viewpoint, of using this technique.

Figure C.4.1 is the time history of one 2 minute trial showing how the parameters can be greatly disturbed by a sudden increase in remnant, when the conventional linear parameter adjustment technique is used. This was one of the worst cases encountered in all of the tests conducted.

Figure C.4.2 is the same run as above with k_K and k_τ set at the same values, but with the nonlinear gradient now in use. The parameters are seen to behave in a much smoother manner. It is apparent from this one example that significant improvement in response occurs even when limiting occurs over only a small portion of the total time interval of the trial. Continuous limiting is not necessary, and is not desirable, since the probability of biasing should increase with the severity of the limiting.

It has been previously noted that the limited gradient technique was

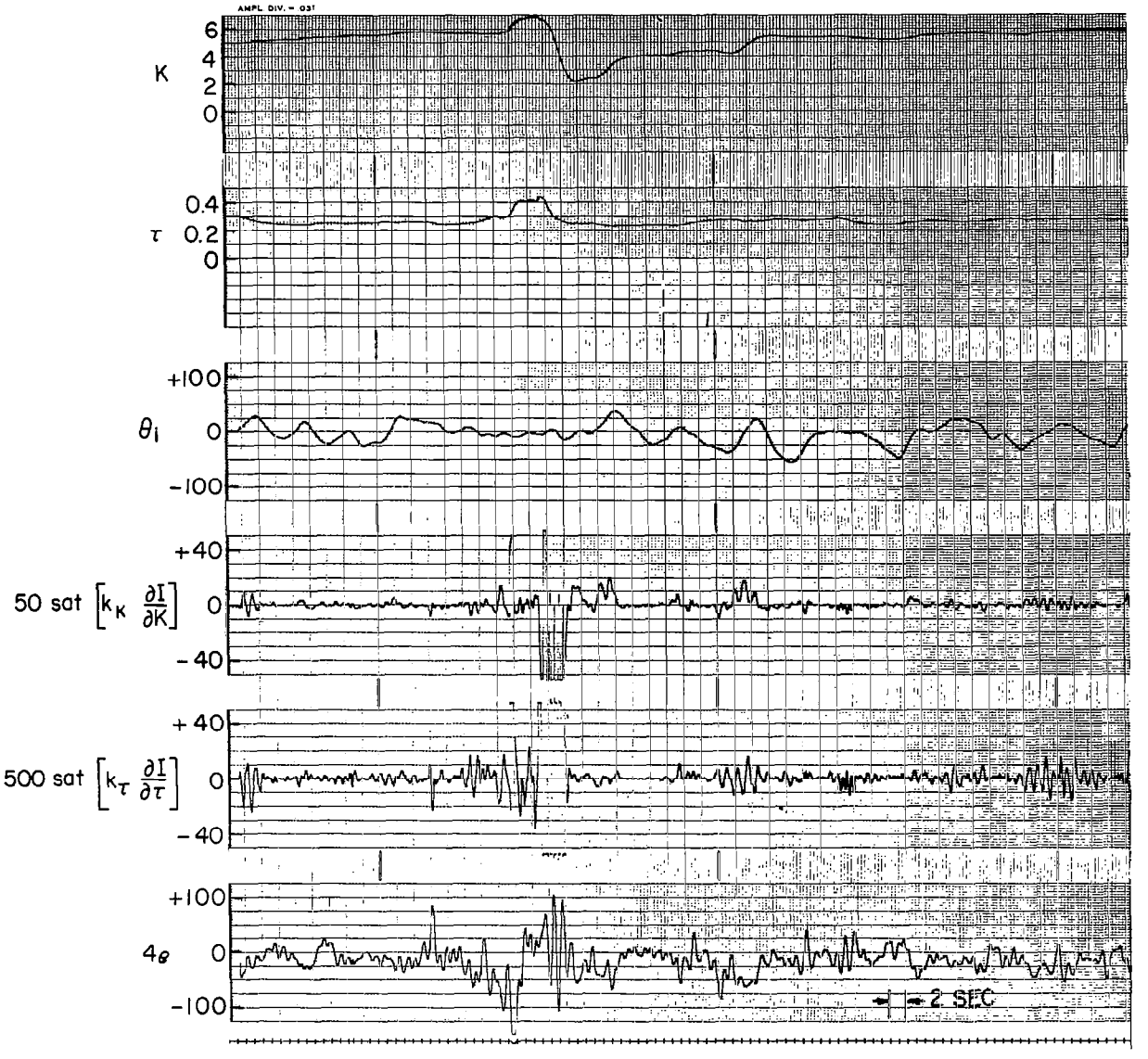

Figure C.4.1 Time History—Subject 3—Day 13—$Y_C(p) = K_2/p^2$—ω_i = 1 radian/second. $k_K = 30 \times 10^{-3}$ and $k_\tau = 24 \times 10^{-5}$. No Parameter Adjustment Limiting.

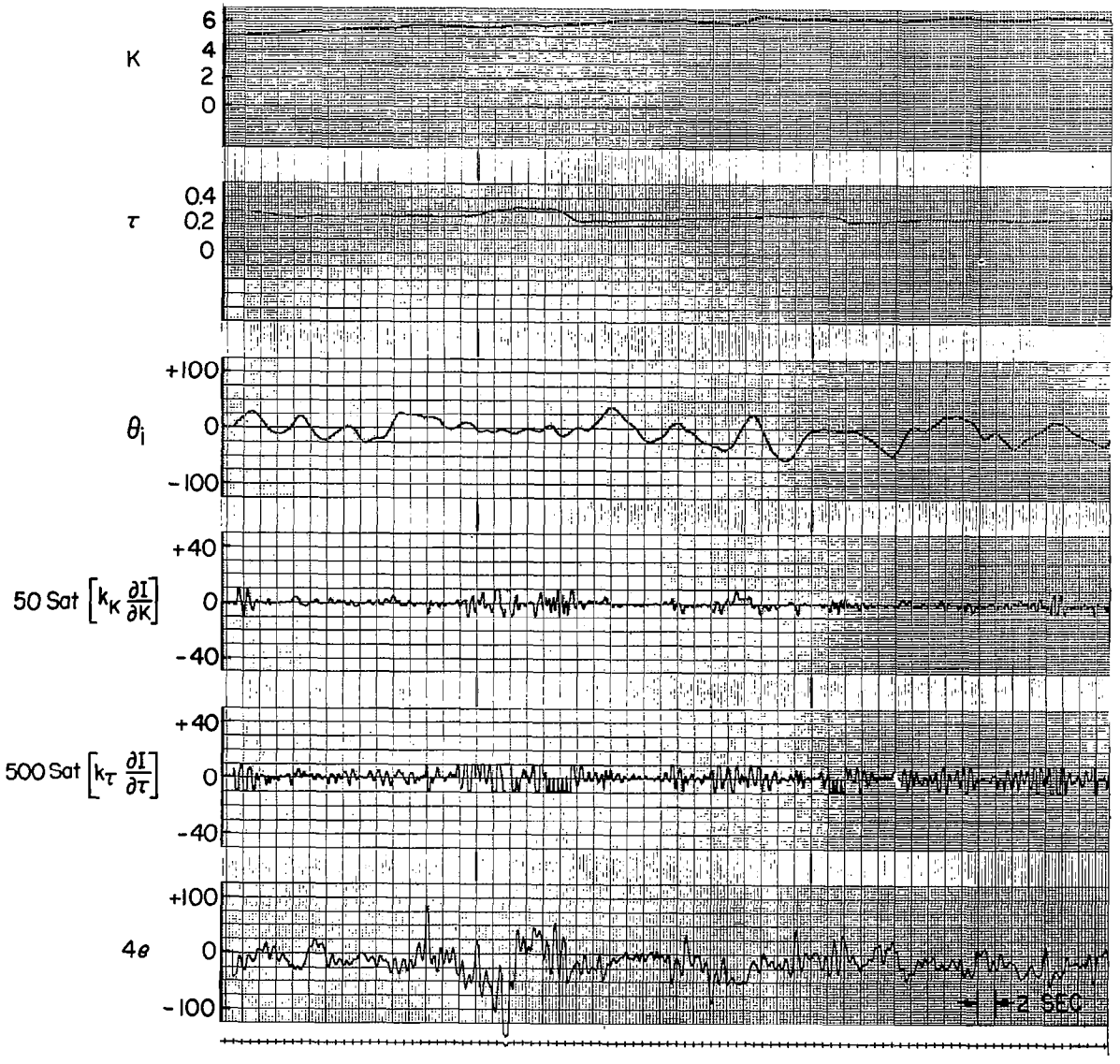

Figure C.4.2 Time History—Subject 3—Day 13—$Y_C(p) = K_2/p^2$—ω_i = 1 radian/second. $k_K = 30 \times 10^{-3}$ and $k_\tau = 24 \times 10^{-5}$. Parameter Adjustment Limiting.

used on all runs in the K_2/p^2 experiment. It should also be noted that in spite of the large amount of remnant power present in these runs, the tracking system did not go unstable a single time. This success is felt to be partly attributable to the limited gradient technique.

The stabilizing effect of the limiter is very encouraging from an experimental viewpoint. Further theoretical work on its overall effect is needed.

Appendix D

SAMPLE TIME HISTORIES

Included in this appendix are a few sample time histories from one subject from each of the two experiments. These are the same two subjects that were analyzed spectrally in Chapter 6.

D.1 Sample Time Histories from the $Y_C(p) = K_1/p$ Experiment

Figures D.1.1 through D.1.4 are sample time histories from Subject 1 of the first compensatory tracking experiment. In each case the initial conditions on K(t) and τ(t) have purposely been set far enough away from their final values so that the convergence rates can be observed.

In actual subject testing, the initial conditions on K(t) and τ(t) were adjusted after the first run at each test condition so that the parameters were not far from their probable final values. The initial conditions on the first run of each block of five runs were set away from the probable final values so that convergence could be observed.

The gradient gains used in these figures are the same ones used in actual data reduction.

D.2 Sample Time Histories from the $Y_C(p) = K_2/p^2$ Experiment

Figures D.2.1 through D.2.4 are sample time histories from Subject 3 of the second compensatory tracking experiment. The

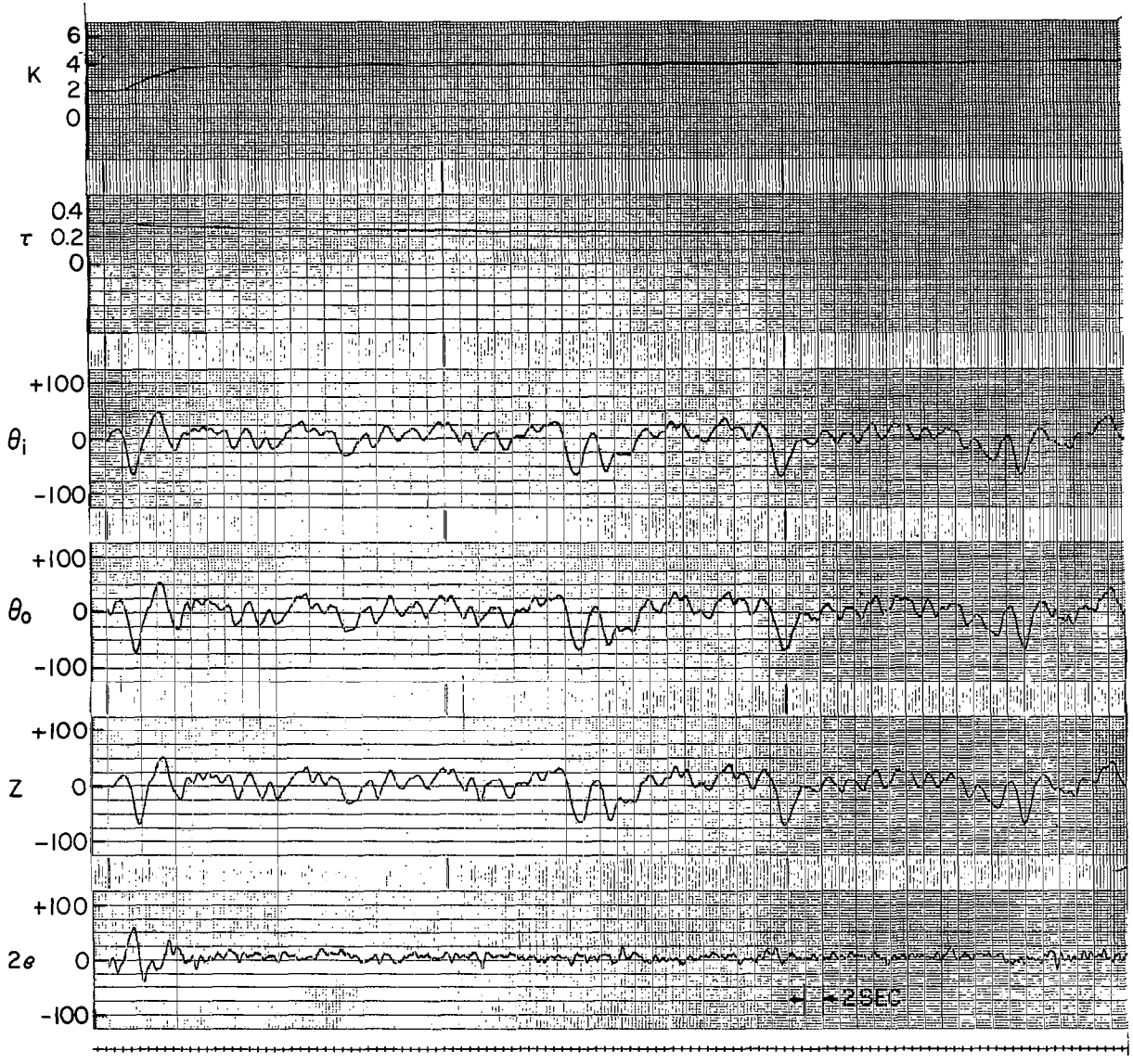

Figure D.1.1 Time History—Subject 1—Day 2—ω_i = 2 radians/second—Run 5—$Y_C(p) = K_1/p$—$k_K = 6 \times 10^{-3}$—$k_\tau = 1.6 \times 10^{-5}$.

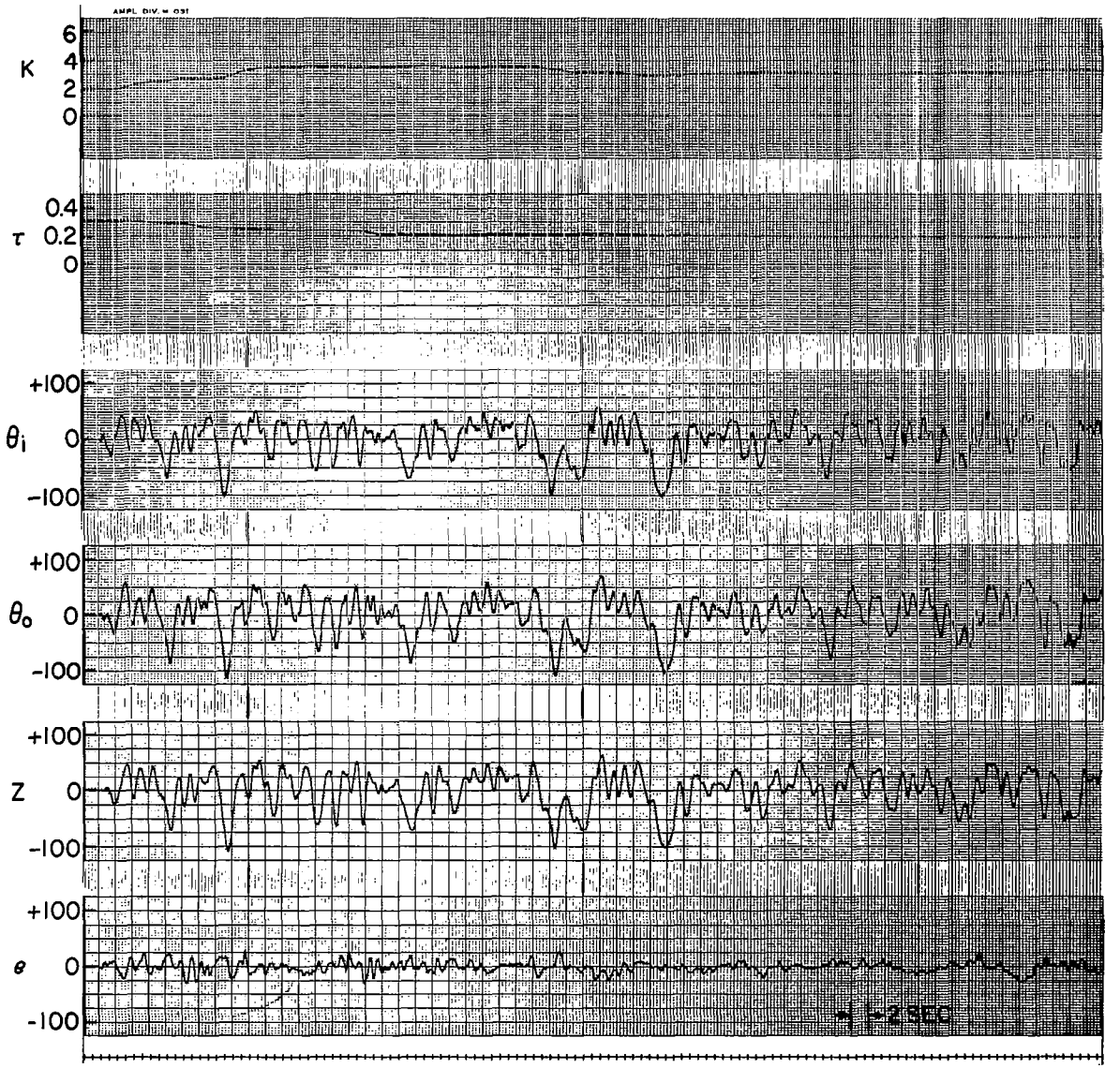

Figure D.1.2 Time History—Subject 1—Day 2—ω_i = 4 radians/second—Run 1—$Y_C(p) = K_1/p$—$k_K = 1.25 \times 10^{-3}$—$k_\tau = 4 \times 10^{-6}$.

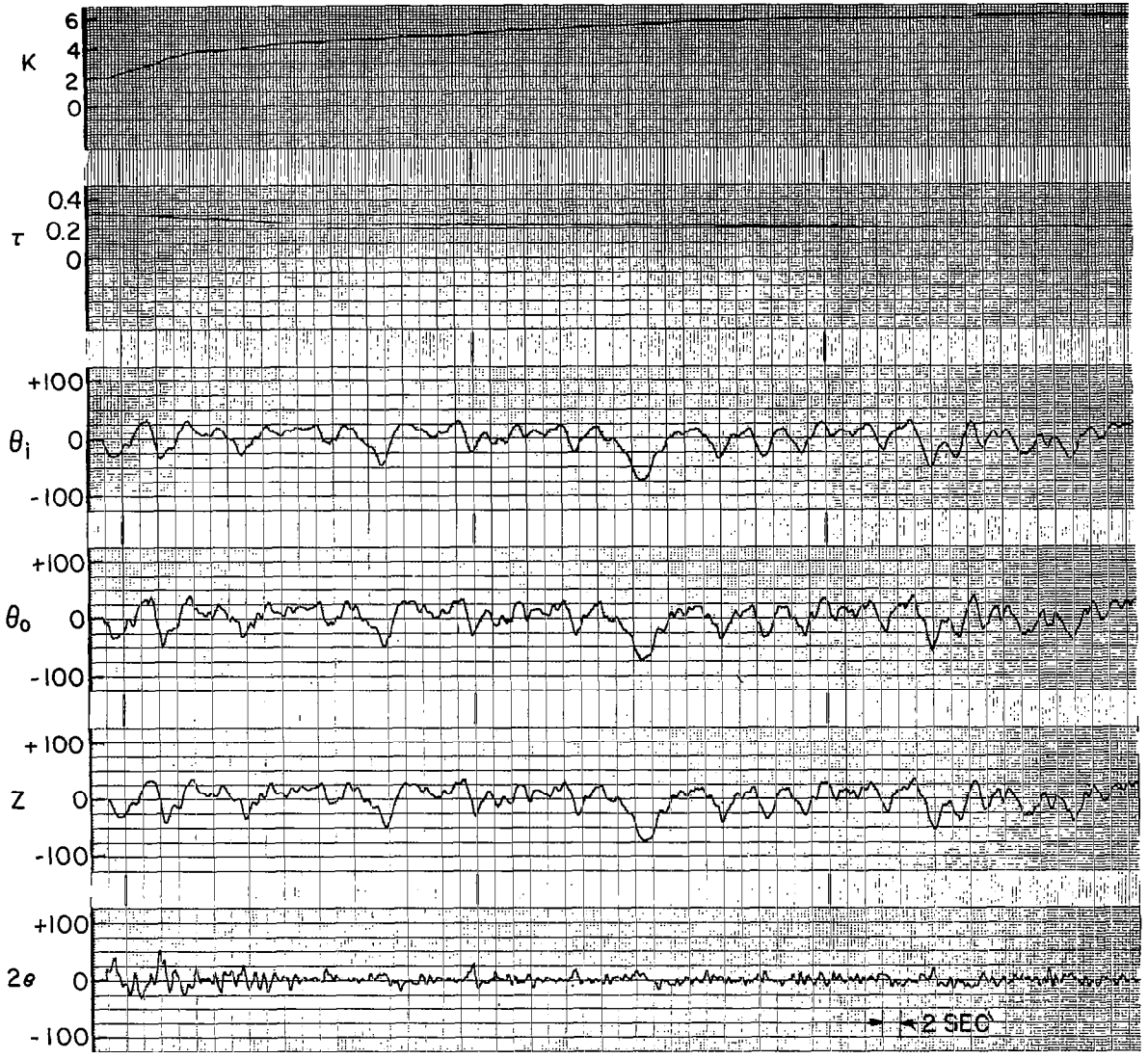

Figure D.1.3 Time History—Subject 1—Day 10—ω_i = 2 radians/second—Run 1—$Y_C(p) = K_1/p$—$k_K = 1.2 \times 10^{-4}$—$k_\tau = 1.6 \times 10^{-5}$.

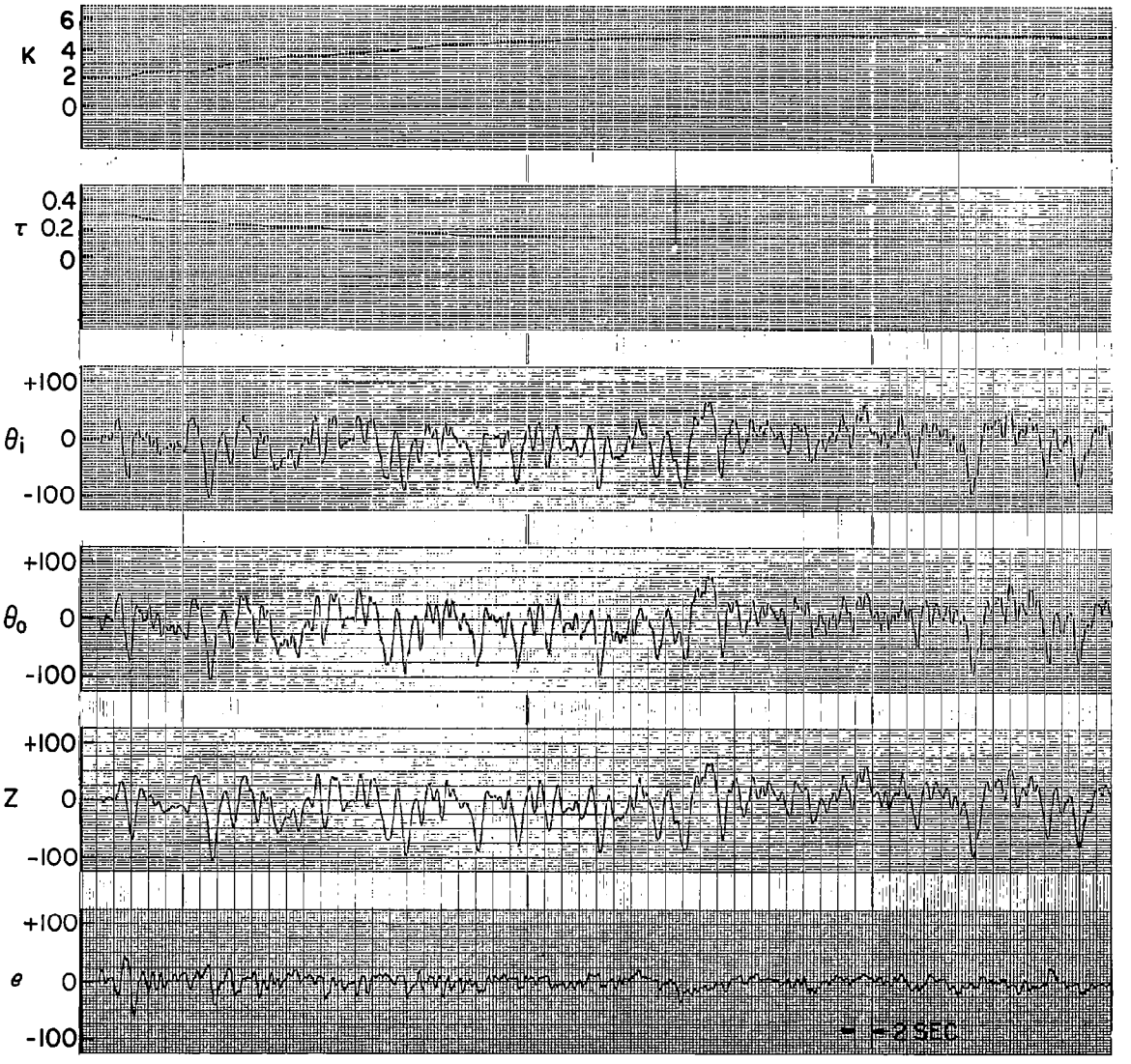

Figure D.1.4 Time History—Subject 1—Day 10—ω_i = 4 radians/second—Run 1—$Y_C(p) = K_1/p$—$k_K = 1.25 \times 10^{-3}$—$k_\tau^i = 4 \times 10^{-6}$.

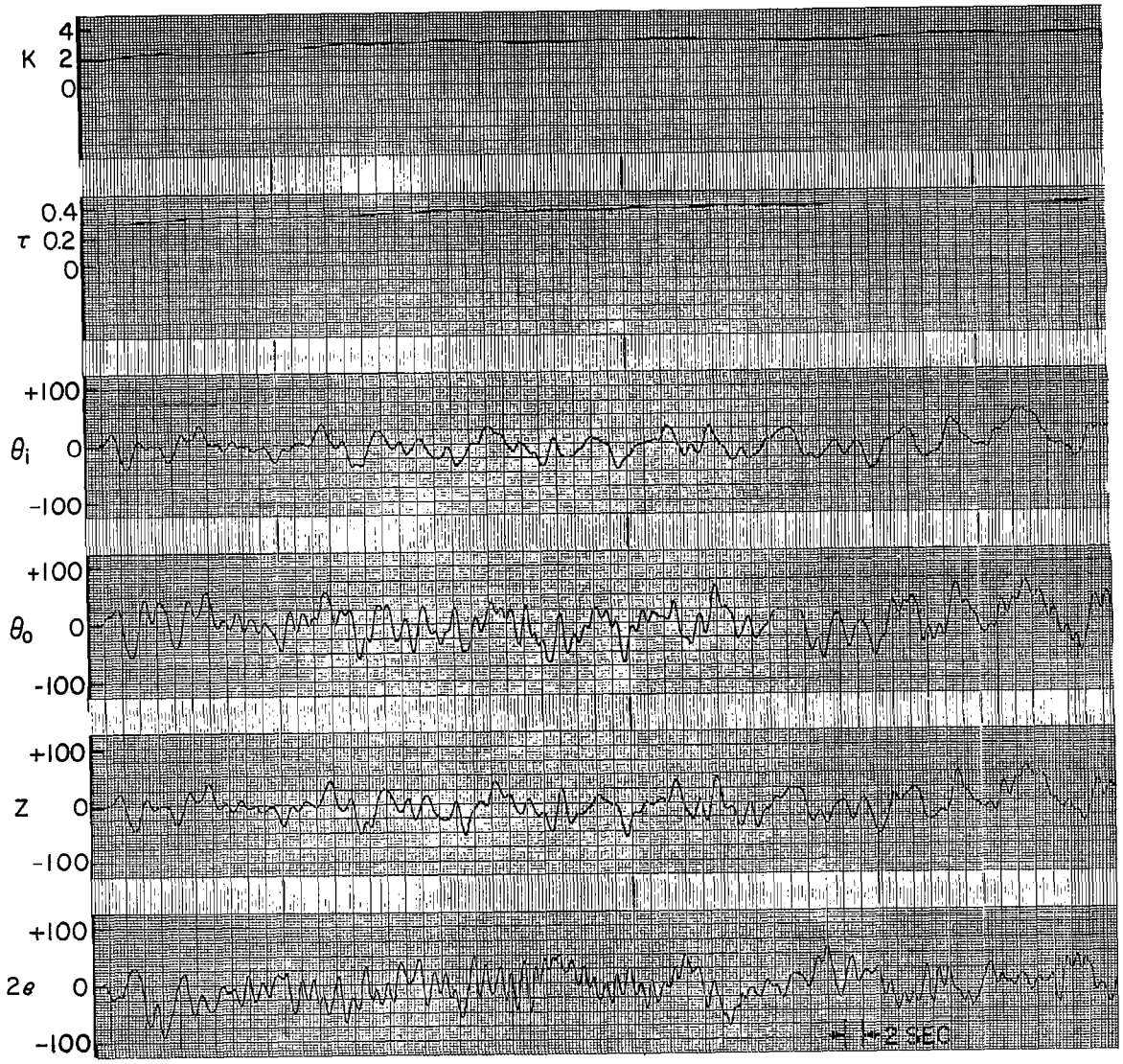

Figure D.2.1 Time History—Subject 3—Day 5—ω_i = 2 radians/second—Run 1—$Y_C(p) = K_2/p^2$—$k_K = 4 \times 10^{-3}$—$k_\tau = 1.6 \times 10^{-5}$.

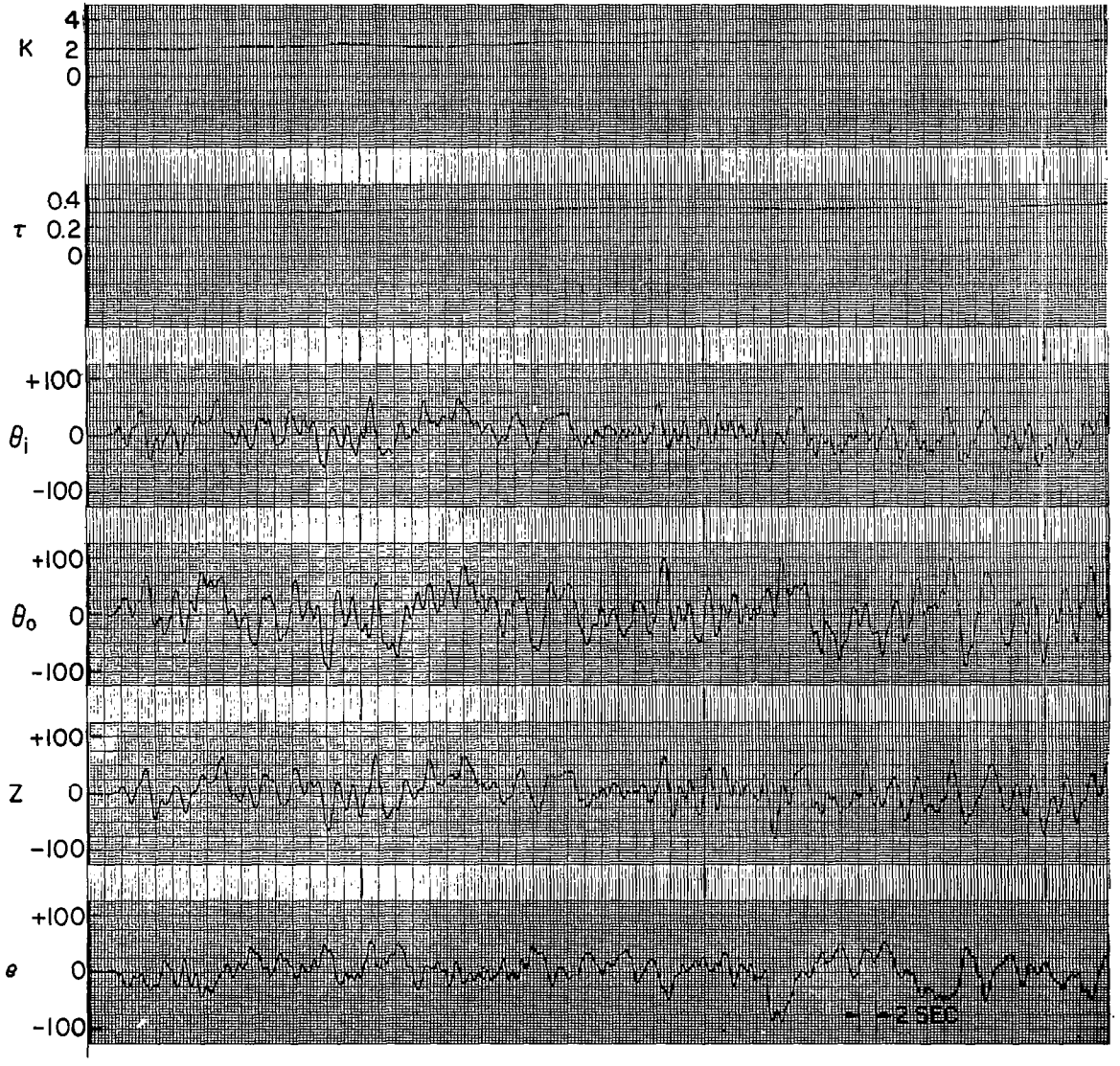

Figure D.2.2 Time History—Subject 3—Day 5—ω_i = 4 radians/second—Run 1—$Y_C(p) = K_2/p^2$—$k_K = 1 \times 10^{-3}$—$k_\tau = 4 \times 10^{-6}$.

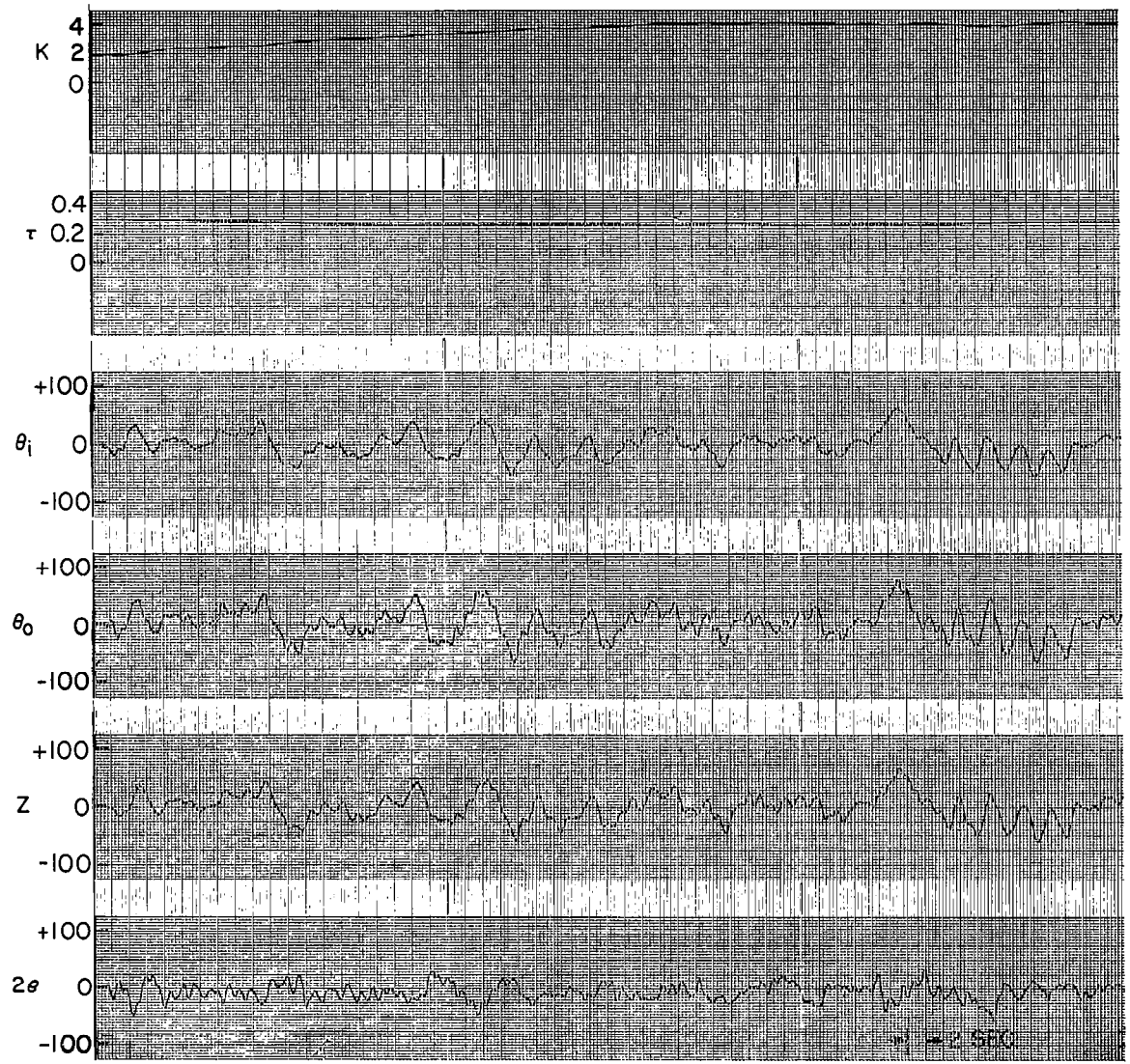

Figure D.2.3 Time History—Subject 3—Day 13—ω_i = 2 radians/second—Run 1—$Y_C(p) = K_2/p^2$—$k_K = 4 \times 10^{-3}$—$k_\tau = 1.6 \times 10^{-5}$.

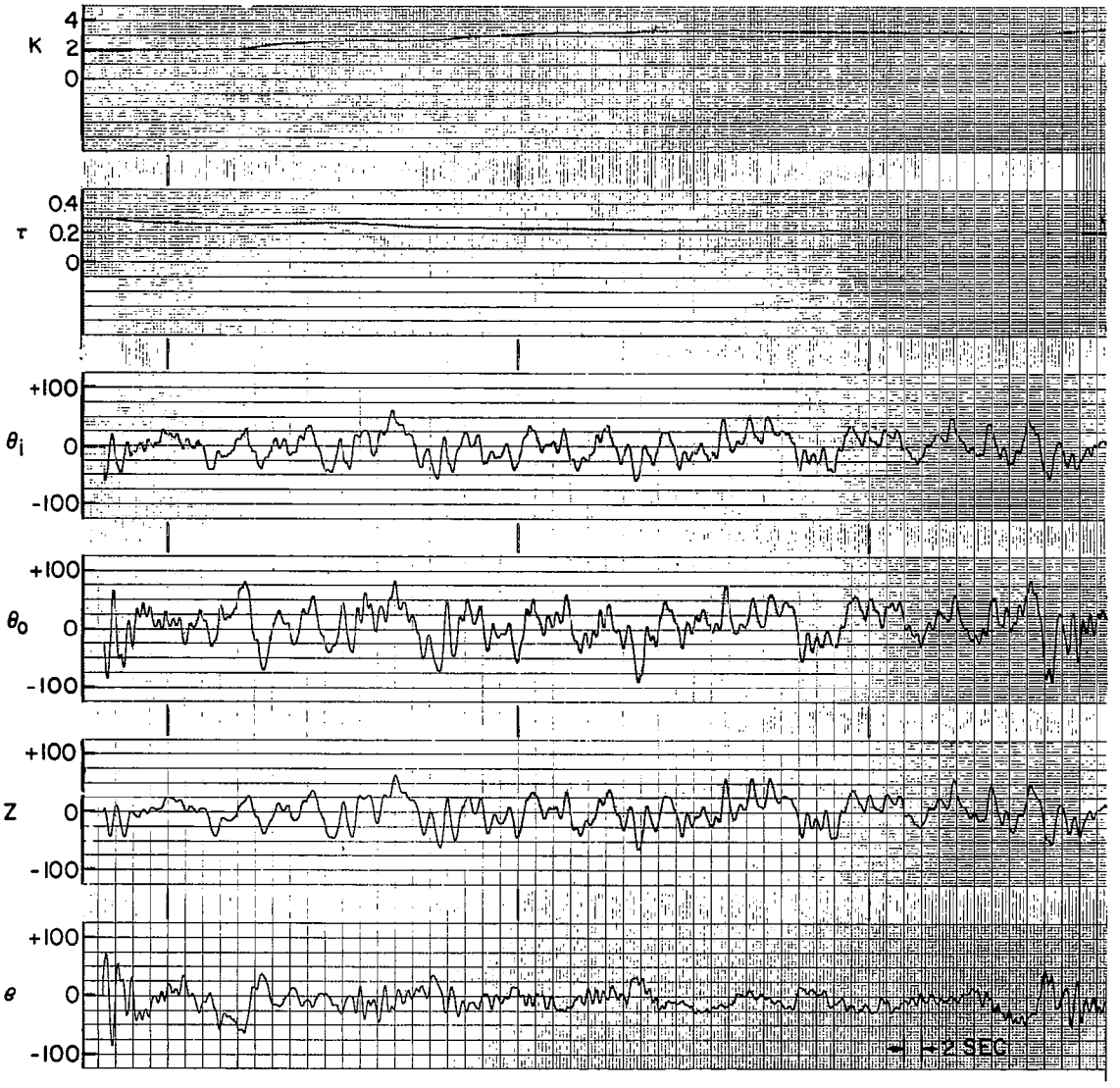

Figure D.2.4 Time History—Subject 3—Day 13—ω_i = 4 radians/second—Run 4—$Y_C(p) = K_2/p^2$—$k_K = 1 \times 10^{-3}$—$k_\tau = 8 \times 10^{-6}$.

initial conditions on K(t) and τ(t) have again been chosen to show convergence.

The gradient gains used in these figures are the same ones used in actual data reduction.

Appendix E

SPECTRAL ANALYSIS

The spectral analyses discussed in Chapter 6 were all done digitally using PDP-1 and CDC-160A computers. The spectral densities were developed on the PDP-1, while all averaging and transfer function calculations were performed on the CDC-160A.

The computer equations used to determine the spectral densities for each two minutes of recorded data will be discussed in this appendix.

E.1 Sampling Rates and Analog-Digital Conversion

The input signal $\theta_i(t)$ and the output signal $\theta_o(t)$ for each two minute run that was spectrally analyzed were converted from analog to digital signals by sampling their recorded values. The sampling was done in an A-D converter while the data was being fed from the magnetic tape recorder into the PDP-1 for spectral calculations.

The sampling rate was set at 20 samples per second. It was felt that $\theta_o(t)$ and $\theta_i(t)$ had negligible power above five cycles per second and that the sampling rate used was high enough to eliminate frequency aliasing.

Of the 120 seconds of data recorded from each run, only the last

110 seconds was sampled. The first 10 seconds of each run was omitted to assure that the speed of the magnetic tape recorder had stabilized before sampling started. Also, this eliminated those portions of the signals which contained the transient behavior of the subjects tracking start-up.

E. 2 Spectral Calculation

To describe the spectral program the following nomenclature is defined:

T_n = Record length per run

= 110 seconds

n = Number of samples per run

= 20 samples per second X 110 seconds

= 2200 samples

T_m = Maximum length of lag used in the calculation of the approximate correlation functions

= 10 seconds

m = Maximum length of lag in terms of samples

= 200

Δt = Time between samples

= 1/ sampling rate

= 1/ 20 seconds

These definitions are taken from the work of Blackman and Tukey [9], as is the general method of analysis.

The general procedure is to find the auto- or cross-correlation function for each two minutes of data, and then Fourier transform these functions to obtain the spectral or cross-spectral densities for that particular run. Estimates of the true densities for a given subject, on a given day, at a given test condition are then determined by averaging the individual run densities over the five runs. This procedure is discussed in Section 6.1.

The auto-correlation function determined for the qth two minute run of $\theta_o(t)$ is given in Eq. (6.1-9). This is calculated digitally by

$$C_{ooq}(\xi \Delta t) = \frac{W(\xi \Delta t)}{T_n - \xi \Delta t} \sum_{r=0}^{2200 - \xi} \theta_{oq}(r\Delta t)\, \theta_{oq}(r\Delta t + \xi \Delta t) \quad , \text{(E.2-1)}$$

$$\xi = 0, 1, 2, \ldots, m$$

where the smoothing function $W(\alpha)$ is defined as

$$W(\alpha) = 0.54 + 0.46 \cos \frac{\pi \alpha}{T_m} \quad , \quad |\alpha| \leq m \ . \qquad \text{(E.2-2)}$$

The equation for the spectral density of $\theta_o(t)$, as determined from the qth two minute run, is given in Eq. (6.1-10). This was calculated as

$$\phi_{ooq}(\omega) = \sum_{\xi = -m}^{+m} C_{ooq}(\xi \Delta t)\, e^{-j\omega \xi \Delta t}\, \Delta t$$

$$= C_{ooq}(0)\, \Delta t + 2 \sum_{\xi = 1}^{m} C_{ooq}(\xi \Delta t) \cos(\omega \xi \Delta t)\, \Delta t \ , \quad \text{(E. 2-3)}$$

since $C_{ooq}(\alpha)$ is an even function.

Equation (E. 2-3) was calculated only at the discrete frequencies $\omega_\beta = 2\pi f_\beta$, where

$$f_\beta = \frac{\beta}{2(\Delta t)m} \text{ cps} \quad , \quad \beta = 0, 1, 2, \ldots m \qquad \text{(E. 2-4)}$$

so that

$$\phi_{ooq}(\omega_\beta) = \left\{ C_{ooq}(0) + 2 \sum_{\xi = 1}^{m} C_{ooq}(\xi \Delta t) \cos\left(\frac{\xi \pi \beta}{m}\right) \right\} \Delta t \ . \quad \text{(E. 2-5)}$$

$\phi_{iiq}(\omega_\beta)$ was calculated in exactly the same manner as the method described above for $\phi_{ooq}(\omega_\beta)$. For the cross-spectral case the equation for the approximate cross-correlation function, as determined from the qth two minute run, was

$$C_{ioq}(\xi \Delta t) = \frac{W(\xi \Delta t)}{(T_n - |\xi \Delta t|)} \sum_{r = -1100 + |\xi|}^{1100 - |\xi|} \theta_{iq}(r \Delta t)\, \theta_{oq}(r \Delta t + \xi \Delta t) \quad \text{(E. 2-6)}$$

and the corresponding cross-spectral density function

$$\phi_{ioq}(\omega_\beta) = \sum_{\xi = -m}^{m} C_{ioq}(\xi \Delta t) \cos\left(\frac{\xi \pi \beta}{m}\right) \Delta t$$

$$- j \sum_{\xi = -m}^{m} C_{ioq}(\xi \Delta t) \sin\left(\frac{\xi \pi \beta}{m}\right) \Delta t \quad . \qquad \text{(E. 2-7)}$$

E. 3 Confidence Band for the Spectral Calculations

The equations necessary to determine the confidence in the spectral densities are given in Blackman and Tukey [9]. The 90% confidence band (in decibels) is

$$20 \sqrt{\frac{m}{2n - \frac{5m}{3}}} = 4.44 \text{ db} \quad . \qquad \text{(E. 3-1)}$$

This means that 90% of the time the magnitude of the spectral density, as calculated from each two minute run, will fall within ± 2. 22 db of the true value.

E. 4 Sample Transfer Function Calculation

To test the accuracy of the spectral calculations and the method of generating transfer functions the following test was run: A random signal of filtered Gaussian white noise was put through a closed loop system with a forward loop consisting of the parameter tracking

version of the crossover model. The value of K was set at 3.0 and the value of τ at 0.35. $\theta_i(t)$ and $\theta_o(t)$ were recorded during five runs of two minutes duration. The forward loop gain-phase curves of the model were then calculated using the spectral density approach as developed for actual subject evaluation. The results are given in Fig. E.4.1. It is seen that the experimental curves match the theoretical gain and phase curves for the forward loop quite well.

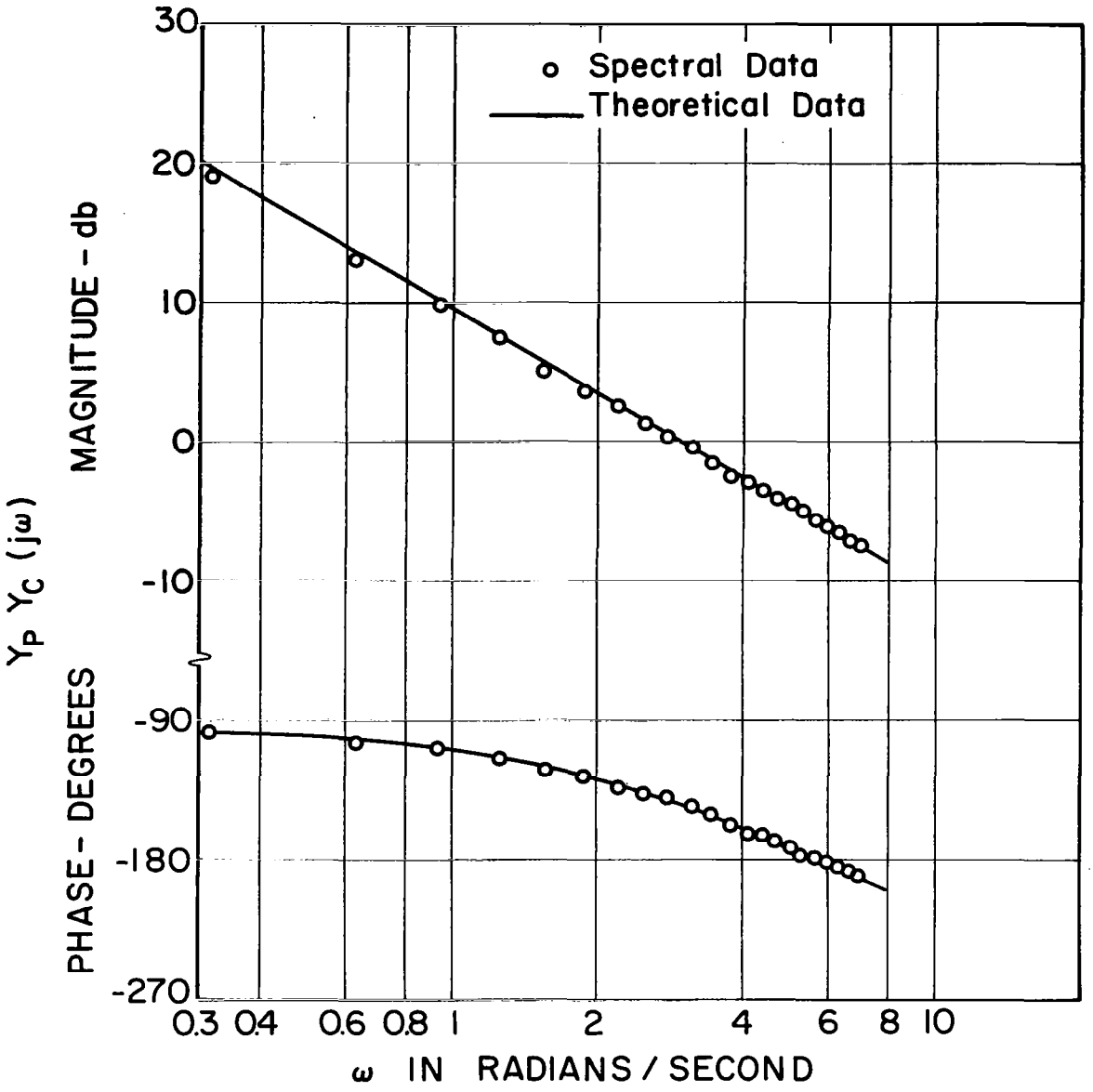

Figure E. 4. 1 Checking the Transfer Function of a Known Approximate Crossover Model Using Spectral Analysis. $K^* = 3.0$ and $\tau^* = 0.35$. Random Input Signal with $\omega_i = 4$ radians/ second.

Appendix F

AN OBSERVATION ON PARAMETER TRACKING SYSTEMS USING ITERATIVE PARAMETER ADJUSTMENT

The sensitivity equations used in the continuous parameter tracking system were developed in Chapter 3 under the assumption that the assumed model parameters K and τ were constant. The equations were implemented so that both K and τ could be adjusted continuously. This means, of course, that the parameter adjustment equations are in error, except in the limit as K(t) and τ(t) approach constant values. In spite of this error which exists during the convergence interval, it was shown theoretically in Chapter 4 and experimentally in Appendices C and D, that the parameters do converge to the correct values.

One would guess that a straightforward way to circumvent this problem, and to completely eliminate the use of the erroneous equations, is to use the iterative adjustment technique discussed in Chapter 3. In this method the assumed model parameters are held constant during a computational period of T seconds. At the end of this period the parameters α_i are step changed by an amount $\Delta\alpha_i$, where

$$\Delta\alpha_i(t_1) = -k \frac{\partial I}{\partial \alpha_i}(t_1, \vec{\alpha})$$

$$= -\frac{k}{T} \int_{t_1 - T}^{t_1} e \frac{\partial Z}{\partial \alpha_i}(t, \vec{\alpha})\, dt \quad ,$$

and $\frac{\partial Z}{\partial \alpha_i}(t, \vec{\alpha}) = u_i(t, \vec{\alpha})$ is the sensitivity coefficient for α_i. At time t_1 this adjustment is made on all the α_i, and a new period of T seconds is initiated.

The first impression on the use of this method is that it is completely accurate. The α_i are held constant during the entire computation interval, and the sensitivity equations should be 100% correct. It should be noted, however, that this is not the case.

The sensitivity equations, by definition, are based on information obtained by noting the changes in $Z(t, \vec{\alpha})$ that would be caused by small changes in α_i made at the start of the solution. All initial transients are either specifically accounted for, or are allowed to die out. Therefore, if the parameter tracking system changes any parameter that will introduce a transient into the system, this transient must be allowed to die out before the equations are again error-free.

In the case of the crossover model, transients die out with a basic time constant that can exceed one second. (See the example in Section C.1.) This means that one should wait at least three seconds

after parameter adjustment before starting the next computational period.

It can be argued that the transients introduced by the step changes in the parameters will be negligible, if the $\Delta\alpha_i$ are small. This is undoubtedly true. However, picking the $\Delta\alpha_i$ small dictates that T must also be small to insure convergence in a reasonable length of time. In the limit as $T \rightarrow 0$, the continuous parameter adjustment case is generated.

The purpose of this discussion is merely to point out one distinct possibility: If the convergence rates of the parameters in the continuous adjustment method are slow, (compared to the time constants of the model) the parameter adjustment equations probably will be no more in error than those found in the iterative adjustment technique, if no time is allowed in the latter case for transients to die out.

REFERENCES

1. Adams, J.J., Kincaid, J.K., and Bergeron, H.P.: Determination of Critical Tracking Tasks for a Human Pilot. NASA TN D-3242, Feb. 1966.

2. Adams, J.J. and Bergeron, H.P.: Measurements of the Human Transfer Function with Various Model Forms. NASA TN D-2394, Aug. 1964.

3. Adams, J.J. and Bergeron, H.P.: Measured Variation in the Transfer Function of a Human Pilot in Single-Axis Tasks. NASA TN D-1952, 1963.

4. Adams, J.J.: A Simplified Method for Measuring Human Transfer Functions. NASA TN D-1782, 1963.

5. Bekey, G.A., Meissinger, H.F., and Rose, R.E.: Mathematical Models of Human Operators in Simple Two-Axis Control Systems. IEEE Trans. on HFE, Vol. HFE-6, No. 1, Sept. 1965, pp. 42-52.

6. Bekey, G.A.: Research on New Techniques for the Analysis of Manual Control Systems. Progress Report on NASA Grant NGR-05-018-022, June 15-Dec. 15, 1965.

7. Bekey, G.A., Meissinger, H.F., and Rose, R.E.: A Study of Model Matching Techniques for the Determination of Parameters in Human Pilot Models. TRW-STL-8426-6006-RU00, May 1964.

8. Bellman, R.: Stability Theory of Differential Equations. McGraw-Hill Book Co., Inc., 1953.

9. Blackman, R.B. and Tukey, J.W.: The Measurement of Power Spectra. Dover Publications, Inc., 1958.

10. Davenport, W.B., Jr., and Root, W.L.: An Introduction to the Theory of Random Signals and Noise. McGraw-Hill Book Co., Inc., 1958.

11. Elkind, J.I.: Further Studies of Multiple Regression Analysis of Human Pilot Dynamic Response: A Comparison of Analysis Techniques and Evaluation of Time-Varying Measurements. ASD-TDR-63-618, Mar. 1964.

12. Elkind, J.I., Green, D.M., and Starr, E.A.: Application of Multiple Regression Analysis to Identification of Time-Varying Systems. IEEE Trans. on A.C., Vol. AC-8, No. 2, Apr. 1963, p. 163.

13. Elkind, J.I.: Characteristics of Simple Manual Control Systems. M.I.T. Lincoln Lab. Tech. Report No. 111, Apr. 6, 1956.

14. Eykhoff, P.: Some Fundamental Aspects of Process-Parameter Estimation. IEEE Trans. on A.C., Vol. AC-8, No. 4, Oct. 1963.

15. Fuchs, A.H.: The Progression-Regression Hypothesis in Perceptual-Motor Skill Learning. Jour. of Exp. Psyc., Vol. 63, No. 2, 1962, pp. 177-182.

16. Gilbert, E.G.: Linear System Approximation by Mean Square Error Minimization in the Time Domain. The Univ. of Mich. Engineering Industry Program, Jan. 1957.

17. Goodman, T.P. and Reswick, J.S.: Determination of System Characteristics from Normal Operating Records. Trans. ASME, Vol. 78, Feb. 1956, pp. 259-271.

18. Goodyear Aircraft Corporation Report GEC-4750: Human Dynamic Study, Apr. 8, 1952.

19. Hoffman, L.G., Lion, P.M., and Best, J.J.: Theoretical and Experimental Research on Parameter Tracking Systems. Systems Technology Inc., TR-N-148-1, Oct. 1965.

20. Jones, J.G.: A Note on the Model Matching Technique for the Measurement of Human Operator Describing Functions. Royal Aircraft Establishment Tech. Rept. No. 65290, Dec. 1965.

21. Kryloff, N. and Bogoliuboff, N.: Introduction to Nonlinear Mechanics. Princeton University Press, 1947.

22. Magdaleno, R. and Wolkovitch, J.: Performance Criteria for Linear Constant Coefficient Systems with Random Inputs. ASD-TDR-62-470, Jan. 1963.

23. Margolis, M.: On the Theory of Process Adaptive Control Systems, the Learning Model Approach. AFOSR-TN-60-618, Report No. 60-32, May 1960.

24. McBride, L.E. and Narenda, K.S.: Optimization of Time-Varying Systems. IEEE Trans. on A.C., Vol. AC-10, July 1965, pp. 289-294.

25. McRuer, D.T., Graham, D., Krendel, E.S., and Reisener, W.,Jr.: Human Pilot Dynamics in Compensatory Systems. AFFDL-TR-65-15, July 1965.

26. McRuer, D.T. and Krendel, E.S.: Dynamic Response of Human Operators. WADC-TR-56-524, Oct. 1957.

27. McRuer, D.T. and Graham, D.: Analysis of Nonlinear Control Systems. John Wiley and Sons, Inc., 1961.

28. McRuer, D.T., Graham, D., Krendel, E.S., and Reisener, W.C., Jr.: System Performance and Operator Stationarity in Manual Control Systems. Paper presented at the 3rd IFAC Congress, London, June 1966.

29. Meissinger, H.F. and Bekey, G.A.: An Analysis of Continuous Parameter Optimization Methods Employing Sensitivity Coefficients. Paper presented at IFAC Conference on Sensitivity Analysis, Dobrovnik, Yugoslavia, Aug. 31-Sept. 4, 1964.

30. Meissinger, H.F.: Parameter Influence Coefficients and Weighting Functions Applied to Perturbation Analysis of Dynamic Systems. 3rd International Analogue Computation Meetings.

31. Saaty, T.L. and Bram,J.: Nonlinear Mechanics. McGraw-Hill, Inc., 1964.

32. Siegel, A.I., Lanterman, R.S., Platzer, H.L., and Wolf, J.J.: Techniques for Evaluating Operator Loading in Man-Machine Systems. Applied Psychological Services, Wayne, Pa., Jan. 1966.

33. Summers. L.G. and Ziedman, K.: A Study of Manual Control Methodology with Annotated Bibliography. NASA CR-125, Nov. 1964.

34. Todosiev, E.P., Rose, R.E., Bekey, G.A., and Williams, H.L.: Human Tracking Performance in Uncoupled and Coupled Two-Axis Systems. TRW Systems Rept. 4380-6003-R0000. Dec. 8, 1965.

35. Tomovic, R.: Sensitivity Analysis of Dynamic Systems. McGraw-Hill Book Co., Inc., 1964.

36. Truxal, J.G.: Control System Synthesis. McGraw-Hill Book Co., Inc., 1955.

37. Volkov, A.A.: Simplified Method of Measuring the Transfer Function of an Operator. In NASA TT-F-374, Feb. 26, 1965.

38. Wierwille, W.W.: A Theory for Optimal Deterministic Characterization of Time-Varying Human Operator Dynamics. IEEE Trans. on HFE, Vol. HFE-6, No. 1, Sept. 1965, pp. 53-61.

39. Wierwille, W.W. and Gagne, G.A.: Experimental Study of a Deterministic Method for the Characterization of the Time-Varying Dynamics of Human Operators. Men and Computers, Sixth Annual Symposium of PG-HFE, May 1965.

40. Winer, B.J.: Statistical Principles in Experimental Design. McGraw-Hill Book Co., Inc., 1962.

41. Young, L.R. and Meiry, J.L.: Bang-Bang Aspects of Manual Control in High Order Systems. IEEE Trans. on A.C., Vol. AC-10, No. 3, July 1965, pp. 336-341.

"The aeronautical and space activities of the United States shall be conducted so as to contribute . . . to the expansion of human knowledge of phenomena in the atmosphere and space. The Administration shall provide for the widest practicable and appropriate dissemination of information concerning its activities and the results thereof."

—NATIONAL AERONAUTICS AND SPACE ACT OF 1958

NASA SCIENTIFIC AND TECHNICAL PUBLICATIONS

TECHNICAL REPORTS: Scientific and technical information considered important, complete, and a lasting contribution to existing knowledge.

TECHNICAL NOTES: Information less broad in scope but nevertheless of importance as a contribution to existing knowledge.

TECHNICAL MEMORANDUMS: Information receiving limited distribution because of preliminary data, security classification, or other reasons.

CONTRACTOR REPORTS: Scientific and technical information generated under a NASA contract or grant and considered an important contribution to existing knowledge.

TECHNICAL TRANSLATIONS: Information published in a foreign language considered to merit NASA distribution in English.

SPECIAL PUBLICATIONS: Information derived from or of value to NASA activities. Publications include conference proceedings, monographs, data compilations, handbooks, sourcebooks, and special bibliographies.

TECHNOLOGY UTILIZATION PUBLICATIONS: Information on technology used by NASA that may be of particular interest in commercial and other non-aerospace applications. Publications include Tech Briefs, Technology Utilization Reports and Notes, and Technology Surveys.

Details on the availability of these publications may be obtained from:

SCIENTIFIC AND TECHNICAL INFORMATION DIVISION

NATIONAL AERONAUTICS AND SPACE ADMINISTRATION

Washington, D.C. 20546